UNIVERSITY OF BIRMINGHAM

Ionisation Studies of Chlorinated and Fluorinated Compounds

by

Michael Anthony Parkes

A thesis submitted to
The University of Birmingham
for the degree of
DOCTOR OF PHILOSOPHY

School of Chemistry
The University of Birmingham
Birmingham
B15 2TT

August 2007

Abstract

Ionisation processes in gas-phase polyatomic molecules have been studied using threshold photoelectron photoion coincidence and selected ion flow tube techniques for cations and an electron attachment mass spectrometer for anions. Cation formation has been studied for fluoroform (CHF_3), octafluorocyclobutane (*c*-C_4F_8), octafluorocyclopentene (*c*-C_5F_8), monochloroethene (C_2H_3Cl), the three isomers of dichloroethene ($C_2H_2Cl_2$) (*i.e.* 1,1-dichloroethene, (*Z*)-1,2-dichloroethene and (*E*)-1,2-dichloroethene), trichloroethene (C_2HCl_3) and tetrachloroethene (C_2Cl_4). Comparison between the data from the photoionisation and the ion-molecule reactions show that the dominant charge-transfer mechanism is long-range in nature.

Detailed studies of the reactions of cations with the three dichloroethenes have been performed to look for evidence of isomeric effects. Major differences are seen when the reactant ion is CF_3^+; when 1,1-dichloroethene is the neutral reactant the only ionic product is $C_2H_2Cl^+$, but if the neutral is 1,2-dichloroethene then the only product is $CHCl_2^+$. Only minor differences are seen with other reagent ions. For the reactions of all six chloroethenes with CF_3^+, product ions are observed which can only be formed by extensive rearrangement across the carbon-carbon double bond. Mechanisms are suggested involving bridged trigonal intermediates to explain the production of the different channels.

Studies have been performed on several perfluorocarbons, CHF_3, *c*-C_4F_8 and *c*-C_5F_8, due to their potential for use in industry. They are all excellent at etching substrates and have a lower global warming potential than the currently used gases. CHF_3 shows signs of non-statistical dissociation following photoionisation, and is shown to react *via* a largely long-range charge transfer mechanism in the ion-molecule reactions studied. For *c*-C_5F_8 the ground electronic state of the ion is found to be very weak under threshold conditions whilst being much more intense when He(I) photons are used.

The existing electron attachment mass spectrometer is described, and also extensive modifications which have been made to this apparatus. The use of new electronics and acquisition system give excellent results in the new equipment. The new arrangement has been extensively characterised by studying attachment to seven molecules, including several perfluorocarbon molecules (*e.g.* the isomers of C_4F_8). Some isomeric effects on the measured rate coefficients are observed in the data.

To Ange, thank you.

"The Chemists are a strange class of mortals, impelled by an almost maniacal impulse to seek their pleasures amongst the smoke and vapour, soot and flames, poisons and poverty. Yet amongst these evils I seem to live so sweetly"

Johann Becher – Alchemist and Fraudster (1635 – 1682)

"Why has man rooted himself thus firmly in the earth, but that he may rise in the same proportion into the heavens above?"

Henry David Thoreau (1817 – 1862), *Where I lived, and what I lived for*.

Acknowledgments

Firstly, I would like to thank my two supervisors, Professor Richard Tuckett and Dr Chris Mayhew, without their considerable help during my PhD this thesis would never have happened. I also thank the many people who have in some way helped me during my work. Special thanks go to Sanj Ali and Matt Simpson for all their support and their friendship, both at Birmingham and, perhaps more importantly at Daresbury. Thank you also for Dr Chris Howle for all his help. I have many many thanks for Dr Victor Mikhailov who taught me a great deal of very useful experimental skills, without his mentoring this thesis would not be half the work it is. I wish to express my thanks to the other members of the Molecular Physics group, Margaret, Shane and Sarah for all the useful discussions over the years. A big thank you to David Howse for all his help with the electronics on the EA and to Dr Graham Worth for his crucial advice on using Gaussian 03 and giving me free rein on his servers.

I would also like to thank the various support staff, in both the school of Chemistry and the school of Astronomy and Physics for helping my work go smoothly. I must especially thank Chou in stores for often guiding me to a correct solution and all the members of the physics workshop. They always did an excellent job even when given very vague instructions. Their willingness to get the jobs done was phenomenal.

I have had the pleasure to collaborate with many scientists during my PhD. I must thank all the staff at the Daresbury laboratory, especially Drs David Shaw and Andy Malins. I must also thank all the people who helped me with solving the problems with *c*-C_5F_8. Dr Jeremy Harvey for advice on calculations, Prof. John Dyke for recording the He(I) spectrum, Prof. George King and Dr Michele Siggel-King for the high-resolution TPES and Prof. Colin Latimer and Dr Ken Dunn for the ion-pair study. I would also like to thank Prof. Geoff Ritchie for advice on quadrupole moments for *c*-C_4F_8.

Finally, I would like to acknowledge my friends and family. The biggest thanks are of course for my wife Ange for all her patience and understanding. Also thanks to my parents and my brother for their support. The last thank you is to Tom, thank you for making sure I was always up on time.

Table of Contents

List of Figures

List of Tables

Chapter 1: Introduction

This thesis is concerned with ionisation of a range of halogenated hydrocarbon molecules in the gas phase. The main aim is to study what happens upon ionisation; what the initial products are and how they decay with time. Ultimately, the aim is to understand how, following ionisation of an isolated molecule, energy is partitioned within a molecular cation and how different types of ionisation compare. For example, what are the breakdown products from photon ionisation and how do they differ from the products formed from an ion-molecule reaction? A secondary aim of this thesis is to understand how molecular structure affects the ionisation process. This has been achieved by replacing hydrogen atoms systematically with halogen atoms in a series of molecules to see how ionisation dynamics alter with the number and position of halogen-atom substituents.

At a more applied level the results for the reactions reported here may find use in many areas of science and technology. Several of the compounds studied in this thesis are important industrially and atmospherically. Monochloroethene, also known as vinyl chloride, is a crucial component of plastics, while tetrachloroethene is used as a dry cleaning agent. The perfluorocarbon molecules studied in chapters 4-6 and 10 are used in technological plasmas for etching of silica substrates. Knowledge of the rates and products of ionisation processes can help understand industrial reactions. Such knowledge can also aid the modelling of atmospheric lifetimes of many halocompounds. For example, Ravishankara *et al.*[1] showed how the lifetime of perfluorocompounds can be longer than human civilisation, and subsequently Morris *et al.*[2] showed that proper allowance for both ion-molecule and electron-molecule reactions can shorten the estimated lifetimes. Therefore, it is crucial that this information is available.

1. Types of isomerism

There are many different types of isomers. For simplicity they can be split into two broad categories; constitutional isomerism and stereoisomerism. Constitutional isomers are molecules which have the same molecular formula but the constituent atoms are bonded in different ways. Several types of constitutional isomer can occur. A simple example would be chloropropane which exists in two forms:

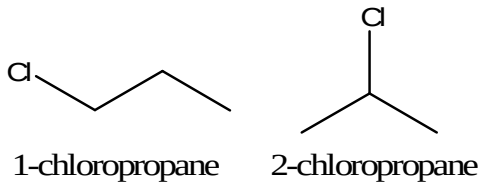

Figure 1.1: Example of constitutional isomerism, variation in position of atoms for C_3H_7Cl.

Here the chlorine can be in two distinct positions, either on a terminal carbon or on a chain carbon. Another example is C_4F_8 which can exist in several forms and show various functional groups:

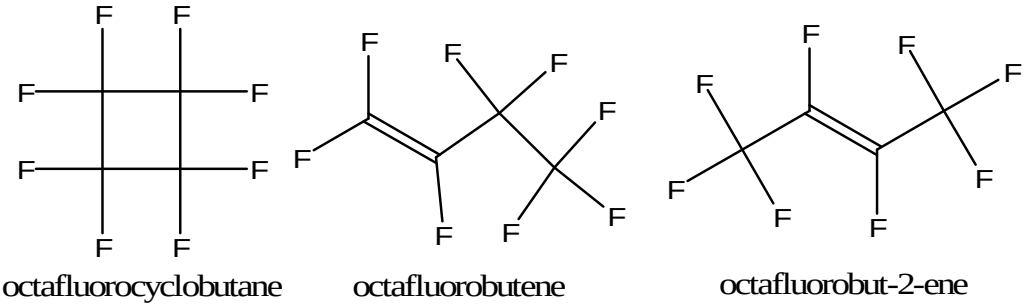

Figure 1.2: Example of constitutional isomerism, variation in functional groups for C_4F_8.

It is expected that most constitutional isomers will show huge variations in both physical properties and chemical reactivity. Such variation will be clearest when the isomeric differences are in the types of functional group, see Figure 1.2 where the molecules are either cyclic alkanes or linear alkenes. If the differences are in the position of the functional group, as shown in Figure 1.1, less variation will be expected, but some differences may still occur.

Stereoisomerism, sometimes called geometric isomerism, is a more subtle effect than constitutional isomerism. It occurs for molecules which have the same molecular formula and bonding of atoms; if the spatial arrangement of the atoms is different then isomerism arises. This type of isomerism can be broken down into two further classes, diastereomers and enantiomers.

Enantiomers are chiral molecules which are non-superimposable mirror images of each other. Enantiomers show optical activity, *i.e.* they rotate the plane of polarized light. In a general reaction enantiomers will show no difference in reactivities and their physical properties will be essentially the same. For differences in chemical properties to show up between the enantiomers, chiral reactants must be used either a chiral reactant ion,[3,4] polarized light or spin-polarized electrons.[5-8] An example of a simple chiral molecule is bromochlorofluoromethane.

(*S*)-bromochlorofluoromethane (*R*)-bromochlorofluoromethane

Figure 1.3: Example of enantiomeric isomerism for CBrClFH.

Most biological molecules show some form of enantiomeric effect, and in some cases there are major differences between the reactions of the enantiomers with other chiral molecules. A famous example is thalidomide, where one enantiomer has desirable effects while the other is toxic and teratogenic.

Diastereomers are any stereoisomers which are not related as mirror images. Examples are *E*-*Z* isomerisation, conformal isomerism and mesoisomerism. *E*-*Z* isomers and conformers are related in that these forms of isomerisation are due to constrained rotation around chemical bonds. *E* and *Z* isomers typically arise from the presence of carbon-carbon double bonds, but also occur in ring structures. *E* and *Z* isomers are often referred to as *trans* and *cis* isomers for double bonds. For ring structures the terms *E* and *Z* are never used, only *trans* and *cis*. An example of *E* and *Z* isomerisation with double bonds is shown in Figure 1.4, and this type of isomerisation in a ring structure is shown Figure 1.5.

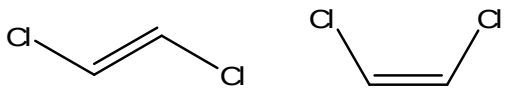

(*E*)-1,2-dichloroethene (*Z*)-1,2-dichloroethene

Figure 1.4: Example of *E* and *Z* isomerism across a double bond for $C_2H_2Cl_2$.

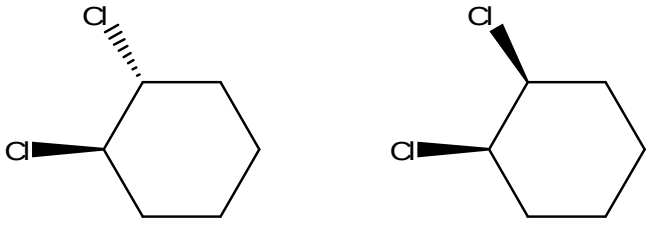

trans-1,2-dichlorocyclohexane *cis*-1,2-dichlorocyclohexane

Figure 1.5: Example of *trans* and *cis* isomerism in a ring structure for $C_6H_{10}Cl_2$.

In the *E* isomer the two highest priority atoms (as determined by the Cahn-Ingold-Perlog priority rules) are on opposite sides of the double bond. For the *Z* isomer the two highest priority

atoms are on the same side of the double bond. This makes *E* equivalent to *trans* and *Z* equivalent to *cis* in the old nomenclature. *Cis* and *trans* are not used because if more than two distinct substituents are present it is no longer a rigorous nomenclature.

E and Z isomers often have quite different physical properties; for example, the Z form tends to have a higher boiling point than the *E* form. Thus (*Z*)-1,2-dichloroethene has a melting point of 193.0 K and boiling point of 333.5 K while (*E*)-1,2-dichloroethene has a melting point of 223 K and a boiling point of 321 K.[9] This is because in the *Z* isomer the dipole moments induced by the substituents will tend to add while in the *E* form they will tend to cancel out. However, chemical reactivities tend to be fairly similar, and most differences in reactivity come from steric effects.

Conformational isomers, conformers, arise from restricted rotation around a single bond. In general, due to low barriers to rotation, there is free rotation and different conformers cannot be isolated. However, there are conditions where it can become important. This can be when temperatures are so low that the molecule can no longer surmount the barrier to rotation, or in cases where the barriers to rotation are intrinsically high. When large molecules are introduced into the gas phase, conformational locking can often occur. An interesting example of this form of isomerism is that many sugars have a specific conformation due to interaction between oxygen and carbon orbitals, the so-called anomeric effect.[10] In the anomeric effect a heteroatom attached to another heteroatom which is part of a cyclohexane ring prefers an axial orientation rather than the sterically more stable equatorial orientation.

In many ways *E* and *Z* isomers are a special case of conformers with a very large barrier to rotation due to the carbon-carbon double bond. If the temperature is increased until k_BT becomes equivalent to the strength of the double bond (about 300 kJ mol^{-1}) then rotation around the double bond becomes free and the *E* and *Z* isomers will no longer be differentiated. However, this corresponds to a very high temperature. In most situations there will be no measurable difference in reactivity between conformers. However, in some reactions, for example E_2 elimination where an antiperiplanar configuration is needed between the attacked substituent and the leaving group, differences between conformers can occur. This can be especially important when considering reactions of ring compounds.

2. Positive ionisation processes

2.1 Formation of positive ions

If enough energy is deposited into a neutral species, either an atom or a molecule, then it is possible that a positive ion, or cation, will be formed. The incident energy, E_i, must be greater than the ionisation energy, IE, of the species under study. The energy can be given to the molecule in several ways. If AB is a general molecule then:

$$h\nu + AB \rightarrow AB^+ + e^- \quad \textbf{(re 1.1)}$$

$$e^- + AB \rightarrow AB^+ + e^- + e^- \quad \textbf{(re 1.2)}$$

$$C^+ + AB \rightarrow AB^+ + e^- + C^+ \quad \textbf{(re 1.3a)}$$

$$C^+ + AB \rightarrow AB^+ + C \quad \textbf{(re 1.3b)}$$

$$M^* + AB \rightarrow AB^+ + e^- + M \quad \textbf{(re 1.4)}$$

$$\bar{E} + AB \rightarrow AB^+ + e^- \quad \textbf{(re 1.5)}$$

A negative species must be formed as a partner to the cation in all cases but reaction 1.3b. This negative species is shown to be an electron in the reactions given here but it is possible that the partner could be an anion, in that case the products would then be $A^+ + N^-$. The forms of excitation listed here are photons, $h\nu$ (reaction 1.1), electrons, e^- (reaction 1.2), positive ions, C^+ (reaction 1.3), excited neutrals, M^* (reaction 1.4) and large electric fields, $\bar{E}$ (reaction 1.5); the most general case is shown where a positive ion (AB^+) is formed. How the ionisation process occurs and what products are formed depends on the method of excitation.

2.1.1 Absorption of photons

When a molecule, or atom, absorbs a photon which is of short enough wavelength (high enough energy), ionisation can occur. As both the photon and molecule are electrically neutral a negative partner must be produced along with the cation to maintain conservation of charge. This partner could be either an electron or a negative ion. Formation of the anion, ion-pair production or polar dissociation, tends to be a much weaker process than production of the electron, photoelectron production. Only diatomics show ion-pair cross-sections which are comparable to photoionisation cross-sections.[11] In general, ion-pair production has a very small cross-section due to poor Franck-Condon factors for direct formation and the necessity of curve-crossing for

indirect formation.[12,13] Production of a photoelectron tends to be the major ionisation phenomena to occur after absorption of a photon above the ionisation limit.

Absorption of a photon below the ionisation limit is a resonant process. The energy of the photon must match exactly the energy of a transition from one state to another. If the energy is higher or lower than the transition energy then the photon will not be absorbed. Selection rules apply to these transitions. In general these rules arise due to conservation of angular momentum, though other quantum variables, such a spin and parity, can also be important. Above the ionisation limit photon absorption can also be a resonant process to form a super-excited state, an electronic state of the neutral which is unstable with respect to ionisation. However, for the photoionisation process itself the absorption of a photon is non-resonant. This arises because the photoelectron is released into a continuum and so can accommodate any excess energy as kinetic energy. There are no strict selection rules for photoionisation. This is because when the photoelectron is ejected it can take on an appropriate value of angular momentum to satisfy conservation laws. The change in angular momentum, ΔL, of the system is given by:

$$\Delta L = \pm l \qquad \textbf{(eq 1.1)}$$

where l is the angular momentum of the electron. Conservation then requires that the angular momentum of the ejected electron is equal to $l \pm 1$. For example, if the electron is removed from a *d*-orbital then the outgoing electron wave will have *p* and *f* character, *i.e.* have one or three units of angular momentum. This means that the nature of the orbital from which an electron is removed can be found by studying the angular distribution of the photoelectrons.[14]

The only technically-forbidden process in photoionisation is one that involves two electrons, because the electronic structure of atoms and molecules is well described by a one-electron model. In this model the motion of electrons is independent and they are present in separate molecular orbitals. Due to these assumptions a transition which affects one electron must leave all other electrons unchanged. Two-electron processes do occur because in reality electrons are correlated. These two-electron processes occur as satellite bands in a photoelectron spectrum, where they are described as the ionisation of one electron and the simultaneous excitation of another electron. Another common two-electron process is the formation of a doubly-charged cation.

There is a second process, termed autoionisation, by which ionisation occurs after absorption of a photon. Autoionisation is an indirect process and can be described by the following scheme:

$$h\nu + AB \rightarrow AB^{*} \rightarrow AB^{+} + e^{-} \qquad \textbf{(re 1.6)}$$

Here the photon excites the neutral into a high-lying electronic state, AB^{*}, these states are often termed super-excited because they are unstable with respect to ionisation. The majority of these super-excited states are Rydberg in character. Here the electron is excited to a high principal quantum number, and has a large, sometimes macroscopic, orbital radius. Series of these Rydberg states converge upon every ionisation energy. As the photon absorption is to a normal, if highly-energetic state, the process is resonant and normal dipole selection rules will apply. Once the super-excited state is formed it can decay in several ways. The first way is by predissociation to form neutral fragments; in this case no charged species will be formed and it will have no bearing on photoionisation measurements. Another decay path is for the super-excited state to fluoresce to a lower neutral electronic state. Again, in this case no charged species are formed. A decay channel which does produce charged species is autoionisation.

There are three main autoionisation mechanisms postulated.[15] The first is conversion of excess rotational energy of the ion core into electronic energy, causing the ejection of the Rydberg electron. The second is conversion of excess vibrational energy of the core into electronic energy, leading to ejection of the Rydberg electron. These two processes will produce electrons with a very low kinetic energy. A third mechanism is the conversion of excess electronic excitation energy into kinetic energy of the electron. This process involves two electrons. One electron falls into an orbital hole while a second is ejected, and this mechanism can produce electrons with significant kinetic energy.[14]

Autoionisation can often populate regions on the potential energy curve of the molecular ion outside the Franck-Condon region. This can lead to different populations of the various ionic states when compared to direct photoionisation. Autoionising decay by any of the three mechanisms can lead to changes in photoionisation measurements. There can be alterations in vibrational distributions within electronic bands, because there is a Franck-Condon transition to the super-excited state followed by another Franck-Condon transition to the ionic state.[14]

It has been shown by Wigner that the behavior of the cross-section at threshold is given by the following equation:[16]

$$\sigma = C\left(E - E_0\right)^{n-1} \qquad \textbf{(eq 1.2)}$$

where C is a constant, E is the ionizing energy, E_0 is the threshold energy and n is the number of outgoing electrons. As only one electron is produced following photoionisation the power becomes zero. This means that for photoionisation the cross-section will show a sharp onset in

the form of a step function. Therefore a measured photoionisation cross-section should consist of a series of steps for each onset of ionisation in a molecule.[17] In theory, each rovibrational level constitutes an onset in such an experiment, but in practice the resolution is never sufficient to observe the structure, or the steps are obscured by autoionisation.[17] The subsequent decay of the positive ion will be dealt with in a later section.

2.1.2 Interaction with electrons

The interaction of an electron with a neutral is in many ways analogous with the absorption of a photon with a neutral. There are, however, several differences. The first is that the electron is not absorbed by the molecule. Instead the electron and the neutral partner collide and the electron scatters off. This collision can occur either elastically or inelastically. It is the inelastic processes which will concern us here. These inelastic collisions can be divided into two broad regimes. In the first the incident electrons have a huge kinetic energy, *i.e.* large compared to the orbital velocities of electrons in the molecule. In this regime the incident electron moves so quickly that the excitation occurs when the electron and neutral are close together, and there is little interaction as the electron arrives and departs. In the second regime the incident electrons have low kinetic energies and the interaction time is long, comparable to the orbital period of the electrons. In this case the incident electron and the electrons in the molecule have significant effects upon each other. In some cases the electron-neutral complex is best considered as a transient negative ion, a regime which will be treated more thoroughly later.

It can be shown that at high electron energies the differential electron scattering cross-section is given by the Bethe-Born theory:[18]

$$\frac{d^2\sigma}{d\theta dE} = \frac{2k_n}{Ek_0K^2} f(K,E) \qquad \textbf{(eq 1.3)}$$

where E is the energy transferred to the target, k_n and k_0 are the magnitudes of the incident and scattering momenta and K is the momentum transfer. $f(K,E)$ is the generalized oscillator strength and is given by:

$$f(K,E) = f(0,E) + aK^2 + bK^4 + ... \qquad \textbf{(eq 1.4)}$$

$f(0,E)$ is the dipole-only term and is the same as the value which would be measured in a photon absorption experiment. Therefore measurements made with a small momentum transfer between the electron and the molecule will be analogous to photon excitation, results which have been

experimentally tested.[17] At low incident electron energies the Bethe-Born theory does not apply because it assumes that the interaction is rapid, and impulsive. An examination of electron ionisation cross-sections from threshold to high energies requires other theories. Several semi-rigorous methods have been used, including the Deutsch-Märk formalism and the binary-encounter-dipole method.[19,20] Both methods have been improved and extended with time to the extended Deutsch –Märk formalism and the binary-encounter-Bethe method.[21,22] In general it appears that the Deutsch-Märk method overestimates the cross-section while the binary encounter-Bethe method underestimates it,[23] although this seems to depend on the initial calculation used to obtain molecular structures. Another difference between the interaction of electrons and photons with neutrals is that selection rules are relaxed. This is because the incident electron can actually exchange with a target electron, allowing spin flipping to occur.

Photoionisation and electron ionisation are similar, except for two major differences. First, the behaviour at threshold is different for the two ionisation methods. As shown in equation 1.2 the dependence of the cross-section on the number of electrons is proportional to $(\Delta E)^{n-1}$. After electron ionisation there are two electrons produced, therefore the cross-section is raised to the power of unity. This leads not to a step function for the cross-section but a linear onset, with a value of zero at threshold. This should be compared to photoionisation which will have a non-zero value at threshold. This is one of the main difficulties with obtaining ionisation energies from electron ionisation. It should be noted that the Wigner threshold rules are only correct under very restrictive assumptions; currently, the best method to obtain IE values is to fit the experimental cross-sections with a model based on the work of Wannier which involves fitting at least four variables.[24] Second, one must consider the behaviour of super-excited states. These states are no longer formed resonantly with electron ionisation, but are excited at all energies above their threshold. They are therefore very common in electron ionisation spectra, and the excitation cross-section to these states is no longer constant but varies with electron energy.[17]

2.1.3 Interactions with positive ions

A neutral molecule can be ionised in several ways using positive ions as a source of energy. If the collision energy of the system is high enough, above ~0.2 MeV, then 'pure' ionisation occurs,[25] reaction 1.3a.

$$C^+ + AB \rightarrow C^+ + AB^+ + e^- \qquad \textbf{(re 1.3a)}$$

This process is similar to both photon and electron ionisation. In fact, high-energy ion impact can be modelled using theories which are similar to the Bethe-Born theory which was described for electrons earlier.[26] In general, small charged species such as H^+ and He^+ are used. Use of high-energy ion beams forms the basis of proton therapy for treatment of cancers. At lower energies charge transfer takes place instead. A better description of the process would be electron transfer, as charge can also be transferred by other species, such as chloride or fluoride transfer, but for historical reasons charge transfer is the terminology used. Charge transfer is represented in reaction 1.3b.

$$C^+ + AB \rightarrow C + AB^+ \qquad \textbf{(re 1.3b)}$$

At very low, thermal collision energies the reaction energy is given by the difference between the recombination energy, RE, of the ion and the IE of the neutral. The recombination energy is the energy of adding an electron to a cation, it can be essentially viewed as the reverse of the IE of the appropriate neutral. Two extreme mechanisms have been postulated for the charge-transfer process. They are known as long-range and short-range charge transfer.[27]

In long-range charge transfer the cation (C^+) and the neutral (AB) approach under the influence of a charge induced-dipole interaction. At some critical internuclear distance (r_c) the reactant potential curve ($C^+ - AB$) and the product potential curve ($C - AB^+$) cross. At this point an electron is transferred from AB to C^+. The potential energy curves can be modelled assuming that the only interaction is due to the attraction between a charge and an induced dipole. This neglects interactions due to repulsion of the electron clouds of C^+ and AB at close range, but at the large internuclear separations considered here is reasonable. If the potential is expressed as the charge induced-dipole interaction then r_c is given by:

$$r_c = \left(\frac{q^2}{8\pi\varepsilon_0} \frac{(\alpha'(AB) - \alpha'(C))}{RE(C^+) - IE(AB)} \right)^{1/4} \qquad \textbf{(eq 1.4)}$$

where q is the ionic charge on the ion, ε_0 is the permittivity of free space and α' is the polarisability volume of the neutral. It should be noted that from this equation if RE = IE, *i.e.* at resonance, then r_c will be at infinity. Figure 1.6 shows how r_c changes as the energy difference [$RE(C^+)$ – IE(AB)] is varied. The potential energy curves were modelled assuming that the values of α' for AB and C are 12.0×10^{-30} and 2.5×10^{-30} m^{-3}, respectively. The energy differences are (a) 0 eV (resonance) (b) 0.5 eV (c) 1 eV (d) 5 eV (e) 10 eV. It is clear that as the energy difference increases r_c rapidly shifts to smaller internuclear separation. Therefore, for charge transfer to occur at large internuclear separation the difference between $RE(C^+)$ and

IE(AB) must be small. This appears a strict criterion. However, for most polyatomic species there are so many different electronic and rovibrational levels of AB^+ that some will be accessible at the RE of the reactant ion. For small species, especially diatomics, this resonance criterion is likely to be much stricter due to the large spacings of energy levels. Another criteria is that the orbital from which the electron is removed must be unshielded for efficient charge transfer.

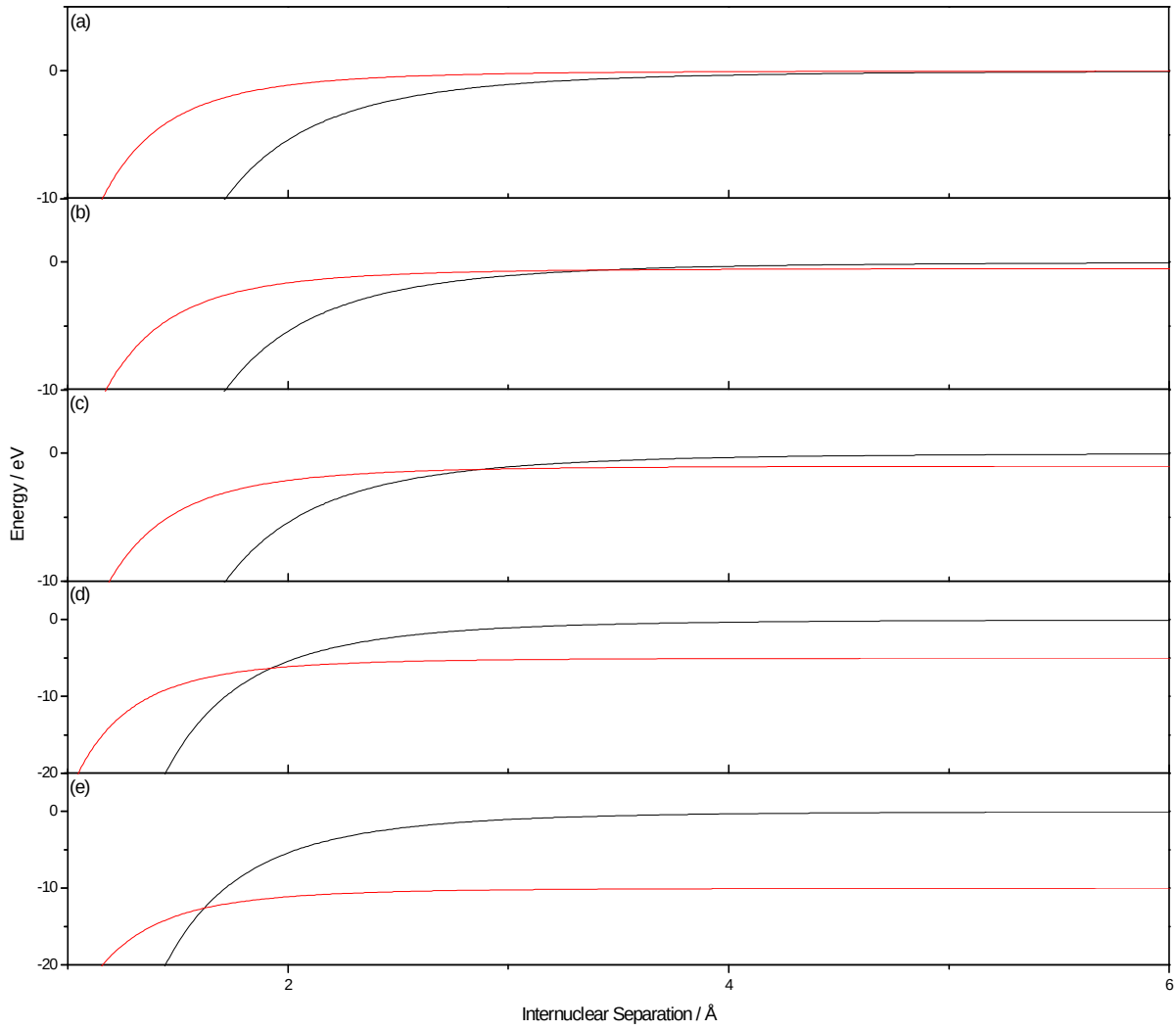

Figure 1.6: Potential energy surfaces for the interaction of C^+ and AB with an energy difference of (a) 0 eV (b) 0.5 eV (c) 1 eV (d) 5 eV (e) 10 eV. Note that as the energy difference is increased, the two potential energy curves cross at a smaller internuclear distance. The black curve is the reactant curve (C^+ – AB) the red the product curve (C – AB^+)

The Landau-Zener model for electron transfer has been successfully applied to various types of charge-transfer reactions in an adapted form as the window model.[28] This suggests that

for charge transfer to be favourable it should take place in a window of internuclear separations around 5 Å. At larger separation the probability of an electron transfer taking place is essentially zero, at smaller separation the probability of charge transfer is such that it will probably re-occur as the new ion and neutral separate, reforming the original reaction system. The Landau-Zener model is simplistic and was originally developed to model charge-transfer in atom-atom collisions.[29,30] The model neglects several details of the interactions and so suffers from incorrect energy dependence at high energies, and it does not take into account interference phenomena which lead to oscillations in scattering cross-sections.[31] However, it is useful for estimating reaction probabilities to within a factor of 2 or 3. This theory complements the long-range charge transfer theory as it estimates when long-range charge transfer will occur.

The long-range charge transfer mechanism takes place in the Born-Oppenheimer approximation, therefore the electron jump is assumed to take place so quickly that there is no change in the nuclear coordinates and the potential energy surfaces remain unchanged. This has been assumed to imply that the Franck-Condon principle can be used to indicate if long-range charge transfer is favourable. If the Franck-Condon principle is important, then it is assumed that for efficient charge-transfer to occur the Franck-Condon factors for both transitions $AB \rightarrow AB^+$ and $C^+ \rightarrow C$ must be reasonable. It also implies that if long-range charge transfer is taking place then the products are the same as for photon ionisation if the photon energy is the same as the RE of C^+. This means that the products, and their branching ratios if more than one product channel is formed, from reactions 1.7 and 1.8 will be the same:

$$C^+ + AB \rightarrow C + (AB^+)^* \rightarrow \text{Products} \qquad \textbf{(re 1.7)}$$

$$h\nu + AB \rightarrow e^- + (AB^+)^* \rightarrow \text{Products} \qquad \textbf{(re 1.8)}$$

Studies of the reactions of rare gas ions with diatomics and simple polyatomics have shown that Franck-Condon factors and energy resonances are indeed important.[32] However, studies of more complicated ion-molecule reactions have suggested that the Franck-Condon factors merely need to be non-zero for efficient ion-molecule reactions to take place.[27,33-36]

If long-range charge transfer is not favourable, then the ion and neutral will move closer together. If the C^+-AB and C-AB^+ potential energy curves cross, then ionisation can take place. If no curve crossing occurs then, especially if the ion and neutral are highly polarisable, a curve crossing can arise due to distortion of the potential energy surface. If ionisation occurs through these close-range curve crossings, the product ion will now be formed in the presence of a highly perturbing neutral, in contrast to long-range charge transfer where the product ion is formed well

separated from any perturbations. Now there is unlikely to be agreement in product yields from photon ionisation and ion-molecule reactions. It is noted that both charge-transfer mechanisms face the energetic constraint that RE(C^+) must be greater than or equal to IE(AB). It should also be noted that for both long-range and short-range charge transfer the parent ion is initially formed and then subsequently decays.

If neither of these mechanisms is favourable then the ion and neutral will get very close together and a chemical reaction may take place. There is now no energetic requirement that the RE(C^+) is greater than IE(AB). In a chemical reaction bonds are broken and formed, with ionisation occuring *via* these bond-forming and bond-breaking processes. The parent ion will not be formed in what we define as a chemical reaction. It is also expected that steric and orientation effects will be very important in such reactions.

It is assumed in all charge transfer experiments that, upon reaction, the entire RE is available to the products. However, this may not strictly be true. The RE depends on the Franck-Condon factors connecting the ion and neutral states. If there is a large change in geometry between the ion and neutral then it is unlikely that all the energy will be available due to a poor Franck-Condon factor for the (0,0) transition. For most ions even if the Franck-Condon factor is poor the amount of unreleased energy will be small. However, there are some extreme cases such as the reactions of Ne_2^+.[37] In this case the neutral Ne_2 dimer is unbound. This leads to very unfavourable Franck-Condon factors because the values of r_e are so different, and approximately 2 eV of energy is not available for ionisation but instead goes into the kinetic energy of the two Ne atoms.

In this thesis, we have discovered another example where the total expected RE is not available for ionisation; the reactions of N^+ with various neutral species.[33-36] Here the products formed from the reaction of N^+ produce far less fragmentation than would be expected from comparison with the reactions of ions with similar RE values. A possible explanation is that not all the RE, 14.53 eV, is available to ionise the neutral reactant. If some of the neutral N atoms which are formed as products from charge-transfer are formed in an excited electronic state, then a reduced amount of energy is available ionise the neutral. It is unclear why this happens in some of the reactions of N^+.

2.1.4 Ionisation by excited neutral species

Many neutral excited states can be very long lived as, although energetically unstable with respect to the ground state, transitions to lower states are forbidden. If the energy of these metastable species is higher than the ionisation energy of a neutral, then following collisions ionisation can occur. This process is known as Penning ionisation after the discoverer.[38] Electrons released in this process can be detected in the same ways as photoelectrons.[39,40]

To provide good energy resolution the metastables are generally excited rare gas atoms.[39] For example He ($1s^1 2s^1$) has an energy of either 19.818 or 20.614 eV depending on which spin state is formed. If a molecule is used instead of a rare gas atom then it is very difficult to populate only a single rovibronic level, leading to a lack of energy resolution. Metastable molecules are therefore rarely used in Penning studies.

The detected Penning ionisation spectra are equivalent to the photoelectron results, but with some small differences.[17] The measured energy of the electrons relates to molecular orbitals and the energy depends on the energy of the metastable and the IE of the orbitals. There is also another energy term which is the shift in IE between the photoelectron and Penning results. This term is generally small and represents interactions between the neutral target and the metastable probe.[41]

2.1.5 Electric field ionisation

When a very high electric field is applied to a molecule the Stark effect can become so high that the potential barrier binding an electron to a molecule drops below the energy of the electron's orbital. This leads to the formation of a molecular ion. In practice the high fields are produced by applying 10 to 20 kV between a cathode and a very fine needle point. Ions formed in this way tend to show little fragmentation when compared to electron or photon ionisation methods.[17]

Another type of ionisation induced by electric fields occurs with high power lasers. This is a special case compared to the field ionisation described above because the electric fields produced by an intense laser beam rapidly vary, leading to strong interactions between electron and field.[42] In many cases the electron can be forced to recombine with the ion at relativistic speeds by the rapidly varying fields. This is the basis for generation of ultra-short laser pulses.[43]

3. Decay processes of positive ions

In general, after ionisation has occurred the ion formed will have excess energy above its ground state. Subsequently this ion will decay. It is interesting to determine how ions decay, and how these decay channels vary depending on the ionising process used. In theory all ions should decay in the same manner if they are ionised with the same amounts of energy.[44] To start, we consider ionisation and decay of an isolated species.

3.1 Isolated ionisation

The best example of an ion formed in isolation is one created following photon ionisation. In this process the photon is absorbed to leave just a cation and departing electron. Once the energy has been deposited in the ion several relaxation processes can occur. In general, these processes will try to move the ion into a lower-energy state. This could occur by emission of a photon. This is termed fluorescence if the transition is between states with the same spin multiplicity, and is therefore an allowed transition. If the transition is between states with different spin multiplicity, *e.g.* triplet to singlet, it is a forbidden transition and the emitted radiation is termed phosphorescence.[45] The lifetime for emission of fluorescence is about 10^{-6} – 10^{-9} s. As phosphorescence is a forbidden process the emission lifetimes are much longer, from seconds to microseconds. Emission of radiation can be considered a non-statistical process. Fluorescence is very common for small molecules, but as the size of the molecules increases it becomes less likely to occur as it competes with other decay paths.

A statistical process corresponds to energy randomisation within the molecule. This can occur non-radiatively. If the transition is between states of the same spin multiplicity it is termed internal conversion, if the states have different spin multiplicities it called intersystem crossing. A final way the ion can relax is by dissociation. Here the excited AB^+ ion fragments, for example into A^+ and B. This process can be described as either impulsive or statistical, depending on the timescale of dissociation. If dissociation is faster than energy randomisation, normally assumed to be on the order of a vibrational period, it is an impulsive dissociation. If the timescale is slower than energy randomisation the process is statistical, and can be modelled using statistical models,[46] see chapter 3. How quickly dissociation occurs depends on the potential energy curve for fragmentation. Figure 1.7 shows some schematic potential energy curves for the generic

polyatomic cation, AB^+, along the A–B bond length. One assumption behind these curves is that, if either A or B is not an atom but a molecular group, then AB^+ can still be treated as a pseudo-diatomic. This assumes that there is zero coupling between the vibrational modes, and they are normal modes. In reality, if either A or B is molecular then any dissociation will take place on a potential energy surface which has as 3N-6 dimensions and these curves only represent cuts through this surface. Curve 1 is the ground state of the neutral AB molecule from which ionisation occurs. The red arrow marked *hv* indicates the transition caused by absorption of a photon. Curve 2 represents a situation where AB^+ is bound. There is a deep potential energy well which supports vibrational and rotational energy levels. In this situation only AB^+ will be detected until the incident excitation energy, from a photon or an electron *etc*., reaches an energy above the dissociation limit. At that energy A^+ fragments will be detected.

Curve 3 is a repulsive potential energy curve. Once this state is populated the nuclei A^+ and B start to move apart and the potential energy is converted into kinetic energy. In this situation A^+ may be detected at its thermochemical threshold but, depending on Franck-Condon factors, is more likely to be formed at an energy above the threshold. The dissociation is impulsive, so occurs rapidly with little redistribution of energy within the different modes of the molecule. This leads to a large proportion of the available energy being converted into kinetic energy of the fragments, and usually there is little vibrational excitation of the fragments. Curve 4 is a bound curve but this time there is a barrier in the exit channel. Due to this barrier the fragments will not be detected at the energy of the $A + B^+$ asymptote but $+\Delta E$ higher in energy. Such barriers can arise due to tight transition states. Finally, it should be noted in this diagram that curves 3 and 4 cross at the $v = 2$ level of curve 4. This can lead to predissociation if, after population of curve 4, there is a jump to curve 3. It is also possible to have curves whose situation is intermediate to curves 2 and 3. Here the curve is largely repulsive but may have a shallow minima in it.

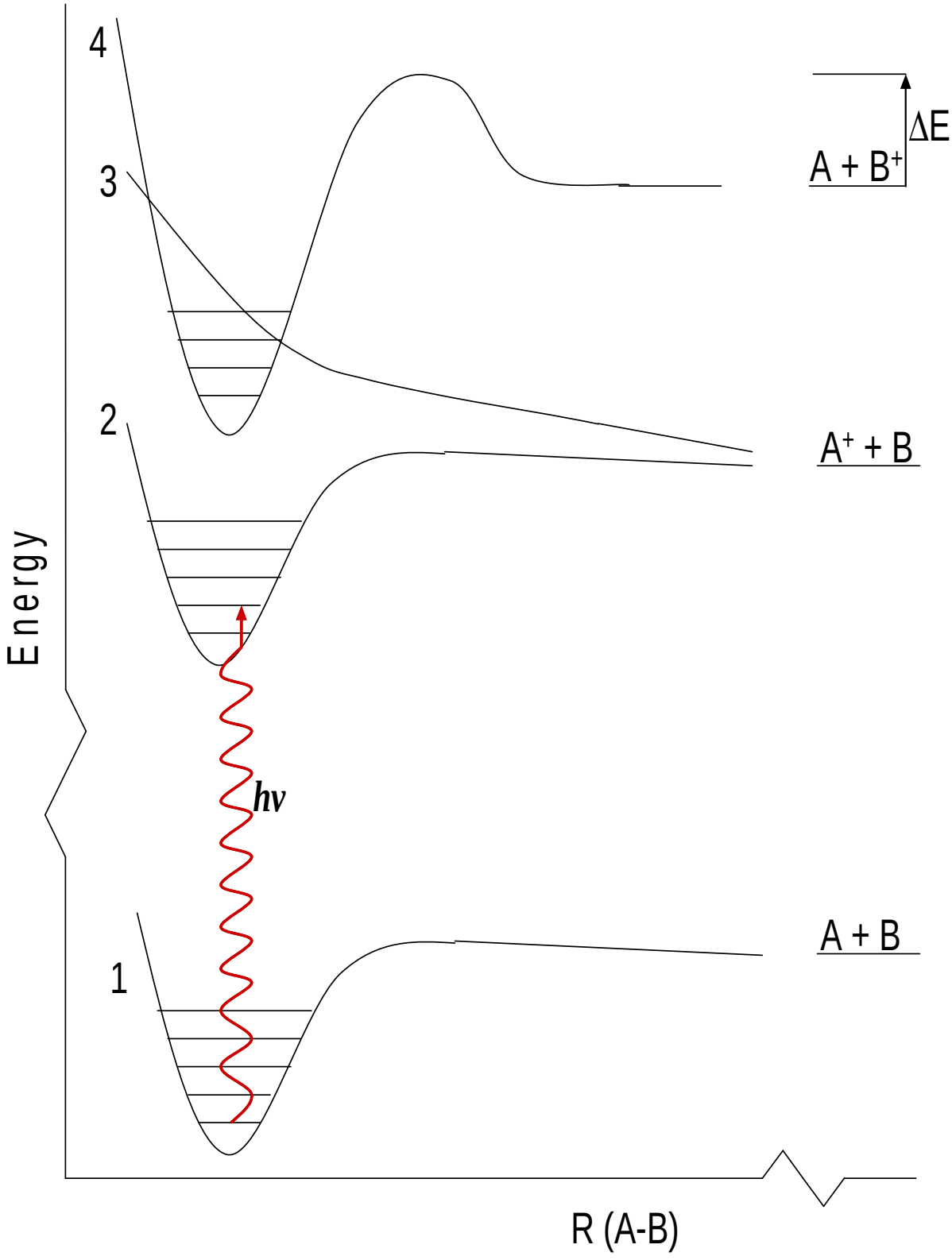

Figure 1.7: Examples of different types of potential energy curves for a molecule AB.

If dissociation is statistical it can be modelled using the Rice-Ramsperger-Kessel-Marcus (RRKM) or quantum equilibrium theories (QET).[46] Here all energy in the ion is assumed to be completely randomised into all vibrational modes of the electronic ground state of the ion. The most important assumption of these theories is that there exists a molecular structure which defines the barrier between the products and the reactant. This is the so-called transition state (TS). An example of a statistical dissociation process can be shown using curve 2. If we assume that AB^+ is polyatomic, *i.e.* A has more than one atom, then there will be several other vibrations than the A^+–B vibration shown. Energy will be randomised between all available modes. If there is enough energy present to place the molecule above the dissociation limit of curve 2 then we would expect to see A^+ and B formed. However, this dissociation will only take place when all the energy is in the A^+-B vibration. Therefore, although thermodynamically there is enough energy to dissociate AB^+ the daughter ion, A^+, will only be visible when the rate of unimolecular dissociation becomes measurable. This forms the basis of the kinetic shift, an idea first explicitly stated by Chupka in 1959.[47] The kinetic shift relates to the measurement of appearance energies of ionic fragments. If dissociation takes place on a timescale which is longer than the transit time of the ions through the detector then the dissociation will not be measured. The dissociation will only become measurable when there is enough excess energy above threshold for the rate of dissociation to increase to a measurable rate. This means that the measured appearance energy will be higher than the actual energy. The size of the kinetic shift depends on the size of the molecule but values are normally around 0.1 – 1.0 eV, the magnitude increasing as the size of the molecule increases. If the dissociation is impulsive then it is more difficult to model. It can only be modelled well using a full reactive scattering calculation, although some analytical solutions are available.

3.2 Perturbed ionisation

We now consider the situation where the ion, AB^+, is formed and decays while interacting with another species. This will be the situation for reactions 1.2-1.4 where the ionising species are electrons, cations or excited neutrals. In these reactions, after the ionisation event has occurred there will be another species in the vicinity of the ion, either an electron or neutral species. This may affect how the energetic ion relaxes. We will deal exclusively with reaction 1.3, ionisation by cations. Earlier it was explained that charge transfer can take place by two extreme mechanisms, either long-range or short-range. If long-range charge transfer takes place,

then the electron jump takes place at a large internuclear distance between C^+ and AB to form AB^+ and C. It is assumed in this model that AB^+ is essentially isolated from C. If this is true, then relaxation of AB^+ by dissociation, IVR *etc*., will be the same as when AB^+ is formed in an isolated situation. This implies that the process is the same as for photon ionisation. This is often found to be the case, and breakdown diagrams of product ions recorded as a function of energy for photoionisation and ion-molecule reactions agree within experimental error. However, we must appreciate that this is an inherent contradiction; AB^+ may fragment as if it is an isolated ion, but it is still part of a collision system with C since AB^+ and C are on an attractive potential energy curve due to the ion induced-dipole interaction. This means that while dissociation is occurring it is possible that some collisions will occur between AB^+ and C, so why does the fragmentation proceed as if it is unimolecular? It is possible that even though AB^+ and C are in a complex the interaction does not have a large effect on the TS. In this case it means that fragmentation should largely occur as if the ion was isolated. It is possible that minor changes in the rate of dissociation may occur due to the slight alterations of the TS. This could lead to a small difference between photoionisation and long-range charge transfer, in that the appearance energy of a fragment ion may be shifted slightly due to the change of vibrational frequencies and hence change the kinetic shift of the appearance energy. For short-range charge transfer the assumption of isolated ionisation is no longer valid, and there is a strong interaction between AB^+ and C. This interaction could easily lead to different fragmentation patterns when compared with photoionisation. If AB^+ and C come even closer, then the extent of interaction will increase and a chemical reaction may take place.

The three possible mechanisms should be considered as forming a spectrum of possible reactions depending on the extent of interaction between C^+ and AB. At the one extreme is long-range charge transfer where there is no interaction and the parent ion, AB^+, is formed and dissociates as if isolated. As the interaction is increased the short-range mechanism takes over. Here the parent ion is formed but the interaction between C^+ and AB^+ will affect fragmentation. At the other extreme is when the interaction is so strong that the parent ion is not formed at all, fragments are formed directly from reaction of C^+ and AB in a tight collision complex.

It is also possible that more than one mechanism could be operative in any ion-molecule reaction. Several studies were performed by Leone *et al* in a flowing afterglow apparatus where the vibrational distributions of products could be measured with LIF.[48,49] They studied the reactions of CO with both Ar^+ and N^+ and the vibrational state distribution of CO^+ was determined. It was found that the distribution is essentially the same as the Franck-Condon

distribution from photoionisation. However there was some non-Franck-Condon intensity in certain vibrational modes. The explanation for this was that there were several charge transfer reactions occurring in competition, leading to different CO^+ (v) distributions.

4. Experimental techniques

4.1 Photoionisation

In this section some of the experimental techniques used to measure photoionisation processes will be reviewed. One of the simplest techniques to measure photoionisation is to detect the photoelectron produced as the negative counterpart to the cation.

4.1.1 Photoelectron spectroscopy

Upon ionisation the electron is released with a kinetic energy which is equal to the difference between the photon energy and the IE of the removed electron. In the most common, and in many ways simplest, version of photoelectron spectroscopy a fixed-energy light source is used to ionise the species under study. The kinetic energy of the released electrons is then analysed by an electron detector. The different kinetic energies of the electron represent the photoelectron spectrum (PES). There are several different monochromatic light sources used, the main types being rare-gas discharge lamps. Many designs have been developed and are detailed in several monographs, for examples see the books of Eland and Samson.[14,50] The general design involves some form of electrical discharge through the rare gas which produces light due to transitions between electronic states. The most common gas used in these discharges is He, and more specifically the He(I) line at 21.22 eV (584.3 Å).[14] This line is energetic enough to ionise most valence electrons, and to ionise the ground state of all gas-phase molecules. It is also highly monochromatic, other transitions in He having much weaker intensity, and is very intense. Other rare gases can also be used in the same design of discharge lamp, and often Ne is used as an alternative to He. Now the Ne(I) line at 16.67 eV is used, but unfortunately due to spin-orbit effects there is a second Ne(I) line at 16.85 eV which causes complications in the measured PES. A final line source of interest is the He(II) line at 40.81 eV. A photon of this energy not only allows access to the complete valence shell of all molecules, but also many double ionisation processes can be excited.

Several designs of electron energy analyser have been developed. The first are retarding-energy analysers.[17] In these only electrons with a kinetic energy higher than a retarding voltage can reach the detector. As this retarding voltage is successively reduced, steps are produced for each group of electrons of a discrete kinetic energy. A major problem with these detectors is the difficulty of examining low-energy electrons. A different type of analyser is a deflection analyser.[14] In these analysers electric or magnetic fields are used to make electrons of different energies follow different trajectories, and hence separate them in space. Figure 1.8 shows a schematic of a simple parallel plate deflection analyser. Only electrons of the correct energy will have a path which leads from the entrance to the exit slit. By varying the pass voltage (–V in Figure 1.8) electrons of different energies will have the correct path. This type of analyser produces distinct peaks for each discrete set of electrons energies. The spectra are the differential of the step spectra obtained using a retarding field analyser.

One of the best deflection-type analysers is the 180° hemispherical analyser. This is very commonly used in high resolution He(I) spectrometers.[51] It provides first-order double focusing and its characteristics match the He(I) lamps used very well. Difficulties with deflection-type analysers are the distortions of electric fields at the slits as they do not lie in an equipotential plane. These distortions can be corrected using lens systems or fringing field correctors, but can still cause difficulties.

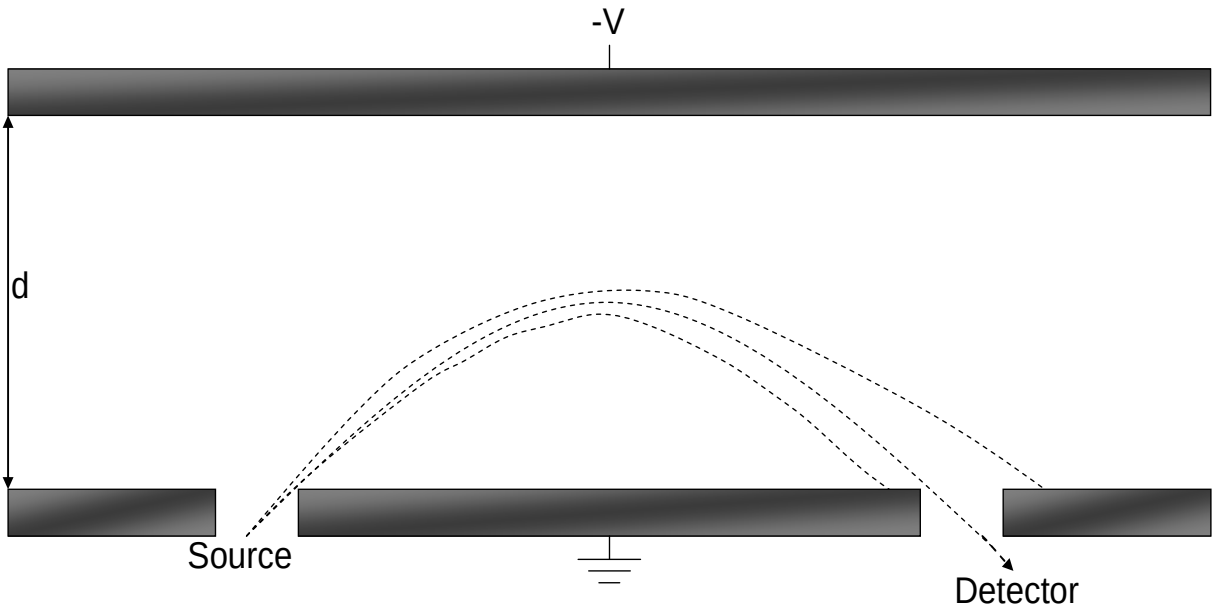

Figure 1.8: Schematic of a parallel plate electrostatic analyser. Dashed lines represent electron trajectories within the analyser.

A variation on these fixed photon energy photoelectron studies is to use a continuum light source and scan the photon energy. The most common continuum source is a Synchrotron, a type of particle accelerator. Here electrons, or sometimes other charged particles, move around a large evacuated ring. As the bunches of electrons go around corners they are accelerated, this leads to the emission of electromagnetic radiation. This radiation is emitted as a smooth continuum of almost 100 % plane-polarised light. The energy range covered depends on the energy of the electrons (on the order of 1 GeV) but is normally ~ 5 – 1000 eV.[14] Laboratory-based sources have been developed, such as the hydrogen many-lines source or the Hopfield Helium continuum.[50] Unfortunately these sources tend to be very weak and only cover small energy ranges. If a continuum source is used, a monochromator must also be used to select the required wavelength of light.

Using a tuneable photon source leads to two ways to detect the electrons. They can be detected at a fixed energy as the photon energy is scanned, or the kinetic energy of every electron can be analysed as for a normal PES. This second method, constant ion state spectroscopy, gives a PES for each photon energy and can be used to follow how the cross-section for ionisation from each photoelectron varies with photon energy.[52] This can give valuable insight into the nature of the orbital from which the electron is removed. For example if the orbital has one radial nodal (*e.g.* 2s, 3p, 4d…) then there is usually a deep minima in the cross-section due to interference between partial waves from the inner and outer parts of the orbital. They are known as Cooper minima, and if they arise it indicates that the ionising orbital must have a radial node.[53]

For the first method, where the electron energy is held constant, the electron energy can be fixed at any energy. There are some advantages to the use of a non-zero value, but in general zero kinetic energy (threshold) electrons are chosen to be detected.[54] These threshold electrons can be detected with high efficiency using electric fields. Many different threshold detectors have been developed, such as the penetrating field and steradiancy detectors.[55] The aim of all these threshold analysers is to detect only low-energy electrons. This has led to several techniques to remove the contribution from high-energy electrons which only have a velocity component along the detector axis. The presence of these electrons leads to the so-called ‘hot-electron tail’ in threshold photoelectron spectra. One recent technique of Sztáray and Baer uses velocity-focussing optics and specially positioned detectors to remove this contribution from hot electrons.[56] By using concentric multichannel electron multiplers subtraction of the signal from

the outer ring (only hot electrons) from that of the inner ring (hot and threshold electrons) removes the hot-electron tail.

One major difference between threshold and He(I) PES is that autoionisation is generally absent in He(I) PES unless there is an energy coincidence, whereas in the threshold photoelectron spectra (TPES) they are fairly ubiquitous. The effect of autoionising resonances on the TPES depends on which type it is: rotational, vibrational, or electronic. If electronic autoionisation occurs, then an electron with high kinetic energy is released. This electron will not be detected by a threshold analyser, so the TPES should not be affected. If vibrational or rotational autoionisation takes place then a low-energy electron will be produced. This electron will be detected in the threshold analyser. Vibrational autoionisation can lead to distortion of the structure of the photoelectron bands due to non-Frank-Condon transitions leading to excitation of different vibrational progressions in the bands.[57]

4.1.2 Photoion spectroscopy

Another technique to study photoionisation is to detect the positive ions formed after interaction with a photon, known as photoion spectroscopy (PIS).[17] It can also be used to detect negative ions formed in the ion-pair process.[58] The ions are in general detected mass-selectively to give partial photoionisation cross-sections for each ion. From this it can be deduced which fragments are formed at any photon energy. In this arrangement it is possible to determine the appearance energies at 298 K (AE_{298}) for any fragment ions formed. The measured signal is from a non-resonant process, and so the cross-section into each ion channel is a step function. Each step on the cross-section represents a new onset of ionisation to produce the detected ion. Autoionisation will also have an effect on this cross-section. As autoionisation is a resonant phenomenon it only occurs for certain energies. It will therefore show up as peaks superimposed on the step functions. Both vibrational and electronic autoionisation will show up as peaks, and therefore comparison to the TPES can indicate what mechanism of autoionisation is taking place as electronic autoionisation will be absent from the TPES.[57]

4.1.3 Photoelectron photoion coincidence spectroscopy

A problem with normal photoelectron and photoionisation spectra is that it is not clear whether the electron and ion come from the same molecule, *i.e.* do they correlate with each

other? A very powerful method to study photoionisation is to combine detection of the photoelectron with a photoion. If the measurement is done in coincidence then what is obtained is the energy-selected ion yield into product ions as a function of photon energy. This technique has been performed with the energy of the photoelectron fixed at non-zero values, so called photoelectron-photoion coincidence (PEPICO) spectroscopy,[54,59] or as the threshold photoelectron variant (TPEPICO).[60,61] A large body of PEPICO work has been performed by Eland and co-workers, recently this has been extended to study double ionisation events with coincidence detection.[62,63] We will concentrate on TPEPICO as it is this type of experiment which we perform. A non-pulsed TPEPICO experiment with time of flight mass detection is a good match to the high intensity pseudo-continuous light which is produced by a Synchrotron. It is important in all coincidence experiments to reduce the number of false coincidences and maximise the number of true coincidences. False coincidences are caused by the detection of an ion which was not formed in the same event which created the photoelectron. It can be shown that the signal-to-noise ratio (*s/n*) of a non-pulsed TPEPICO measurement is given by:[64]

$$s/n = \frac{ag}{m}\left(\frac{Nf_1 f_2 T}{\frac{ag}{m} + N\tau}\right)^{1/2} \qquad \textbf{(eq 1.6)}$$

N is the number of ionisation events per second, f_1 and f_2 are the collection efficiencies of ions and electrons, *g* is the fraction of events of the required type, *a* is an overlap factor in space, *m* is the number of channels of a time-to-digital-converter over which the signal is spread, τ is the time the coincidence gate is open for and *T* is the measurement time. The *s/n* ratio is not quite the same as the ratio of true to false coincidences but is a useful measure. Equation 1.6 shows that, to maximise the *s/n* ratio, the spatial overlap, collection efficiency and fraction of events of the type to be studied must all be maximised. *a* can be maximised by careful alignment of the two detectors with the light source and beam of gas, while *g* depends on the aims of the experiment. The most important effect is to maximise the collection efficiency of the detectors, so that when there is an ionisation event it will be detected.[65] However, maximising the efficiencies causes other difficulties. If only a TPES or PIS experiment is being performed then it is very easy to tune the electron or ion optics to give very high collection efficiencies. The voltages that give a high ion collection efficiency, however, will give a very poor electron efficiency, and *vice-versa*. The important efficiency is the total collection efficiency, F_T, which is the product of f_1 and f_2. This means the best F_T value is usually obtained by having a reasonable, but not over-high, collection

efficiency for both electrons and ions. Simplistically, it also appears that by increasing N by increasing the sample pressure or flux of light, good spectra will be obtained, however, this is not the case. Although the rate of true coincidences goes up with N the rate of false coincidences goes up as well but is now proportional to N^2. In terms of *s/n* ratio, this means that the best *s/n* is obtained when $N \rightarrow 0$. This cannot be realised in any real experiment, but does show that the best statistics are obtained at low event rates. For pulsed TPEPICO experiments it is much harder to deal with false coincidences because the true and false coincidences are now correlated in time.

4.1.4 ZEKE and MATI photoionisation

An extension of detecting threshold electrons is zero electron kinetic energy (ZEKE) spectroscopy and the photoion analogue, mass analysed threshold ionisation (MATI).[66] In these methods a species is excited to a very high-lying Rydberg state. Application of a specific sequence of voltage pulses remove any electrons or photoions produced by direct ionisation. After a short time delay another sequence of voltage pulses then extracts the photoelectron which resides in the Rydberg state by field ionisation. This technique can produce a resolution which is limited by the electric fields and the excitation source, not by the kinetic energy of the photoelectron. In general, lasers are used as the excitation source due their high resolution and pulsed nature, which allows synchronisation with the pulsed electric fields.

4.2 Ion-molecule reactions

Several techniques are available to study ion-molecule reactions, generally labelled C^+ + AB. A brief overview will be given here.

4.2.1 Flowing afterglow

The flowing afterglow (FA) was developed in the early 1960s at Boulder, Colorado, USA by Ferguson.[67] Conceptually, the FA is a very simple experiment. Buffer gas, usually He, flows through a tube at pressures of between 0.2 and 1 Torr, and is evacuated by a large roots pump. This allows very high flow rates to be achieved inside the flow tube. A microwave or d.c. discharge is induced in the buffer gas to produce a plasma. At a point downstream from this discharge, a source gas is added to prepare the reagent ions. A reactant gas can then be leaked in

and the reactions between this and the reagent ion studied. Ions are detected at the far end of the flow tube by a quadrupole mass spectrometer. Standard analysis is to monitor the disappearance of the reagent ion (C^+) as a function of neutral (AB) flow rate, leading to the rate coefficient for the reaction. Product ions can also be detected and branching ratios determined. Modern versions of this instrument contain more advanced detection techniques to the fixed mass spectrometer.[68] One apparatus has a moveable mass spectrometer to change the reaction time. Also commonly used are Langmuir probes and laser induced fluorescence (LIF) detection of neutral products. Langmuir probes are special electrodes which can measure the number density and temperature of charged species. They have found great use in monitoring electrons, allowing the study of electron attachment and dissociative recombination reactions.[69] The greatest disadvantage of the FA is that the reagent ions are generated inside the flow tube. The generation of these ions is rarely clean, and often several different ions will be present as reagents. This can lead to very complex kinetics, and in some cases makes it impossible to determine product channels.

4.2.2 Selected ion flow tube

A solution to the problems of the FA was developed as the Selected Ion Flow Tube (SIFT) at the University of Birmingham in the 1970s.[70] In this apparatus the ion source is separated from the flow tube by a quadrupole mass filter. In ideal conditions only a single reagent ion will enter the flow tube. This greatly simplifies the reaction kinetics, and it is much simpler to determine branching ratios than on the FA. The SIFT has shown great versatility with versions capable of being heated to ~900 K or cooled to liquid N_2 temperatures.[71] Other adaptations have included drift tubes inserted into the flow tube, allowing studies of the reactions with different energy distributions. Several different ion sources have also been adapted to the SIFT. These include flowing afterglow, cluster and electrospray sources.[68] A recent development by Böhme attached an inductively-coupled plasma torch to the SIFT.[72] This allows atomic ions to be formed from anywhere in the periodic table. However, there are some disadvantages in using a SIFT rather than a FA. The reactions of electrons with neutrals, *i.e.* electron attachment, or with ions, *i.e.* dissociative electron recombination, cannot be studied in the SIFT as no electrons enter the flow tube from the source. Another disadvantage is that the densities of ions, and hence products are lower in the SIFT, and this means that LIF detection of products is no longer feasible.

4.2.3 Other high-pressure techniques

Another very important high pressure apparatus is the CRESU which stands for Cinetique de Reactions en Ecoulement Supersonique Uniforme (Kinetics of Reactions in Uniform Supersonic Flow). It is based on wind tunnel techniques which are used to measure aerodynamics at low pressure and supersonic speeds.[73,74] The technique is to expand the reactant ion, or neutral, in a buffer gas isentropically through a Laval nozzle. This creates a supersonic isentropic flow, which has been described as a reaction vessel without walls. By altering the divergence of the Laval nozzle different flow temperatures can be achieved,[75] and normally the CRESU is operated at temperatures of astrochemical importance, down to ~10 K. Reaction rate coefficients are measured in a similar way to the SIFT, by following the decrease in reactant ion as a function of the neutral reagent. An improvement to the CRESU was to include a quadrupole mass filter to allow mass selection of the reagent ion, this is the CRESUS (Kinetics of Reactions in Uniform Supersonic Flow with Selection).[73] One major disadvantage of the CRESU technique is the huge gas flows involved, about 50 standard cubic centimetres per second (sccm), which requires massive pumping requirements.[75]

A very recent variation of flow tube techniques is the turbulent ion flow tube, TIFT.[76] This apparatus allows studies of ion-molecule reactions at very high pressures (up to 700 Torr). The main difference is that with the pressures and flow rates used, the flow is turbulent rather than laminar. Rate coefficients are measured in the normal way. A final high-pressure technique is the ion mobility spectrometer. In this apparatus the ions move along a drift-tube under the influence of an electric field at atmospheric pressures. By varying the electric field rate coefficients can be measured as a function of collision energy.[77]

4.2.4 Ion cyclotron resonance

Another technique to measure rate coefficient and products of ion-molecule reactions is the ion cyclotron resonance (ICR) instrument, often referred to as a Fourier transform mass spectrometer (FTMS) in more modern versions. In contrast to the other techniques reported above, it operates at very low pressure, around 10^{-7} mbar. In an FTMS a small chamber has a large magnetic field (~5 T) from a superconducting magnet applied across it. Any ions in this

chamber will be constrained in a circular orbit due to the magnetic field, called the cyclotron orbit, with a frequency given by:

$$\omega_c = \frac{v}{r} = \frac{zeB}{mc} \qquad \textbf{(eq 1.7)}$$

ω_c is the cyclotron frequency, v is the velocity of the ion, r is the orbital radius, z the ionic charge, e is the charge of an electron, B is the magnetic field strength, m is the mass of the ion and c is the speed of light.[78] A radio frequency voltage is applied perpendicular to the magnetic field. If the frequency matches that of the ion it is excited into larger orbits. As the radio frequency voltage is scanned a mass spectrum is obtained. In modern versions a specially shaped radio frequency voltage pulse is applied that excites all ions at once, the so called SWIFT pulse.[79] The resulting ion current is then Fourier transformed to give a frequency spectrum. The resolution of a FTMS is much greater than other mass spectrometers, and they are very powerful tools.[17] Ion-molecule reactions can be studied by leaking a small amount of neutral gas into the ICR chamber.[80] Mass spectra are then obtained as a function of time, or as a function of neutral concentration. To simplify reaction schemes, special excitation pulses can be applied that remove all ions but the one of interest before the reaction begins. It is also possible to measure ion-molecule reactions from broadening of the lines in the mass spectrum. Although rate coefficients can be measured in an FTMS, it should be noted that there are several issues with obtaining *absolute* values. Firstly, from the equations of cyclotron motion, only the ratio of v to r is defined by ω_c, and they can therefore take any combination of values. This means that the translational energy of ions inside the trap after excitation by the RF pulse is undefined and possibly non-thermal. This will lead to deviations from the true, thermal rate coefficients measured, for example, by the flowing afterglow experiment. However, it has been pointed out that, if enough non-reactive collisions take place, there should be a thermal distribution of velocities.[81] Also, if ion storage times are long enough, then thermalisation will occur due to blackbody radiation from the trap itself.[82] Another difficulty in measuring absolute rate coefficients is measuring the pressure in the ICR cell. The pressure gauge is usually a long distance from the cell and so there will be on offset due to this.[80] Also at the low pressures in an FTMS pressures are measured on an ion gauge and calibration becomes difficult.[83] Due to these limitations it is common to record *relative* rate coefficients, for example by including Ar in the reaction mixture.[84]

5. Electron attachment

5.1 Theories

There are several ways in which negative ions can be formed, for example from ion-pair production after photoionisation or electrosprayed into vacuum from a solution. In this thesis only formation of negative ions following attachment of electrons by neutral species will be considered.

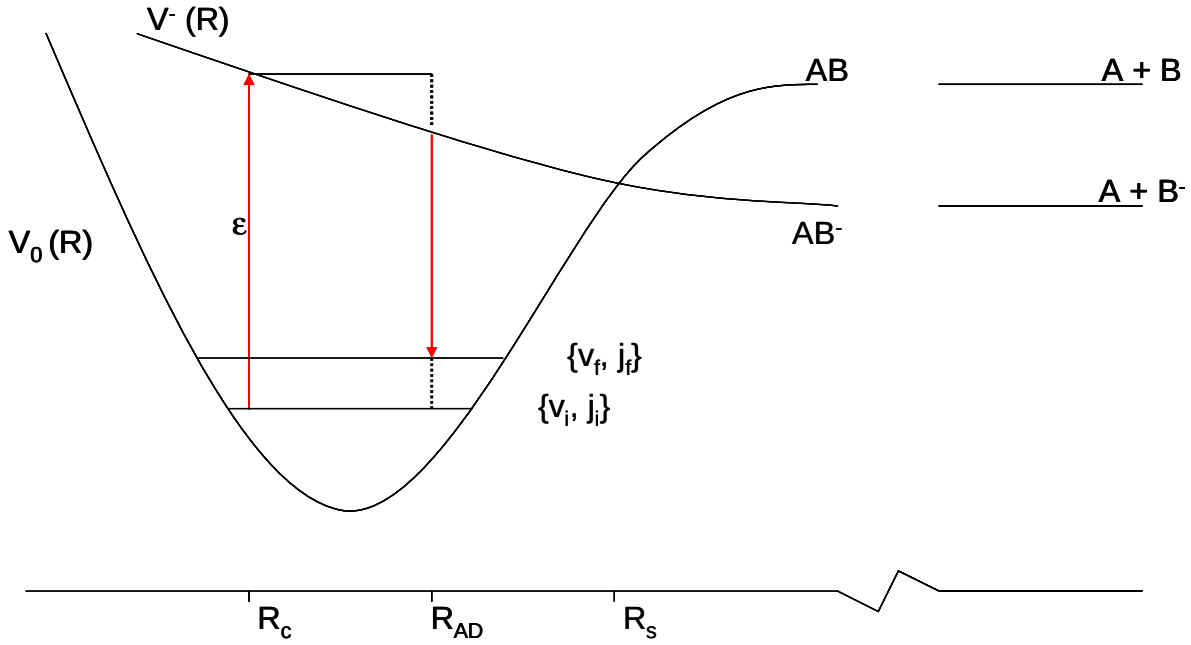

Figure 1.9: Potential energy curves for dissociative electron attachment to AB, adapted from ref 85.

In general, if electron attachment occurs it must do so *via* a dissociative pathway. It is normal to describe the dissociative attachment (DA) process in the resonance model.[17,85] In this model DA proceeds through a temporary negative ion (TNI) state. Figure 1.9 shows potential energy curves for the attachment of an electron to a molecule AB. Firstly, an electron of energy ε is captured by the nuclei in a particular rovibrational level, indicated as v_i and j_i on the potential curve $V_0(R)$. The capture populates the anion potential curve $V^-(R)$. R_c is the most probable point of capture. In this picture $V^-(R)$ is repulsive, though it is possible for there to be a shallow bound region. If $V^-(R)$ is repulsive then the nuclei A and B begin to separate so that their potential energy is converted into kinetic energy. The electron can autodetach at any point and return to the continuum. If, for example, it autodetaches at R_{AD} then the molecule will be left excited in v_f and

j_f. The autodetachment rate depends on the resonance lifetime. If the state is sufficiently long lived, the nuclei may separate past R_s where autodetachment is no longer possible. Past this point DA will occur. The DA cross-section was given by O'Malley as:[86]

$$\sigma_{DA} = \frac{\pi^2}{\varepsilon}\Gamma\left|F_C\right|^2 s \qquad \textbf{(eq 1.8)}$$

where $|F_C|^2$ is the Franck-Condon factor between the initial and anion state, Γ is the width of the resonance and s is the survival factor of the resonance. The survival factor is given by the ratio of the time it takes the products to dissociate past R_s and the autodetachment lifetime. If the curve $V^-(R)$ is not repulsive then DA cannot take place. If the lifetime of the TNI is long enough, it may be possible to detect the parent anion in a mass spectrometer.

This is the most general mechanism and is a single-electron excitation. However, there are situations were attachment of an electron is accompanied by excitation of another electron in the molecule: a two-electron process. If the energy of this resonance is above the energy of the excited electronic state of the molecule, the electron can decay by autodetachment to this excited state. This is known as a core-excited resonance. If the excited state of the molecule is below the resonance energy, then decay to this neutral excited state is forbidden to occur by a one-electron detachment process. The decay into the neutral ground state requires rearrangement of the electronic configuration, and this can lead to long anion lifetimes. This is known as an electronic Feshbach resonance. If the electron couples to a molecular vibration then transfer of electronic energy to vibrational energy can take place. This can prevent autodetachment taking place. Previously these have been known as nuclear-excited Feshbach resonances, but the preferred name now is vibrational Feshbach resonances. As vibrational Feshbach resonances couple electronic and nuclear degrees of freedom, the Born-Oppenheimer picture developed in Figure 1.9 is no longer applicable. A final type of resonance is a shape resonance. These resonances only occur for electrons with non-zero angular momentum. These resonances are due to a potential well which arises from the interaction of the attractive polarisation between the electron and the neutral and the repulsive centrifugal barrier due to conservation of angular momentum.[17]

It should be noted that, for the majority of resonances, if subsequently a collision occurs between the TNI and another neutral molecule, energy can be transferred which will stabilise the anion. This leads to one of the major differences between electron attachment studied at high and low pressure. At low pressure there will be no collisional stabilisation, while there will be many such collisions in a high pressure environment. This can lead to an increase in the measured yield

of parent ions and measured rate coefficients or cross-sections in high-pressure experiments compared to low-pressure experiments.

5.2 Experiments

Many different types of experiments have been performed to study electron attachment, thoroughly reviewed by Chutjian and Hotop *et al*.[85,87] They can be classed into two broad areas of study. The first uses a beam of monoenergetic electrons and work under very low, single-collision pressure conditions.[88] The second type is performed at high, generally atmospheric, pressures and the electrons are in a swarm.[89] The term swarm means that the electrons are present in a distribution of energies. The electron-energy distribution depends on the electric field applied, the number density of neutral molecules and the type of buffer gas used. Attempts to calculate this distribution have been performed by Druyvestan assuming that the electrons only undergo elastic collisions with the buffer gas.[90] Major errors with this approach are that it ignores the contribution of inelastic processes, and it is independent of type of buffer gas. This last point is remedied by including the momentum transfer cross-section of the buffer gases. Other methods to calculate the energy function have been based on the Boltzmann transport equation.[91]

For the first type of experiment, which will be referred to as beam experiments, a method of production to generate a beam of electrons with a well-defined and with very low energy is needed. Several different electron sources have been used,[85] the most common types being electrostatic or trochoidal monochromators. The trochoidal monochromator uses a combination of electric and magnetic fields to energy-select electrons.[17,92] These sources easily allow electrons with energies down to ~ 0.5 eV to be produced with a reasonable resolution. However, below this energy results can be unreliable.

One method developed to overcome these problems is to collide high-*n* Rydberg atoms (where *n* is the principal quantum number) with a neutral molecule under study.[93] The main assumptions in this method are that when the electron is removed from a very high-lying Rydberg orbital, it behaves essentially as a free electron of the same energy.[85] This method can give resolutions down to 0.05 meV. The major limit of this technique is poor knowledge of the collision complex between the Rydberg atom and the neutral and what the precise energy of the Rydberg electron is. A second method has been used extensively by Chutjian and Alajajian,[94] in which the electron is produced by photoionisation of Kr by a Hopfield lamp close to threshold. This has been extended by Hotop *et al*.[95,96] who performed the ionisation using a two-laser

excitation process. Careful tuning of the laser energy allows formation of either high *n*-Rydberg atoms or free electrons. This laser photoionisation attachment technique has an energy width which is now limited by the Doppler effect and by any stray fields, and it has been used to measure EA cross sections at electron energies as low as 20 μeV with 20 μeV resolution.[96]

The swarm experiments have been performed for many years, an especially large body of work in this area being due to Christophorou and co-workers. The most common type of swarm apparatus is based on that developed by him.[97] This consists of two parallel plates inside a large vacuum chamber with a high voltage between them. This chamber can either be heated or cooled. The chamber is filled with buffer gas and a certain amount of sample gas. Some excitation source is then used to form free electrons near one of the plates; the electrons rapidly reach equilibrium in the buffer gas. The electron current is then measured at the positively biased plate. This process is repeated with different concentrations of sample gas to extract the electron attachment coefficient. A main difficulty with this equipment is that the chamber must be emptied and refilled for each measurement at different concentrations. Also attachment products cannot be detected. Several different types of exciting source have been used, including laser pulses and radioactive sources. Another type of swarm apparatus which has found wide spread use is the electron capture detector developed by Lovelock.[98]

A variation on the static swarm apparatus is the flowing swarm.[99-101] These devices are based on negative ion mobility mass spectrometers.[102] They consist of a drift tube through which the ions and electrons move under the influence of an electric field. Inside this drift tube is some form of gate system which allows the swarm of electrons to be pulsed. By measuring the change in pulse height as an attaching gas is injected into the drift tube, the electron attachment coefficient can be measured. By interfacing the drift tube with a mass spectrometer, for example a quadrupole, attachment products can also be measured.

6. Thermochemistry

6.1 Affinity values

In general, the affinity of a species A for species X is given by reaction 1.9

$$A + X \rightarrow AX \qquad \textbf{(re 1.9)}$$

The affinity is then the negative of the enthalpy of this reaction. That is, an exothermic reaction has a positive affinity, an endothermic reaction a negative affinity. From this definition it follows that if the reaction 1.10 occurs, then the affinity of B for X is greater than the affinity of A for X.

$$AX + B \rightarrow BX + A \qquad \textbf{(re 1.10)}$$

Perhaps the most well-known affinity is the electron affinity which describes the reaction:

$$A + e^- \rightarrow A^- \qquad \textbf{(re 1.11)}$$

If the value of the electron affinity is positive, then addition of an electron is an exothermic reaction.[103] In this thesis values have been estimated for proton affinities (PA) and fluoride ion affinities (FIA) for several chemical species. Reaction 1.12 shows the generic reaction for PA, reaction 1.13 for FIA:

$$A + H^+ \rightarrow HA^+ \qquad \textbf{(re 1.12)}$$

$$A + F^- \rightarrow FA^- \qquad \textbf{(re 1.13)}$$

For PA the proton source is normally H_3O^+. If the following reaction occurs:

$$H_3O^+ + A \rightarrow HA^+ + H_2O \qquad \textbf{(re 1.14)}$$

then the PA[A] is greater than or equal to the PA[H_2O]. The value for the PA[H_2O] is well known, 691.0 kJ mol^{-1}.[104] For two species studied in this thesis, reactions were also performed with NH_4^+ and the PA of NH_3 is 853.6 kJ mol^{-1}.[104] If protonation reactions occur with H_3O^+ but not with NH_4^+, then this brackets the PA of the neutral under study as greater than PA[H_2O] but less than PA[NH_3]. This method has been used successfully by many workers to estimate the PA of chemicals in the gas phase.[105]

Less well known than proton affinity is fluoride ion affinity, though there is still a reasonable body of literature published on the subject.[106,107] In our studies of ion-molecule reactions several fluorinated ions and fluorinated neutral reactants have been used. If any F^- anions are transferred in these reactions then a limit can be placed on the FIA of some of the species. It is easy to calculate the FIA of the reactant cations used in the SIFT as these are founded on well-known thermochemistry. Table 1.1 lists the FIA for these reagent ions. These values were calculated from standard thermochemical values and agree with other determinations of FIAs.[106]

Table 1.1: Calculated fluoride ion affinities for a range of fluorinated ions.

Ion	Fluoride Ion Affinity / kJ mol^{-1}
CF_2^+	1139
CF_3^+	1090
CF^+	1067
SF_4^+	1056
SF^+	1045
SF_5^+	1001
SF_2^+	886
SF_3^+	881

Table 1.1 shows that the reactant ion with the greatest FIA is CF_2^+, the ion with the smallest is SF_3^+. An example of the measurement of a FIA is given for the reactions of *c*-C_5F_8 in chapter 6. Reaction 1.15 shows one of these reactions, reaction 1.16 indicates the relation between each species and the generic affinity reaction, reaction 1.10.

$$C_5F_8 + CF_3^+ \rightarrow C_5F_7^+ + CF_4 \qquad \textbf{(re 1.15)}$$

$$AX + B \rightarrow A + BX \qquad \textbf{(re 1.16)}$$

c-C_5F_8 reacts with CF^+, CF_3^+ and CF_2^+ to produce $C_5F_7^+$. There is no reaction with SF_3^+, SF_2^+ or SF_5^+, and only a very slow reaction with SF^+ to form $C_5F_7^+$. These results show that the FIA of $C_5F_7^+$ is greater than SF_5^+ but less than SF^+, *i.e.* $1001 \leq FIA[C_5F_7^+] \leq 1045$ kJ mol^{-1}. Using the calculated enthalpy of formation of *c*-C_5F_8 of −1495 kJ mol^{-1}, see chapters 3 and 6, and reaction 1.17, we can set bounds on the enthalpy of formation of $C_5F_7^+$.

$$C_5F_7^+ + F^- \rightarrow C_5F_8 \qquad \textbf{(re 1.17)}$$

This gives the following inequality for the enthalpy of formation of $C_5F_7^+$:

$$-245 \leq \Delta_f H^o_{298}[C_5F_7^+] \leq -201 \text{ kJ mol}^{-1}.$$

7. Aims

As mentioned earlier one of the main aims of this work is to attempt to understand how charge transfer occurs in ion-molecule reactions. Along side this aim are several other aims. Perhaps the most important is related to the work on the six chloroethene molecules (chapters 7 – 9). Both the photoionisation of these molecules and their reactions with a range of different ions have been studied. These studies have given insight into fundamental ionisation processes and the affect of replacing hydrogen atoms with chlorine atoms. Perhaps most interesting is reactions of the three dichloroethenes, molecules which are related to each other as different isomers. Here differences in reaction rate coefficients and products highlight the importance of steric effects.

Another aim of the work has been towards the application of the recorded data. The perfluorocarbon molecules studied in chapters 4 – 6 and 10 are all, or have the potential to be, major industrial gases, especially in technological plasmas. The properties of these plasmas depend on how its constituent chemical species behave upon ionisation. The work in this thesis will help understand how the plasmas will evolve with time. The photoionisation results give some indication of what neutrals and radicals will be produced, while the ion-molecule reactions show how their concentrations will vary. The electron attachment data (chapter 10) is also important in understanding plasmas where high concentrations of electrons are present. The electron attachment studies can also be used to put the relative electron attachment cross-sections measured in beam studies onto an absolute scale. To do this it was necessary to upgrade the existing electron attachment apparatus to improve data acquisitions.

8. References

1 A.R. Ravishankara, S. Solomon, A.A. Turnipseed, R.F. Warren, *Science*, **259**, (1993) 194.
2 R.A. Morris, T.M. Miller, A.A. Viggiano, J.F. Paulson, S. Solomon, G. Reid, *J. Geo. Res.*, **100**, (1995) 1287.
3 G. Grigorean, X. CongCarlito, B. Lebrilla, *Int. J. Mass Spec.*, **234**, (2004) 71.
4 A. Filippi, A. Giardini, S. Piccirillo, M. Speranza, *Int. J. Mass Spec.*, **198**, (2000) 137.
5 K.B. Wiberg, Y.-G. Wang, M.J. Murphy, P.H. Vaccaro, *J. Phys. Chem. A*, **108**, (2004) 5559.
6 D.G. Thompson, M. Kinnin, *J. Phys. B*, **28**, (1995) 2473.
7 M. Speranza, M. Satta, S. Piccirillo, F. Rondino, A. Paladini, A. Giardini, A. Filippi, D. Catone, *Mass Spec. Rev.*, **24**, (2005) 588.
8 M. Musigmann, A. Busalla, K. Blum, D.G. Thompson, *J. Phys. B*, **34**, (2001) L79.
9 P.J. Linstrom, W.G. Mallard, *NIST Chemistry WebBook, NIST Standard Reference Database Number 69*, National Institute of Standards and Technology,, Gaithersburg MD, 20899, (June 2005)
10 E. Juaristi, G. Cuevas, *Tetra.*, **48**, (1992) 5019.
11 J. Berkowitz, *VUV and Soft X-ray Photoionisation*. U. Becker, D.A. Shirley ed., Plenum Press, New York, (1996).
12 A.G. Suits, J.W. Hepburn, *Annu. Rev. Phys. Chem.*, **57**, (2006) 431.
13 A.J. Yencha, A. Hopkirk, *J. Elec. Spec. Rel. Phen.*, **79**, (1996) 377.
14 J.H.D. Eland: *Photoelectron Spectroscopy*, Butterworths, London, (1984).
15 T.P. Softley, *Int. Rev. Phys. Chem.*, **23**, (2004) 1.
16 E.P. Wigner, *Phys. Rev.*, **73**, (1948) 1002.
17 E. Illenberger, J. Momigny: *Gaseous Molecular Ions*, Steinkopff Verlag, Darmstadt, (1992).
18 M. Inokuti, *Rev. Mod. Phys.*, **43**, (1971) 297.
19 H. Deutsch, T.D. Märk, *Int. J. Mass Spec. Ion Proc.*, **79**, (1987) R1.
20 Y.K. Kim, M.E. Rudd, *Phys. Rev. A*, **50**, (1994) 3954.
21 H. Deutsch, P. Scheier, S. Matt-Leubner, K. Becker, T.D. Märk, *Int. J. Mass Spec.*, **243**, (2005) 215.
22 Y.K. Kim, W. Hwang, N.M. Weinburger, M.A. Ali, M.E. Judd, *J. Chem. Phys.*, **106**, (1997) 1026.
23 M. Bart, P.W. Harland, J.E. Hudson, C. Vallance, *Phys. Chem. Chem. Phys.*, **3**, (2001) 800.
24 T. Fiegele, G. Hanel, I. Torres, M. Lezius, T.D. Märk, *J. Phys. B*, **33**, (2000) 4263.
25 C.J. Latimer, *Adv. Atom. Mol. Phys.*, **30**, (1992) 105.
26 R.F. King, C.J. Latimer, *J. Phys. B*, **12**, (1979) 1477.
27 G.K. Jarvis, R.A. Kennedy, C.A. Mayhew, R.P. Tuckett, *Int. J. Mass Spec.*, **202**, (2000) 323.
28 S.D. Price, *Phys. Chem. Chem. Phys.*, **5**, (2003) 1717.
29 M. Manning, S.D. Price, S.R. Leone, *J. Chem. Phys.*, **99**, (1993) 8695.
30 C. Wittig, *J. Phys. B*, **109**, (2005) 8428.
31 R.E. Olson, F.T. Smith, E. Bauer, *Appl. Optic.*, **10**, (1971) 1848.
32 J.B. Laudenslager, W.T. Huntress Jr, M.T. Bowers, *J. Chem. Phys.*, **61**, (1974) 4600.
33 M.A. Parkes, R.Y.L. Chim, C.A. Mayhew, V.A. Mikhailov, R.P. Tuckett, *Mol. Phys.*, **104**, (2006) 263.
34 M.A. Parkes, S. Ali, R.P. Tuckett, V.A. Mikhailov, C.A. Mayhew, *Phys. Chem. Chem. Phys.*, **8**, (2006) 3643.

35 V.A. Mikhailov, M.A. Parkes, R.P. Tuckett, C.A. Mayhew, *J. Phys. Chem. A*, **110**, (2006) 5760.
36 M.A. Parkes, S. Ali, R.P. Tuckett, V.A. Mikhailov, C.A. Mayhew, *Phys. Chem. Chem. Phys.*, **9**, (2007) 5222.
37 C.A. Mayhew, *J. Phys. B*, **25**, (1992) 1865.
38 F. Penning, *Naturwissenschaften*, **15**, (1927) 818.
39 P.E. Siska, *Rev. Mod. Phys.*, **65**, (1993) 337.
40 M.J. Druyvesteyn, F.M. Penning, *Rev. Mol. Phys.*, **12**, (1940) 87.
41 A. Borodin, M. Yamazaki, N. Kishimoto, K. Ohno, *J. Phys. Chem. A*, **110**, (2006) 1783.
42 B. Sheehy, L.F. DiMauro, *Annu. Rev. Phys. Chem.*, **47**, (1996) 463.
43 P.B. Corkum, M.Y. Ivanov, J.S. Wright, *Annu. Rev. Phys. Chem.*, **48**, (1997) 387.
44 H.M. Rosenstock, V.H. Dibeler, F.N. Harlee, *J. Chem. Phys.*, **40**, (1964) 591.
45 J.M. Hollas: *High Resolution Spectroscopy*, John Wiley & Sons, Chichester, (1998).
46 T. Baer, W.L. Hase: *Unimolecular Reaction Dynamics: Theory and Experiments*, Oxford University Press, New York, (1996).
47 W.A. Chupka, *J. Chem. Phys.*, **30**, (1959) 191.
48 C.E. Hamilton, V.M. Bierbaum, S.R. Leone, *J. Chem. Phys.*, **83**, (1985) 2284.
49 C.E. Hamilton, V.M. Bierbaum, S.R. Leone, *J. Chem. Phys.*, **83**, (1985) 601.
50 J.A.R. Samson: *Techniques of vacuum ultaviolet spectroscopy*, John Wiley & Sons, New York, (1967).
51 J.M. Dyke, A. Morris, N. Jonathon, *Int. Rev. Phys. Chem.*, **2**, (1982) 3.
52 A.W. Potts, J.M. Benson, I. Novak, W.A. Svensson, *Chem. Phys.*, **115**, (1987) 253.
53 J. Berkowitz: *Photoabsorption, photoionization and photoelectron spectroscopy*, Academic Press, New York, (1979).
54 J.H.D. Eland, *Int. J. Mass Spec. Ion Phys.*, **31**, (1979) 161.
55 R.I. Hall, A. McConkey, K. Ellis, G. Dawber, L. Avaldi, M.A. MacDonald, G.C. King, *Meas. Sci. Technol*, **3**, (1992) 316.
56 B. Sztáray, T. Baer, *Rev. Sci. Instrum.*, **74**, (2003) 3763.
57 G.K. Jarvis, PhD Thesis, University of Birmingham, (1998).
58 K. Mitsuke, S. Suzuki, T. Imamura, I. Koyano, *J. Chem. Phys.*, **93**, (1990) 8717.
59 M.F. Erben, Rosana M. Romano, C.O. Della Védova, *J. Phys. Chem. A*, **109**, (2005) 304.
60 W. Zhou, D.P. Seccombe, R.P. Tuckett, M.K. Thomas, *Chem. Phys.*, **283**, (2002) 419.
61 E.E. Rennie, A.-M. Boulanger, P.M. Mayer, D.M.P. Holland, D.A. Shaw, L. Cooper, L.G. Shpinkova, *J. Phys. Chem. A*, **110**, (2006) 8663.
62 J.H.D. Eland, *Chem. Phys.*, **323**, (2006) 391.
63 J.H.D. Eland, O. Vieuxmaire, T. Kinugawa, P. Lablanquie, R.I.H.a.F. Penent, *Phys. Rev. Letts.*, **90**, (2003) 053003.
64 J.H.D. Eland, *Vacuum UV Spectrscopy and Dynamics*. C.Y. Ng ed., World Scientific, London, (1991).
65 J.H.D. Eland, *Int. J. Mass Spec. Ion. Phys.*, **8**, (1972) 143.
66 F. Merkt, *Annu. Rev. Phys. Chem.*, **48**, (1997) 675.
67 E.E. Ferguson, F.C. Fehsenfeld, A.L. Schmeltekopf, *Adv. At. Mol. Phys.*, **5**, (1969) 1.
68 S.T. Graul, R.R. Squires, *Mass Spec. Rev.*, **7**, (1988) 263.
69 J.L. McLain, V. Poterya, C.D. Molek, L.M. Babcock, N.G. Adams, *J. Phys. Chem. A*, **108**, (2004) 6704.
70 D. Smith, N.A. Adams, *Adv. Atom. Mol. Phys.*, **24**, (1988) 1.
71 D.K. Böhme, *Int. J. Mass Spec.*, **200**, (2000) 97.
72 G.K. Koyanagi, V.V. Lavrov, V. Baranov, D. Bandura, S. Tanner, J.W. McLaren, D.K. Bohme, *Int. J. Mass Spec.*, **194**, (2000) L1.

73 B.R. Rowe, J.-B. Marquette, C. Rebrion, *J. Chem. Soc., Faraday Trans. 2*, **85**, (1989) 1631.
74 I.W.M. Smith, B.R. Rowe, *Acc. Chem. Res.*, **35**, (2000) 261.
75 I.W.M. Smith, *Chem. Soc. Rev.*, **31**, (2002) 137.
76 A.A. Viggiano, A.I. Fernandez, J. Troe, *Phys. Chem. Chem. Phys.*, **7**, (2005) 1533.
77 K. Giles, E.P. Grimsrud, *J. Phys. Chem.*, **96**, (1992) 6680.
78 J.D. Baldeschwieler, *Science*, **159**, (1968) 263.
79 A.G. Marshall, *Acc. Chem. Res.*, **29**, (1996) 307.
80 M.L. Anderson, M.S. Ford, P.J. Derrick, T. Drewello, D.P. Woodruff, S.R. Mackenzie, *J. Phys. Chem. A*, **110**, (2006) 10992.
81 W.J. Chesnavich, T. Su, M.T. Bowers, *J. Chem. Phys.*, **65**, (1976) 990.
82 R.C. Dunbar, T.B. McMahon, *Science*, **279**, (1998) 194.
83 D. Schröder, H. Schwarz, D.E. Clemmer, Y. Chen, P.B. Armentrout, V.I. Baranov, D.K. Böhme, *Int. J. Mass Spec. Ion. Proc.*, **161**, (1997) 175.
84 C.Q. Jiao, C.A. DeJoseph Jr, A. Garscadden, *J. Phys. D*, **40**, (2007) 409.
85 A. Chutjian, A. Garscadden, J.M. Wadegra, *Phys. Reports*, **264**, (1996) 393.
86 T.F. O'Malley, *Phys. Rev.*, **150**, (1966) 14.
87 H. Hotop, M.-W. Ruf, M. Allan, I.I. Fabrikant, *Adv. Atom. Mol. Phys.*, **49**, (2003) 85.
88 S.H. Alajajian, A. Chutjian, *J. Phys. B*, **20**, (1987) 2117.
89 L.G. Christophorou, J.K. Olthoff: *Fundamental Electron Interactions with Plasma Processing Gases*, Kluwer Academic / Plenum Publishers, New York, (2004).
90 M.J. Druyvestan, *Physica*, **10**, (1930) 61.
91 R. Winkler, *Adv. Atom. Mol. Phys.*, **43**, (2000) 19.
92 V. Grill, H. Drexel, W. Sailer, M. Lezius, T.D. Märk, *Int. J. Mass Spec.*, **205**, (2001) 209.
93 S. Marienfeld, I.I. Fabrikant, M. Braun, M.-W. Ruf, H. Hotop, *J. Phys. B*, **39**, (2006) 105.
94 A. Chutjian, S.H. Alajajian, K.-F. Man, *Phys. Rev. A*, **41**, (1990) 1311.
95 A. Schramm, J.M. Weber, J. Kreil, D. Klar, M.-W. Ruf, H. Hotop, *Phys. Rev. Letts.*, **81**, (1998) 778.
96 I.I. Fabrikant, H. Hotop, M. Allan, *Phys. Rev. A*, **71**, (2005) 022712.
97 S.M. Spyrou, L.G. Christophorou, *J. Chem. Phys.*, **82**, (1985) 2620.
98 J.E. Lovelock, *Anal. Chem.*, **33**, (1961) 163.
99 C.A. Mayhew, A.D.J. Critchley, D.C. Howse, V. Mikhailov, M.A. Parkes, *Eur. Phys. D*, **35**, (2005) 307.
100 M. Tabrizchi, A. Abedi, *J. Phys. Chem. A.*, **108**, (2004) 6319.
101 M. Tabrizchi, A. Abedi, *Int. J. Mass Spec.*, **218**, (2002) 75.
102 Y. Liu, C.A. Mayhew, R. Peverall, *Int. J. Mass Spec. Ion Phys.*, **152**, (1996) 225.
103 P. Muller, *Pure & Appl. Chem.*, **66**, (1994) 1077.
104 S.G. Lias, J.E. Bartmess, J.F. Liebman, J.L. Holmes, R.D. Levin, W.G. Mallard, *J. Phys. Chem. Ref. Data*, **17**, (1988) supplement no 1.
105 D.K. Bohme, G.I. Mackay, H.I. Schiff, *J. Chem. Phys.*, **73**, (1980) 4976.
106 M. O'Keeffe, *J. Am. Chem. Soc.*, **108**, (1986) 434`.
107 J.C. Haartz, D.H. McDaniel, *J. Am. Chem. Soc.*, **95**, (1973) 8562.

2. Experimental

For the studies discussed in this thesis three major pieces of apparatus have been used. They are the selected ion flow tube (SIFT), the threshold photoelectron photoion coincidence (TPEPICO) spectrometer, and the electron attachment mass spectrometer (EAMS). The operation of the three experiments will be described, along with how data is obtained and analysed.

1 Selected ion flow tube

1.1 Apparatus details

The Selected Ion Flow Tube (SIFT) is a well-established technique which has developed much in the past 30 years. The development of the SIFT has been described in detail in several publications,[1,2] with several describing innovations to the source.[3-6] The SIFT is used to study ion-molecule reactions; it produces both rate coefficients and also product ion distributions. It can be used with either cations or anions but, for the reactions studied for this thesis, only cations have been used.

The SIFT can be broken down into three basic segments; the source region, the flow tube and the detector region. Each section will be dealt with in turn. Figure 2.1 shows a schematic of the apparatus. The source currently in use in Birmingham is a closed high pressure electron impact source; there is also a flowing afterglow cluster source which has not been used for the experiments reported here. During operation a high pressure (~10^{-4} mbar) of neutral precursor gas flows past a tungsten filament. 70 eV electrons emitted by this filament ionise the gas to produce cations. Electrostatic lenses then focus and transmit the swarm of ions into a quadrupole mass filter. The quadrupole is then used to select ions according to their mass-to-charge ratio. Subsequently, in ideal situations, only the chosen ion is injected into the SIFT flow tube.

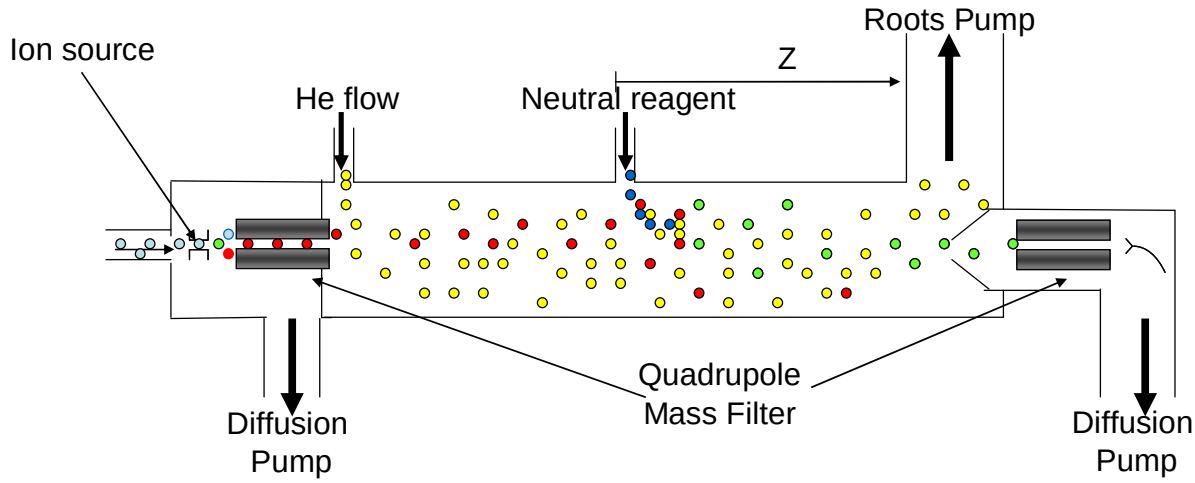

Figure 2.1: Schematic of the SIFT, not to scale. Yellow dots represent the He buffer gas blue the neutral reagent, other colours represent various ions.

The flow tube is 1 metre in length and is normally used with a pressure of ~ 0.5 Torr Helium buffer gas (99.997% purity). The design of the interface between the source and the flow tube is such that there is no back streaming of buffer gas into the source and turbulence is kept to a minimum.[1] In the flow tube collisions with the buffer gas should rapidly thermalise any ions which are in excited states. However previous studies by several groups have shown that this is not always the case,[7-9] and this aspect will be dealt with in detail later. The flow of He buffer is maintained by a roots pump (Edwards EH 2600) backed by an Edwards rotary pump (Edwards E1M176) which is sufficient to give a buffer gas velocity of about 100 m s^{-1}. In the flow tube there are two ring ports (RP), these are used to admit the neutral reagent into the system. Each RP consists of a ring with holes drilled around its circumference through which the neutral reactant flows. The two ports are at different points along the tube, so give different reaction lengths (z) which in a flow tube represent different reaction times. The current design of RP is used to minimise the end correction (c) to z due to the difference in the velocities between the injected and tube gases as well as the finite mixing time. The value of c is in the range -1 to +1 cm which is small compared to the z values of around 40 cm. Upon entering the flow tube reaction can, if it is possible, begin, and from this position forward product ions are formed. By use of either RP1 (z = 42.74 cm, long reaction time) or RP2 (z = 17.31 cm, short reaction time) the reaction progress can be monitored. The ions in the flow tube (both reactant and product) move on down to a sampling cone which leads into the detector. The flow tube itself is brazed with copper tubing and heating jackets which allows the temperature of the SIFT to be controlled. Use of heaters allows temperatures up to 400 K, use of liquid N_2 pumped through the copper tubing

allows temperatures below 0 °C. However, all the reactions reported here were performed at 298 K.

The ions enter the detector region through a small (~1 mm) hole drilled in the sampling cone end plate. This end plate is electrically isolated from the rest of the system and is used as a Faraday plate to allow detection of the total ion current reaching the end of flow tube. This is especially important for reactions with anions where electron detachment can occur. As an electron is so much lighter than any cation there will be a large drop in total current at the Faraday plate due to greater diffusive loss of the electrons relative to the initial reactant signal. The detector used in the Birmingham SIFT is a quadrupole mass spectrometer (SXP Elite 300) and the ion signal is detected *via* an on-axis channeltron. Use of an on-axis detector gives an improvement in signal compared to off-axis detectors, but is only possible because the SIFT ion source itself is off-axis, so no stray photons produced in the source can reach the channeltron. All measurements were made at the lowest mass resolution to reduce any mass discrimination effects. At this resolution most peaks are resolved, only those which are very close in mass may not be. When such peaks do occur they are treated, initially, as one peak in low-resolution scans. High-resolution scans are then taken of these unresolved peaks so correct branching ratios can be recorded. Figure 2.2 shows a high-resolution mass scan in the range 162-172 amu of the $C_2Cl_4^+$ peak formed by the reaction of an ion with C_2Cl_4. The peaks due to the different isotopes of chlorine are clearly visible in the expected ratios of 8 : 10 : 5 : 1 : 0.08. The final peak of mass 172 is not visible because it has essentially zero intensity compared to the other peaks, it has a signal which is 0.8 % of the signal at mass 166 amu. This separation of peaks is routinely achieved with our quadrupole mass spectrometer.

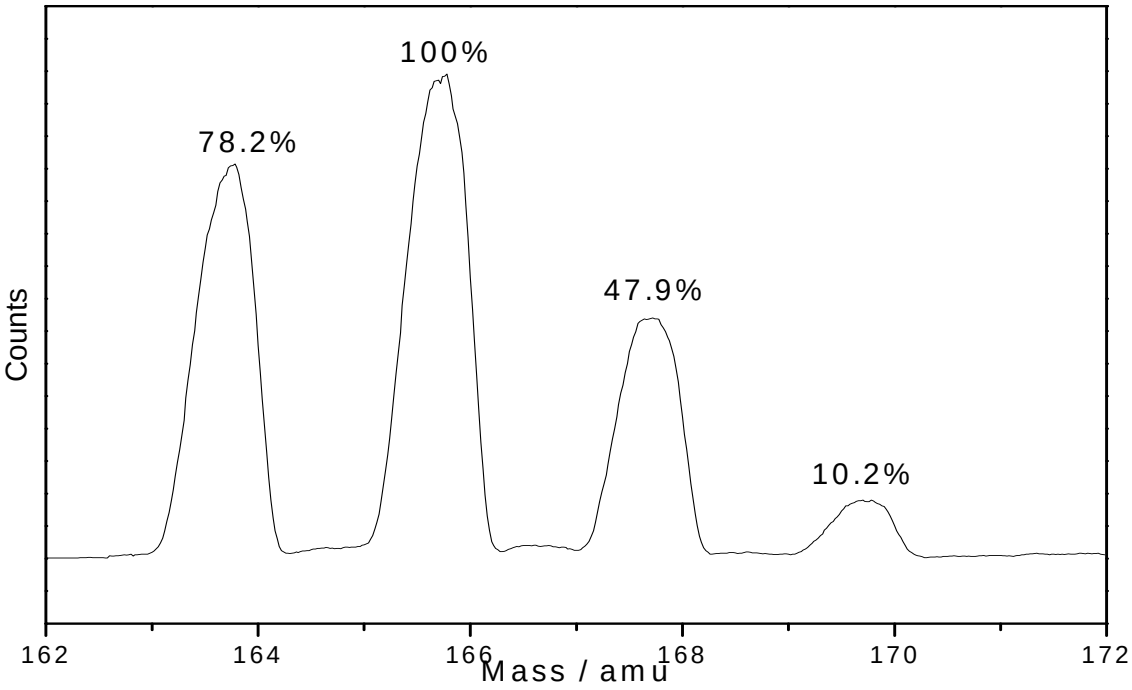

Figure 2.2: An example mass scan from the SIFT. This shows the parent ion peak produced from C_2Cl_4 showing the resolution of all chlorine isotopomers. The numbers show the signal strengths relative to the peak at mass 166.

1.2 Experimental issues

To measure rate coefficients using a SIFT the standard technique is as follows. For a general ion-molecule reaction where A^+ is the reactant ion, B the reactant neutral and C^+ and D are various ionic and neutral products respectively:

$$A^+ + B \xrightarrow{k} C^+ + D \qquad \textbf{(eq 2.1)}$$

The rate coefficient (k) is defined, if the signal of A^+ ions is monitored as a function of the flow rate of neutral gas B, by this first order rate equation, where v_i is the ion velocity:

$$\frac{d[A^+]}{dt} = v_i \frac{\partial[A^+]}{\partial t} = -k[A^+][B] \qquad \textbf{(eq 2.2)}$$

In SIFT experiments $[B] \gg [A^+]$ so measurements are made under pseudo-first order kinetics. Hence [B] is effectively constant and integrating equation 2.2 gives:

$$\ln\left(\frac{[A^+]_t}{[A^+]_0}\right) = -k't \qquad \textbf{(eq 2.3)}$$

where *k'* is the pseudo-first order rate coefficient which is equal to $k[B]$. From the fact that in a flow tube time is equal to the reaction length divided by the ion velocity, it can be seen that a plot of $\ln[A^+]$ against $[B]$ will give a gradient of $-\frac{kz}{v_i}$. It is clearly important to determine v_i accurately so as to obtain an accurate value for *k*, Smith and Adams have given a thorough overview of how to measure the ion velocity in the SIFT.[1] In the current experimental apparatus only rate coefficients which are greater than 10^{-13} cm^3 $molecule^{-1}s^{-1}$ can be measured. It is estimated that that the error in rate coefficients is ± 20 %. Figure 2.3 shows an example of a plot of $\ln[A^+]$ against $[B]$.

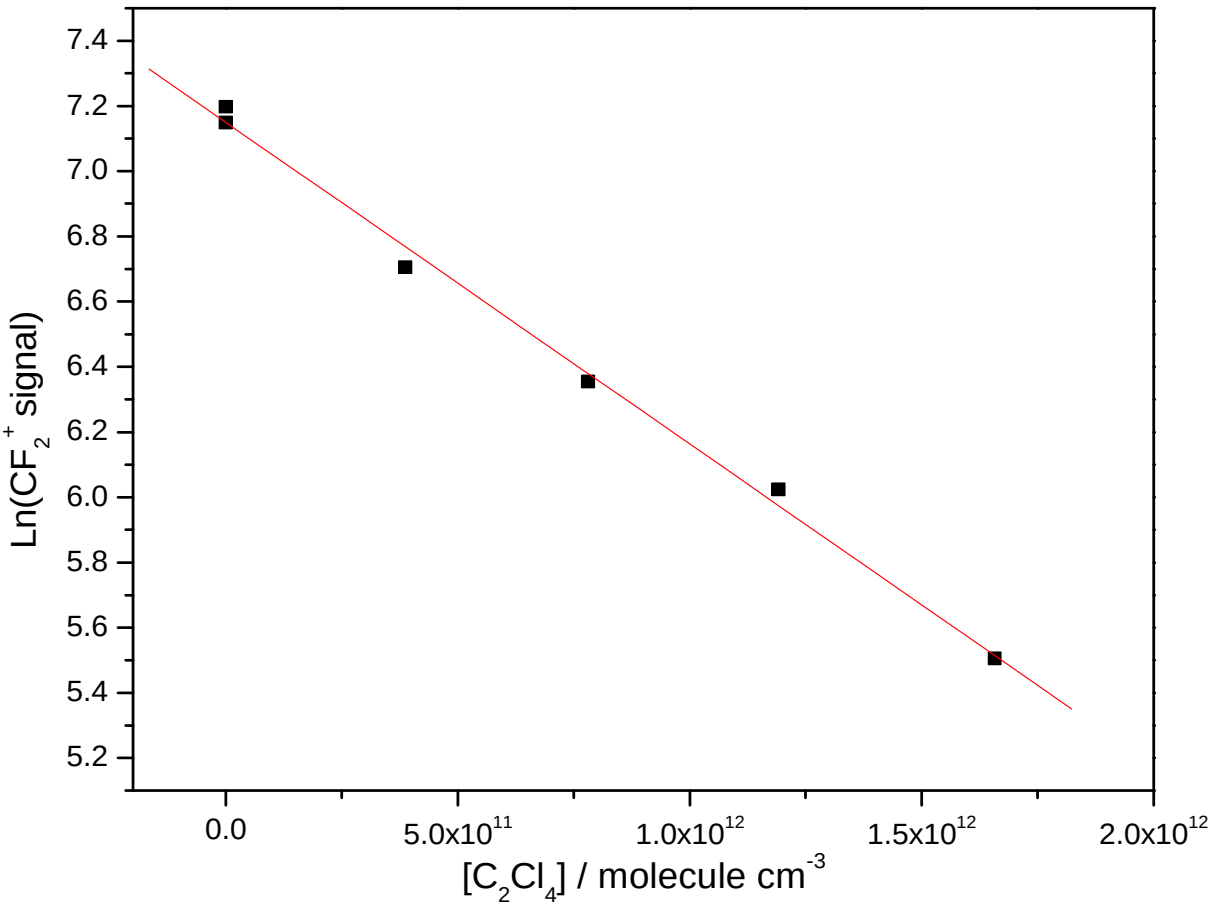

Figure 2.3: Example rate plot from the reaction of C_2Cl_4 + CF_2^+ showing the decrease in the CF_2^+ signal with increasing $[C_2Cl_4]$.

The SIFT can also be used to measure product ion branching ratios. When working out branching ratios it is necessary to make allowances for any possible secondary reactions, *i.e.* any

reactions between product ions and the neutral reagent itself. To allow for this effect, the ion yields are measured using RP2 so there has only been a short reaction time, decreasing the prevalence of secondary reactions. The ion yields are then extrapolated to zero neutral concentration. By following this procedure, the branching ratios produced should be the true distributions.

As mentioned earlier, collisions of the ions with the helium buffer should quench any excited states. This is not, however, always true. In previous studies we have shown that *ca* 20 % of the O_2^+ is present in the $v = 1$ and 2 vibrational levels.[8] CF^+ and NO^+ are also known to be vibrationally excited in a SIFT depending on operating conditions,[10,11] as is N_2.[12] There is also some possibility of electronic excitation due to spin-orbit splitting; this is especially important with the rare gas ions Kr^+ and Xe^+ where the splitting is as large as 0.67 and 1.31 eV respectively.[13] Such a large splitting can lead to the upper and lower states having differing reaction rates and products.[14,15] Any differences in reactivity should show up in the pseudo-first order plots as curvature. In the studies reported here no curvature was visible. This means two things; either that there are no excited states present in the flow tube, or that the two levels react at the same rate. Where this is relevant to specific results, it will be discussed further.

A common impurity in the flow tube when using ions whose recombination energy (RE) is greater than 12.61 eV is H_3O^+. This is due to proton transfer to any residual water present in the flow tube. When present the ion lenses are tuned to reduce any H_3O^+ signal to < 10 % of the reagent signal. The presence of H_3O^+ is further reduced by using a liquid nitrogen trap on the helium inlet and regularly baking the flow tube to temperatures above 100 °C to remove any traces of water.

As part of the studies reported here the data acquisition system of the Birmingham SIFT has recently been upgraded. Originally it was running on a 486 PC using a Visual Basic based programme. This has been changed to a new labVIEW-based system. The programme is custom written in the labVIEW programming language. It runs on a Pentium based computer with a National Instruments PCI data acquisition card (PCI 6014) that has several analogue and digital inputs and outputs to control and monitor the SIFT apparatus. This development has allowed the time for individual experiments to be decreased, and given easy access to high powered analysis techniques.

2. Threshold photoelectron photoion coincidence spectrometer

2.1 Apparatus detail

The Threshold Photoelectron Photoion Coincidence Spectrometer is an apparatus which is used to measure what happens following photoionisation of a neutral. It is specifically designed to detect zero energy (*i.e.* zero to a few meV) electrons in coincidence with the associated ions. The equipment has been described in detail in the literature.[16,17]

As the TPEPICO apparatus detects threshold electrons it needs a source of continuum light and a monochromator. This is in comparison with normal photoelectron experiments where the standard source is the He(I) lamp which has just one peak at 58.4 nm (21.22 eV), this is the transition from the excited state (1s 2p, ^{1}P) to ground state He ($1s^2$, ^{1}S). Such a line source does not require any dispersion before use. The continuum source used for all the experiments in this thesis is the Daresbury Synchrotron Radiation Source (SRS). A Synchrotron is a large storage ring in which bunches of charged particles (electrons at the SRS, other charged particles are in use at different Synchrotrons) circulate. As the electron bunches are bent around the corners by bending magnets they accelerate and this causes them to lose energy as radiation. The properties of Synchrotron radiation that make it especially useful for this work are that it covers smoothly a broad energy range (IR to X-ray) and is very intense. Due to the spectral nature of the radiation produced it must be dispersed before it can be used. The experiment in this thesis were mainly performed on beamline 3.2 at the SRS where the dispersion is through a 5 m vacuum-UV McPherson normal incidence monochromator, and a post-focusing mirror box. The beamline and monochromator have been detailed in the literature.[18] For two molecules, CHF_3 and *c*-C_5F_8, the TPEPICO experiments were performed on beamline 3.1. For the CHF_3 data the monochromator was a Seya type. Recently a new monochromator was commissioned for this beamline.[19] It is of the Wadsworth type and was used for the *c*-C_5F_8 experiment. More details are given in chapters 4 and 6. Both beamlines are designed specifically for VUV experiments, 3.1 is optimised for high flux, while 3.2 is for high resolution work.

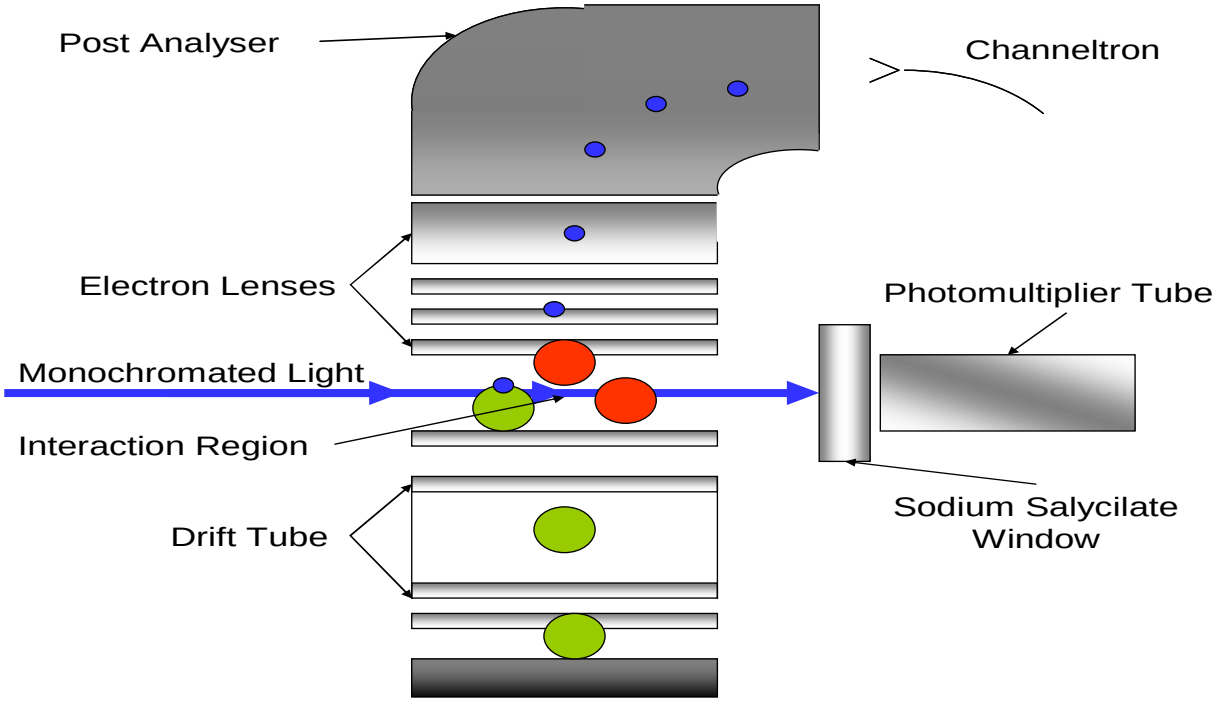

Figure 2.4: Schematic of the TPEPICO apparatus, not to scale. Blue dots are electrons, the green dots are cations and the red dots are neutral molecules.

A diagram of the TPEPICO apparatus is shown in Figure 2.4, it consists of two electrostatic detectors (for the ions and electrons) and a photomultiplier tube (PMT) to detect incident photons. Monochromatic light from the beamline monochromator is coupled into the interaction region *via* a 100 mm long quartz capillary. Gas is allowed into the interaction region through a needle as an effusive beam. A pressure of around 10^{-5} mbar is maintained, higher pressures are not used to avoid any absorption affects. The light, if it has a high enough energy, ionises the gas. The resultant electrons and ions are initially extracted into their respective detectors by a 20 V cm^{-1} extraction field. The threshold electron detector has been previously described,[20] it is a combination of steradiancy and low extraction field analysers. In the steradiancy type, electrons are accelerated by an electric field into a field free region, and most high-energy electrons will have an off-axis component to their velocity and will be lost from the system. The problem with this is that some high-energy electrons will have only on-axis velocity and so pass through this region into the detector, so producing the so called “hot electron tail” in spectra. Use of a post-analyser can remove this tail. In a low extraction field detector, the electrons are extracted from the interaction region by a small electric field. It is configured so that only low-energy electrons can be brought to focus on the entrance of a post analyser. Our detector in the TPEPICO spectrometer combines the two techniques. The first electron lens has a

large chromatic aberration; this performs in a similar way to a steradiancy analyser removing electrons with an off-axis velocity component. The remaining optics then brings the threshold electrons into focus on a 127° cylindrical post-analyser. This removes any remaining high-energy electrons before the threshold electrons hit a channeltron (Phillips X818BL) and are detected. Computer simulations show that this analyser is capable of a resolution of 3.5 meV,[20] though the resolution achieved in these studies is more modest at *ca* 10 meV.

Unlike the quadrupole mass spectrometers used in the other apparatus described in this Chapter, the TPEPICO ion detector is a time-of-flight (TOF) mass spectrometer. Ions pass through a two-stage acceleration region before entering a linear drift region. The design of the acceleration region is such that the space focussing condition is met and all ions of the same *m/z* and initial velocity arrive at the same time on the detector.[21] The ions are detected by two microchannel plates (MCP) (Hamamatsu F4296-10) in the chevron configuration. In this experiment the start pulse to the TOF is provided by an electron being detected in the threshold analyser, because electrons move so much faster than ions the time they take to reach their detector can be neglected compared to the ion TOF.

The photon flux from the synchrotron is monitored by a photomultiplier tube (EMI 9924B) which detects the fluorescence from a sodium salicylate coated Pyrex window. The flux is monitored as it allows the data to be flux normalised *in situ*. Figure 2.5 shows the flux curve for the high energy grating of the 5m McPherson monochromator on beamline 3.2 at the Daresbury SRS.

The signals from the MCPs and channeltron are first discriminated before been sent to pulse-shaping electronics. The resultant pulses are then sent to a time-to-digital (TDC) card where the electron signal provides a start and the ion signal a stop to the timing. A counter card working alongside the TDC measures the total electron, ion and photon signals. Descriptions of basic experimental setups and considerations are readily available.[22]

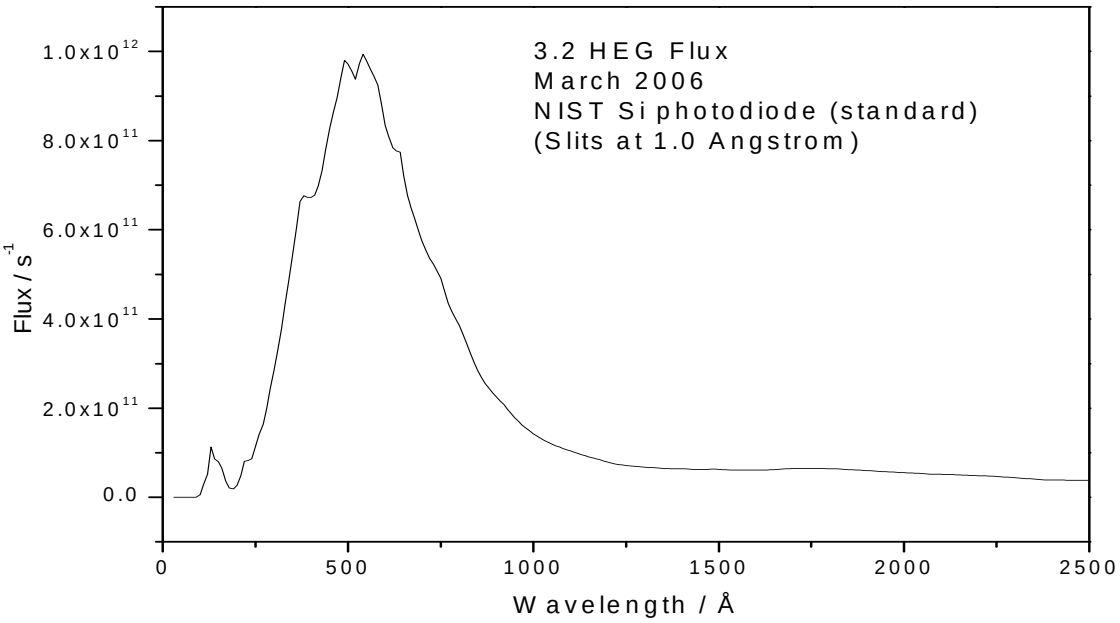

Figure 2.5: Flux curve for the high energy grating on beamline 3.2 at the SRS.

2.2 Calibration

Before any new sample gas can be studied the TPEPICO energy and mass scale must be calibrated, and the threshold electron analyser must also be tuned to accept only zero energy electrons. These necessities can all be achieved using argon. The positions of both spin-orbit components of the ground state of Ar^+ ($^2P_{3/2}$ 15.759 eV, $^2P_{1/2}$ 15.937 eV)[17] are known with high precision as is its mass, so both energy and the mass scale can be calibrated. Figure 2.6 shows an example of a TPES and photoionisation cross section for Ar recorded with a resolution 0.025 nm (or 0.005 eV). Clearly visible are the two spin-orbit states of Ar^+ and the autoionisation states converging on the upper $^2P_{1/2}$ state. Recording a TOF spectrum of Ar^+ at high time resolution is also necessary in setting up the TPEPICO experiment. The TOF of Ar^+ (normally around 11 μs) is used to calibrate the TOF mass scale from the relationship:

$$\mathrm{TOF(x)} = \mathrm{TOF(Ar)}\sqrt{\frac{m_x}{m_{Ar}}} \qquad \textbf{(eq 2.4)}$$

where TOF(x) and TOF(Ar) are the TOF of the unknown ion and Ar^+, respectively, and m_x and m_{Ar} are the masses of the unknown and Ar^+. The width of the Ar^+ peak allows measurement of the sample temperature and instrumental effects.

From the equation of Franklin (chapter 3 equation 3.20) the theoretical width of the Ar^+ TOF peak at 298 K and a 20 V cm^{-1} extraction voltage is 121 ns. Figure 2.7 shows an Ar TOF spectra recorded on beamline 3.2, the fwhm value measured here of 120 ns is in excellent agreement with the Franklin value.[23]

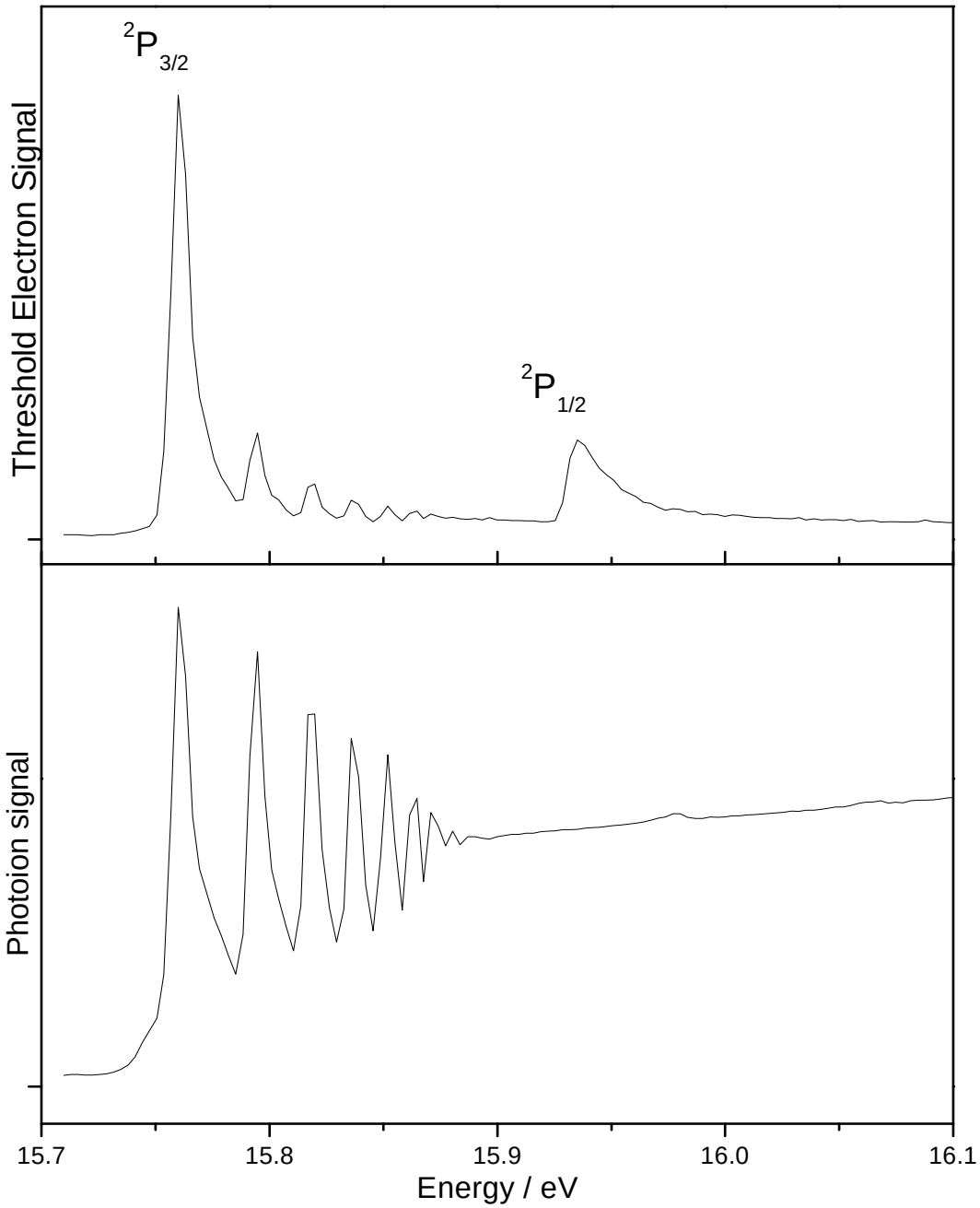

Figure 2.6: TPES and PIS for Ar recorded from 15.7 to 16.1 eV with 0.025 nm resolution on beamline 3.2.

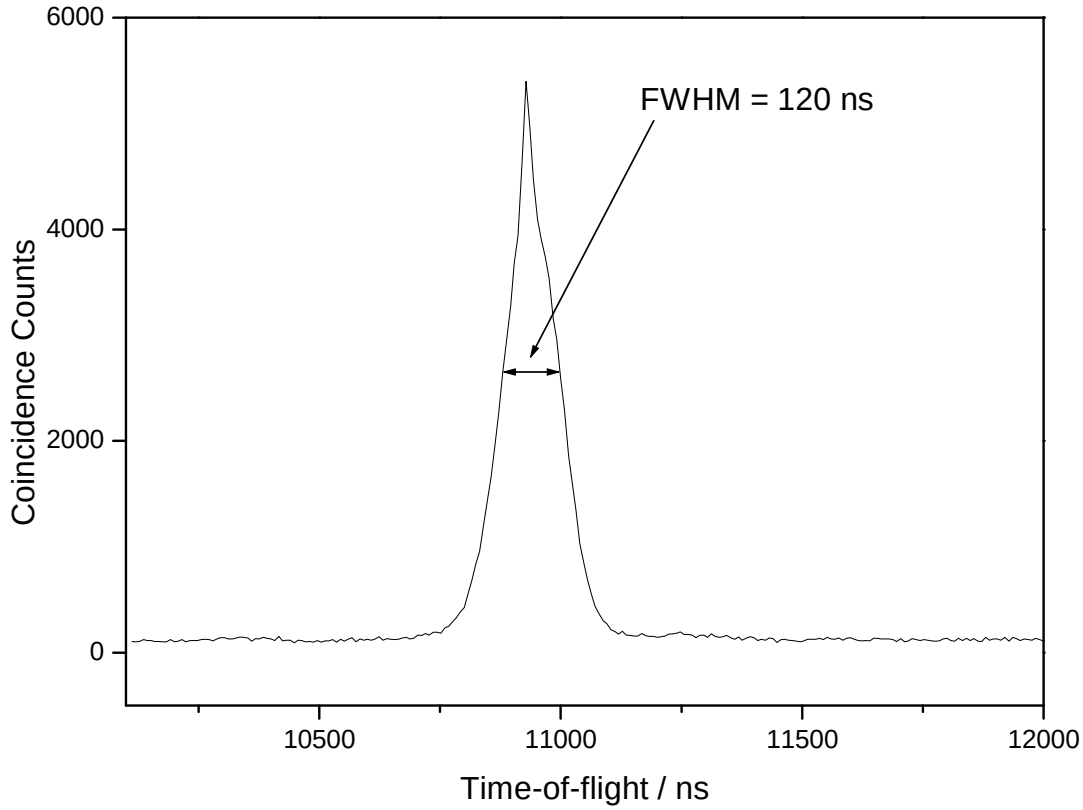

Figure 2.7: Ar coincidence TOF spectra recorded on beamline 3.2 with 0.025 nm resolution

2.3 Experimental details

Two main experiments can be performed with the TPEPICO apparatus. The first is a scanning energy TPEPICO measurement. Here the wavelength of incident radiation is scanned and any electrons or ions produced at this energy detected in coincidence are recorded. This produces a 3D plot of wavelength *vs.* coincidence signal *vs.* ion TOF, and example is shown in Figure 2.8. This experiment also has the added bonus of producing the threshold photoelectron spectra (TPES) and total photoion yield for the neutral under study. Taking a cut through the 3D plot at a fixed TOF will produce the ion yield curve for the particular ion as a function of wavelength. By taking such cuts for all ions, ion branching ratios can easily be extracted. A cut at fixed wavelength produces the mass spectrum for that wavelength. This is useful for seeing which fragments are present but no further analysis is performed due to a reduced TOF resolution. The ultimate resolving power ($M/\Delta M$) of the TOF analyser is ~150-200, however the TDC card limits the resolution to 8 ns. When recording 3D maps this resolution is even further degraded so that *all* wavelengths and *all* ion fragments can be recorded on one 3D map consisting of 256 x 256

channels. This can cause problems in that ionic fragments, especially where the difference between product ions is as small as one hydrogen atom, cannot always be resolved at the TOF resolutions used. In cases where this problem is encountered, the unresolved fragments will be treated as one fragment when calculating branching ratios.

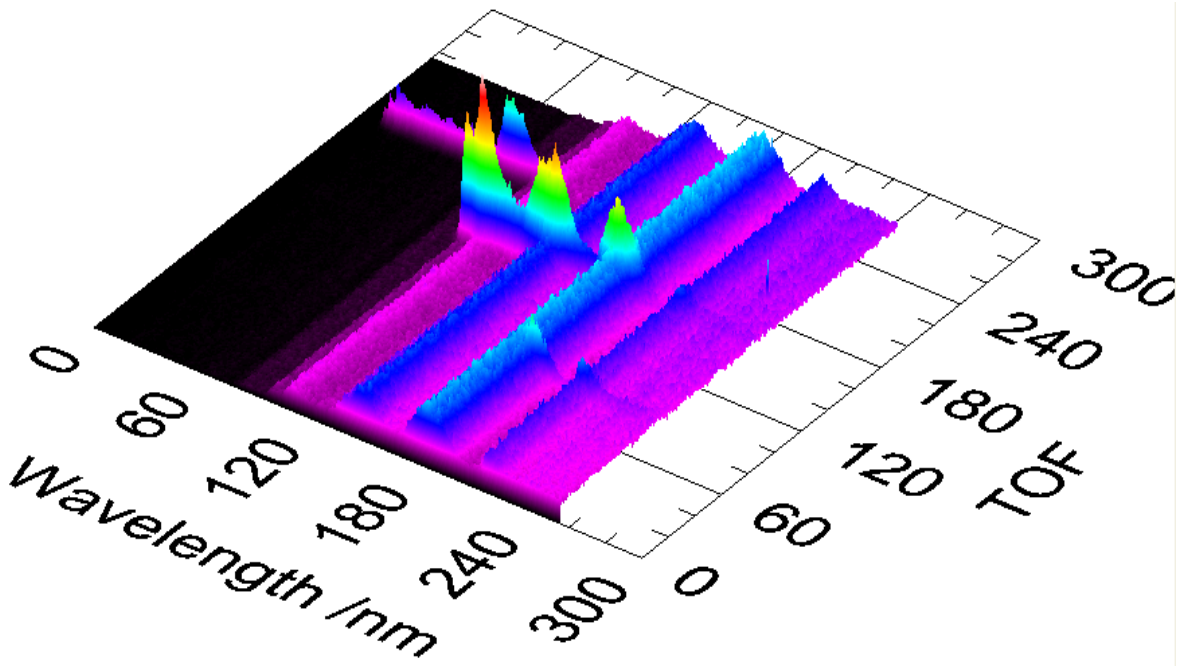

Figure 2.8: 3D map of coincidences for *c*-C_5F_8. Time-of-flight is in ns, cuts at a fixed TOF will produce the ion yield curve for a particular ion.

The second experiment that can be performed can alleviate, to a certain extent, the difficulties in separating the fragments. Fixed-energy high-resolution TOF scans are recorded. Here the wavelength of the radiation is fixed and a window is placed around just one of the ions fragments using a high TOF resolution (8 ns). At this resolution most fragments will be resolvable. From such fixed-energy scans can be calculated kinetic energy release distributions (KERDS) and hence how much energy is released into translation of fragments. This theory is covered in detail in chapter 3 of the thesis.

3. Electron attachment mass spectrometer

3.1 Apparatus details

The Electron Attachment Mass Spectrometer (EAMS) is used to study electron attachment to neutral molecules at high pressure. The original EAMS was an adapted ion mobility spectrometer[24] though it has gone through several extensive upgrades since then.[25,26] Several variations on this apparatus have been developed across the world.[27,28] The EAMS operates with an electron swarm, *i.e.* the electrons produced by the source do not have a single clearly defined energy but have a range of energies, and at atmospheric pressure. The energy distribution is in general non-thermal and must be determined for each buffer gas, so that data can be compared with electron beam experiments where the electrons emanate from a monoenergetic beam under single collision conditions.[29]Almost uniquely for a swarm technique, our EAMS can not only give attachment rate coefficients but also detect the product anions.[25,29] A schematic of the apparatus is shown in Figure 2.9.

The electron source is a planar sample of ^{63}Ni which is an 11 mCi β-radiation source. The emitted radiation continuously ionises the buffer gas in the drift tube. The electrons produced in these interactions will, after many collisions, come to an equilibrium with the surrounding gas. The final energy distribution depends on the buffer gas used and the voltage applied along the drift tube.

The drift tube is inside a large vacuum chamber which is filled with the buffer gas. The buffer gas pressure is maintained by a mass flow controller (MKS 1159-B) and the buffer gas is injected against the drift of electrons and anions; this helps to reduce concentration gradients, a problem encountered with earlier versions of this apparatus which used two gas flows. The first containing buffer gas, the second from the opposite direction was a mixture of the buffer and sample gas.[26] A high voltage (50-3400 V) is applied between the β-source and the Faraday plate. The upper limit on the voltage range is dependent on the breakdown voltage of the buffer which is being used. The lower limit is chosen because below this the detected signal strength becomes too small to perform useful measurements. Under the influence of this voltage the electrons drift towards the Faraday plate where they can be collected and monitored over time. Any anions formed due to electron attachment will also drift down the tube.

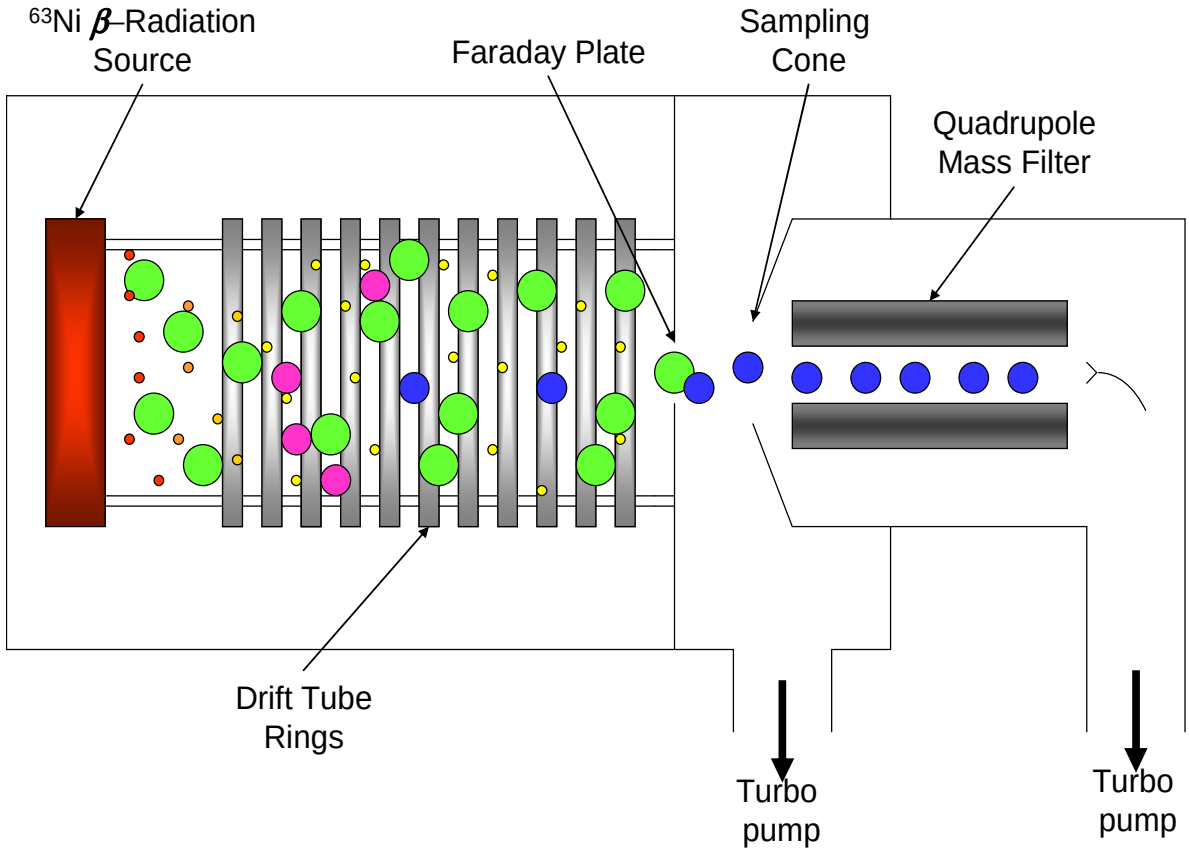

Figure 2.9: Schematic diagram of the EAMS, note that there are more rings between the β source than shown, the others have been removed for clarity. Not to scale. Small dots are electrons, large green dots are the buffer gas, magenta dots are the neutral attaching gas. The blue dots represent the anionic products following attachment.

The drift tube itself (see Figure 2.10) consists of a series of ring electrodes with a total length of 9.7 cm from the β source to the Faraday plate. Each electrode ring is made of aluminium coated in molybdenum, this is known to reduce charging effects.[30] Each of the electrodes is electrically isolated from the next using a ceramic spacer. Electrical connection is maintained by a chain of 10 MΩ resistors. In the centre of the tube is an electron gate which is used to pulse the electron swarm. At the end of the drift tube is a Faraday plate which has a 70 μm hole in it leading to the detection region of the apparatus. The Faraday plate is electrically isolated from the drift tube by a PTFE spacer ring.

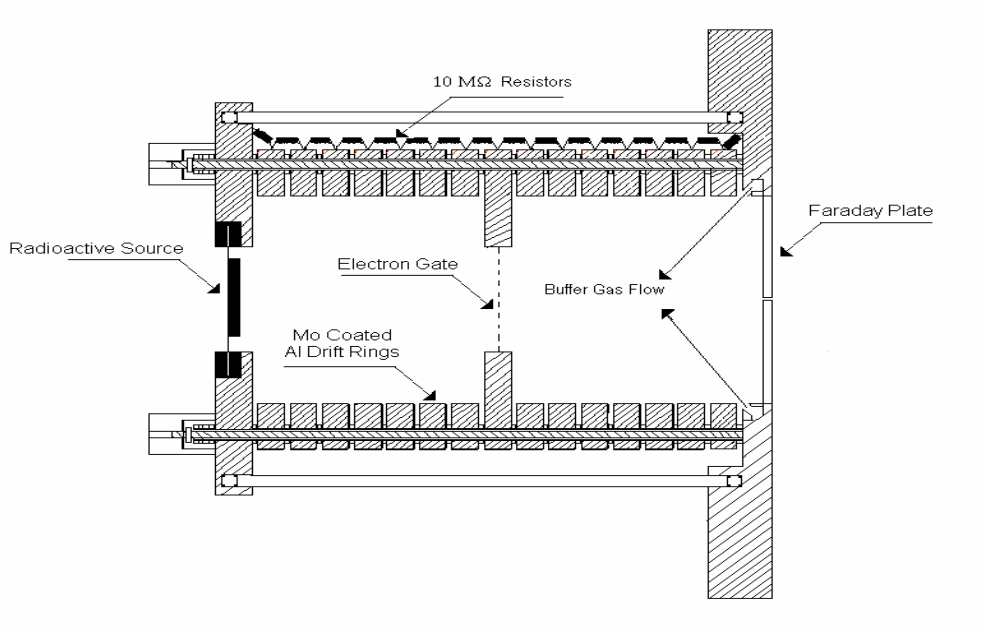

Figure 2.10: Diagram of the EAMS drift tube.

The electron gate is used to convert the constant stream of electrons generated by the β-source into discreet pulses. The gate is positioned approximately halfway through the drift tube, and is made up of two sets of interdigitated wires and is based on the Bradbury-Nielson design. The wires are made of molybdenum (thickness 0.05 mm) placed on top of a glass circuit board with a 25×25 mm^2 square hole in the centre. The wire spacing is 0.32 mm between consecutive wires. The wires are glued down using non-conducting epoxy resin. By snipping alternative wires two separate arrays of wire are created, conducting epoxy is then used to join all wires in each discreet set together (see Figure 2.11).

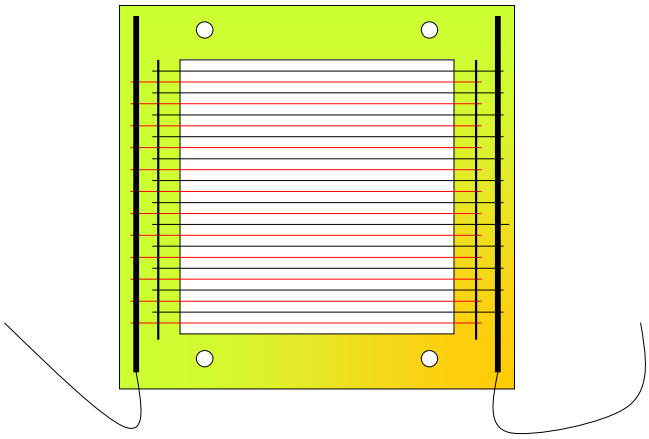

Figure 2.11: EAMS electron gate. The wires are coloured differently to highlight the interdigitation.

Batteries are used to apply up to ± 15 V + V_d, to the wire arrays, where V_d is the voltage at the position of the gate in the drift tube. One of the arrays has a positive voltage applied, for the other array it is negative. Application of the voltages closes the gate to electrons. When the gate is closed the electrons experience a large sideways deflection, stopping them from continuing into the rest of the drift tube. The gate is opened by switching the voltage on both sets of wire to V_d. In this instrument voltages of ~18 V are adequate to close the gate for E/N values of 2×10^{17} V cm^2. Typically electron pulses are produced with widths of 0.2-1 ms with a 40 ms gap between them. An initial TTL pulse is generated by a commercial pulse generator (GEPL logic pulse generator) this is passed to the pulse switch. The pulse switch itself consists of two Schmitt triggers which are optically isolated from V_d. Due to the electronics fast response time the pulsed swarm has a well defined start time.

It can be shown that the position of the gate has no effect on the detected signal. If the intensity of electrons at the start of the drift tube is I_0, then if the distance between source and gate is l_1 then the intensity at the gate $I(l_1)$ is given by:

$$I(l_1) = I_0 \exp -(n\eta + \beta)l_1 \qquad \textbf{(eq 2.5)}$$

where η is the electron attachment coefficient, β is the diffusive loss coefficient (the probability of diffusive loss of electrons per unit length) and n is the number density of attaching gas. A fraction of this signal, γ, will be pulsed into the next section of the drift tube, where the initial pulse intensity will be:

$$A(l_1) = \gamma I(l_1) = \gamma I_0 \exp -(n\eta + \beta)l_1 \qquad \textbf{(eq 2.6)}$$

By the time the pulse reaches the Faraday plate further losses will have been caused due to diffusion and attachment, so the amplitude at the Faraday plate, l_2 the full length of the drift tube, will be:

$$A(l_2) = A(l_1)\exp -(n\eta + \beta)(l_2 - l_1) = \gamma I_0 \exp -(\beta l_1)\exp -(n\eta l_2) \qquad \textbf{(eq 2.7)}$$

$A(l_2)$ is clearly independent of the gate position, and it can be seen that η can easily be extracted from measurements at different values of n.

Any electrons and anions which manage to reach the Faraday plate will produce a current. This current is converted to a voltage pulse by a current-to-voltage converter. A fast preamplifier, which has a gain range of 10^9 V A^{-1}, amplifies the signal. The amplified pulse is passed to a gated boxcar integrator, which monitors the pulse amplitude. The pulse amplitude is subsequently passed to a DOS 6.0 based acquisition programme for storage. The process of amplification will

impose a time constant on the measurement which must be known if electron drift velocities are to be measured.[26]

Behind the Faraday plate is a differentially pumped region. This region is necessary to reduce the high pressure of the drift region down to the ~ 10^{-5} mbar needed to operate a quadrupole mass spectrometer. In this region is positioned a sampling cone with a 1 mm hole leading to the quadrupole mass spectrometer. Due to going from high pressure to low pressure through a small orifice the gas undergoes an adiabatic expansion to form a supersonic beam.[31] This expansion will rapidly cool the gas and can lead to cluster formation. Figure 2.12 shows an example of ion clustering. For this mass scan the drift tube was removed and a cylindrical β-source was positioned directly in front of the Faraday plate. The majority of peaks in this spectrum are due to clustering of common atmospheric gases. It is necessary to be aware of the distortion of product yields that such ion clustering can cause. The cone is positioned in the so called silent zone to maximise transmission and also because there is no mingling of any background gas into the jet in this region. Between the cone and the Faraday plate a voltage can be applied; this not only aids in transmission of ions but also can lead to collision induced dissociation (CID). CID can be a useful probe of ion identification, but in general the voltage is kept low (10-15 V) to minimise CID but maximise transmission so that only the unaffected ion yields are measured.

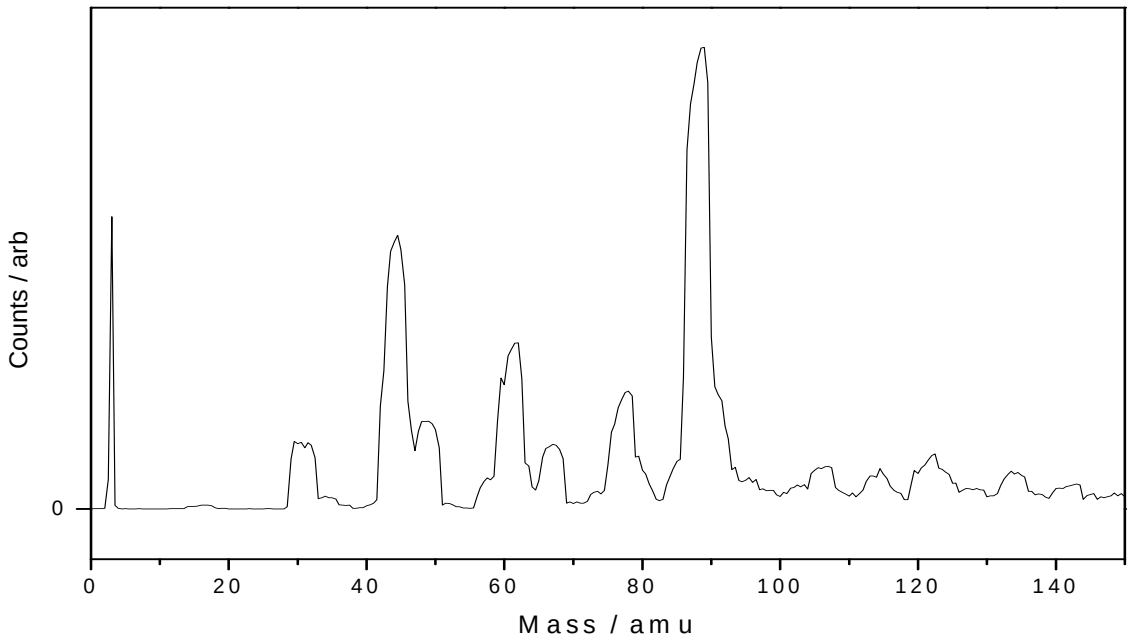

Figure 2.12: Example of a mass spectrum produced by electron attachment in air.

The ions are detected after the cone by a quadrupole mass spectrometer (SXP Elite 600). The same resolution issues as identified with the SIFT quadrupole are also pertinent here. The mass range of the quadrupole is 0 – 600 amu allowing a larger range of molecules to be studied in this system compared to the SIFT.

3.2 Sample handling

Samples are injected into the flow of buffer gas in the EAMS. Sample preparation is an important part of correct operation of the EAMS; the sample concentrations must be kept very low, *ca* 10^{13} molecule cm^{-3}. If the concentration of a sample is too high then it can interfere with, and alter, the electron energy distribution, it is for this reason that the buffer gas should be as pure as possible. Another reason for low concentrations is that if a neutral gas attaches electrons it tends to be with a very high rate of attachment, so by keeping sample concentration low better control over the measurement can be achieved. The method used to prepare the samples is:

1. Sample is let into a large evacuated chamber (evacuated to ~10^{-6} mbar) up to a pressure of around 10 – 100 mbar.
2. The chamber is then filled up to 1900 – 2000 mbar with the appropriate buffer gas.
3. The mixture is left to stand for 24 hours to allow full mixing.
4. The chamber is then evacuated down to around 10 – 100 mbar.
5. The chamber is then refilled with buffer gas to 1900 – 2000 mbar.
6. Steps 3-5, the sequence of evacuations and refilling, are repeated until the required concentration (*ca* 10^{13} molecules cm^{-3} or lower) of the sample is reached.

The process of removal of gas by pumping can lead to large errors in concentration as it is possible that, proportionally, more buffer gas is pumped off than the sample or *vice-versa*. It can also be problematic that samples must be prepared days in advance, as wall loses can become important. It is likely that the biggest error in the measurements of electron attachment rate coefficients arises due to errors in sample concentration. Samples are removed from the tank for injection into the apparatus using either a syringe, and injected via a septum into the buffer gas flow. The flow rate is controlled with a digital syringe drive (World Precision Instruments, sp100i).

3.3 Buffer gas

The selection of buffer gas will affect the electron energy distribution which is achieved in the EAMS. Three gases are used regularly, nitrogen, argon and carbon dioxide. Figure 2.13 shows a graph of the mean electron energy, <ε>, for the different values of the reduced electric field strength, E/N, for all three buffer gases. It is clear that using argon as a buffer will give access to a higher <ε> for a given value of E/N than for nitrogen. So these two gases give a complimentary range of <ε> values, allowing study of electron attachment from high energies to close to thermal energy ($3k_BT$ / 2 or 0.038 eV). However, it has been found that in some cases the rate coefficients measured at the same <ε> in different buffer gases do not agree.[32] This arises because although <ε> is the same, the underlying electron energy-distribution is different. It should be noted that to reach thermal energy with N_2 is very difficult because the applied voltage on the drift tube is below 100 V and the pulse amplitude becomes very small, this makes it necessary to extrapolate data from higher energies down to 0.038 eV. The most interesting plot in Figure 2.13 is that for carbon dioxide. For CO_2 our group and others[25,33] have found that the electron energy-distribution is thermal over a broad range of E/N values (~ 0 – 16 × 10^{-18} V cm^2). This means that the thermal attachment rate coefficient and also the product ion distribution at thermal energies are facile to measure. In this thesis, in general, measurements are performed using CO_2. However, on some occasions N_2 has been used for the useful extra information it can provide on how the attachment process changes as a function of energy.

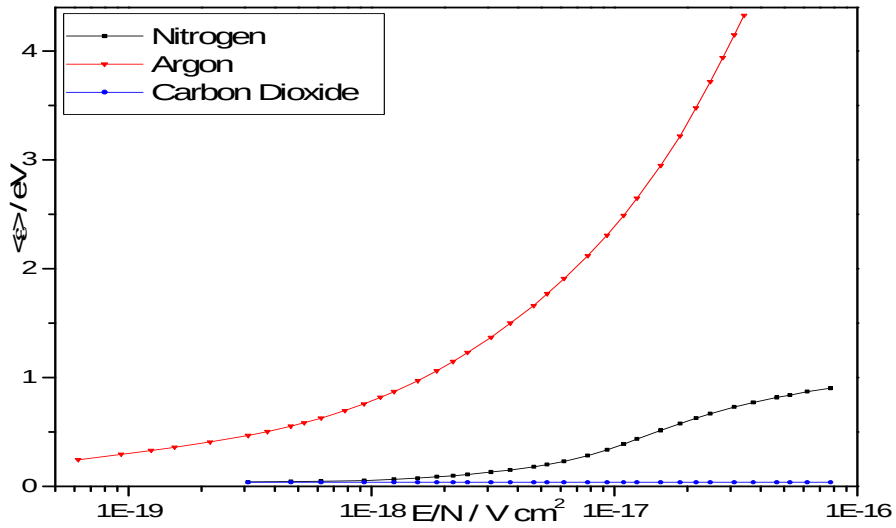

Figure 2.13: How the mean electron energy <ε> of a swarm varies with the reduced electric field (E/N) for N_2, Ar and CO_2 from 25,26,34.

3.4 Experimental Details

There are several different experiments which can be run on the EAMS. The main experiment is to measure the electron attachment rate coefficient. For this experiment the system is pulsed and the electron pulses detected at the Faraday plate. A small flow of sample gas is then injected and the change in electron current measured. This process is repeated until the signal has been depleted by around 80 %. There are two ways to extract the density normalized electron attachment coefficient (η) from the data. The first is a plot of attaching gas concentration (n) versus I_c:

$$I_c = I_0 \exp(-n\eta l) \qquad \textbf{(eq 2.8)}$$

where I_c is the intensity at the concentration (n) of the attaching gas and I_0 is the intensity at zero gas concentration. Fitting an exponential function to a I_c versus n plot results gives η. The second method is to use a Beer-Lambert analysis. This is done by plotting n versus $\ln(I_c/I_0)$. This will yield a straight line with a gradient equal to $-\eta l$. It should be noted that I_0 has contributions to its value from the diffusive loss coefficient and attachment due to any impurities in the buffer gas. Once η has been calculated then the rate coefficient (k_a) can be determined from the relationship of η to the electron drift velocity (w):

$$k_a = \eta w \qquad \textbf{(eq 2.9)}$$

The drift velocity depends on the reduced electric field, the temperature and the buffer gas used. For N_2 and Ar extensive tabulations of w are available for use in this calculation.[26,34] For CO_2 w is calculated using:

$$w = \mu_n \left(\frac{1013}{P}\right)\left(\frac{T}{273}\right)\frac{E}{N} \qquad \textbf{(eq 2.10)}$$

where μ_n is the reduced electron mobility in CO_2 which has been measured in this apparatus to be $(1.81 \pm 0.05) \times 10^{22}$ V^{-1} cm^{-1} s^{-1}.[25] Figure 2.14 shows an example of an experimental data for electron attachment to c-C_4F_8 with an exponential fit, Figure 2.15 shows this data following the Beer-Lambert analysis. The preferred method is to take the exponential fit to the experimental data. This avoids the Beer-Lambert analysis which assumes that the zero point of the measurement is correct to obtain the unity value.

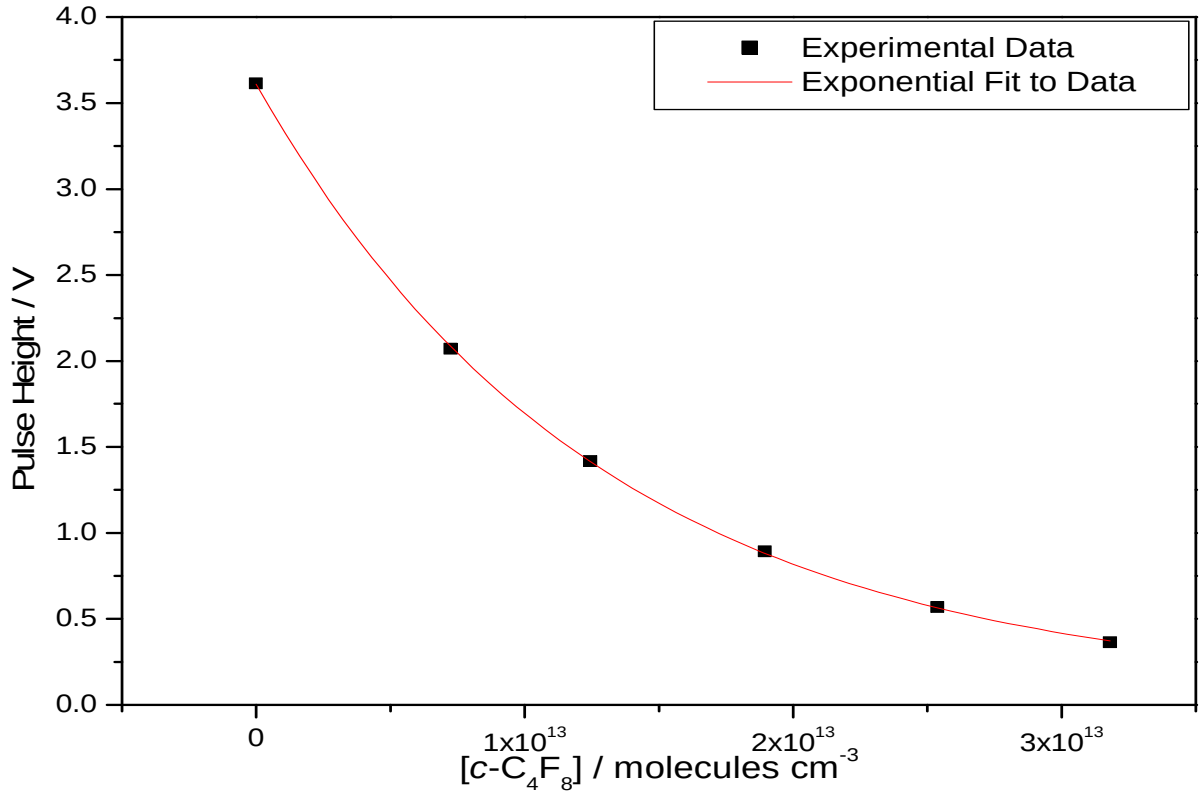

Figure 2.14: Plot of experimental measurements of electron signal against [*c*-C_4F_8], with exponential fit

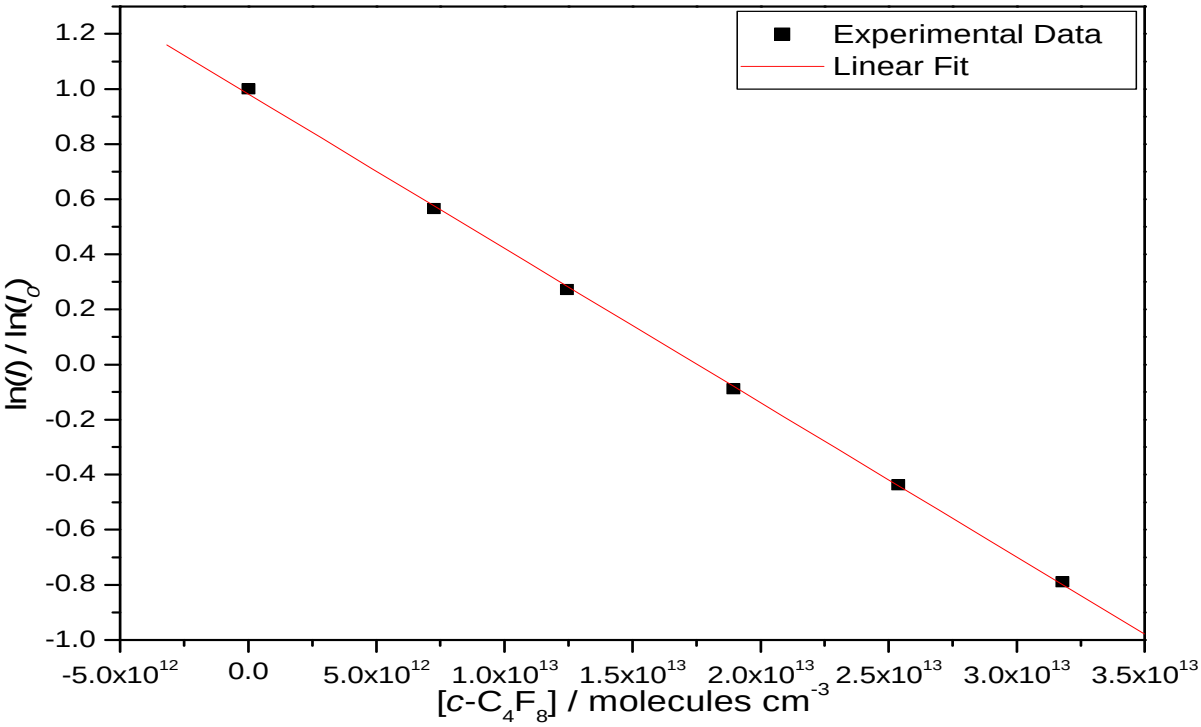

Figure 2.15: Data from Figure 2.14 following Beer-Lambert analysis with a linear fit to the results.

Mass spectra of the product ions from the electron attachment process can also be recorded. Now the electron gate is no longer pulsed. Ion yields can be recorded as a function of attaching gas concentration, or reduced field strength. The effects of CID can be studied by recording the ion yields versus the voltage between the Faraday plate and the sampling cone. By extrapolating the CID voltage to zero any dissociation of the product ions distribution can be allowed for. As in the SIFT experiment allowance is made for any secondary reactions by extrapolating to zero attaching gas concentration. By these means we can be fairly confident that we are getting undistorted branching ratios, except with one caveat; there may be the reactions of anions with neutrals taking place in the drift tube.

Which buffer gas is used will alter subtly the experiments performed. If CO_2 is being used, varying the reduced electron field will not reveal any extra data as the electron energy distribution remains unchanged. If N_2 or Ar are used, then varying E/N can give a wealth of extra data on how the attachment resonances behave with changing electron energy.

4. References

1 D. Smith, N.A. Adams, *Adv. Atom. Mol. Phys.*, **24**, (1988) 1.
2 D.K. Böhme, *Int. J. Mass Spec.*, **200**, (2000) 97.
3 S.T. Graul, R.R. Squires, *Mass Spec. Rev.*, **7**, (1988) 263.
4 G.K. Koyanagi, V.V. Lavrov, V. Baranov, D. Bandura, S. Tanner, J.W. McLaren, D.K. Böhme, *Int. J. Mass. Spec.*, **194**, (2000) L1.
5 J.C. Poutsma, R.A. Seburg, L.J. Chyall, L.S. Sunderlin, B.T. Hill, J. Hu, R.R. Squires, *Rap. Comm. Mass. Spec*, **11**, (1997) 489.
6 X. Yang, X. Zhang, A.W. Castleman, Jr., *Int. J. Mass Spec. Ion Proc.*, **109**, (1991) 339.
7 R.A. Morris, A.A. Viggiano, S.T. Arnold, J.F. Paulson, *Int. J. Mass Spec. Ion Proc.*, **149/150**, (1995) 287.
8 G.K. Jarvis, C.A. Mayhew, R.P. Tuckett, *J, Phys. Chem*, **100**, (1996) 17166.
9 E.E. Ferguson, *J. Phys. Chem.*, **90**, (1986) 731.
10 R.A. Morris, A.A. Viggiano, J.F. Paulson, *J. Phys. Chem.*, **97**, (1993) 6208.
11 A.A. Viggiano, R.A. Morris, F. Dale, J.F. Paulson, E.E. Ferguson, *J. Chem. Phys.*, **90**, (1989) 1648.
12 C. Atterbury, A.D.J. Critchley, R.A. Kennedy, C.A. Mayhew, R.P. Tuckett, *Phys. Chem. Chem. Phys.*, **4**, (2002) 2206.
13 M.W. Chase, *J. Phys. Chem. Ref. Data*, (1998) Monograph no. 9.
14 N.G. Adams, D. Smith, E. Alge, *J. Phys. B*, **13**, (1980) 3235.
15 P. Spanel, M. Tichy, D. Smith, *Int. J. Mass. Spec. Ion Proc.*, **129**, (1993) 155.
16 P.A. Hatherly, D.M. Smith, R.P. Tuckett, *Zeit. Phys. Chem.*, **195**, (1996) 97.
17 D.M. Smith, R.P. Tuckett, K.R. Yoxall, K. Codling, P.A. Hatherly, J.F.M. Aarts, M. Stankiewicz, *J. Chem. Phys.*, **101**, (1994) 10559.
18 D.M.P. Holland, J.B. West, A.A. Macdowell, I.H. Munro, A.G. Beckett, *Nucl. Instrum. Meth. B*, **44**, (1989) 233.
19 C.R. Howle, S. Ali, R.P. Tuckett, D.A. Shaw, J.B. West, *Nuc. Instru. Meth. Phys. Res. B*, **237**, (2005) 656.
20 P.A. Halherly, M. Stankiewiczt, K. Codlingt, J.C. Creasey, H.M. Jones, R.P. Tuckett, *Meas. Sci. Technol.*, **3**, (1992) 891.
21 W.C. Wiley, I.H. McLaren, *Rev. Sci. Instr.*, **26**, (1955) 1150.
22 J.H.D. Eland, *Int. J. Mass Spec.*, **8**, (1971) 143.
23 J.L. Franklin, P.M. Hierl, D.A. Whan, *J. Chem. Phys.*, **47**, (1967) 3148.
24 Y. Liu, C.A. Mayhew, R. Peverall, *Int. J. Mass Spec. Ion Phys.*, **152**, (1996) 225.
25 C.A. Mayhew, A.D.J. Critchley, D.C. Howse, V. Mikhailov, M.A. Parkes, *Eur. Phys. D*, **35**, (2005) 307.
26 G.K. Jarvis, R.A. Kennedy, C.A. Mayhew, *Int. J. Mass Spec.*, **205**, (2001) 253.
27 D.H. Williamson, C.A. Mayhew, W.B. Knighton, E.P. Grimsrud, *J. Chem. Phys.*, **113**, (2000) 11035.
28 M. Tabrizchi, A. Abedi, *J. Phys. Chem. A.*, **108**, (2004) 6319.
29 A. Chutjian, A. Garscadden, J.M. Wadehra, *Phys. Rep.*, **264**, (1996) 393.
30 J.E. Pollard, D.J. Trevor, Y.T. Lee, D.A. Shirley, *Rev. Sci. Instrum.*, **52**, (1981) 1837.
31 J.B. Fenn, *Int. J. Mass Spec.*, **200**, (2000) 459.
32 G.K. Jarvis, C.A. Mayhew, L. Singleton, S.M. Spyrou, *Int. J. Mass Spec. Ion Proc.*, **164**, (1997) 207.
33 I. Szamrej, M. Forys, *Radiat. Phys. Chem.*, **33**, (1989) 393.

34 S.R. Hunter, J.G. Carter, L.G. Christophorou, *J. Chem. Phys.*, **90**, (1989) 4879.

3. Theoretical Studies

The experimental work performed for this thesis has been supported by theoretical studies. An overview of this theoretical work will be given in this chapter.

1. Ion-molecule reactions

1.1 Ion-molecule reaction rate coefficients

1.1.1 Ion-non-polar neutral molecule collisions

Using the selected ion flow tube (SIFT) it is relatively simple to measure experimental reaction rate coefficients (k_{exp}). To aid in interpreting these results from ion-molecule reactions it is useful to know the reaction efficiency. This is simply k_{exp}/k_c, where k_c is the collisional rate coefficient when reaction occurs upon every collision between an ion and a neutral molecule. There are several models to predict k_c which are mostly based upon Langevin theory.[1] This model uses an ion-induced dipole interaction and was formulated in its modern version by Gioumousis and Stevenson.[2]

The model is founded on similar assumptions as the kinetic model of gases. That is, the ion (A^+) and neutral (B) are hard-shell point particles with no internal energy, however, unlike the kinetic model the ion and neutral are interacting. The interaction between the ion and neutral is modelled using the classical ion-induced dipole potential:

$$V(r) = -\frac{\alpha' q^2}{8\pi\varepsilon_0 r^4} \qquad \textbf{(eq 3.1)}$$

Here r is the distance between the ion and neutral, q is the charge on the ion, α' is the polarisability volume of the non-polar neutral molecule, and ε_0 is the permittivity of free space whose value is 8.85×10^{-12} C^2 m^{-1} J^{-1}. The polarisability volume has units of m^3 and is related to the polarisability, α, by:

$$\alpha' = \frac{\alpha}{4\pi\varepsilon_0} \qquad \textbf{(eq 3.2)}$$

α has the complicated SI units of C^2 m^2 J^{-1}, so α' values (in m^3) are used for simplicity. It should be noted that a polarisability reported in c.g.s units has the same value as a polarisability volume

in SI units. In this model, as the ion and neutral approach each other, the charge on the ion induces a dipole in the neutral and this creates an attraction. For the singly charged ions studied in this work, the magnitude of the induced dipole depends on the polarisability of the neutral reactant.

This potential energy can be combined with the potential due to the relative rotation of the two particles to give an effective potential energy given by:

$$V_{eff}(r) = -\frac{\alpha' q^2}{8\pi\varepsilon_0 r^4} + \frac{\mu v^2 b^2}{r^2} \qquad \textbf{(eq 3.3)}$$

where μ is the reduced mass of the interacting system in kg, v is the relative velocity between A^+ and B and b is the impact parameter. Above a critical impact parameter b_c, the total relative energy of the system is less than the energy of the centrifugal barrier, which arises due to conservation of angular momentum in the system, and no reaction can occur. Below b_c, the relative energy is greater than the centrifugal barrier and a collision will take place. Thus all ions that travel through a circle of radius b_c towards the neutral will react. The area of this circle, πb_c^2, is equal to the collisional cross-section for a given velocity. From V_{eff} it is easy to calculate b_c, the collisional cross-section (σ_c), and hence the Langevin collisional rate coefficient (k_{Lan}):

$$\sigma_c = \pi b_c^2 = \pi q \left(\frac{2\alpha'}{4\pi\varepsilon_0 E_r} \right)^{1/2} \qquad \textbf{(eq 3.4)}$$

Note that E_r is the total relative energy of the system with value of $\mu v^2 / 2$. Thus:

$$k_{Lan} = \sigma_c v = v\pi q \left(\frac{4\alpha'}{4\pi\varepsilon_0 \mu v^2} \right)^{1/2} = \pi q \left(\frac{\alpha'}{\pi\varepsilon_0 \mu} \right)^{1/2} \qquad \textbf{(eq 3.5)}$$

Therefore, the temperature dependent cross-section becomes a temperature-independent rate coefficient. This is usually expressed in a simpler form:

$$k_{Lan} = \left(\frac{\pi\alpha' q^2}{\varepsilon_0 \mu} \right)^{1/2} \qquad \textbf{(eq 3.6)}$$

1.1.2 Ion-polar neutral molecule collisions

The Langevin theory has been found to be an excellent model of reactive collisions between ions and non-polar neutral molecules, especially at low energies.[3] However, it has been noted that if the collision partner is a polar neutral molecule then Langevin theory fails, underestimating rate coefficients by a considerable amount. Theard and Hamil[4] and Moran and Hamil[5] determined that if a molecule has a permanent dipole moment then its effect is too large to ignore when calculating collisional cross-sections. Allowance must be made for the ion-dipole interaction in the modelling. This allowance is made by introducing an extra term in the potential representing this ion-dipole interaction:

$$\phi = -\left(\frac{q\mu_D}{4\pi\varepsilon_0 r^2} \right) \cos\,\theta \qquad \textbf{(eq 3.7)}$$

Here μ_D is the permanent dipole moment of the neutral molecule in units of C m. The $\cos\theta$ term arises because the dipole is a vector property and so the interaction depends on the angle between the ion and the direction of the dipole. In initial treatments of the problem, to simplify the complex calculations needed if the dipole rotates freely, θ was set to 0.[4] This assumes that the dipole of the neutral molecule 'locks' completely towards the oncoming ion, and there is no residual relative rotation of the ion-molecule system. This method was called locked dipole (LD), and with a similar derivation to Langevin theory gives rate coefficients with the following formula:

$$k_{LD} \propto \left(\frac{\pi q^2}{\varepsilon_0 \mu} \right)^{1/2} \left[\alpha'^{1/2} + \frac{\mu_D}{v} \right] \qquad \textbf{(eq 3.8)}$$

This rate coefficient depends on the relative velocity of the collision system, and so clearly will depend on temperature. As this is the case *v* can be replaced by a Maxwell-Boltzmann velocity distribution:

$$k_{LD} = \left(\frac{\pi q^2}{\varepsilon_0 \mu} \right)^{1/2} \left[\alpha'^{1/2} + \mu_D \left(\frac{2}{\pi k_B T} \right)^{1/2} \right] \qquad \textbf{(eq 3.9)}$$

where k_B is the Boltzmann constant and T is the temperature in K. The locked dipole gives an upper limit for the ion-dipole collision rate. In practice the systems rotational angular momentum is never fully quenched and the locked dipole model therefore overestimates the reaction rate coefficients. To take account of this rotation a parameter, *c*, was introduced which can take

values between 0 and 1. A value of 0 represents a freely rotating dipole which does not interact with the ion, a value of 1 represents a dipole which is fully 'locked' onto the ion. This model is known as average dipole orientation (ADO) theory:[5]

$$k_{ADO} = \left(\frac{\pi q^2}{\varepsilon_0 \mu}\right)^{1/2}\left[\alpha'^{1/2} + c\mu_D\left(\frac{2}{\pi k_B T}\right)^{1/2}\right] \qquad \textbf{(eq 3.10)}$$

This was then further parameterised by Su to give modified ADO theory (MADO) which is more user friendly.[6,7] To develop MADO Su *et al* used variational transition state theory trajectory methods to model thermal ion-polar molecule collisions.[7] They showed that the ratio of the trajectory rate coefficient (k_{traj}) to k_{Lan} depends on two reduced parameters T_R and I^*:

$$\frac{k_{traj}}{k_{Lan}} = K_{cap}\left(T_R, I^*\right) \qquad \textbf{(eq 3.11)}$$

where $T_R = \frac{2\alpha' k_B T}{\mu_D^2}$ and $I^* = \frac{\mu_D I}{\alpha' q \mu}$ where I is the moment of inertia of the neutral molecule around its principal axis. In a real system I^* is small and K_{cap} is insensitive to its value. From this result Su[6,8] presented parameterised equations to calculate K_{cap}:

$$K_{cap} = \begin{cases} \frac{(x + 0.5090)^2}{10.526} + 0.9754; & x \le 2 \\ 0.4767\,x + 0.6200; & 2 \le x \le 3 \\ 0.5781\,x + 0.3165; & 3 \le x \le 35 \\ 0.6201\,x - 1.153; & 35 \le x \le 60 \\ 0.6347\,x - 2.209; & x \ge 60 \end{cases} \qquad \textbf{(eq 3.12)}$$

where $x = 1/\sqrt{T_R}$ and the MADO rate coefficient (k_{MADO}) is equal to K_{cap} x k_{Lan}. Unless otherwise stated, the rate coefficients in this thesis have been calculated using MADO theory.

1.1.3 Ion-multipolar neutral molecule collisions

For the reactions of *c*-C_4F_8 with a range of cations reported in this thesis (chapter 5) it was found that, in general, $k_{exp} > k_{MADO}$. One possible explanation for why experimental rate coefficients could be greater than calculated rate coefficients is that there is an extra attractive potential between the ion and the neutral molecule. This extra attraction would increase the collision rate between the ion and neutral in the experiment relative to the MADO calculations.

To attempt to model this it was assumed that the extra term was due to an ion-quadrupole potential (ϑ):

$$\vartheta = -\frac{\Theta q\left(3\cos^2\theta - 1\right)}{8\pi\varepsilon_0 r^3} \qquad \textbf{(eq 3.13)}$$

where Θ is the static quadrupole moment of the neutral molecule and θ is the angle the quadrupole axis makes with *r*. It should be noted that many attempts have been made to model the quadrupolar interaction with intermolecular potentials. These attempts have been, in general, unsuccessful.[9] Bhowmik and Su[10] used a trajectory method to derive:

$$k_\Theta = k_{Lan} \times K_{cap} \qquad \textbf{(eq 3.14)}$$

where:

$$K_{cap} = \left\{ \begin{array}{l} 0.627\ \lambda + 0.789\ \text{ Odd Case} \\ 0.573\ \lambda + 0.811\ \text{ Even Case} \end{array} \right\} \lambda > 0.4 \qquad \textbf{(eq 3.15)}$$

and

$$\lambda = \frac{1.12|\Theta|}{\alpha'^{3/4} T^{1/4}} \qquad \textbf{(eq 3.16)}$$

If $\lambda < 0.4$ then K_{cap} can be considered as unity. An 'even' case means that *q* and Θ have the same sign, 'odd ' means they have the opposite sign. This parameterised formula has only been used for calculating the rate coefficients of *c*-C_4F_8.

1.2 Calculation of parameters for neutral molecules

1.2.1 Polarisability

For many neutral molecules studied in this thesis, no data on their polarisability volume is available. One solution to this problem is to calculate the molecular polarisability. This can be done using *ab initio* methods but an easier and very successful method was developed by Miller.[11] Miller's method empirically estimates the average molecular polarisability volume using atomic hybridisation. The formula is:

$$\alpha'(ahc) = \left(\frac{4}{N}\right)\left[\sum_A \tau_A(ahc)\right]^2 \qquad \textbf{(eq 3.17)}$$

Here N is the total number of electrons in the molecule, while τ_A is an atomic hybrid component for each atom A which has been tabulated by Miller. This method estimates values of α' which are comparable with experimentally measured values.

1.2.2 Calculation of multipoles

If the value of a neutral multipole (*e.g.* dipole or quadrupole moments) is not available experimentally, then there is no simple method analogous to Millers method to calculate the value. The only solution is then to use *ab initio* methods. The accuracy of these results therefore depends on how good a representation the structure of the neutral is, the level of theory, and on the quality of the basis set used in the calculation.

2. Threshold photoelectron photoionisation measurements

2.1 Determination of appearance energies at 298 K

From the threshold photoelectron-photoion coincidence (TPEPICO) experiment, energy selected ion yields can be measured and from these the appearance energies at 298 K (AE_{298}) for any fragment ions can be determined. These AE_{298} values can then be converted into the enthalpy change at 298 K for the corresponding unimolecular reaction ($\Delta_r H^0_{298}$). Due to thermal effects, it is not correct to set AE_{298} equal to $\Delta_r H^0_{298}$. Figure 3.1 shows an example of a possible fragmentation pathway and the effect of a change in temperature. At 0 K the first onset of signal for a fragment will correspond to ionisation from the ground state of the reactants (which is all that will be populated at 0 K) to the ground state of the products. This transition is represented by the arrow E_0 in figure 1. If the temperature is increased above 0 K then some fraction of the product molecules will be in excited states. If ionisation occurs from these molecules then the measured appearance energy will be lower than the 0 K value. This transition is indicated by the arrow E_{298} in Figure 3.1.

One method to convert the AE_{298} into $\Delta_r H^0_{298}$ values was developed by Traeger and McLoughlin for photoionisation measurements.[12] They showed that the enthalpy change for the unimolecular reaction $AB + h\nu \rightarrow A^+ + B + e^-$ is related to AE_{298} by:

$$\Delta_r H^0_{298} \leq AE_{298}(A^+) + \int_0^{298} C_p(A^+)dT + \int_0^{298} C_p(B)dT - \frac{5RT}{2} \qquad \textbf{(eq 3.18)}$$

C_p is the heat capacity of a fragment and is calculated using standard statistical thermodynamic equations, whilst the final 5RT / 2 term is due to the translational heat capacity of the parent molecule.

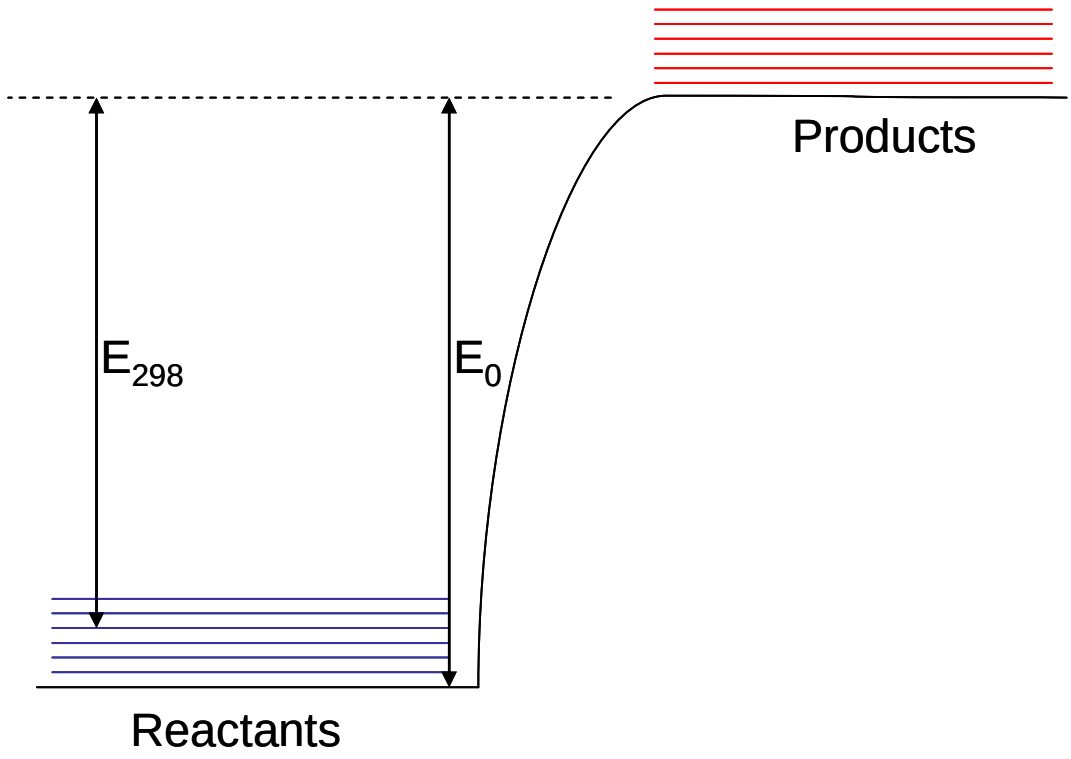

Figure 3.1: Effect of temperature on appearance energies.

For the corrections calculated in this thesis the following equation has been used:

$$H_T^0 = \frac{5RT}{2} + \frac{3RT}{2} + \sum_i \frac{N_a h\nu_i}{\exp\left(\frac{h\nu_i}{k_b T}\right) - 1} \qquad \textbf{(eq 3.19)}$$

This equation sums up all the separate contributions to the enthalpy of a molecule at temperature T from translational and pV work term, rotational and vibrational motion. No correction is needed to convert the IE of the parent to $\Delta_r H^0_{298}$ as the contributions will be essentially the same in both neutral and ion structures.

There are several caveats to the use of the Traeger and McLoughlin method when applied to energy-selected ion yields. Firstly, as stated earlier, the method was developed for photoionisation measurements, whereas the TPEPICO ion yields are the derivative of the photoionisation yields. Secondly, the experimental AE_{298} values should be extracted from an extrapolation of the linear portion of the photoionisation cross-section, rather than from the first

onset of signal as we have determined them by. In all measurements made for this thesis, these two points can be neglected. This is because, with the resolution and step size used, the determination of AE_{298} from the first onset of signal is equivalent to the extrapolation of the linear portion of the photoionisation cross-section. Thirdly, the method is strictly applicable to fragmentations in which only a single bond is broken. The method has still been used in this thesis for some fragments in which more than one bond is broken, as this can indicate what neutral partner is formed during the fragmentation. Notwithstanding these three caveats, we have applied the Traeger and McLoughlin correction, because we believe it introduces more error to neglect thermal effects and assume $AE_{298} = \Delta_r H^0_{298}$.

2.2 Kinetic energy release from unimolecular fragmentation

The TPEPICO experiment detects ions using a time-of-flight (TOF) technique. One of the advantages of such TOF mass spectrometers is that they not only give information of the mass of any ionic products but also their velocity distribution. From an analysis of the TOF peak shapes the kinetic energy of the fragment can then be determined. The size of this kinetic energy release can give insight into the fragmentation mechanism.

The width of a TOF peak represents the distribution of velocities of ions created in the photoionisation event. If the ion detected is the parent ion, rather than a fragment, then the velocity distribution will be simply a thermal distribution. Franklin *et al*[13] have shown that parent ions produce Gaussian peaks whose full width at half maximum (FWHM) can be given by:

$$FWHM = \frac{1.664\left(2k_B T m_P\right)^{1/2}}{\bar{E}} \qquad \textbf{(eq 3.20)}$$

where T is the temperature of the molecule, m_P is the mass of the parent ion, and $\bar{E}$ is the ion extraction field.

More interesting results arise from analysis of the widths of TOF peaks due to daughter ions. These peaks are made of two components: the first is the thermal distribution (eq 3.20) and the second is a 'fission energy' distribution. This 'fission energy' distribution is rectangular and represents the energy released into translation from the breaking of bonds. Analysis of these peaks gives the kinetic energy release distribution (KERD) and from this the mean translational kinetic energy release ($<KE>_t$) for the ionic fragment. Several methods have been suggested to extract such kinematic information, most recently that $<KE>_t$ is proportional to the variance of the TOF peak.[14] However, this method has not been extended to make allowance for the possible

presence of isotopes in a sample. The analysis used in this thesis are based on the method of Powis *et al.*[15] and has been described in detail elsewhere.[16]

A calculation of the KERD is performed in the following manner. Initially a basis set of TOF peaks is calculated. Each peak in this basis set has a discrete energy release ε_t given by:

$$\varepsilon_t = (2n-1)^2 \Delta E \qquad \textbf{(eq 3.21)}$$

where n is a non-zero integer and ΔE is the kinetic energy release into the first TOF peak of this basis set. The number of peaks used in a basis set to fit to the experimental TOF peak depends on the values of n and ΔE used. Each peak is modelled with the two components outlined above. The thermal component is modelled with eq 3.20, the 'fission energy' distribution with the following equation:

$$FWHM \propto \frac{(m_D \varepsilon_t(n))^{1/2}}{\overline{E}} \qquad \textbf{(eq 3.22)}$$

Here m_D is the mass of the fragment ion. Each peak in the basis set is assigned a reduced probability, defined as the probability of a given energy release divided by the range of energies. The probability of each peak is varied using linear regression methods to get the best fit to the experimental data. This fitting gives the KERD and $\langle KE \rangle_{ion}$, the kinetic energy of the ionic product. Although the KERD is often found to be dependent on the values of n and ΔE used, $\langle KE \rangle_{ion}$ is usually independent. Thus $\langle KE \rangle_{ion}$ can be converted into a $\langle KE \rangle_t$ value:

$$\langle KE \rangle_t = \left(1 + \frac{m_{ion}}{m_{neutral}}\right) \langle KE \rangle_{ion} \qquad \textbf{(eq 3.23)}$$

where m_{ion} and $m_{neutral}$ are the masses of the two products formed in the fragmentation process. The fitting procedure takes into account contribution from any isotopes in the fragment ion. To do this, each peak in the basis set is made up of more than one peak representing the different isotopomers in the appropriate statistical ratio.

Once $\langle KE \rangle_t$ has been calculated, careful examination of its value can give insight into the type of fragmentation mechanism that has taken place. To do this $\langle KE \rangle_t$ is divided by the energy available (E_{av}) to give the fraction of energy that is channelled into translation of the fragments ($\langle f \rangle_t$). E_{av} is equal to the incident photon energy plus the thermal energy of the parent molecule minus the thermochemical threshold to form the fragment. The parent thermal energies are due to rotations and vibrations and are calculated using statistical thermodynamics. Experimental values of $\langle f \rangle_t$ can then be compared to theoretically calculated values from both impulsive and statistical models. This comparison can suggest whether the fragmentation is impulsive or statistical.

Impulsive models assume that the fragmentation occurs on a timescale which is quick compared to intramolecular vibrational redistribution (IVR) or electronic relaxation. This means that the majority of the energy released from the fragmentation goes into translational energy between the fragments. In this model $\langle f \rangle_t$ can be estimated from the simple relationship given by Holdy *et al*:[17]

$$\langle f \rangle_t = \frac{\langle KE \rangle_t}{E_{av}} = \frac{\mu_B}{\mu_f} \qquad \textbf{(eq 3.24)}$$

where μ_B is the reduced mass of the two atoms whose bond is broken and μ_f is the reduced mass of the two products formed from the fragmentation.

Statistical models assume that, after initial photoexcitation of the ion, enough time occurs before fragmentation that complete relaxation occurs to the electronic ground state of the ion. This results in low kinetic energy releases as the initial excitation energy is shared between all the different modes of the molecule. From quasi-equilibrium theory coupled to Langevin collision theory for the reverse bimolecular reaction, Klots[18] derived the following relationship between E_{av} and $\langle KE \rangle_t$:

$$E_{av} = k_B T^* + \frac{(R-1)}{2} k_B T^* + \sum_i \frac{h\nu_i}{\exp\left(\frac{h\nu_i}{k_B T^*}\right) - 1} \qquad \textbf{(eq 3.25)}$$

where T^* is a microcanonical temperature defined simply as $T^* = \langle KE \rangle_t / k_B$. This microcanonical distribution will have a different distribution to the true canonical distribution but will have the same average energy.[19] This equation is for loose transition states. For tight transition states the R–1 term is replaced by R–2.[18] A lower limit for $\langle f \rangle_t$ from statistical fragmentations can be estimated from $1/(x+1)$, where x is the number of vibrational degrees of freedom in the transition state (TS). This can be calculated from 3N-7, where N is the number of atoms in the TS.[20]

2.3 Unimolecular dissociation modelled by Rice Ramsperger Kassel and Marcus (RRKM) methods

If fragmentation of photoexcited ions occurs statistically then it can be modelled using the RRKM method. As this is a well established technique with many books on the subject,[19] only brief details will be given here. This model is statistical in basis and assumes that the internal energy of the ion is randomly distributed into all modes of the electronic ground state of the ion

prior to dissociation. It also assumes that there is some point on the potential energy surface which completely separates the products and reactants, *i.e.* a TS. In the TS one of the vibrational modes of the reactant has transformed into a translation between the product fragments. For example if the molecule is ABC then in the TS $[AB\text{-}C]^{\ddagger}$ the B-C bond will now break instead of vibrating. Dissociation occurs when enough energy becomes concentrated into this dissociating mode to break the bond and lead to the separation of B and C. How the energy becomes distributed into this mode depends on the density of states of the dissociating species, essentially how many states are available for the energy to be shared into. The more states there are the less likely it is the energy will enter the fragmentation mode. It also depends on how many states there are in the transition state above the dissociation threshold. The general expression to calculate the unimolecular rate is:

$$k(E) = \alpha(E)\sigma\frac{G(E-E_0)}{hN(E)} \qquad \textbf{(eq 3.26)}$$

where $\alpha(E)$ is the transmission coefficient which allows for tunnelling effects close to threshold, it is set to 1 for most cases studied, and σ is the reaction symmetry which allows for fragmentation to occur in more than one way. E_0 is the energetic threshold for the fragmentation process. $G(E\text{-}E_0)$ is the sum of states of the transition state relative to threshold, for semiclassical rovibrational states it is given by:

$$G_{v,r} = \frac{\left(E-E_0\right)^{v-\frac{r}{2}}}{h^{v-r}\prod_{j}^{v-r}\nu_j} \qquad \textbf{(eq 3.27)}$$

In eq 3.27, v and r are the vibrational frequencies and number of rotations in the transition state. It should be noted that the number of vibrational frequencies in the transition state is reduced by one compared to the fragmenting molecule. $N(E)$ is the density of states of the fragmenting species at the exciting energy E, given by:

$$N_{v,r} = \frac{E^{(v-1)-\frac{r}{2}}}{h^{v-r}\prod_{j}^{v-r}\nu_j} \qquad \textbf{(eq 3.28)}$$

Here v and r are the vibrational frequencies and number of rotations in the fragmenting species.

In this thesis $k(E)$ is evaluated using a steepest descent method rather than a direct count method, based on a programme outlined in the book of Baer and Hase.[19] This method is more approximate than the direct count method, mainly as it assumes that $G_{v,r}$ is a continuous function

when quantum mechanically it is a series of step functions. However, above 500 cm^{-1} steepest descent is found to give excellent agreement with the direct count method, and is much simpler to use and implement. Examples of use of this method is given in appendix 1.

Once the rate for unimolecular dissociation has been calculated then a breakdown diagram can be calculated. By varying E_0 until the experimental and theoretical breakdown diagrams agree, the actual dissociation threshold can be obtained without any contributing kinetic shift.

3. Electron attachment reactions

3.1. Attachment rate coefficients

Although several attempts have been made to calculate electron attachment cross-sections and rate coefficients, arguably the results in this field have not been as successful as for calculating ion-molecule reaction rate coefficients. Best results have been achieved using complicated *ab initio* R-matrix methods.[21] In theory the Langevin model should be applicable to modelling the electron attachment process. Here the ion would be replaced by the electron. However, in practise the Langevin model fails when applied to electron attachment. The reason for this is the de Broglie wavelength (more correctly its square) is comparable to the collision cross-section for electron attachment, and quantum effects cannot be ignored in this situation.[22] One of the first attempts to solve this problem was made by Vogt and Wannier.[22] Starting from the Langevin model they used quantum mechanical calculations to show that the collision cross-section, in the limit of the electron energy $\varepsilon \rightarrow 0$, is twice the Langevin value and can be written in the form:

$$\sigma_c = 4\pi a_0^2 \left(\frac{\alpha' R_H}{a_0^3 \varepsilon} \right)^{1/2} \qquad \textbf{(eq 3.29)}$$

where a_0 is the Bohr radius (5.292 x 10^{-11} m) and R_H is the Rydberg energy (2.180 x 10^{-18} J). This formula was then used by Klots[23] who proposed the following analytical form which assumes that *s*-wave capture is the dominate mechanism:

$$\sigma_c = \left(\frac{\pi R_H a_0^2}{\varepsilon} \right)^{1/2} \left(1 - \exp\left[-4 \left(\frac{\alpha' \varepsilon}{a_0^3 R_H} \right)^{1/2} \right] \right) \qquad \textbf{(eq 3.30)}$$

This form agrees well with the Vogt and Wannier model as $\varepsilon \to 0$, and can be extended to give the geometric cross-section as ε increases. From this the thermal rate coefficient for electron attachment (k_a) is given by:

$$k_a(\varepsilon) = \frac{2}{m_e}\int_0^{\infty} \sigma(\varepsilon)\varepsilon^{1/2} f(\varepsilon) d\varepsilon \qquad \textbf{(eq 3.31)}$$

where $f(\varepsilon)d\varepsilon$ is the electron energy distribution, which, for a thermal rate, is taken to be a Maxwell velocity distribution:

$$f(\varepsilon)d\varepsilon = 2\pi\left(\frac{1}{\pi k_b T}\right)^{3/2} \varepsilon^{1/2} \exp\left[-\frac{\varepsilon}{k_b T}\right] d\varepsilon \qquad \textbf{(eq 3.32)}$$

Any calculations of attachment rates have been made using this *s*-wave model. An extension of the Vogt and Wannier model has been suggested called the extended Vogt Wannier model.[21] This makes allowances for the presence of a dipole moment in the neutral molecule. This model has not been used because it is only for dipole moments below a critical threshold, 1.625 D. The only molecule for which EA was studied in this thesis which has a known dipole moment is *c*-C_5F_8. The dipole moment of *c*-C_5F_8 has a value above the critical dipole moment and so use of the extended model is inappropriate.

4. *ab initio* calculations

4.1 Standard calculations

To aid in interpretation of the experimental results a project was initiated to use *ab initio* procedures to calculate important molecular properties. These *ab initio* calculations were performed using the commercial quantum chemistry package Gaussian 03.[24] This package allows easy access to high-level *ab initio* techniques. For all calculations performed the following general method was used:

1. An initial molecular structure is generated using experimental structural parameters. If experimental data is not available then the parameters will be a first guess.
2. This initial structure is then optimised using the Hartree-Fock (HF) level of theory.
3. The structure from this calculation is then optimised using Density Functional Theory (DFT) with a B3LYP functional.

4. Finally the DFT structure is optimised using second order Møller-Plesset perturbation theory (MP2).

It is this MP2 structure which is then used for further analysis, and if necessary this optimisation can be continued to higher levels of theory, *e.g.* MP3. In general the calculations are performed using a G-311G + (d,p) basis set, as this gives a good balance of quality of results to calculation time. No attempt is made to correct for use of a finite basis set.

Many useful molecule properties can be extracted from the final structure. The most relevant properties to the work presented in this thesis are the molecular structure itself; the detailed information on molecular orbitals (MO) such as orbital symmetry, eigenvalues and MO coefficients; and values for the molecules multipoles and harmonic frequencies.

4.2 Calculation of ionisation energies

For comparison to the TPEPICO results it is useful to know the ionisation energy of each orbital (IE). A simple method to arrive at this value is to take the energy of the highest occupied molecular orbital as the IE. This is the basis of Koopmans' Theorem. This theory assumes that there is no change in the MOs when going from the neutral to the ion; this includes the idea that the relativistic effects and electron correlation energies are the same in both ion and neutral. Clearly these assumptions are not correct. Electron correlation depends largely on interactions between pairs of electrons. Therefore, the removal of an electron will change the correlation energy. If only outer electrons are removed it is likely that relativistic effects will be similar between ion and neutral, but core electrons have massive kinetic energies and hence will have large relativistic effects. Finally, if an electron is removed then all the MOs will be changed as there will be a rearrangement of the one-electron wavefunctions. These problems have been realised for a long time.[25] Koopmans' theorem is strictly true only for HF calculations though it has been reformulated for calculations performed using DFT.[26] An improvement over Koopmans' theorem is to calculate the energy of the neutral molecule and the energy of the cation. The difference in energies is then the IE. However, this method will give energies which are too low in value, and can lead to difficulties for the relative ordering of the MOs.[25]

Currently one of the best methods to calculate IEs is to use Outer Valence Green's Functions (OVGF). This is an electron propagating technique in which the electrons wavefunction is propagated and the poles of the Green's function represent the binding

energies.[27] This method calculates the IE directly, without recourse to subtracting two calculated energy values from each other. A version of the OVGF method is implemented in Gaussian 03, and this has been used to calculate the vertical IE for molecules studied in this thesis. The OVGF calculations are only applicable to outer valence electrons and so Gaussian 03 operates a cut-off of 20 eV above which it will not calculate the IE of the orbitals. This cut-off is applied to an initial first-iteration IE, before further more complicated calculations are performed. Because of this imposed threshold, some orbitals which lie below 20 eV will not be calculated as the initial guess places them above the cut-off. Green's functions have also been applied to inner valence processes which take into accounts the effect of valence holes on the IE.[28,29] It should also be noted that OVGF is only useable at the HF level of theory in Gaussian 03.

4.3 Calculation in support of the Traeger and McLoughlin correction

The calculation of the Traeger and McLoughlin correction (section 3.1) requires that the vibrational frequencies of the fragments are known. In many case, especially for ions, these frequencies are unknown. To solve this the vibrational frequencies were calculated using Gaussian 03. The calculations have all been performed using DFT B3YLP with a 6-311G + (d,p) basis set.

4.4 Calculation of unknown enthalpies of formation.

For the work on *c*-C_5F_8 it was found that no value existed for the enthalpy of formation of the neutral molecule. This made interpretation of the results from both the SIFT and TPEPICO experiments difficult. To this end attempts have been made to calculate $\Delta_f H^0_{298}$[*c*-C_5F_8]. Following advice given by Dr Jeremy Harvey of the University of Bristol the following method was used.[30] DFT B3LYP calculations were performed on a series of perfluorocarbons such as CF_3, C_2F_4 and *c*-C_4F_8 (see appendix 2 for a full list) to provide the calculated enthalpy of formation ($\Delta_f H^0_{calc}$). This value was also calculated for *c*-C_5F_8. A series of reactions were then written for which *c*-C_5F_8 was a product. For example:

$$3C_2F_4 \rightarrow c\text{-}C_5F_8 + CF_4 \qquad \textbf{(Re 3.1)}$$

Using Hess' cycles the $\Delta_r H^0_{calc}$ values for these reactions was calculated. For example if $\Delta_f H^0_{calc}$ = –475.6, –989.4 and –437.6 Hartrees for C_2F_4, *c*-C_5F_8 and CF_4, respectively, then $\Delta_r H^0_{calc}$ =

−358.9 kJ mol^{-1}. Values were then taken from the literature for values of $\Delta_f H^0_{calc}$ which were reliable. That is performed using high level theories and with allowance made for errors, such as extrapolating to the basis set limit. Most of the numbers were taken from the work of Bauschlicher *et al*,[31-34] where the errors in the these literature values are suggested to be ~ 8 kJ mol^{-1}. Using the value for $\Delta_r H^0_{calc}$ taken from our calculations and the literature values for $\Delta_f H^0_{calc}$ then using a second Hess' cycle a value for $\Delta_f H^0_{298}$[*c*-C_5F_8] could be arrived at. So for the example shown in reaction 3.1 from the work of Bauschlicher the calculated enthalpies of formation are -677 and -933 kJ mol^{-1} for C_2F_4 and CF_4. Using these numbers with our calculated enthalpy of reaction, for reaction 3.1 gives $\Delta_f H^0_{298}$[*c*-C_5F_8] = −1455.5 kJ mol^{-1}. A total of nine reactions were studied in this way to arrive at an average value of $\Delta_f H^0_{298}$[*c*-C_5F_8] of −1495 ± 20 kJ mol^{-1}. The error of 20 kJ mol^{-1} is considered to be conservative. This value seems reasonable as the experimental enthalpy of formation for *c*-C_4F_8 is −1515 kJ mol^{-1}.[35]

After the success of this calculation a similar method was used to calculate $\Delta_f H^0_{298}$[*c*-C_5F_7] which was then combined with a calculated IE to give $\Delta_f H^0_{298}$[*c*-$C_5F_7^+$]. This gave a value of −173 ± 50 kJ mol^{-1}.

4.5 Transition state calculations

To calculate the RRKM rate of unimolecular dissociation (section 2.3) it is necessary to know the sum of states in the TS. This requires knowledge of the TS vibrations. To acquire this information TS calculations were performed using Gaussian 03. The optimisation was performed to find a Berny-TS. An optimised structure was considered a TS if only a single frequency was imaginary.

5. References

1 P.M. Langevin, *Ann. Chim. Phys.*, **5**, (1905) 245.
2 G. Gioumousis, D.P. Stevenson, *J. Chem. Phys.*, **29**, (1958) 294.
3 J.H. Futrell, T.O. Tiernan, *Science*, **162**, (1968) 415.
4 T.W. Moran, W.H. Hamill, *J. Chem. Phys.*, **39**, (1963) 1413.
5 T. Su, M.T. Bowers, *J. Chem. Phys.*, **58**, (1973) 3027.
6 T. Su, *J. Chem. Phys.*, **89**, (1988) 5355.
7 T. Su, W.J. Chesnavich, *J. Chem. Phys.*, **76**, (1982) 5183.
8 T. Su, *J. Chem. Phys.*, **88**, (1988) 4102.
9 G. Ritchie, *Private Communication*, **2006**
10 P.K. Bhowmik, T. Su, *J. Chem. Phys.*, **94**, (1991) 6444.
11 K.J. Miller, *J. Am. Chem. Soc.*, **112**, (1990) 8533.
12 J.C. Traeger, R.G. McLoughlin, *J. Am. Chem. Soc.*, **103**, (1981) 3647.
13 J.L. Franklin, P.M. Hierl, D.A. Whan, *J. Chem. Phys.*, **47**, (1967) 3148.
14 F. von Busch, *J. Phys. B*, **34**, (2001) 431.
15 I. Powis, P.I. Mansell, C.J. Danby, *Int. J. Mass Spec. Ion Phys.*, **32**, (1979) 15.
16 G.K. Jarvis, D.P. Seccombe, R.P. Tuckett, *Chem. Phys. Letts.*, **315**, (1999) 287.
17 K.E. Holdy, L.C. Klotz, K.R. Wilson, *J. Chem. Phys.*, **52**, (1970) 4588.
18 C.E. Klots, *J. Chem. Phys.*, **58**, (1973) 5364.
19 T. Baer, W.L. Hase: *Unimolecular Reaction Dynamics: Theory and Experiments*, Oxford University Press, New York, (1996).
20 J.L. Franklin, *Science*, **193**, (1976) 725.
21 H. Hotop, M.-W. Ruf, M. Allan, I.I. Fabrikant, *Adv. Atom. Mol. Phys.*, **49**, (2003) 85.
22 E. Vogt, G.H. Wannier, *Phys. Rev.*, **95**, (1954) 1190.
23 C.E. Klots, *Chem. Phys. Letts.*, **38**, (1976) 61.
24 Gaussian 3, *Revision C.02*, M.J. Frisch, G.W. Trucks, H.B. Schlegel, G.E. Scuseria, M.A. Robb, J.R. Cheeseman, J.A.M. Jr., T. Vreven, K.N. Kudin, J.C. Burant, J.M. Millam, S.S. Iyengar, J. Tomasi, V. Barone, B. Mennucci, M. Cossi, G. Scalmani, N. Rega, G.A. Petersson, H. Nakatsuji, M. Hada, M. Ehara, K. Toyota, R. Fukuda, J. Hasegawa, M. Ishida, T. Nakajima, Y. Honda, O. Kitao, H. Nakai, M. Klene, X. Li, J. E. Knox, H. P. Hratchian, J. B. Cross, V. Bakken, C. Adamo, J. Jaramillo, R. Gomperts, R. E. Stratmann, O. Yazyev, A. J. Austin, R. Cammi, C. Pomelli, J. W. Ochterski, P. Y. Ayala, K. Morokuma, G. A. Voth, P. Salvador, J. J. Dannenberg, V. G. Zakrzewski, S. Dapprich, A. D. Daniels, M. C. Strain, O. Farkas, D. K. Malick, A. D. Rabuck, K. Raghavachari, J. B. Foresman, J. V. Ortiz, Q. Cui, A. G. Baboul, S. Clifford, J. Cioslowski, B. B. Stefanov, G. Liu, A. Liashenko, P. Piskorz, I. Komaromi, R. L. Martin, D. J. Fox, T. Keith, M. A. Al-Laham, C. Y. Peng, A. Nanayakkara, M. Challacombe, P. M. W. Gill, B. Johnson, M. W. Chen, W. Wong, C. Gonzalez, J.A. Pople, Gaussian Inc., Wallingford CT, 2004
25 W.G. Richards, *Int. J. Mass Spec. Ion Phys.*, **2**, (1969) 419.
26 J.L.Z.Q. Xue, W.M. Liu, J.L. Wu, Z.Q. Yang, *J. Phys. Chem. A*, **110**, (2006) 12005.
27 V.G. Zakrzewski, V. Ortiz, J.A. Nichols, D. Heryadi, D.L. Yeager, J.T. Golab, *Int. J. Quant. Chem.*, **60**, (1995) 29.
28 J. Schirmert, W. Domcket, L.S. Cederbaumt, W.v. Niessen, *J. Phys. B*, **11**, (1978) 1901.
29 J. Schirmer, L.S. Cederbaum, *J. Phys. B*, **11**, (1978) 1889.
30 J. Harvey, *Private Communication*, **2006**
31 C.W. Bauschlicher, A. Ricca, *J. Phys. Chem. A*, **104**, (2000) 9026.

32 C.W. Bauschlicher, A. Ricca, *J. Phys. Chem. A*, **104**, (2000) 4581.
33 A. Ricca, *J. Phys. Chem.*, **103**, (1999) 1876.
34 C.W. Bauschlicher, A. Ricca, *Chem. Phys. Letts*, **315**, (1999) 449.
35 S.W. Benson, H.E. O'Neal, *Natl. Stand. Ref. Data Ser.*, (1970) NBS.

Chapter 4: Fluoroform

1. Introduction

Fluoroform (CHF_3), or more formally trifluoromethane, is a major industrial gas. It is now often used to replace common feedgases, such as $CHBr_3$, $CHCl_3$ and CF_4, in plasma applications.[1] All four gases are, like most halocarbons, greenhouse gases and thus contribute to global warming. In addition $CHBr_3$ and $CHCl_3$ are serious ozone depleters. CHF_3 has neither Br nor Cl atoms in its structure, so does not deplete ozone.[2] With respect to CF_4, CHF_3 has about twice the global warming potential over a hundred year period, however the lifetime of CHF_3 is far shorter (~ 250 yrs *cf* 50,000 yrs),[3] this suggests that CHF_3 has much stronger IR transitions than CF_4. This large difference in lifetimes is due to the presence of a H atom on CHF_3, which allows reaction with OH in the troposphere.[2] Taken together these points show why CHF_3 is an ideal replacement gas.

Not only is CHF_3 important for industrial, but also for more fundamental reasons. CHF_3 is a small molecule and can be considered part of several homologous chemical series. It is part of the CH_nF_{4-n} and the CXF_3 (where X is a halogen or hydrogen atom) series, as well as other series with various combinations of hydrogen and halogen atoms. As such, CHF_3 forms a keystone in examining the effect of atomic substitution on the chemical properties of molecules. For these reasons it is important to understand the properties of this molecule under photon, electron and ion impact.

Many of these studies have been performed previously. There have been several on the interaction of electrons with CHF_3 which have been collected and summarised by Christophorou and Olthoff.[4] Previously, low energy electron attachment to CHF_3 have been studied in this laboratory,[5] however, it was not possible to measure the attachment rate ($<10^{-14}$ cm^3 $molecule^{-1}$ s^{-1}). This is consistent with results from several different experiments.[4] Electron ionisation has been extensively studied[6-9] and there has also been measurement of an electron energy loss spectrum.[10] A study of positron impact has also been performed.[11]

There are also extensive photon studies. Many VUV photoelectron studies have been performed,[12-19] as well as the measurement of the VUV absorption spectrum.[20-23] From microwave spectroscopy the structure of CHF_3 has been determined and the IR vibrations are well known.[24,25] No previous threshold photoelectron spectrum has been reported though there is

a report of two photoionisation studies.[26,27] One of these only reports onset of ionisation, the other is at a higher energy than is studied here. Several groups have studied the fluorescence following excitation of CHF_3. Excitation methods have included photoionisation, high energy ion impact and electron impact studies.[28-30]

It is surprising to find that only a limited amount of work has been done on the reaction of CHF_3 with gas-phase ions.[1,31-35] Of these studies most are interested in reactions with plasma-type reactant ions and two are anion studies. In our work we present a threshold coincidence study of CHF_3 and a study of its reactions with a range of industrially- and atmospherically-important gases in a selected ion flow tube.[36]

2. Experimental

Both sets of apparatus were described in chapter 2. The acquisition of the CHF_3 TPEPICO data was performed several years ago at the Daresbury SRS. The coincidence experiment was performed on beamline 3.1 using the now decommissioned 1m Seya-Namika monochromator, the threshold photoelectron spectra (TPES) was recorded on beamline 3.2 (5m McPherson monochromator). This chapter provides the first analysis of this older data. Fluoroform was from Air Products with a stated purity of 99.25 %. It was used without any further purification.

3. Energetics

As discussed in chapter 3, the method of Traeger and McLoughlin is used to convert appearance energies (AE_{298}) to upper limits for $\Delta_r H^\circ_{298}$ for the major fragment ions.[37] The vibrational frequencies of the two major fragments (CF_3^+ and CHF_2^+) were not available so they have been calculated using *ab initio* methods set out in section 4 of chapter 3. All enthalpies of formation were taken from the standard sources,[38,39] apart from values for CF_3 (-466 kJ mol^{-1}), CF_3^+ (406 kJ mol^{-1}),[40] CHF_2^+ (604 kJ mol^{-1}),[41] FOCO (-356 kJ mol^{-1})[42] and HOCO (-179 kJ mol^{-1}).[43] These last two results are both from *ab initio* calculations for the lower energy trans isomer. *Ab initio* calculations have been performed on CHF_3 using Gaussian 03 as outlined in chapter 3 to obtain the eigenvalues and characters of the molecular orbitals (MO) and their ionisation energies (IE).

4. Results

4.1 Threshold photoelectron photoion coincidence results

4.1.1 Threshold photoelectron spectrum

Figure 4.1(a) shows the TPES of CHF_3 recorded on beamline 3.2 from 13.5 – 24.5 eV at an optical resolution of 0.15 nm. Figure 4.1(b) shows the total ion yield recorded on beamline 3.1 with an optical resolution of 0.3 nm. The onset of ionisation is 13.85 ± 0.05 eV, in excellent agreement with Brundle *et al*.[18] and an old spectroscopic value.[20] CHF_3 has C_{3v} symmetry and in this point group the MOs are labelled as:

$….(4a_1)^2\ (5a_1)^2\ (3e)^4\ (4e)^4\ (5e)^4\ (1a_2)^2\ (6a_1)^2$.

this numbering includes all the core orbitals. From our MP2 calculations statements can be made on which atomic orbitals contribute to the each MO and this can help in understanding why particular fragmentation patterns occur. The $6a_1$ highest occupied molecular orbital (HOMO) is largely $\sigma_{C\text{-}H}$ bonding with some $\sigma_{C\text{-}F}$ contribution. The $1a_2$ orbital is F 2pπ non-bonding, whilst the 5e, 4e and 3e are $\sigma_{C\text{-}F}$ bonding. The $5a_1$ orbital is also $\sigma_{C\text{-}F}$ bonding, the $4a_1$ orbital is of mixed bonding character.

At the optical resolution used for the measurement of the TPES clearly-resolved vibrational structure is observed on the low energy side of the $\tilde{D}/\tilde{E}$ band. Figure 4.2 shows an expanded view of this band at 20.74 eV with the vibrations indicated. There is one long progression with an average spacing of 0.056 eV (455 cm^{-1}). Potts *et al* also saw vibrations in the He(I) spectrum of this band with a mean spacing of 480 cm^{-1} which they assigned to a $\nu_6(a_1)$ symmetrical CF_3 deformation.[17] This state not only supports vibrational levels but also fluoresces,[28,29,44] suggesting that this electronic state of CHF_3^+ is bound and decays radiatively. This has also been seen for the equivalent state of CF_4^+.[45] A photoion fluorescence coincidence study showed that photons emitted from this state were in coincidence with ions at around 50 amu, it was not possible to determine if the ion was mass 50 (i.e. CF_2^+) or 51 (i.e. CHF_2^+) in this experiment, though greater weight was placed on it been mass 51.[29] Thus fluorescence occurs from the bound $\tilde{D}\ ^2E$ state of CHF_3^+ to lower electronic states which are dissociative and form either $CF_2^+ + H + F$ (or HF) or $CHF_2^+ + F$. The lifetime of this state was determined by Biehl *et al* to be 12.6 ns.[28] Our TPEPICO data, however, shows that the main fragment produced from this state is not CHF_2^+ (or CF_2^+), but CF^+ (section 4.1.2). We conclude that the dominant decay

channel of the $\tilde{D}/\tilde{E}$ state of CHF_3^+ is non-radiative, and the competing radiative channel has a small quantum yield.

Table 4.1 lists both the experimental vertical ionisation energies and those calculated by the outer valence Greens' functions (OVGF) method for the HOMO and next five valence MOs of fluoroform. The values in brackets in the OVGF columns are the calculated pole strengths of the ionisation process. There is no calculated VIE for $\tilde{D}/\tilde{E}$ because Gaussian 03 does not run the OVGF calculations for values greater than 20 eV. These OVGF values are plotted along the TPES in Figure 4.1(a), in the spectra the pole strengths have been normalised to the height of the $\tilde{X}$ state. As can be seen, the agreement between the poles and the experimental VIE is not very good, especially when compared to other OVGF calculations we have performed (see especially chapter 5 on *c*-C_4F_8). This is even more surprising given the relative simplicity and small number of electrons in CHF_3.

The positions and assignments of these peaks agree well with results from previous non-threshold photoelectron studies,[12-19] but with one major difference. Under threshold conditions a broad band is observed at 19.22 eV. This band has not been seen in previous photoelectron studies, undoubtedly because they are all non-resonant. The peak, must therefore, arise due to autoionisation of a Rydberg state of CHF_3. In a recent absorption study a peak is observed at 19.19 eV.[23] This peak is assigned to the $(4a_1)^{-1}$3s Rydberg state, whilst at a slightly lower resolution Wu *et al* assigned the peak as the (3e or $5a_1)^{-1}$3d transition.[21]

The total ion yield of CHF_3 is shown in Figure 4.1 (b). Interestingly there are extra peaks in the ion yield curve compared to the TPES, a clear example being the peak above 22 eV. As these peaks are not seen in the TPES, it is likely that they are due to electronic autoionisation from super-excited states. The apparent absence of ion yield in the region of the X state of CHF_3^+ is probably due to scaling.

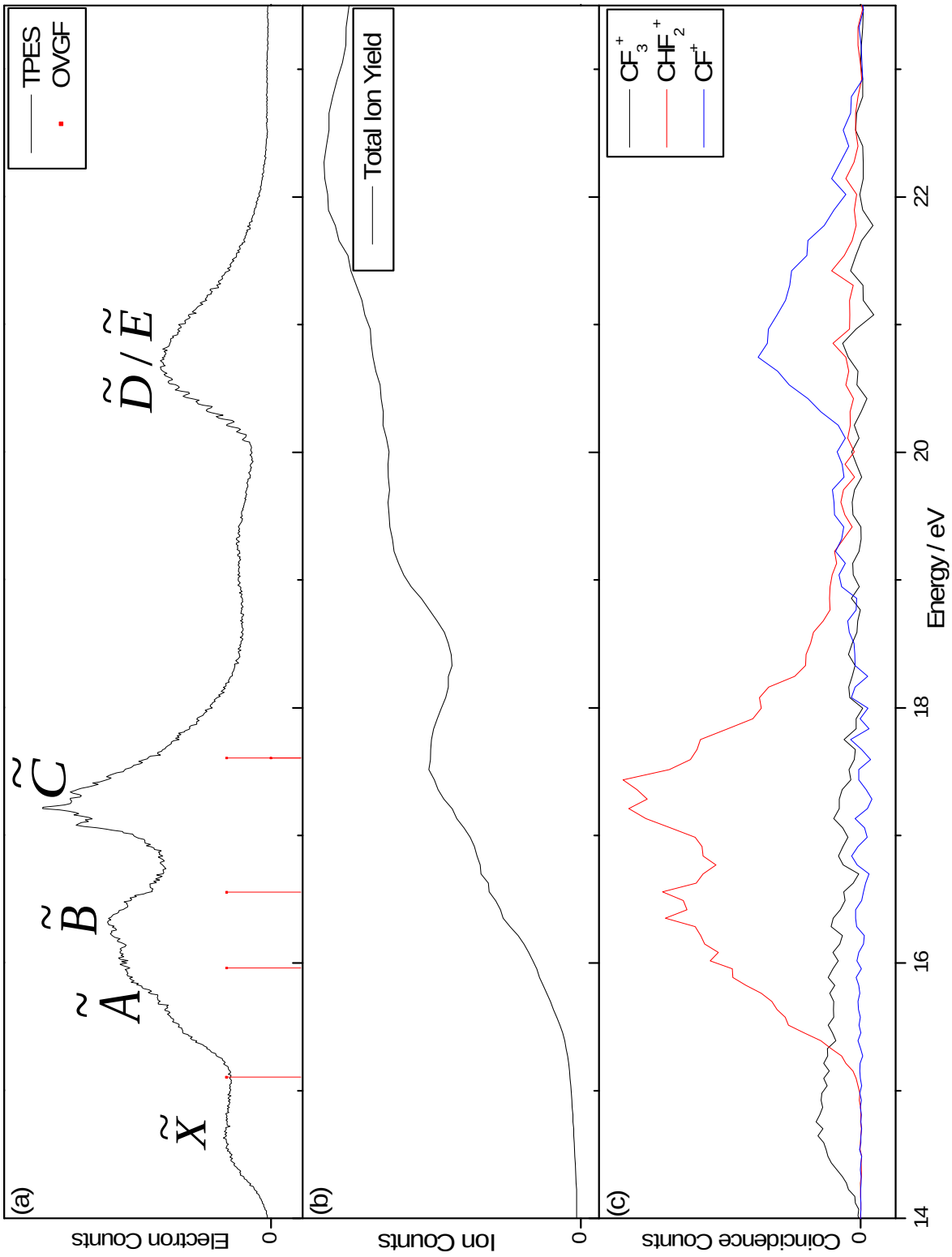

Figure 4.1: (a) Threshold photoelectron spectrum of CHF_3, resolution 0.15 nm. Red drop lines are IE calculated using the OVGF method (b) Total ion yield, resolution 0.3 nm (c) TPEPICO coincidence ion yields of CF_3^+, CHF_2^+ and CF^+, optical resolution of 0.3 nm.

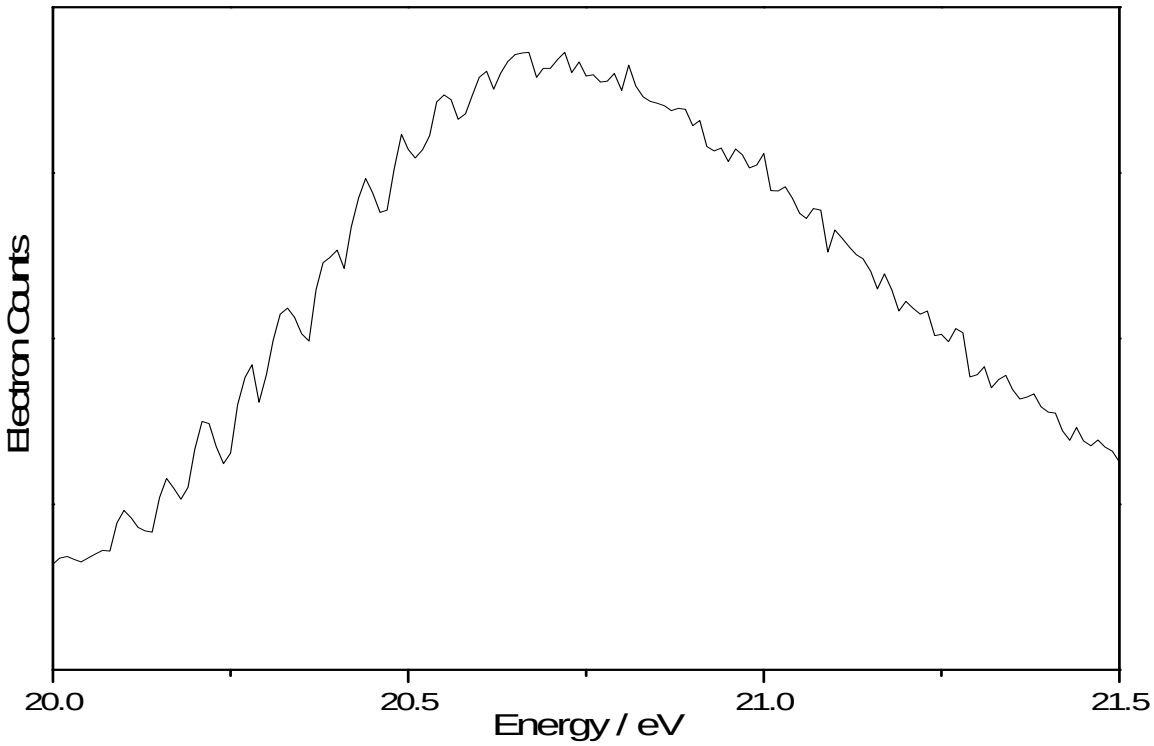

Figure 4.2: Vibrational structure of the $\tilde{D}/\tilde{E}$ peak.

Table 4.1: Experimental and theoretical VIE for fluoroform.

State	VIE / eV	OVGF / eV
$\tilde{X}$ (A_1)	14.81	15.11 (0.936)
$\tilde{A}$ (A_2)	15.57	15.96 (0.933)
$\tilde{B}$ (E)	16.35	16.56 (0.933)
$\tilde{C}$ (E)	17.28	17.61 (0.932)
$\tilde{D}/\tilde{E}$ (E/A_1)	20.74	-

4.1.2 Scanning TPEPICO spectrum

A scanning-energy TPEPICO spectrum was recorded for CHF_3 on beamline 3.1 from 13.5 – 24.5 eV with an optical resolution of 0.3 nm and a TOF resolution of 16 ns. Fragment ion yields are shown in Figure 4.1(c). As explained in chapter 2 it can be difficult to determine whether there is any hydrogen loss in the TOF spectrometer of the coincidence apparatus. However with a resolution of 16 ns it can be stated with confidence that only three fragments were detected; CF_3^+, CHF_2^+ and CF^+. There is no contribution from CHF_3^+, CF_2^+ or CHF^+. The parent ion has never been unambiguously observed in previous electron or photon ionisation studies of CHF_3. CF_2^+ and CHF^+ have both been observed by electron ionisation.[6,8] In a recent photoion-fluorescence coincidence study of electron-impact-excited CHF_3,[30] Furuya *et al* observed CF_2^+ on the shoulder of the CHF_2^+ peak. However, the electron impact energy is relatively high (120 eV) and the presence of CF_2^+ is only deduced through simulations. CF_2^+ was also observed by Fiegele *et al* after electron impact at 15.25 eV, so from the same states which produce CHF_2^+.[9] However, the signal is at least an order of magnitude lower than the CHF_2^+ signal in the same experiment.

Fragment ion yields abstracted from the 3D map are shown in Figure 4.1(c). The first product observed is CF_3^+ at the onset of ionisation of CHF_3, 13.85 ± 0.05 eV. This is the only ionic product formed from the ground state of CHF_3^+. Looking at the results of the MP2 calculations it can be seen that the HOMO of CHF_3 is essentially $\sigma_{C\text{-}H}$ in character. If intramolecular vibrational redistribution (IVR) is slow, then it is expected that the most likely bond to break will be C-H as the energy will be localised in this bond. The next ion to be observed is CHF_2^+ with an appearance energy (AE_{298}) of 15.03 ± 0.05 eV and is the major fragment from the $\tilde{A}$, $\tilde{B}$ and $\tilde{C}$ states of CHF_3^+, in fact, it is the only product for the $\tilde{C}$ state. Calculations show that these states arise from ionisation of predominately F2pπ non-bonding orbitals so, again if IVR is slow, breaking of a C-F bond and production of CHF_2^+ is the most likely consequence of ionisation to these states. The final fragment, CF^+, has a weak onset of 18.9 ± 0.2 eV, which is probably due to autoionisation from the Rydberg state of CHF_3 at 19.22 eV, showing that the Rydberg state is converging on the $\tilde{D}/\tilde{E}$ state of CHF_3^+. The CF^+ signal then rises rapidly for energies greater than 20 eV, reaching a maximum at 20.6 eV; these values correspond exactly to the adiabatic and vertical IEs of the blended $\tilde{D}\ ^2E$ and $\tilde{E}\ ^2A_1$ states of CHF_3^+, respectively.

Table 4.2: Thermochemistry of dissociative ionisation pathways of CHF_3 at 298 K. All values in first column are in kJ mol^{-1}.

	AE_{298} / eV	$\Delta_r H^0_{298,\,exp}$ / eV	$\Delta_r H^0_{298,\,calc}$ / eV
Major products of CHF_3 (-697)			
CF_3^+ (+406) + H (+218) + e^-	13.85 ± 0.05	13.96 ± 0.05	13.69
CHF_2^+ (+604) + F (+79) + e^-	15.03 ± 0.05	15.14 ± 0.05	14.30
Minor products of CHF_3 (-697)			
CF^+ (+1134) + HF (-273) + F (+79) + e^-	18.9 ± 0.2		16.97

The data on the fragment AE_{298} values is collected in Table 4.2. In column 1 are the ionic and proposed neutral products for the dissociation of CHF_3, in brackets are the 298 K enthalpies of formation in kJ mol^{-1} of each chemical species. The appearance energies at 298 K are listed in column 2, the experimental enthalpies of reaction in column 3, and the calculated enthalpies of reaction are in column 4. For CF_3^+ and CHF_2^+ the appearance energies at 298 K have been converted into enthalpies of reaction for the appropriate unimolecular reaction using the procedure of Trager and McLoughlin.[37] Comparing values of $\Delta_r H^0_{298}$ shows that for the reaction:

$$CHF_3 \rightarrow CF_3^+ + H + e^- \qquad \textbf{(re 4.1)}$$

that the measured $\Delta_r H^0_{298}$ is 0.27 eV above the calculated value. This shows that the onset of the CF_3^+ signal does not relate to the thermochemical threshold, but to the energy of the ground electronic state of CHF_3^+. Therefore, this state of CHF_3^+ is not bound but probably repulsive along the C-H coordinate. Similarly the same argument holds for the reaction:

$$CHF_3 \rightarrow CHF_2^+ + F + e^- \qquad \textbf{(re 4.2)}$$

which is endothermic by 0.84 eV. Thus it seems that the $\tilde{A}$, $\tilde{B}$ and $\tilde{C}$ states of CHF_3^+ are probably repulsive along the C-F coordinate, and dissociate state-selectively to CHF_2^+ + F. This indicates that CHF_3^+ is behaving non-statistically in the small molecule limit.[46]

The methodology of Trager and McLoughlin is only applicable to fragmentations where only one bond breaks. As such it is inappropriate to use it for the formation of CF^+. With this in mind we note that CF^+ appears to form around 2 eV above the thermochemical threshold for the reaction:

$$CHF_3 \rightarrow CF^+ + HF + F + e^- \qquad \textbf{(re 4.3)}$$

It appears that CF^+ relates to state-selected dissociation of both the autoionising Rydberg state of CHF_3 at 19.22 eV and to the $\tilde{D}$ and $\tilde{E}$ states of the parent ion.

4.1.3 Fixed-energy TPEPICO spectra

Fixed energy spectra were recorded with a TOF resolution of 8 ns for CF_3^+ at 14.76 eV and for CHF_2^+ at 16.35 and 17.36 eV, representing the VIEs of the $\tilde{X}$, $\tilde{B}$ and $\tilde{C}$ states of CHF_3^+, respectively. Mean translational kinetic energy releases, $\langle KE \rangle_t$, were obtained from each of these spectra as described in chapter 3. Figure 4.3 shows the TOF spectrum for CHF_2^+ at 17.36 eV, with the fit to the data, and the agreement is excellent. Table 4.3 lists the experimental $\langle KE \rangle_t$ and $\langle f \rangle_t$ values, as well as the calculated impulsive and statistical $\langle f \rangle_t$ values. The statistical values are calculated using the formula proposed by Klots ($\langle f \rangle_t$ Klots) and by calculating a lower limit based on the vibrational degrees of freedom of the parent ion ($\langle f \rangle_t$ stat), see chapter 3 section 3.2. Without over interpreting this data, there is clear indication that the $\tilde{B}$ and $\tilde{C}$ states of CHF_3^+ dissociate non-statistically by cleavage of a C-F bond, with a value for $\langle f \rangle_t$ close to the dynamical, impulsive limit. The ground state of CHF_3^+ also seems to dissociate by C-H bond cleavage *via* a mechanism that has a significant impulsive component. Both these observations are consistent with the yield data for these two ions described in Section 4.1.2.

Table 4.3: Total mean kinetic energy releases $\langle KE \rangle_t$ of for the two-body fragmentation of valence states of CHF_3. $\langle f \rangle_t$ is the fraction of energy released into translation calculated by various methods.

Electronic State of Parent Ion	Daughter Ion	hν / eV	E_{avail} [a] / eV	$\langle KE \rangle_t$ / eV	$\langle f \rangle_t$ experimental	$\langle f \rangle_t$ Klots	$\langle f \rangle_t$ stat	$\langle f \rangle_t$ impulsive
CHF_3^+ $\tilde{X}$ $^2A_1$	CF_3^+	14.7	1.24	0.66	0.53	0.16	0.10	0.94
$\tilde{B}$ ^2E	CHF_2^+	16.3	2.22	1.02	0.46	0.15	0.10	0.53
$\tilde{C}$ ^2E	CHF_2^+	17.3	3.23	1.18	0.37	0.14	0.10	0.53

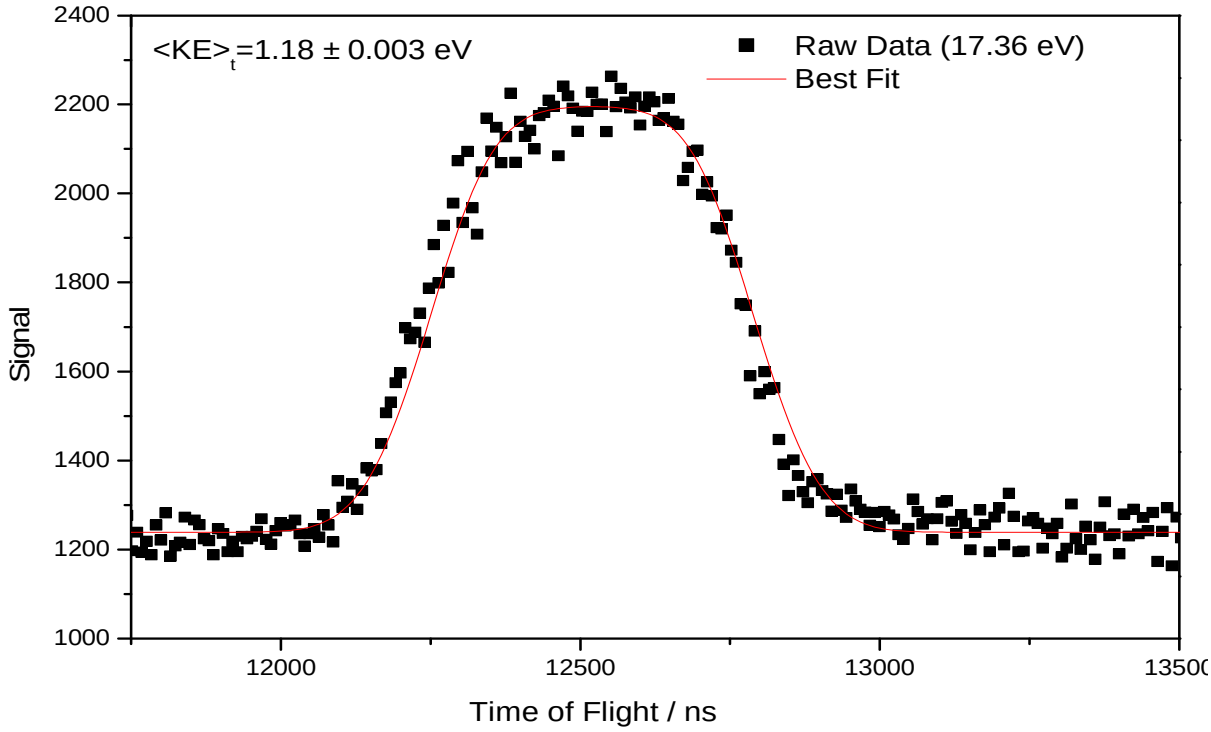

Figure 4.3: Time of flight spectrum (dots) for the CHF_2^+ fragment ion produced from dissociative photoionisation of CHF_3^+. The solid line is a best fit using the method described elsewhere. The measured $<KE>_t$ corresponds to 37% of available energy.

4.2 Selected ion flow tube results

4.2.1 Rate coefficients

The reactions of CHF_3 and a series of cations with recombination energies (RE) in the range 6.27 – 21.56 eV were studied using the selected ion flow tube. For each reaction we have measured a second order rate coefficient (k_{exp}) and have calculated a theoretical rate (k_c) using MADO as explained in chapter 3 section 1. The dipole moment and polarisability volume used were 1.65 D and 3.15 x 10^{-30} m^3 respectively.[4] Data for k_{exp} and k_c is shown in column 2 of Table 4.4, k_c are the values in square brackets.

For those cations whose RE exceeds the IE (CHF_3), 13.85 eV, k_{exp} is very similar to k_c, implying that these are efficient reactions which occur upon nearly every collision. The one exception is Kr^+ (RE = 14.00 eV), just above the IE (CHF_3), where the efficiency is only 0.5. There is no obvious correlation between efficiency of reaction and RE of the cation. For cations with RE below the IE (CHF_3), only seven of the seventeen collision systems studied exhibited

any reactivity. Of these seven, all but O^+ and OH^+ have a k_{exp} value which is somewhat lower than k_c, and for CO_2^+ and CF_3^+ the reaction efficiency falls to *ca*. 0.25. Energetics alone cannot explain the observed values of k_{exp}. For example, O^+ and CO_2^+ differ in RE by only 0.16 eV, yet the former reacts with unity efficiency whereas the latter has an efficiency less than 0.25. This suggests that steric effects for this group of reactions may be important. Such reactions can only occur *via* a short-range intermediate and subsequent chemical reaction (chapter 1), so it is not surprising that such effects may play an important role.

4.2.2 Ion-molecule branching ratios

For the ion-molecule reactions studied on the SIFT branching ratios of the product ions have also been recorded, these are shown in column 3 of table 4.4. Column 4 and 5 of Table 4.4 show proposed neutral products and enthalpies of reaction at 298 K. We do not observe the parent ion (CHF_3^+) in accord with the TPEPICO results, and the three major products are CF_3^+, CHF_2^+ and CF^+. The only exceptions are that CF_2OH^+ is the only product formed from reaction with H_2O^+ (RE = 12.56 eV) and that there is a small yield of CF_2^+ in the reaction with Ne^+ (Re 21.56 eV). Clearly both the SIFT and the TPEPICO experiments detect essentially the same ionic products.

The proposed neutral products are those which are both chemically feasible and most exothermic. For nearly all of the reactions studied there are clear exothermic pathways which form reasonable products, that is the neutrals are not too exotic. There is one clear exception, the reaction of CO_2^+ to form CHF_2^+. Both possible neutral channels:

$$CHF_3 + CO_2^+ \rightarrow CHF_2^+ + CO_2 + F \qquad \textbf{(re 4.4)}$$

and

$$CHF_3 + CO_2^+ \rightarrow CHF_2^+ + FOCO \qquad \textbf{(re 4.5)}$$

are slightly endothermic. For the CO_2 + F channel, $\Delta_r H^0 = 52$ kJ mol^{-1} while for the FOCO channel, $\Delta_r H^0 = 10$ kJ mol^{-1}. Previous work has shown that such slightly endothermic reactions can be driven by entropy effects,[47] as the key thermodynamic property to consider is $\Delta_r G^0$ and not $\Delta_r H^0$. We note that an entropy change of only 30 J mol^{-1} K^{-1} would be enough to make this a favourable process. Also the experimental value for the $\Delta_f H^0$ of FOCO has an associated error of ~12 kJ mol^{-1}, which would be enough for the reaction to possibly be exothermic.[42] For the

reaction with Kr^+, ignoring any entropic effects, to produce the minor product CHF_2^+ (16 %) via an exothermic reaction Kr^+ must be in the upper $^2P_{1/2}$ spin-orbit state.

The CF_x^+ (x = 1-3) series of ions all react with efficiencies of 0.3 - 0.8. They react to produce CHF_2^+ as the only ionic product. The process is driven by abstraction of a F^- from CHF_3 to produce neutral CF_{x+1}. This reaction is therefore a measure of the fluoride ion affinity (FIA) of CHF_2^+. A detailed definition of FIA is given in chapter 1. CHF_3 reacts with CF^+ and CF_3^+ and CF_2^+ to form CHF_2^+ but does not react at all with the SF_n^+ (n = 1-5). This places the FIA of CHF_2^+ between the FIA of CF^+ and SF_4^+. The FIA of CHF_2^+ has been measured previously in an ICR, and it was found to be less than the FIA of CF_3^+,[48] in agreement with the findings of this study. A second interesting comparison is between the reactions of CHF_3 with Kr^+ and CO^+. Both cations have RE greater than IE of CHF_3 but have almost the same RE (Kr^+ = 14.00 eV CO^+ = 14.01 eV) different by only 0.01 eV. Yet the product ratios of CHF_2^+ to CF_3^+ change from 0.2 for Kr^+ to 32 for CO^+. This is a drastic change for such a small difference in energy. This is discussed in more detail in a later section.

There have been relatively few studies of the reactivity of CHF_3 with positive ions, and very surprisingly none, to our knowledge, in a selected ion flow tube. The reaction of CF_3^+ with CHF_3 has been studied using a crossed beam electrostatic trapping cell at a range of collision energies,[1] the rate coefficient was not measured but the ionic products were. The results do not agree, as Peko *et al.* observe the products CF^+, CF_3^+ and CHF_2^+, whereas on the SIFT only CHF_2^+ is observed. The discrepancy may be due to the high collisional energy (20-400 eV) used in their study compared to the SIFTs thermal energy. Pabst *et al.* studied the reaction of CHF_3 with fragment ions produced from electron impact ionisation of CHF_3 under relatively high pressure conditions.[35] They observed the same fragments from electron impact as are observed from our photon-induced study (Section 4.1), but in addition they observed CF_2^+, F^+ and the parent ion. However, these three ions occurred only as very small percentage yields, especially CHF_3^+ (0.5 %). We note that the ions in the study of Pabst *et al.* were generated at high electron impact energies of 150-200 eV, compared to photon energies of 13-25 eV in our TPEPICO study. The rates of the reactions of CF_3^+ and F^+ with CHF_3 are in fairly good agreement with our measurements, but their rates for the reaction of CF_2^+ and CF^+ with CHF_3 are much lower. Chau and Bowers used the ion cyclotron resonance technique to study the reactions of CHF_3 with the rare gas ions and N_2^+, CO^+, CO_2^+ and N_2O^+.[34] They were unable to measure product distributions but commented that charge transfer dominates over chemical reaction channels. The majority of the rates they measured are in good agreement to those from the SIFT. Blint *et al* also used an

ICR to measure the reactions of CHF_3 with its fragmentation products.[48] The major products due to electron impact were found to be CF_3^+ and CHF_2^+. They found that CF_3^+ reacts with CHF_3 to form CHF_2^+ with a rate of 2.1 x 10^{-10} cm^3 $molecule^{-1}$ s^{-1}, in fair agreement with our result. Jiao *et al*. used Fourier Transform mass spectrometry to study the reactions of Ar^+, CF_2^+ and CF_3^+ with CHF_3.[33] They measure rate coefficients which are much lower than ours, but their product yields are similar.

Table 4.4: Rate coefficients at 298 K, product cations and branching ratios, and suggested neutral products for reactions of gas-phase cations with CHF_3. The calculated enthalpy of reaction at 298 K is shown in the fifth column. The dashed line represents the onset of ionisation of CHF_3.

Reagent ion (RE [b] / eV)	Rate coefficient / 10^{-9} cm^3 $molecule^{-1}$ s^{-1}	Product ions (%)	Proposed neutral products	$\Delta_r H^o_{298}$ / kJ mol^{-1}
H_3O^+ (6.27)	- [2.3]	No Reaction	-	-
SF_3^+ (8.32)	- [1.4]	No Reaction	-	-
CF_3^+ (9.04)	0.4 [1.5]	CHF_2^+ (100)	CF_4	-38
CF^+ (9.11)	1.3 [1.9]	CHF_2^+ (100)	CF_2	-15
NO^+ (9.26)	- [2.0]	No Reaction	-	-
SF_5^+ (9.78)	- [1.3]	No Reaction	-	-
SF_2^+ (10.24)	- [1.5]	No Reaction	-	-
SF^+ (10.31)	- [1.7]	No Reaction	-	-
CF_2^+ (11.44)	1.4 [1.7]	CHF_2^+ (100)	CF_3	-87
SF_4^+ (11.99)	- [1.4]	No Reaction	-	-
O_2^+ (12.07)	- [1.9]	No Reaction	-	-

Xe^+ (12.13)	- [1.3]	No Reaction	-	-
H_2O^+ (12.62)	1.5 [2.4]	CF_2OH^+ (100)	HF + H	-102
N_2O^+ (12.89)	- [1.7]	No reaction	-	-
OH^+ (13.25)	2.2 [2.4]	CHF_2^+ (68) CF_3^+ (32)	HOF HF + O H_2O	-90 -15 -432
O^+ (13.62)	2.5 [2.4]	CHF_2^+ (100)	OF	-153
CO_2^+ (13.76)	0.4 [1.7]	CHF_2^+ (55) CF_3^+ (45)	FOCO HOCO CO_2 + H	10 -11 -8
Kr^+ (14.00 (& 14.67))	0.8 [1.5]	CHF_2^+ (16) CF_3^+ (84)	Kr + F Kr + H	30 (or -35) -30 (or -95)
CO^+ (14.01)	2.0 [2.0]	CHF_2^+ (97) CF_3^+ (3)	CO + F FCO CO + H HCO	29 -112 -30 -95
N^+ (14.53)	2.3 [2.6]	CHF_2^+ (61) CF_3^+ (39)	N + F or NF N + H or NH	-22 -96 -81 -395
N_2^+ (15.58)	2.1 [2.0]	CHF_2^+ (46) CF_3^+ (54)	N_2 + F N_2 + H	-123 -182
Ar^+ (15.76)	1.8 [1.8]	CHF_2^+ (72) CF_3^+ (28)	Ar + F Ar + H	-141 -200
F^+ (17.42)	1.9 [2.3]	CHF_2^+ (100)	F + F F_2	-300 -459
Ne^+ (21.56)	1.9 [2.2]	CHF_2^+ (7) CF_2^+ (15) CF^+ (78)	Ne + F Ne + HF Ne + HF + F	-700 -734 -442

5. A comparison of product branching ratios from TPEPICO and SIFT data

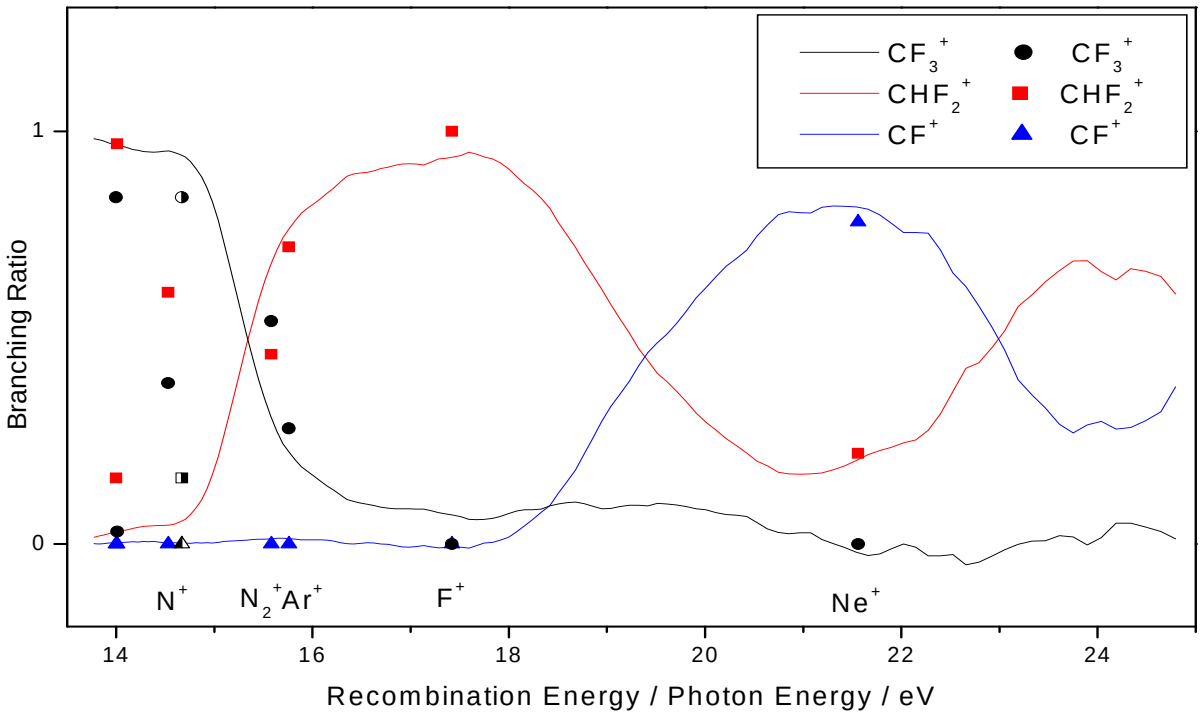

Figure 4.4: Comparison of the ionic products from ion-molecule studies of CHF_3 with TPEPICO photoionisation branching ratios over the range 14 – 25 eV. The half filled symbols at 14.67 eV correspond to Kr^+ in the $^2P_{1/2}$ state. Errors are conservatively estimated to be ~20 % for both sets of data.

Figure 4.4 shows the branching ratios for both TPEPICO and SIFT studies as a function of photon and recombination energy respectively. The former are the continuous graphs the latter data points at the defined RE of each ion reactant. As described in chapter 1 comparison of the branching ratios from the two experiments may indicate which mechanism is in operation for the cation reactions. Only seven out of the twenty four cation ion reactions studied have RE > IE (CHF_3) so it is only for these seven that non-dissociative charge transfer is possible. The four ions with RE > than 15 eV show some interesting features. For the atomic ions in this range Ar^+, F^+, Ne^+ the agreement is quite good. For N_2^+ there is a significant difference, a ratio of 48% CHF_2^+ to 52% CF_3^+ in the ion-molecule reaction to be compared with 68% CHF_2^+ to 32% CF_3^+ in the TPEPICO experiment at a photon energy of 15.58 eV. For N_2^+, Ar^+ and F^+ there is a significant Franck-Condon intensity in the TPES (Figure 4.1(a)) at the RE of these three ions and the

electron is removed from an unshielded F 2pπ molecular orbital, whereas at the RE of Ne^+, 21.56 eV, the Franck-Condon activity is low and the electron is removed from a mixture of σ_{C-H} and σ_{C-F} shielded orbitals.

In several previous studies it has been suggested that energy resonance and the transfer of an unshielded electron are sufficient criteria for long-range charge transfer to occur; an appreciable Franck-Condon vibrational overlap factor between $BC_{v=0}$ and $(BC^+)^{(*)}_v$, was not a necessary condition.[49,50] The evidence from these reactions with CHF_3 is not so clear. For N_2^+, despite all three criteria being satisfied, the branching ratio agreement is poor, suggesting that long-range charge transfer may not be the dominant mechanism. However looking at the figure 4.4 shows that RE of N_2^+ is in line with a rapidly changing region in the TPEPICO breakdown diagram, in this region small errors in measurement may be magnified. As such it could be suggested that the results for N_2^+ are not in too bad a disagreement with the TPEPICO data. For Ar^+ all three criteria are satisfied, and the agreement between branching ratios is excellent; long-range charge transfer is apparently dominant. We note that, despite only a small difference between the RE of N_2^+ and Ar^+, 0.18 eV, the branching ratios from the two SIFT experiments are very different. A simplistic argument is that the difference is that N_2^+ is molecular while Ar^+ is atomic, leading to different interactions. However, another explanation is possible, as stated earlier N_2^+ falls on a rapidly changing region of the breakdown diagram. If we assume that some form of long-range charge transfer takes place for N_2^+ and Ar^+ than this steep change in the TPEPICO results should be mirrored in the SIFT data, which it appears to be. For F^+, there is a small discrepancy between the branching ratios of the two experiments, in that CHF_2^+ (100 %) is the only observed product ion, whereas the TPEPICO experiment at 17.42 eV photon energy produces CHF_2^+ (93 %) and CF_3^+ (7 %). However, the F^+ signal was very weak, and it is possible that we did not have the sensitivity to observe the CF_3^+ channel. It seems likely that long-range charge transfer is dominant. For Ne^+, the RE of 21.56 eV corresponds to the very edge of the Franck-Condon region of the $\tilde{D}/\tilde{E}$ states of CHF_3^+, and the electron is removed from a shielded orbital. Despite the excellent agreement between the branching ratio data, therefore, we suggest that Ne^+ charge transfers with CHF_3 *via* a short-range intermediate.

For the three ions with RE in the range 13.9-15.0 (Kr^+, CO^+ and N^+), there is significantly poorer agreement between the branching ratios from the two experiments. Indeed, for CO^+ there is total disagreement in that the bimolecular chemical reaction produces CHF_2^+ (97%) as its main product whereas the photon-induced reaction produces CF_3^+ (*ca.* 90%). The agreement of the

branching ratios for N^+ (RE=14.53 eV) is poor, the discrepancy for CF_3^+ and CHF_2^+ yields being greater than a factor of two. This odd behaviour has been observed in many cases,[51,52] and one possible explanation is given in chapter 1. For CO^+ long-range charge transfer cannot be the preferred reaction mechanism. We note that the electron would have to transfer from the highest occupied molecular orbital of CHF_3, a σ_{C-H} bonding orbital which will be shielded by three fluorine atoms. The data points for Kr^+ are in better agreement, within 10-15 % of the photon-induced branching ratios, this being true at the energies of both of its spin-orbit components, $^2P_{3/2}$ at 14.00 and $^2P_{1/2}$ at 14.67 eV. As stated earlier, CHF_2^+ (16 %), only becomes energetically allowed if Kr^+ exists in its excited spin-orbit state (Table 4.3). Unfortunately, we are unable to determine how thermalised Kr^+ is in the SIFT apparatus. It is interesting that Kr^+ reacts by long-range charge transfer while CO^+ does not, even though they have essentially the same RE (~14.0 eV). It may be that long-range charge transfer is not favourable this close to the IE of CHF_3. This may be confirmed by the rate coefficients; Kr^+ is only 50 % efficient while CO^+ has 100 % efficiency. Kr^+ can only react by charge transfer, and if this is unfavourable explains the low efficiency of the reaction. CO^+ cannot only react *via* charge transfer but also by a chemical reaction, and it is possible that the chemical reaction could be very efficient.

6. A comparison of the results of photon and ion chemistry of the CXF_3 series

It is of interest to see how the results for CHF_3 given here compare to the results for other molecules in the CXF_3 series (where X is Br, Cl or F). TPEPICO studies on CF_3Br and CF_3Cl have been reported,[53] and there are several such studies for CF_4.[45,54] Very few ion molecule reactions have been studied for CF_3Br or CF_3Cl.[55-58] Threshold photoelectron–fluorescence photon coincidence measurements have been performed on all four molecules.[28,45]

Table 4.5 shows the ionic products formed from photoionisation using the TPEPICO experiment for CHF_3, CF_4, CF_3Cl and CF_3Br.[53,54] The ions highlighted in bold are the major ions formed from a ionic state. States labelled with a # show radiative decay, so the interpretation of these branching ratios assuming non-radiative decay needs caution. At threshold the parent ion of CF_3Br and CF_3Cl is formed, although weakly. No parent is observed for either CHF_3 or CF_4. This shows that the ground electronic state of the parent ion for bromo- and chloro-trifluoromethane is weakly bound, while there is no equivalent bound state, at least at threshold, for fluoroform or tetrafluoromethane.

Table 4.5: Comparison of TPEPICO product ions for CXF_3^+ (X = H, F, Cl and Br), ions in bold are the main product channels from this state. States marked with # fluoresce.

State	CHF_3^+	CF_4^+	CF_3Cl^+	CF_3Br^+
$\tilde{X}$	**CF_3^+**	**CF_3^+**	**CF_3^+**, CF_3Cl^+	**CF_3^+**, CF_3Br^+
$\tilde{A}$	**CHF_2^+**, CF_3^+	**CF_3^+**	**CF_3^+**	**CF_3^+**
$\tilde{B}$	**CHF_2^+**, CF_3^+	**CF_3^+**	**CF_3^+**	**CF_3^+**, CF_2Br^+
$\tilde{C}$	**CHF_2^+**, CF_3^+	CF_3^+, $CF_2^{+\#}$	**CF_2Cl^+**, CF_3^+	**CF_2Br^+**, CF_3^+
$\tilde{D}$	**CF^+**, CHF_2^+, $CF_3^{+\#}$	CF_3^+, $CF_2^{+\#}$	**CF_2Cl^+**, CF_3^+	**CF_2Br^+**, CF_3^+
$\tilde{E}$	**CF^+**, CHF_2^+, CF_3^+	-	**$CF_2^{+\#}$**	**CF_2^+**, CF_2Br
$\tilde{F}$	-	-	**CF_2^+**	**CF_2^+**

All four ions show similar fragmentation patterns; at low energy they all lose the X atom (H, F, Cl or Br). At slightly higher energies a competing dissociation channel opens which is loss of a F atom. There is variation in the relative yields of these two channels, but they still occur for all the ions. At higher energies, around 20 eV, a third channel opens. For CF_4^+, CF_3Cl^+ and CF_3Br^+ this channel is loss of an XF fragment to form CF_2^+. For CHF_3^+ no CF_2^+ is detected. Instead CF^+ is formed.

There have been fewer studies on the ion-molecule reactions of CF_3Cl and CF_3Br. Morris *et al* have studied the reactions of both molecules and CF_4 with H_2O^+ and CF_n^+ (n = 1-3),[57,58] while Mayhew *et al* have studied the reactions of CF_3Br with a range of small ions.[55,56] The reactant ions studied by Mayhew *et al* all had RE values greater than the IE of the neutral molecule, thus charge transfer is energetically allowed. Comparison of this SIFT data with the TPEPICO data suggests that CF_3Br reacts mainly by charge transfer. The data of Morris *et al* on the reactions of H_2O^+ and H_3O^+ with CF_3Cl and CF_3Br show some interesting differences to the same reactions with CHF_3. CHF_3 reacts with H_2O^+ to produce exclusively CF_2OH^+. CF_3Cl and CF_3Br produce the same ion but in a small fraction, and CF_3^+ and CF_2X^+ are also formed. This difference can be rationalised on the basis that RE(H_2O) is greater than both IE(CF_3Cl) and IE(CF_3Br), while it is lower than IE(CHF_3). This means that charge transfer is a competing

process to the reaction which forms CF_2OH^+ for the reactions of both CF_3Cl and CF_3Br. The reactions of the CF_n^+ sequence of ions also show some interesting differences for reactions with CHF_3. CHF_3 reacts by F^- abstraction with all three CF_n^+ ions. For the reactions of CF^+ and CF_3^+ with CF_3Cl and CF_3Br this is also essentially true, but a small amount of CF_3^+ is also formed from the reaction of CF^+ with CF_3Cl. The reaction of CF_2^+ with either CF_3Cl or CF_3Br produces both CF_2X^+ and CF_3^+ in large abundance. The process of Cl^- or Br^- transfer is more favourable than the analogous H^- transfer in CHF_3 because the C-Cl and C-Br bonds are far weaker than the C-H bond.

7. Conclusions

The threshold photoelectron photoion coincidence spectrum of CHF_3 has been recorded over the photon energy range 13.5 – 24.5 eV. Ion yields and branching ratios have been determined for the three fragments produced. No parent ion has been observed, the lowest-energy fragment is CF_3^+, and as the photon energy increases first CHF_2^+ and then CF^+ are formed. The mean kinetic energy releases into fragment ions involving one bond cleavage have been measured and compared with statistical and impulsive models. This work has showen that CHF_3^+ behaves in a non-statistical manner characteristic of the small-molecule limit, with the ground state and low-lying excited states of CHF_3^+ being largely repulsive along the C-H and C-F coordinates, respectively. The rate coefficients and branching ratios have been measured at 298 K for the reactions of CHF_3 with H_3O^+, CF_n^+ (n=1-3), SF_x^+ (x=1-5), NO^+, O_2^+, Xe^+, H_2O^+, N_2O^+, OH^+, O^+, CO_2^+, Kr^+, CO^+, N^+, N_2^+, Ar^+, F^+ and Ne^+. Comparison with theory shows that for reactions where charge transfer is exothermic, *i.e.* RE (ion) > IE (CHF_3), most of the reactions occur efficiently, *i.e.* $k_{exp} \approx k_{calc}$. For reactions at lower energies, the efficiency can be significantly reduced. Comparisons between TPEPICO and SIFT branching ratios, together with an analysis of the TPES of CHF_3, show that long-range charge transfer probably occurs for the Ar^+ and F^+ atomic ions with recombination energies above *ca.* 15 eV. The importance or otherwise of an appreciable Franck-Condon factor for the neutral molecule, CHF_3, at the RE of the ion is unclear. Below 15 eV, a combination of short-range charge transfer and chemical reactions take place.

Comparison of the results with the CXF_3 series of molecules (X = F, Cl or Br) shows some interesting similarities and differences with CHF_3. All four molecules fragment *via* similar

pathways except at higher energies, where CHF_3 fragments to form CF^+. For the three other neutrals CF_2^+ is formed instead. This could be due to the production of HF as the neutral partner. HF has a very strong bond and formation of this bond could drive production of CF^+. None of the neutral products which could be formed from the other molecules will have such a large thermodynamic driving force. For the ion-molecule reactions of these four molecules, where results are available, again similar patterns are observed. The differences being rationalized on differing ionisation energies of the different molecules. However for the chemical reactions which occur when CF_2^+ is the reagent ion loss of both F^- and X^- is seen from CF_3Cl and CF_3Br, but only loss of F^- is seen with CHF_3. This difference is explained as due to the relative bond strengths between carbon and hydrogen, chlorine and bromine.

8. References

1 B.L. Peko, R.L. Champion, M.V.V.S. Rao, J.K. Olthoff, *J. Appl. Phys.*, **92**, (2002) 1657.
2 M.J. Molina, L.T. Molina, C.E. Kolb, *Ann. Rev. Phys. Chem.*, **47**, (1996) 327.
3 Intergovernmental Panel on Climate Change, *The 1994 Report of the Scientific Assessment Working Group of IPCC*, 28.
4 L.G. Christophorou, J.K. Olthoff: *Fundamental Electron Interactions with Plasma Processing Gases*, Kluwer Academic / Plenum Publishers, New York, (2004).
5 G.K. Jarvis, C.A. Mayhew, L. Singleton, S.M. Spyrou, *Int. J. Mass. Spec. Ion Proc.*, **164**, (1997) 207.
6 I. Torres, R. Martinez, F. Castano, *J. Phys. B*, **35**, (2002) 2423.
7 I. Torres, R. Martinez, M.N.S. Rayo, F. Castano, *J. Chem. Phys.*, **115**, (2001) 4041.
8 M. Goto, K. Nakamura, H. Toyodo, H. Sugai, *Jpn. J. Appl. Phys.*, **33**, (1994) 3602.
9 T. Fiegele, G. Hanel, I. Torres, M. Lezius, T.D. Mark, *J. Phys. B*, **33**, (2000) 4263.
10 J.F. Ying, K.T. Leung, *Phys. Rev. A*, **53**, (1995) 1476.
11 J. Moxom, D.M. Schrader, G. Lancchia, J. Xu, L.D. Hulett, *Phys. Rev. A*, **62**, (2000) 52708.
12 I. Novak, A.W. Potts, F. Quinn, G.V. Marr, B. Dobson, I.H. Hillier, J.B. West, *J. Phys. B*, **18**, (1985) 1581.
13 S. Elbel, H. tom Dieck, R. Demuth, *J. Fluor, Chem.*, **19**, (1982) 349.
14 G. Bieri, L. Aasbrink, W. Von Niessen, *J. Electron Spec. Rel. Phen.*, **23**, (1981) 281.
15 T.A. Carlson, R.M. White, *Faraday Dissc. Chem. Soc.*, **No. 54**, (1972) 285.
16 A.W. Potts, T.A. Williams, W.C. Price, *Faraday Dissc. Chem. Soc.*, **No. 54**, (1972) 104.
17 A.W. Potts, H.J. Lempka, D.G. Streets, W.C. Price, *Phil. Trans. R. Soc. A*, **268**, (1970) 59.
18 C.R. Brundle, M.B. Robin, H. Basch, *J. Chem. Phys.*, **53**, (1970) 2196.
19 B.P. Pullen, T.A. Carlson, W.E. Moddeman, G.K. Schweitzer, W.E. Bull, F. Grimm, *J Chem. Phys.*, **53**, (1970) 768.
20 S. Strokes, A.B.F. Duncan, *J. Am. Chem. Soc.*, **80**, (1958) 6177.
21 C.Y.R. Wu, L.C. Lee, D.L. Judge, *J. Chem. Phys.*, **71**, (1979) 5221.
22 P. Sauvageau, R. Gilbert, P.P. Berlow, C. Sandorfy, *J. Chem. Phys.*, **59**, (1973) 762.
23 S. Ali, Thesis, University of Birmingham, (2007).
24 G. Gazzoli, L. Cludi, G. Cotti, L. Dore, C.D. Esposti, M. Bellini, P.d. Natale, *J. Mol. Phys*, **163**, (1994) 521.
25 T. Shimanouchi: *Tables of Molecular Vibrational Frequencies Consolidated Volume I*, National Bureau of Standards, (1972).
26 F.C.Y. Wang, G.E. Leroi, *Ann. Isra. Phys. Soc.*, **6**, (1984) 210.
27 I. Novak, J.M. Benson, A.W. Potts, *J. Elec. Spec. Rel. Phenom.*, **41**, (1986) 175.
28 H. Biehl, K.J. Boyle, D.M. Smith, R.P. Tuckett, *Chem. Phys.*, **214**, (1997) 357.
29 U. Müller, M. Lange, W. Haas, R. Brenn, *J. Chem. Phys.*, **100**, (1994) 5550.
30 K. Furuya, K. Matsuo, E. Koto, K. Maruyama, Y. Hatano, T. Ogawa, *J. Phys. B*, **35**, (2002) 1015.
31 C.A. Mayhew, R. Peverall, C.M. Timperley, P. Watts, *Int. J. Mass Spec.*, **233**, (2004) 155.
32 R. Peverall, R.A. Kennedy, C.A. Mayhew, P. Watts, *Int. J. Mass Spec. Ion Proc.*, **171**, (1997) 51.
33 C.Q. Jiao, R. Nagpal, P.D. Haaland, *Chem. Phys. Lett.*, **269**, (1997) 117.
34 M. Chau, M.T. Bowers, *Int. J. Mass Spec. Ion Phys.*, **24**, (1977) 191.
35 M.J.K. Pabst, H.S. Tan, J.L. Franklin, *Int. J. Mass. Spec. Ion Phys.*, **20**, (1975) 191.

36 M.A. Parkes, R.Y.L. Chim, C.A. Mayhew, V.A. Mikhailov, R.P. Tuckett, *Mol. Phys.*, **104**, (2006) 263.
37 J.C. Traeger, R.G. McLoughlin, *J. Am. Chem. Soc.*, **103**, (1981) 3647.
38 M.W. Chase, *J. Phys. Chem. Ref. Data*, (1998) Monograph no. 9.
39 S.G. Lias, J.E. Bartmess, J.F. Liebman, J.L. Holmes, R.D. Levin, W.G. Mallard, *J. Phys. Chem. Ref. Data*, **17**, (1988) supplement no 1.
40 G.A. Garcia, P.M. Guyon, I. Powis, *J. Phys. Chem. A*, **105**, (2001) 8296.
41 W. Zhou, D.P. Seccombe, R.P. Tuckett, M.K. Thomas, *Chem. Phys.*, **283**, (2002) 419.
42 D.W. Arnold, S.E. Bradforth, E.H. Kim, D.M. Neumark, *J. Chem. Phys.*, **102**, (1995) 3493.
43 T.V. Duncan, C.E. Miller, *J. Chem. Phys.*, **113**, (2000) 5138.
44 H. Biehl, K.J. Boyle, R.P. Tuckett, H. Baumgaertel, H.W. Jochims, *Chem. Phys.*, **214**, (1997) 367.
45 D.M. Smith, R.P. Tuckett, K.R. Yoxall, K. Codling, P.A. Hatherly, J.F.M. Aarts, M. Stankiewicz, *J. Chem. Phys.*, **101**, (1994) 10559.
46 P.A. Hatherly, D.M. Smith, R.P. Tuckett, *Zeit. Fur Phys. Chem.*, **195**, (1996) 97.
47 K.K. Irikura, *J. Am. Chem. Soc.*, **121**, (1999) 7689.
48 R.J. Blint, T.B. McMahon, J.L. Beauchamp, *J. Am. Chem. Soc.*, **96**, (1974) 1269.
49 C.R. Howle, C.A. Mayhew, R.P. Tuckett, *J. Phys. Chem. A*, **109**, (2005) 3626.
50 G.K. Jarvis, R.A. Kennedy, C.A. Mayhew, R.P. Tuckett, *Int. J. Mass Spec.*, **202**, (2000) 323.
51 M.A. Parkes, S. Ali, R.P. Tuckett, V.A. Mikhailov, C.A. Mayhew, *Phys. Chem. Chem. Phys.*, **8**, (2006) 3643.
52 V.A. Mikhailov, M.A. Parkes, R.P. Tuckett, C.A. Mayhew, *J. Phys. Chem. A*, **110**, (2006) 5760.
53 J.C. Creasey, D.M. Smith, R.P. Tuckett, K.R. Yoxall, K. Codling, P.A. Hatherly, *J. Phys. Chem.*, **100**, (1996) 4350.
54 J.C. Creasey, H.M. Jones, D.M. Smith, R.P. Tuckett, P.A. Hatherly, K. Codling, I. Powis, *Chem. Phys.*, **174**, (1993) 441.
55 C.A. Mayhew, R. Thomas, P. Watts, *Int. J. Mass Spec.*, **223-224**, (2003) 91.
56 R.D. Thomas, R.A. Kennedy, C.A. Mayhew, P. Watts, *J. Phys. Chem. A*, **101**, (1997) 8489.
57 R.A. Morris, A.A. Viggiano, J.M. Van Doren, J.F. Paulson, *J. Phys. Chem.*, **96**, (1992) 3051.
58 R.A. Morris, A.A. Viggiano, J.M. Van Doren, J.F. Paulson, *J. Phys. Chem.*, **96**, (1992) 2597.

Chapter 5: Positive Ion Chemistry of Octafluorocyclobutane

1. Introduction

Octafluorocyclobutane (*c*-C_4F_8) is an important industrial gas, especially in plasma technologies.[1-3] It has also found use in surgical procedures.[4] It is used for dry etching where, in mixtures with CH_3F, it has high selectivity for etching SiO_2 over Si_3N_4 compared to other gas mixtures;[1] there is also high selectivity for SiO_2 over Si.[5] *c*-C_4F_8 is used in high-voltage insulation applications, especially when mixed with SF_6. The rapid rate coefficient for non-dissociative electron attachment to *c*-C_4F_8 and the ease of purification make it more suitable for such applications than other insulating mixtures.[6] For such a significant industrial gas it is also important to be aware of the atmospheric implications of its use.

Ravishankara *et al.*[7] have reported on the lifetime of *c*-C_4F_8 in the Earth's atmosphere. Assuming that photolysis is the dominant loss process and that electron attachment does not dissociate the molecule, the estimated lifetime is ~ 3200 years. By allowing for the effect of reactions with both ions and electrons, Morris *et al.*[8] gave a lower value of ~ 1400 years. The differences between the lifetimes show the significant effect of neglecting reactions with charged species. However, it is normal to neglect these reactions due to the low concentrations of charged species in the atmosphere. It was decided to study further the reactions of *c*-C_4F_8 with both ions and with electrons; this chapter will deal exclusively with cations, electron attachment reactions will be covered in chapter 10.

There have already been many studies of *c*-C_4F_8 with electrons.[4,6,9] There have also been studies of the dissociation of the neutral molecule initiated by both infrared radiation and thermal decomposition.[10-12] Spectroscopic measurements include both gas-phase electron diffraction and IR measurements.[13,14] There have been only three measurements of the positive ion chemistry of *c*-C_4F_8,[15-17] and there is only one on the negative ion chemistry.[18] A previous photoionisation and photoelectron measurement was taken by the Tuckett group eight years ago.[19] This experiment was performed on the now-decommissioned 1m Seya VUV monochromator at the SRS. The TPEPICO results presented in this chapter were performed on the higher flux 5m McPherson monochromator also at the SRS.

2. Experimental

The two apparatus used to obtain the data reported in this chapter are the same as described in chapter 2. *c*-C_4F_8 was obtained from Fluorochem UK with a stated purity of 99 %, and was used without further purification.

3. Energetics

From the TPEPICO data we determine appearance energies at 298 K (AE_{298}) for each ionic product formed. These AE_{298} values can be converted into an upper limit for $\Delta_r H^0_{298}$, the enthalpy change for the corresponding unimolecular reaction, using the procedure of Traeger and McLoughlin,[20] a methodology discussed in detail in section 2.1 of chapter 3. As noted in that chapter the method is only applicable in cases where a single bond is broken. Although the two main fragments detected in the TPEPICO experiment, $C_3F_5^+$ and $C_2F_4^+$, are formed *via* multiple bond cleavage, we have applied the correction factor to these ions, noting that this is only an approximation to aid in interpretation of the results. The vibrational frequencies of the two ions, necessary for application of the Traeger and McLoughlin procedure, were obtained from Gaussian 03 calculations performed at the B3LYP level with a 6-311-G + (d,p) basis set. All other vibrational frequencies required were taken from standard sources.[21] The enthalpies of formation at 298 K were from standard sources, apart from *c*-C_4F_8 (–1515 kJ mol^{-1}),[22] C_3F_3 (-134 kJ mol^{-1}), C_3F_5 (–729 kJ mol^{-1}), $C_3F_5^+$ (+45 kJ mol^{-1}),[23] CF_3 (–466 kJ mol^{-1}), CF_3^+ (406 kJ mol^{-1}),[24] *c*-C_4F_7 (-1166 kJ mol^{-1}), *c*-$C_4F_7^+$ (-166 kJ mol^{-1}),[25] $O(CHF_2)_2$ (-858 kJ mol^{-1}),[26] CF_3O (-631 kJ mol^{-1}), CF_3CO (-609 kJ mol^{-1}),[27] and C_2F_4O (-1004 kJ mol^{-1}).[28] The ionisation energy (IE) of SF_5 was taken as 9.78 eV.[29]

4. Molecular structure

The structure of *c*-C_4F_8 was calculated using Gaussian 03. There are two possible basic geometries for the molecule to take: the D_{2d} structure where the C_4 square is puckered, or the D_{4h} structure where the C_4 square is planner. Though older measurements have suggested the planner structure,[30] most recent measurements show that *c*-C_4F_8 has the puckered form,[13] and the puckering motion has been measured in a jet-cooled IR experiment.[31] Some of the *ab intio*

calculations that have been reported by other groups have found the planar structure as the energy minimum, for example Hiroka *et al.*[18] This shows the dangers of a geometry optimisation becoming trapped in local minima or of a poor choice of initial structure.

5. Theoretical rate coefficients

For the SIFT experiments the theoretical rate coefficient was calculated as described in chapter 3 section 1.1. Very surprisingly, it was found that the Langevin rate coefficient consistently underestimated the value of the experimental rate coefficient, i.e. $k_{exp} > k_c$. Such unphysical results have been seen before and were found to be due to the presence of a polar neutral. If the neutral has a dipole moment then an extra attractive term in the potential energy function is required in the calculation of the rate coefficient,[32] see chapter 3 section 1.1.2 for more detail on extensions to the Langevin model. There is no dipole moment for *c*-C_4F_8 as it is a very symmetrical molecule, therefore as a first step it was assumed that there was a higher-order multipole term contributing to the increased measured rate coefficients. The theoretical rate coefficients were therefore calculated using a parameterised equation of Bhowmik and Su which includes the ion-quadrupole potential.[33] More details on this method and its limitations are given in chapter 3 section 1.1.3. For both calculations α', the polarisability volume was required. For α' a value of 1.25 x 10^{-29} m^3 from a semi-empirical calculation was used,[4] details on the value of the average quadrupole moment (Θ) of *c*-C_4F_8 will be given later.

6. Results

6.1 Threshold photoelectron photoion coincidence results

6.1.1 Threshold photoelectron spectrum

Figure 5.1 shows the threshold photoelectron spectrum (a) and total ion yield (b) of *c*-C_4F_8 recorded from 11 – 25 eV with 0.3 nm resolution. The stick spectrum in Figure 5.1(a) represents the ionisation energies of the twelve highest energy orbitals calculated by the OVGF method. The onset of ionisation was determined to be 11.60 ± 0.05 eV, in excellent agreement with the previous work from the Tuckett group,[19] but significantly lower than the value of 12.25 eV from an early electron ionisation study.[9] The discrepancy is probably due to the inherent lower

resolution of electron ionisation and the method used to determine the onset by extrapolation with reference to the ionisation energy of argon.

The MOs of *c*-C_4F_8 were calculated using Gaussian 03 to the MP2 level. In D_{2d} symmetry they are labelled

…..$(9a_1)^2$ $(9e)^4$ $(1a_2)^2$ $(8b_2)^2$ $(10e)^4$ $(10a_1)^2$ $(9b_2)^2$ $(2b_1)^2$ $(11e)^4$ $(11a_1)^2$ $(12e)^4$ $(3b_1)^2$

where the numbering includes all atomic orbitals. The ionisation energies (IE) have also been calculated using the outer valence Greens' Functions (OVGF) method. It is clear from Figure 5.1 that there are more MOs than peaks in the spectrum, and this is obviously due to the experiment not having the resolution to resolve such closely spaced peaks. The first peak in Figure 5.1 (vertical IE = 12.4 eV) is due to ionisation from the highest occupied molecular orbital (HOMO) with symmetry b_1 of *c*-C_4F_8. The calculated IE of this peak is 12.1 eV which agrees well with the measured VIE. The calculations show that the orbital is largely C-F antibonding and C-C bonding in character. The next peak at 14.0 eV is due to ionisation from the 12e orbital of *c*-C_4F_8, and again the VIE and OVGF calculation agree well. The next ten orbitals have energies in the range 16.4-18.3 eV and encompass the three large unresolved peaks at ~ 16.0, 16.7 and 17.5 eV. These peaks are so close in energy that their ordering is different between the MP2 calculations and the OVGF calculations which are performed at the HF level of theory. The two weak shoulders at 12.8 and 14.8 eV do not seem to be due to ionisation from a single MO.

The total ionisation cross-section is shown in Figure 5.1(b). If there are no features due to autoionisation, then the total ion yield curve should only show steps at the onset of each electronic state of c-$C_4F_8^+$. However, examination of the total ion yield shows that after these steps are reached there is a subsequent drop in ion signal. This is a clear signature of autoionisation. It seems that the majority of the peaks detected in the TPES are due to, or have contributions from autoionisation. The clearest example is the large peak at around 17 eV which also appears as a peak in the ion yield followed by a large reduction in ion signal. The two small peaks at 12.8 and 14.8 eV almost certainly arise due to autoionisation from a super-excited state. These two shoulders are not present in the recently published He(I) PES of Limão-Vieira *et al.*[34] This confirms that they arise from a resonant process.

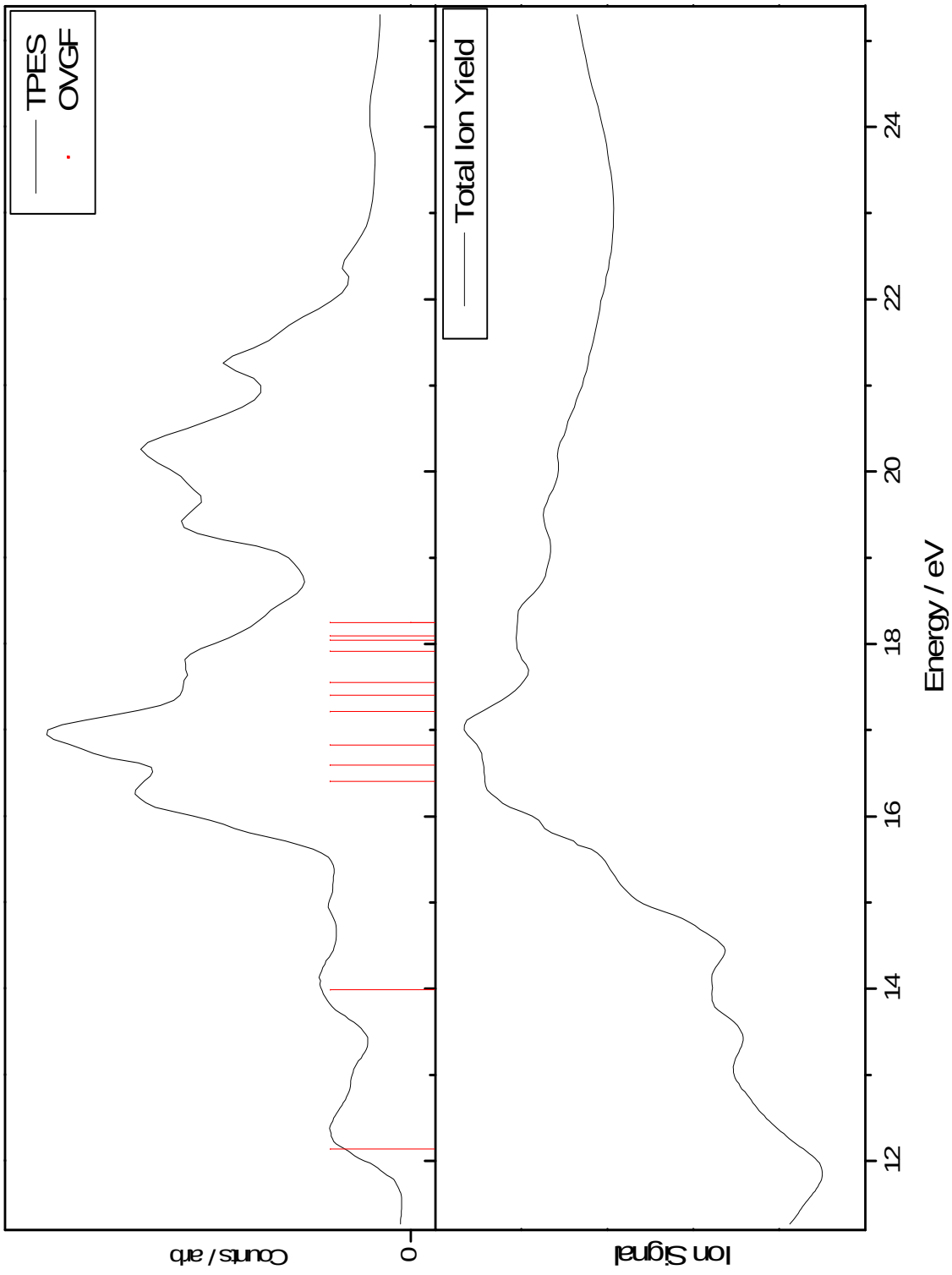

Figure 5.1: (a) Threshold photoelectron spectrum of *c*-C_4F_8, the red drop lines are IE values calculated using the OVGF method and (b) total ionisation cross-section both recorded at a resolution of 0.3 nm recorded on beamline 3.2.

6.1.2 Scanning TPEPICO spectra

The scanning energy TPEPICO spectrum was recorded from 11-25 eV with an optical resolution of 0.3 nm and a time-of-flight resolution of 64 ns. Six ions were observed, $C_4F_8^+$, $C_3F_5^+$, $C_2F_4^+$, CF_3^+, CF_2^+ and CF^+, Table 5.1 Column 2 lists their appearance energies. Our definition of AE_{298} is given in chapter 3.

Table 5.1: Thermochemistry of dissociation pathways of *c*-C_4F_8. Values in the first column are in kJ mol^{-1}.

	AE_{298} / eV	$\Delta_r H^o_{298,exp}$ / eV	$\Delta_r H^o_{298,calc}$ / eV
Products of *c*-C_4F_8 (−1515)			
c-$C_4F_8^+$ (–396) + e^-	11.60 ± 0.05	-	-
$C_3F_5^+$ (45) + CF_3 (–466) + e^-	11.68 ± 0.05	11.95 ± 0.05	11.33
$C_2F_4^+$ (316) + C_2F_4 (–659) + e^-	11.86 ± 0.05	12.13 ± 0.05	12.15
CF^+ (1134) + C_3F_7 (–1335) + e^-	14.7 ± 0.2	-	13.62
CF_2^+ (922) + C_3F_6 (–1125) + e^-	15.0 ± 0.2	-	13.60
CF_3^+ (406) + C_3F_5 (–729) + e^-	15.4 ± 0.2	-	12.36

The breakdown diagram is shown in Figure 5.2, with the TPEPICO data plotted as continuous lines and the SIFT data plotted as symbols at the recombination energy (RE) of the reagent ions; see section 6.2 for the ion-molecule results.

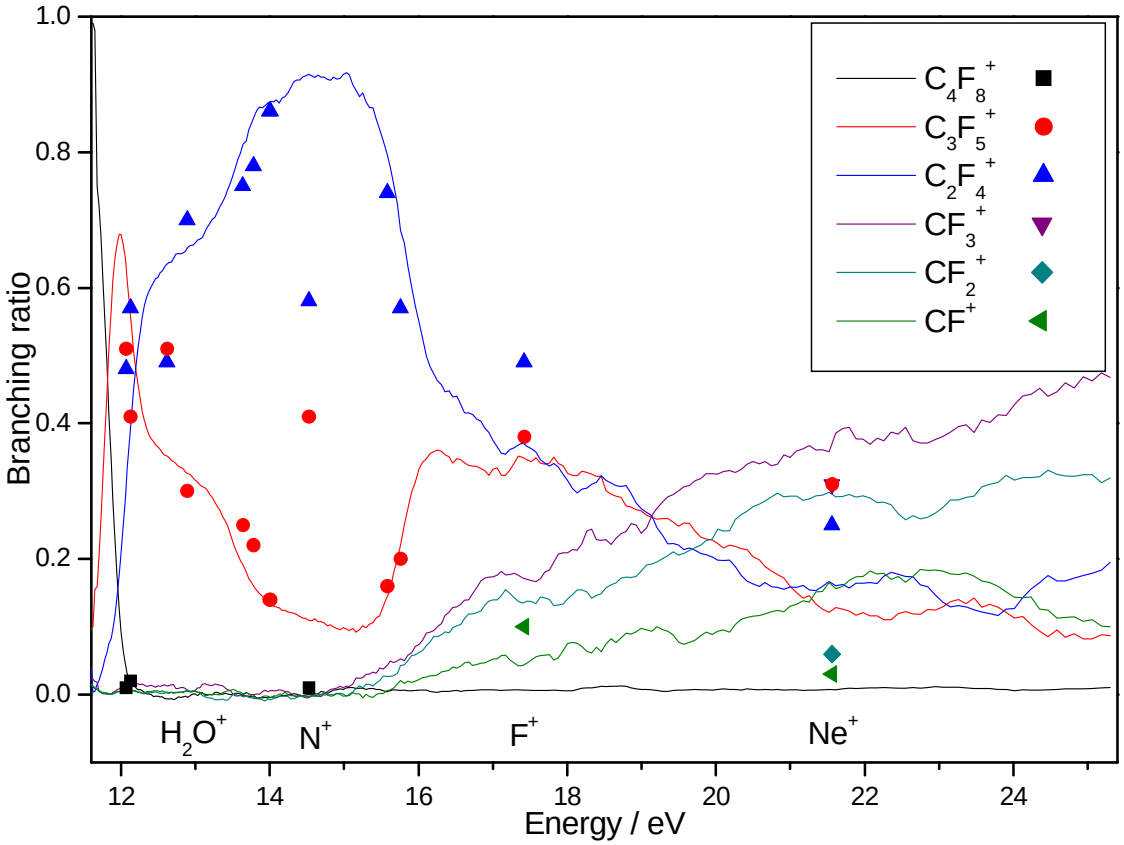

Figure 5.2: Comparison of the product ion branching ratios from photon-induced TPEPICO spectroscopy with ion-molecule studies of *c*-C_4F_8 over the energy range 11 – 25 eV. The former appear as continuous lines, the latter as individual data points at specific values.

Whilst there are no major differences from the data reported in the earlier TPEPICO study,[19] the improved statistics of the present coincidence map mean that this diagram is more accurate. The signal from $C_4F_8^+$ is very weak above its threshold energy for production. As its intensity reduces, $C_3F_5^+$ and $C_2F_4^+$ are the two main fragment ions observed. The smaller three cations have onsets at higher energy and are much weaker. The parent ion is detected from 11.60 eV ± 0.05. For dissociation of the parent ion into $C_3F_5^+$ and $C_2F_4^+$, the appearance energies of 11.68 ± 0.05 and 11.86 ± 0.05 eV have been converted into $\Delta_r H^o_{298}$ values of the corresponding unimolecular reactions; it is assumed that the neutral products are CF_3 and C_2F_4, respectively. The onsets for production of CF_3^+, CF_2^+ and CF^+ are less well defined, and their onsets are quoted with a larger error in each value of ± 0.2 eV.

The parent ion has only been seen previously in a 70 eV electron ionisation mass spectrum with a very low abundance of 0.1%,[35] and this is the first detection by photoionisation

or at such low energies. In other electron ionisation studies no parent ion is seen at all from onset to 200 eV.[15] This suggests that the TPEPICO experiment is sampling a small bound region in an otherwise repulsive ground state of $C_4F_8^+$, a region which electron ionisation lacks the resolution to sample. Recently, Bauschlicher and Ricca looked at the energetics and possible fragmentation pathways of *c*-C_4F_8 upon ionisation using *ab initio* methods.[25] Figure 5.3 is adapted from this paper and shows the low energy decomposition routes open to *c*-$C_4F_8^+$. They calculated an adiabatic ionisation energy for *c*-C_4F_8 of 10.76 eV with a vertical value of 11.24 eV, and it is noted that both values are significantly lower than any experimental measurement.[9,19]

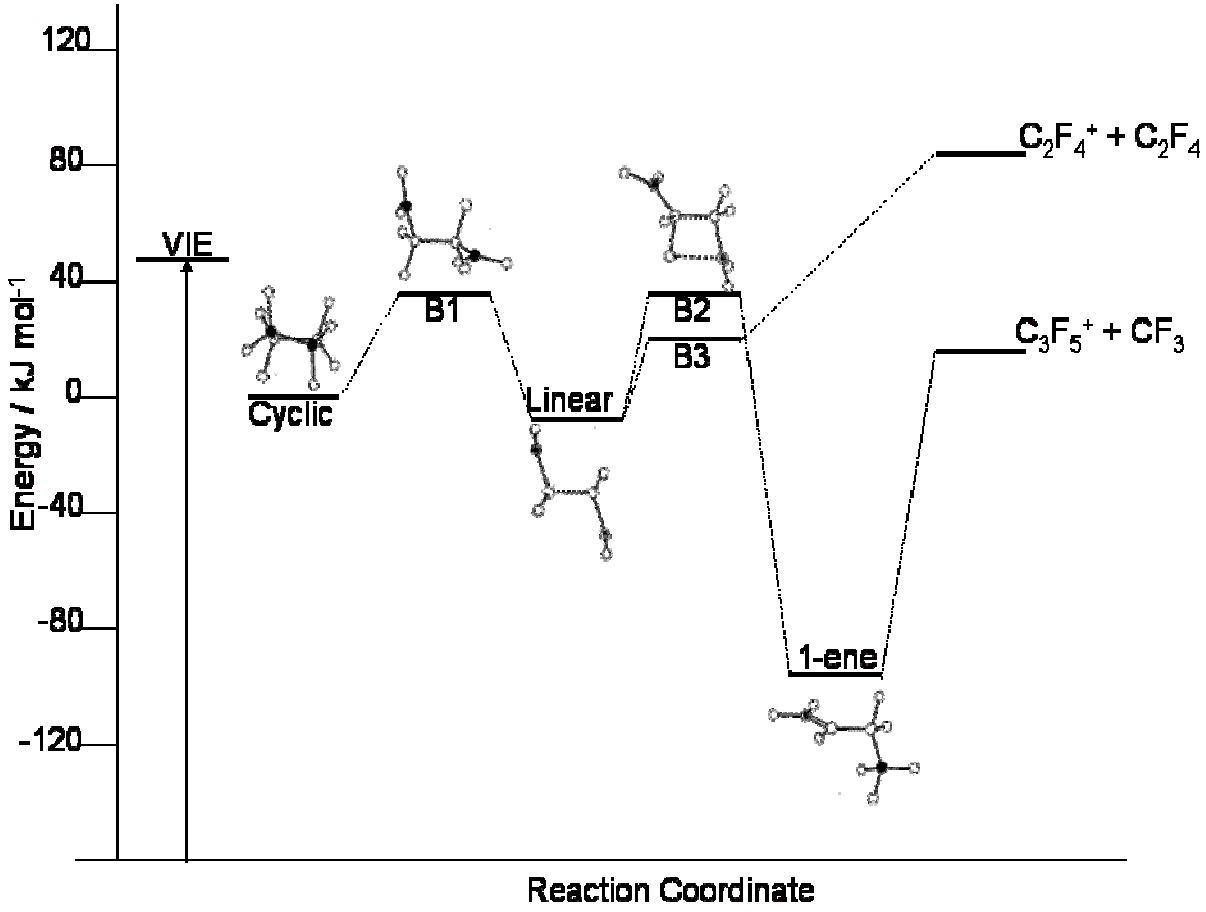

Figure 5.3: Pathways for fragmentation of *c*-$C_4F_8^+$, adapted with permission from reference 25. The units of energy on the y-axis are kJ mol^{-1}, all referenced to a zero level corresponding to the lowest vibrational level of *c*-$C_4F_8^+$.

Bauschlicher and Ricca also showed that the cyclic form of $C_4F_8^+$ lies above the open chain isomer by around 7 kJ mol^{-1} through a barrier, B1 (Figure 5.3). Furthermore vertical ionisation from the ground state of *c*-C_4F_8 will form the ion above this barrier, VIE on Figure 5.3,

and several different routes of fragmentation are then available. The TPEPICO results, which show that the first fragment ions formed are $C_3F_5^+$ and $C_2F_4^+$, agrees with the calculated pathways. Even though the calculated ionisation energies of Bauschlicher and Ricca disagree with experimental data, the *relative* energies of the fragmentation pathways of *c*-$C_4F_8^+$ are more likely to be valid. As such, with the use of the TPEPICO experimental data as a basis for the energetics, the calculations can be used to aid interpretation of the results.

From the TPEPICO data there is no way to state definitely whether the parent ion is formed in the cyclic or linear isomer. However it appears that in the range 11.6 – 12.2 eV it forms as a cyclic ion. The reasons for this belief arise from the theoretical study of Bauschlicher and Ricca. From this study the barrier B1 must be surmounted for the isomerisation from cyclic to linear form to take place. B1 is calculated to lie less than 10 kJ mol^{-1} below the barrier B2 to fragmentation into $C_3F_5^+$. So if photoionisation has sufficient energy to overcome B1 then it is probably sufficient to overcome B2 and hence fragment the parent ion. There is a small range of energies where parent ion occurs with no fragment ions present. This seems good evidence that around these energies the ion is cyclic.

The main fragments formed from 11.60 –16 eV are $C_3F_5^+$ and $C_2F_4^+$. The first fragment formed is $C_3F_5^+$ with an onset of 11.68 eV. At 11.86 eV production of $C_2F_4^+$ begins and it is the dominant ion from 12.5 – 17.5 eV. Between 14 and 16 eV there is a drastic drop in $C_3F_5^+$ production before increasing again at 16.2 eV which is the beginning of the Franck-Condon region of the large unresolved peak system. Above 14.5 eV the CF_x^+ (x = 1-3) series of ions are formed and by around 20 eV they now dominate. As described earlier, the method of Traeger and McLoughlin cannot formally be applied to any of the ionic fragmentations as they involve cleavage of more than one bond. However, bearing in mind that it is only an approximation, we have applied it to $C_3F_5^+$ and $C_2F_4^+$. These approximate values for $\Delta_r H^0_{298}$ of the unimolecular reactions allow some statements to be made on the fragmentation dynamics of ionised *c*-C_4F_8. The following unimolecular reactions have been used:

$$c\text{-}C_4F_8 \rightarrow C_3F_5^+ + CF_3 + e^- \qquad \textbf{(re 5.1)}$$

and

$$c\text{-}C_4F_8 \rightarrow C_2F_4^+ + C_2F_4 + e^- \qquad \textbf{(re 5.2)}$$

First, consider the fragmentation into $C_3F_5^+$. The calculated and experimental $\Delta_r H^0_{298}$ values (Table 5.1) shows that the threshold for this channel occurs *ca.* 0.6 eV above the thermochemical threshold, suggesting the presence of a barrier in the exit channel. Such a barrier

is to be expected as the fragmentation mechanism must contain a 1,3-fluorine migration to allow for production of the CF_3 radical. This would involve a constrained transition state for the migration step, almost certainly leading to a barrier. The presence of a barrier is predicted in the work of Bauschlicher and Ricca.[25] In their study $C_3F_5^+$ is only formed after barrier B2 (Figure 5.3), which is the transistion state for the F migration, is surmounted. It therefore forms above the thermochemical threshold, as we have measured. They calculated the excess energy needed for fragmentation to occur to be 0.31 eV, this should be compared to our approximate value of 0.62 eV.

For the fragmentation into $C_2F_4^+$ there are two possible routes. Firstly the two C-C bonds can be broken in a concerted manner, in effect an inverse cycloaddition, or the bonds could break sequentially. On the basis of frontier molecular theory the concerted mechanism is forbidden on symmetry grounds.[36] Therefore only the sequential mechanism is allowed and the fragmentation will go through a radical intermediate. Our results show that the fragmentation occurs at or near the thermochemical threshold, so there is unlikely to be a barrier in this channel. The calculated barrier from Bauschlichers study (B3, Figure 5.3) lies below the thermochemical threshold for this fragmentation, and therefore the measured appearance energy should be the same as the thermochemical value. This again shows the excellent agreement between this work and that of Bauschlicher and Ricca.

The formation of $C_3F_5^+$ appears to be a non-statistical process. This is indicated by the fact that there is a rise in $C_3F_5^+$ signal at around 15.5 eV (Figure 5.2) which corresponds to the rise in signal for the unresolved states of *c*-$C_4F_8^+$. It also appears that the CF_x^+ series of ions are formed in a non-statistical manner as they are formed well above any thermochemical onset, and the simultaneous rise in signal at ~15.5 eV again suggests that they form from the state-selected fragmentation of these unresolved states. It is possible that the CF_x^+ ions are not formed directly from fragmentation of the parent ion but are in fact formed from further fragmentation of $C_3F_5^+$. It is clear from the total ion yield curves (Figure 5.1(b)) that there is a large concentration of autoionising states in this energy region. Ionisation from these states can lead to population of non-Franck-Condon regions of the potential energy surfaces. This could lead to large alterations in branching ratios at the photon energies of these resonant states.

6.2 Selected ion flow tube results

6.2.1 Rate coefficients

Table 5.2: Selected Ion Flow Tube Results for ion molecule reactions of *c*-C_4F_8 with cations with RE from 6.27 – 21.56 eV. The dashed line indicates IE of *c*-C_4F_8 at 11.6 eV.

Reagent ion (RE / eV)	Rate coefficient / 10^{-9} cm^3 $molecule^{-1}$ s^{-1}	Product ions (%)	Proposed neutral products	$\Delta_r H^o_{298}$ / kJ mol^{-1}
H_3O^+ (6.27)	- [2.0] / (2.5)	No Reaction	-	-
SF_3^+ (8.32)	- [1.1] / (1.3)	No Reaction	-	-
CF_3^+ (9.04)	- [1.2] / (1.5)	No Reaction	-	-
CF^+ (9.11)	- [1.6] / (2.0)	No Reaction	-	-
NO^+ (9.26)	- [1.6] / (2.1)	No Reaction	-	-
SF_5^+ (9.78)	- [0.9] / (1.2)	No Reaction	-	-
SF_2^+ (10.24)	- [1.1] / (1.5)	No Reaction	-	-
SF^+ (10.31)	- [1.3] / (1.7)	No Reaction	-	-
CF_2^+ (11.44)	1.3 [1.3] / (1.7)	$C_4F_7^+$ (60) $C_4F_6^+$ (15) CF_3^+ (25)	CF_3 CF_4 c-C_4F_7 $C_3F_3 + CF_4$ $C_3F_4 + CF_3$	-39 -361 -167 -68 -61
SF_4^+ (11.99)	- [1.0] / (1.3)	No Reaction	-	-
O_2^+ (12.07)	1.9 [1.6] / (2.0)	*c*-$C_4F_8^+$ (1) $C_3F_5^+$ (51) $C_2F_4^+$ (48)	O_2 $O_2 + CF_3$ $COF_2 + OF$ $O_2 + C_2F_4$ $COF_2 + COF_2$	-46 -844 -908 8 -611
Xe^+ (12.13/13.44)	1.3 [0.9] / (1.2)	*c*-$C_4F_8^+$ (2) $C_3F_5^+$ (41)	Xe Xe +CF_3	-51 -77

		$C_2F_4^+$ (57)	Xe + C_2F_4	2
H_2O^+	2.4	$C_3F_5^+$ (51)	COF + 2HF	-136
(12.62)	[2.0] / (2.6)		CF_3 + H_2O	-123
			COF_2 + HF + H	-109
			CHF_3 + OH	-74
		$C_2F_4^+$ (49)	CH_2F_2 + COF_2	-234
			$O(CHF_2)_2$	-228
			CHF_3 + HF + CO	-224
			CHF_3 + HFCO	-218
			CF_4 + H_2CO	-193
N_2O^+	2.2	$C_3F_5^+$ (30)	COF_3 + N_2	-397
(12.89)	[1.4] / (1.7)		COF_2 + F + N_2	-326
			CF_3 + N_2O	-150
		$C_2F_4^+$ (70)	CF_4 + CO + N_2	-539
			C_2F_4O + N_2	-499
O^+	2.3	$C_3F_5^+$ (25)	CF_3O	-634
(13.62)	[2.1] / (2.7)		CF_2O + F	-563
			CF_3 + O	-220
		$C_2F_4^+$ (75)	C_2F_4O	-736
			CF_2O + CF_2	-553
CO_2^+	1.7	$C_3F_5^+$ (22)	CF_3 + CO_2	-235
(13.76)	[1.4] / (1.8)		COF_2 + COF	-190
			COF_3 + CO	-117
		$C_2F_4^+$ (78)	CF_4 + 2CO	-258
			C_2F_4O + CO	-218
Kr^+	1.3	$C_3F_5^+$ (14)	CF_3 + Kr	-257
(14.00)	[1.1] / (1.4)	$C_2F_4^+$ (86)	C_2F_4 + Kr	-178
CO^+	2.0	$C_3F_5^+$ (20)	CF_3CO	-290
(14.01)	[1.7] / (2.1)		CF_3 + CO	-258
		$C_2F_4^+$ (80)	C_2F_4 + CO	-179
N^+	2.8	$C_4F_8^+$ (1)	N	-427
(14.53)	[2.3] / (2.9)	$C_3F_5^+$ (41)	CF_3 + N	-309
			FCN + F_2	-280
			CF_2 + NF	-249
		$C_2F_4^+$ (58)	CF_4 + CN	-542
			CF_3 + FCN	-474
			CF_3CN + F	-460
			C_2F_4 + N	-230
N_2^+	2.2	$C_4F_7^+$ (9)	F + N_2	-74
(15.58)	[1.7] / (2.1)	$C_3F_6^+$ (1)	CF_2 + N_2	-272
		$C_3F_5^+$ (16)	CF_3 + N_2	-410
		$C_2F_4^+$ (74)	C_2F_4 + N_2	-331
Ar^+	1.8	$C_4F_7^+$ (22)	F + Ar	-92
(15.76)	[1.4] / (1.8)	$C_3F_6^+$ (1)	CF_2 + Ar	-290

		$C_3F_5^+$ (20)	CF_3 + Ar	-428
		$C_2F_4^+$ (57)	C_2F_4 + Ar	-349
F^+	2.3	$C_4F_7^+$ (3)	F_2	-410
(17.42)	[2.0] / (2.5)	$C_3F_5^+$ (38)	CF_4	-1133
		$C_2F_4^+$ (49)	C_2F_5	-822
			CF_4 + CF	-607
			CF_3 + CF_2	-577
			C_2F_4 + F	-508
		CF_3^+ (10)	C_3F_6	-964
			C_2F_4 + CF_4	-751
Ne^+	2.5	$C_4F_7^+$ (1)	F + Ne	-651
(21.56)	[1.9] / (2.5)	$C_4F_6^+$ (1)	F_2 + Ne	-586
		$C_3F_5^+$ (31)	CF_3 + Ne	-987
		$C_3F_4^+$ (1)	CF_4 + Ne	-1042
		$C_2F_4^+$ (25)	C_2F_4 + Ne	-908
		$C_2F_3^+$ (1)	C_2F_5 + Ne	-667
		CF_3^+ (31)	C_3F_5 + Ne	-888
		CF_2^+ (6)	C_3F_6 + Ne	-768
		CF^+ (3)	C_3F_7 + Ne	-766

Table 5.2 lists the results from the SIFT study of the ion-molecule reactions of *c*-C_4F_8 with a range of ionic species. Column 2 shows the rate coefficients, both measured and theoretical. There are two theoretical values for each reaction, in square brackets the Langevin value and in parenthesis the quadrupole value. As can be seen there is a large discrepancy between k_{exp} and k_c, with the experimental results all being far higher than the Langevin value. Clearly this is unphysical as it suggests that there are more reactions taking place than there are collisions. Morris *et al*.[16] have previously performed some of these ion-molecule reactions on a SIFT. There is excellent agreement between the values of k_{exp} in this study and in their study, suggesting that there is no fault with the k_{exp} data. Therefore there is some error in the Langevin calculations. Morris *et al* state that all their measured rates go with the collisional value. Since no details are given of how their calculations are performed, this means that the calculations used in this study cannot be checked against their calculations. For this study,[37] the value used for α', the polarisability volume, was the largest available from the literature.[4] Though this gives better agreement with experiment than lower values of α', k_c is still significantly smaller than experimental.

One possible reason for such disagreement could be *c*-C_4F_8 has another ion-neutral interaction which has not been taken into account. As stated earlier it cannot be a dipole moment due to the high symmetry of *c*-C_4F_8. It could, however, be an even higher multipole term such as

a quadrupole moment. Rate coefficients were therefore recalculated using the parameterized formula of Bhowmik and Su,[33] where in addition to the Langevin potential a quadrupole-ion potential is included (see chapter 3 section 1.1.3). For this calculation a value for the quadrupole moment, Θ, of *c*-C_4F_8 is required as well as α'. No value for Θ exists in the literature so it has been estimated to be $7.0 \pm 0.7 \times 10^{-39}$ C m^2. This empirical value and associated error gives values for the rate coefficients of a large number of the ion reactions studied which agree with the experimental values within error. The mean value for Θ, 7.0×10^{-39} C m^2, was determined by the fact that it gives a value for k_c of Ne^+ + *c*-C_4F_8 which is in exact agreement with the experimental rate coefficient; it is assumed that Ne^+ reacts at the collisional, *i.e.* capture rate. A calculation of Θ at the MP2 level of theory gives a similar value, 7.3×10^{-39} C m^2. However, it has been suggested that these values are too high,[38] based on a comparison to the quadrupole moment of C_6F_6 in the gas phase, 2.8×10^{-39} C m^2,[39] which would be expected to have a larger quadrupole moment than *c*-C_4F_8. Rather than an actual quadrupole moment it can be argued that this term is more of a correction factor to the Langevin model. *c*-C_4F_8 is a relatively large and anisotropically polarisable molecule, and many of the assumptions in the Langevin model, such as treating ions as dimensionless point charges, will become invalid. It is interesting to note that the rate coefficients measured for the ion-molecule reactions of *c*-C_5F_8, see chapter 6, were never higher than the MADO value. This is probably due to the presence of a non-zero dipole moment for *c*-C_5F_8 which will mask many of the deficiencies of the Langevin model. Nevertheless, the value of Θ used for *c*-C_4F_8 is useful in allowing qualitative comparisons and statements on reaction efficiency to be made, and to allow different results to be compared.

Using the value for Θ of $7.0 \pm 0.7 \times 10^{-39}$ C m^2, with two exceptions, all reactions proceed at the collisional rate. The two exceptions are CF_2^+ and N_2O^+. CF_2^+ reacts with an efficiency of only 75%. Since the RE (CF_2^+) is less than the IE (*c*-C_4F_8), this reaction can only proceed *via* an intimate chemical pathway, and steric effects may play a role. This is the only ion with a RE below IE (*c*-C_4F_8) where any reaction is observed. N_2O^+ has an experimental rate coefficient 30% higher than the calculated value incorporating an ion-quadrupole interaction. This is outside experimental error, and no explanation for this large value can be offered.

6.2.2 Ion-molecule branching ratios

Table 5.2 lists the ionic products and branching ratios from the SIFT study (column 3) as well as proposed neutral products and corresponding enthalpies of formation (columns 4 & 5). The proposed pathways are those which are both chemically feasible and have the most negative values for $\Delta_r H^o_{298}$. In cases where there are several feasible pathways, only an indicative selection is presented. Emphasis is placed on charge transfer reactions.

CF_2^+ is the only ion with RE < IE (*c*-C_4F_8) which reacts. Three ionic products are observed: $C_4F_7^+$ (60%), $C_4F_6^+$ (15%) and CF_3^+ (25%). These are all exothermic reactions if they are driven by loss of one or more fluorine atom. For formation of CF_3^+ the reaction is driven by fluoride ion abstraction and this allows us to bracket the fluoride ion affinity (FIA) of *c*-C_4F_8. As *c*-C_4F_8 does not react with CF_3^+ but does react with CF_2^+ then $C_4F_7^+$ must have a FIA between the values of CF_3^+ (1090 kJ mol^{-1}) and CF_2^+ (1139 kJ mol^{-1}), see chapter 1. For the reaction of CF_2^+ with *c*-C_4F_8 there was also CF^+ present as a reactant. However as CF^+ does not react with *c*-C_4F_8 this presented no complications to determination of the branching ratios. Jiao *et al* have also studied the reaction of *c*-C_4F_8 with CF_2^+ in a Fourier Transform Mass Spectrometer (FTMS).[15] In this study the major product ion was $C_3F_5^+$, a product that was not seen at all in our SIFT reaction. Also present as minor ions were $C_4F_7^+$, $C_4F_6^+$, $C_2F_4^+$ and CF_3^+. There could be several reasons for such a difference in branching ratios to occur, which all relate to the different conditions used in the two experiments. In the SIFT experiment reactions occur in a thermalised bath of He gas at ~0.5 Torr. In the FTMS the reactions occur under extremely low-pressure (~ 10^{-8} mbar), single-collision conditions. It is easy to show that collisional stabilisation of unstable ions can take place in the SIFT environment but not in a FTMS, and this will tend to ionic products showing less fragmentation in the SIFT compared to the FTMS. Another difference is that due to the bath gas the translational energies are thermal in the SIFT, whereas in the FTMS the translational energies are not clearly defined. Other difficulties are caused by the problems in measuring the pressure inside the ICR cell with an ion gauge. This has lead to differences in both reaction rates and branching ratios between the two experiments previously.[40]

For ions where the RE > IE (*c*-C_4F_8) charge transfer now becomes energetically allowed. Of these ions only SF_4^+ (11.92 eV) does not react. Exothermic pathways are available for this reaction; presumably reaction does not take place due to the reaction cross-section close to threshold being small. For the remaining ions they all react with close to 100% efficiency with a range of ionic products being formed. For ions with RE values up to *ca.* 15 eV, the major

products are $C_3F_5^+$ and $C_2F_4^+$, additionally the parent ion is observed weakly for the reactions with O_2^+, Xe^+ and N^+. For ions with RE values above 15 eV, a larger range of fragment ions are observed ($C_4F_7^+$, $C_4F_6^+$, $C_3F_6^+$, $C_3F_4^+$ $C_2F_3^+$, CF_3^+, CF_2^+ and CF^+), the branching ratios for $C_3F_5^+$ and $C_2F_4^+$ decrease, and parent ion signal is no longer observed. From the SIFT experiment the structure of the parent ion can not be determined to be either cyclic or linear. However as described earlier (section 5.1.2) it is assumed that in the energy range 11.6 – 12.2 eV the ion is cyclic.

The results of Smith and Kevan for reactions of *c*-C_4F_8 with noble gas cations agree broadly with the results presented here.[17] However, the study is performed at much higher average kinetic energies of ~50 eV, this may explain why greater amounts of fragmentation are observed in their product ions. As mentioned above Jiao *et al* studied the reaction of CF_2^+ with *c*-C_4F_8 in a FTMS, they also studied the reaction with the noble gas ions Xe^+, Kr^+ and Ar^+. The results for Kr^+ and Xe^+ are in good agreement with the data in this chapter, but agreement is poor for Ar^+. Probably this is due to uncertainty in the translational energy of the ions in the FTMS experiment. Morris *et al* used a SIFT to study reactions of *c*-C_4F_8 with cations and anions of atmospheric importance. As stated earlier the agreement in rate coefficients is excellent but, whereas the O^+ product branching ratios are in reasonable agreement, those for O_2^+ are poor. They reported $C_3F_5^+$ and $C_2F_4^+$ in the ratio 72 % : 28% and observed no parent ion, whereas in this study the ratio is 51% : 48% with the additional presence of a weak parent ion signal, 1%. It has been shown that thermalisation of excited vibrational levels of O_2^+ does not always occur in a SIFT,[41] so several $O_2^+(v)$ levels may be contributing to the reaction with *c*-C_4F_8. This phenomenon can manifest as curvature in the pseudo-first-order rate plot of *ln*(ion signal) *vs.* neutral concentration.[41] In this study, no such curvature was observed. However, it cannot be ruled out that differing amounts of $O_2^+(v)$ vibrational excitation in the two studies is contributing to the different product ion branching ratios.

7. A comparison of TPEPICO and SIFT branching ratios

Figure 5.2 shows the branching ratios from both the TPEPICO study (continuous lines) and SIFT study (discrete data points at RE of reagent ion), only products seen in both experiments being included on the plot. As described in chapter 1, a comparison of the branching ratios from the two separate experiments may indicate the mechanism by which the ions are

formed, whether it is a chemical reaction or charge transfer, either long or short range. For ions with RE from 11.6 to 12.6 eV (O_2^+, Xe^+ and H_2O^+) there is poor agreement between the SIFT and TPEPICO data. Over this range, however, the TPEPICO branching ratios are changing very rapidly with photon energy, so that small differences can become magnified. The energy of H_2O^+ (12.6 eV) corresponds to what appears to be an autoionisation feature on the edge of the $\tilde{X}$ state of *c*-$C_4F_8^+$ while the REs of the other two ions places them firmly in the $\tilde{X}$ state Franck-Condon region itself. The poor agreement between the experiments over this energy range may suggest that the orbitals involved in the ionisation process are shielded from the approaching ion, making long-range charge transfer an unfavourable process.[42-44] For ions with RE values in the range 12.9–15.8 eV, with the exception of N^+ (RE = 14.53 eV) the branching ratios into $C_3F_5^+$ and $C_2F_4^+$ agree well between the two experiments. From this it can be concluded that the reactions of N_2O^+, O^+, CO_2^+, Kr^+, CO^+, N_2^+ and Ar^+ all probably proceed by long-range charge transfer. The reactions of N^+ are often anomalous on the SIFT apparatus,[42,43] with branching ratios of fragment ions significantly different in the TPEPICO and SIFT studies. One possible explanation for this is given in chapter 1. For the two ions with RE greater than 16 eV, F^+ at 17.42 and Ne^+ at 21.56 eV, the agreement of the two datasets is poor again. For F^+, the difference in branching ratios could possibly be explained by the low signal of ion which can be formed in the high-pressure SIFT source, resulting in difficulties to obtain reliable branching ratios, as products with small percentage yield may not be detectable above background noise. For Ne^+, many more fragments are observed in the ion-molecule reaction than with photoionisation at 21.56 eV, so Ne^+ cannot react *via* a long-range mechanism. It is not clear whether the mechanism is short-range charge transfer or a chemical reaction.

8. Conclusions

The threshold photoelectron and threshold photoelectron photoion coincidence spectra of *c*-C_4F_8 in the range 11–25 eV have been recorded. The parent ion has been observed very weakly at threshold, 11.60 ± 0.05 eV, and it is most likely to have cyclic geometry. Ion yield curves and branching ratios have been determined above the ionisation threshold of *c*-C_4F_8 for the five fragments produced; $C_3F_5^+$, $C_2F_4^+$, CF_3^+, CF_2^+ and CF^+. The first ion formed is $C_3F_5^+$, at slightly higher energy $C_2F_4^+$, then successively CF^+, CF_2^+ and CF_3^+ are formed. The dominant ions are $C_3F_5^+$ and $C_2F_4^+$. It is assumed that the accompanying neutral fragments are CF_3 and C_2F_4,

respectively. In agreement with calculations of Bauschlicher and Ricca, we predict that there is a barrier in the exit channel for formation of $C_3F_5^+$, whilst there is no barrier for production of $C_2F_4^+$.

The branching ratios and rate coefficients have been measured in a selected ion flow tube at 298 K for the bimolecular reactions of *c*-C_4F_8 with H_3O^+, CF_x^+ (x = 1-3), SF_x^+ (x = 1-5), NO^+, O_2^+, Xe^+, H_2O^+, N_2O^+, O^+, CO_2^+, Kr^+, CO^+, N^+, N_2^+, Ar^+, F^+ and Ne^+. Below the energy where charge transfer becomes energetically allowed, *ca.* 11.6 eV, only one of the nine ions, CF_2^+, reacts. Above this energy, all but one of the fourteen remaining ions reacts. It has been difficult to comment on the reaction efficiency (k_{exp} / k_c) due to k_{exp} values which are consistently greater than the collisional values calculated from modified average dipole orientation theory. The inclusion of an additional ion-quadrupole interaction with a sensible choice of quadrupole moment for *c*-C_4F_8 has allowed better agreement to be achieved. With the exception of N^+, a comparison of the fragment ion branching ratios from the TPEPICO and SIFT data suggest that long-range charge transfer is the dominant mechanism for reactions of ions with recombination energy between 12.9 and 15.8 eV. For all other ions, either short-range charge transfer and/or a chemical reaction occurs.

9. References

1 C.O. Jung, K.K. Chi, B.G. Hwang, J.T. Moon, M.Y. Lee, J.G. Lee, *Thin. Sol. Fil.*, **341**, (1999) 112.
2 K. Kubota, H. Matsumoto, H. Shindo, S. Shingubara, Y. Horiike, *Jpn. J. Appl. Phys.*, **34**, (1995) 2119.
3 H. Kazumi, K. Tago, *Jpn. J. Appl. Phys.*, **34**, (1995) 2125.
4 L.G. Christophorou, J.K. Olthoff: *Fundamental Electron Interactions with Plasma Processing Gases*, Kluwer Academic / Plenum Publishers, New York, (2004).
5 Y. Gotoh, T. Kure, *Jpn. J. Appl. Phys.*, **34**, (1995) 2132.
6 C.A. Mayhew, A.D.J. Critchley, D.C. Howse, V. Mikhailov, M.A. Parkes, *Eur. Phys. J. D*, **35**, (2005) 307.
7 A.R. Ravishankara, S. Solomon, A.A. Turnipseed, R.F. Warren, *Science*, **259**, (1993) 194.
8 R.A. Morris, T.M. Miller, A.A. Viggiano, J.F. Paulson, S. Solomon, G. Reid, *J. Geo. Res.*, **100**, (1995) 1287.
9 M.M. Bibby, G. Carter, *Trans. Faraday Soc.*, **59**, (1963) 2455.
10 A. Yokoyama, K. Yokoyama, G. Fujisawa, *Chem. Phys. Lett.*, **237**, (1994) 106.
11 J.M. Simmie, W.J. Quiring, E. Tschuikov-Roux, *J. Phys. Chem.*, **73**, (1969) 3830.
12 J.N. Butler, *J. Am. Chem. Soc.*, **84**, (1962) 1393.
13 C.H. Chang, R.F. Porter, S.H. Bauer, *J. Mol. Struc.*, **7**, (1971) 89.
14 H.H. Claasen, *J. Chem. Phys.*, **18**, (1950) 543.
15 C.Q. Jiao, A. Garscadden, P.D. Haaland, *Chem. Phys. Letts.*, **297**, (1998) 121.
16 R.A. Morris, A.A. Viggiano, S.T. Arnold, J.F. Paulson, *Int. J. Mass Spec. Ion Proc.*, **149/150**, (1995) 287.
17 D.L. Smith, L. Kevan, *J. Chem. Phys.*, **35**, (1971) 2290.
18 K. Hiraoka, T. Mizuno, D. Eguchi, K. Takao, T. Iino, S. Yamabe, *J. Chem. Phys.*, **116**, (2002) 7574.
19 G.K. Jarvis, K.J. Boyle, C.A. Mayhew, R.P. Tuckett, *J. Phys. Chem. A*, **102**, (1998) 3230.
20 J.C. Traeger, R.G. McLoughlin, *J. Am. Chem. Soc.*, **103**, (1981) 3647.
21 T. Shimanouchi: *Tables of Molecular Vibrational Frequencies Consolidated Volume I*, National Bureau of Standards, (1972).
22 S.W. Benson, H.E. O'Neal, *Natl. Stand. Ref. Data Ser.*, (1970) NBS.
23 C. Bauschlicher, A. Ricca, *J. Phys. Chem. A*, **104**, (2000) 4851.
24 G.A. Garcia, P.M. Guyon, I. Powis, *J. Phys. Chem. A*, **105**, (2001) 8296.
25 C.W. Bauschlicher, A. Ricca, *J. Phys. Chem. A*, **104**, (2000) 9026.
26 R. Janoschek, M.J. Rossi, *Int. J. Chem. Kinet.*, **36**, (2004) 661.
27 R. Janoschek, M.J. Rossi, *Int. J. Chem. Kinet.*, **34**, (2002) 550.
28 K.K.S. Lau, K.K. Gleason, B.L. Trout, *J. Chem. Phys.*, **113**, (2000) 4103.
29 R.Y.L. Chim, R.A. Kennedy, R.P. Tuckett, W. Zhou, G.K. Jarvis, D.J. Collins, P.A. Hatherly, *J. Phys. Chem. A*, **105**, (2001) 8403.
30 W.F. Edgell, *J. Am. Chem. Soc*, **69**, (1947) 660.
31 G. Fischer, R.L. Purchase, D.M. Smith, *J. Mol. Struc.*, **405**, (1997) 159.
32 L.P. Theard, W.H. Hamill, *J. Am. Chem. Soc.*, **84**, (1962) 1134.
33 P.K. Bhowmik, T. Su, *J. Chem. Phys.*, **94**, (1991) 6444.
34 P. Limão-Vieira, E. Vasekova, A. Giuliani, J.M.C. Lourenço, P.M. Santos, D. Duflot, S.V. Hoffmann, N.J. Mason, J. Delwiche, M.-J. Hubin-Franskin, *Phys. Rev. A*, **76**, (2007) 032509.
35 NIST Standard Reference Database 69, June 2005: *NIST Chemistry WebBook*

36 R.B. Woodward, R. Hoffmann: *The Conservation of Orbital Symmetry*, Verlag Chemie, Weinham, (1970).
37 M.A. Parkes, S. Ali, R.P. Tuckett, V.A. Mikhailov, C.A. Mayhew, *Phys. Chem. Chem. Phys.*, **8**, (2006) 3643.
38 G.L.D. Ritchie, *Private Communication*, (2006)
39 G.L.D. Ritchie, J.N. Watson, *Chem. Phys. Letts.*, **322**, (2000) 143.
40 D. Schröder, H. Schwarz, D.E. Clemmer, Y. Chen, P.B. Armentrout, V.I. Baranov, D.K. Böhme, *Int. J. Mass Spec. Ion. Proc.*, **161**, (1997) 175.
41 D. Smith, N.A. Adams, *Adv. Atom. Mol. Phys.*, **24**, (1988) 1.
42 V.A. Mikhailov, M.A. Parkes, R.P. Tuckett, C.A. Mayhew, *J. Phys. Chem. A*, **110**, (2006) 5760.
43 M.A. Parkes, R.Y.L. Chim, C.A. Mayhew, V.A. Mikhailov, R.P. Tuckett, *Mol. Phys.*, **104**, (2006) 263.
44 G.K. Jarvis, R.A. Kennedy, C.A. Mayhew, R.P. Tuckett, *Int. J. Mass Spec.*, **202**, (2000) 323.

Chapter 6: Positive Ion Chemistry of Octafluorocyclopentene

1. Introduction

In the previous chapter the positive ion chemistry of the important industrial gas *c*-C_4F_8, which is used for the dry etching of SiO_2, was described. *c*-C_4F_8 has a high global warming potential.[1] Although it is a replacement for other feedgases such as CF_4 in technological plasmas, it is important to find alternatives which have lower global warming potential. Octafluorocyclopentene (*c*-C_5F_8) has been suggested as just such a gas.[2] The following chapter will outline the positive ion chemistry of *c*-C_5F_8. Surprisingly, even less work has been performed to date on *c*-C_5F_8 than on *c*-C_4F_8. With the exception of electron attachment investigations very few studies have been reported. Chapter 10 will give details on electron attachment to this molecule. This chapter presents the first measurements of the He(I) photoelectron spectrum (PES), the threshold photoelectron photoion coincidence spectrum (TPEPICO), an independent high-resolution threshold photoelectron spectrum (TPES) and a study of the reactions of *c*-C_5F_8 with a range of atomic and molecular ions. Also presented are some results from a new electron ionisation study of *c*-C_5F_8 performed at the University of Innsbruck.

There has been much interest in negative ion formation by *c*-C_5F_8 due to its large attachment rate coefficient of 3.62×10^{-7} cm^3 s^{-1}.[3-5] The structure has been determined by gas phase electron diffraction,[6] and mulitphoton infra-red dissociation of the molecule is well documented.[7,8] Only two studies of the ion-molecule reactions of *c*-C_5F_8 appear to have been published.[9,10] One of these studies used a Fourier transform mass spectrometer (FTMS) to measure the kinetics and products of some cation-molecule reactions. This study also presents the electron impact ionisation cross-sections of *c*-C_5F_8 from 10-200 eV.[9] This electron ionisation study is the first recorded experimental determination of the ionisation energy (IE) of *c*-C_5F_8. The second study is mainly concerned with negative ion reactions in a high pressure environment.[10]

2. Experimental

The apparatus used is the same as described in chapter 2. The TPEPICO experiment was performed on two beamlines, 3.1 and 3.2. The coincidence data was acquired on 3.1 with the Wadsworth monochromator,[11] while the threshold photoelectron spectrum (TPES), total ion yield and kinetic energy releases (KERDS) were acquired using the 5 m McPherson on beamline 3.2.[12] The sample of *c*-C_5F_8 was purchased from Apollo Scientific with a stated purity of 99%, and was used without any further purification.

3. Energetics

For the TPEPICO data we can assign appearance energies at 298 K (AE_{298}) for each ionic fragment formed. As described in chapter 3 these values can be converted into an upper limit for $\Delta_r H^0_{298}$, using the methodology of Traeger and McLoughlin.[13] It must be kept in mind that this procedure was developed for use with photoionisation cross-sections and where only a single bond is broken in the fragmentation process. With these caveats the procedure has been applied to the two fragment ions formed upon ionisation of *c*-C_5F_8; $C_4F_6^+$ and $C_5F_7^+$. The necessary vibrational frequencies of the ions were taken from Gaussian 03 calculations performed at the B3LYP level with a 6-311-G + (d,p) basis set. All other vibrational frequencies were taking from standard sources.[14] Enthalpies of formation at 298 K were taken from the standard sources,[15,16] apart from CF_3 (–466 kJ mol^{-1}) and CF_3^+ (406 kJ mol^{-1}),[17] $C_4F_x^+$ (x = 4–6),[18] $C_3F_5^+$ (45 kJ mol^{-1}),[19] and the SF_n and SF_n^+ (n = 1 – 5) series of molecules.[20] In the calculations of the enthalpy of formation of *c*-$C_5F_8^+$ the IE used was taken from the new electron ionisation study performed at the University of Innsbruck and from the high-resolution TPES of 11.24 eV.

As noted in section 4.4 of chapter 3 no enthalpy of formation was available for *c*-C_5F_8. The absence of this value would have made interpretation of the results very difficult. To remedy this, attempts were made to calculate the enthalpy of formation using Gaussian 03. Full details are given in chapter 3. The value was found to be –1495 kJ mol^{-1}. Similarly there was no enthalpy of formation available for $C_5F_7^+$. In principle it is possible to calculate this value from the TPEPICO results using the following Hess' cycle:

$$c\text{-}C_5F_8 \rightarrow C_5F_7^+ + F + e^- \qquad \textbf{(re 6.1)}$$

From the AE_{298} for this channel, and assuming that after the Traeger and McLoughlin correction has been applied that $\Delta_r H^o_{298,exp}$ is the thermochemical threshold, $\Delta_f H^0_{298}[c\text{-}C_5F_7^+]$ is found to be –84 kJ mol^{-1}. A second method to determine $\Delta_f H^0_{298}[c\text{-}C_5F_7^+]$ uses the bracketed value for the fluoride ion affinity (FIA) of $C_5F_7^+$, $1001 \leq FIA[C_5F_7^+] \leq 1045$ kJ mol^{-1}. The FIA is defined for $C_5F_7^+$ by:

$$C_5F_7^+ + F^- \rightarrow C_5F_7 \qquad \textbf{(re 6.2)}$$

This then gives $-245 \leq \Delta_f H^0_{298}[c\text{-}C_5F_7^+] \leq -201$ kJmol^{-1}, see chapter 1 section 6 for more details. However, both methods are dependent on the value used for $\Delta_f H^0_{298}[c\text{-}C_5F_8]$. To determine a value which is independent of $\Delta_f H^0_{298}[c\text{-}C_5F_8]$, we used the method outlined in section 4.4 of chapter 3 to calculate the value of $\Delta_f H^0_{298}[c\text{-}C_5F_7]$, –1105 kJ mol^{-1}. A value for the adiabatic ionisation energy was then calculated for C_5F_7 using Gaussian 03 to be 9.66 eV. This gives a $\Delta_f H^0_{298}[c\text{-}C_5F_7^+]$ value of –173 kJ mol^{-1}. Thus there is a range of ~160 kJ mol^{-1} for the possible values of $\Delta_f H^0_{298}[c\text{-}C_5F_7^+]$. Due to the closeness in values between the Gaussian calculation of the enthalpy of formation and the FIA value, we have chosen to use a value of -223 kJ mol^{-1}, which is the mid-point of the range determined by the FIA method. This method is also likely to have the least error associated with it.

4. Molecular structure

The structure of *c*-C_5F_8 was calculated using Gaussian 03. The structural optimisation would not converge at the MP2 level of theory, so all calculations were performed using DFT B3LYP 6-311G + (d,p). The molecule has C_s symmetry and the molecule has puckered, not planar, geometry. The carbon atom opposite the C=C bond (at the apex of the ring) is raised out of the plane of the ring with a pucker angle of ~22 °. This is less than the pucker angle in the hydrogen analogue, *c*-C_5H_8.

5. Theoretical Rate Calculations

The theoretical rate coefficients for the ion-molecule reactions were calculated using the MADO theory explained in chapter 3.[21-23] Values for the polarisability volume, α', and the dipole moment, μ, of *c*-C_5F_8 were required. Neither values were available in the literature and so were

estimated. α' was estimated using the additive hybrid atomic orbital method of Miller,[24] see chapter 3 section 1.2.1, the value used was 9.38×10^{-30} m^3. The dipole moment was taken from a DFT Gaussian 03 calculation and was 1.874 D. This value of μ should be compared to the dipole moment of Z-1,2-difluoroethene, 2.42 D. Z-1,2-difluoroethene has a similar configuration of atoms around the C=C bond but would be expected to have a slightly higher dipole moment due to the presence of H atoms rather than CF_2 groups.

6. Results

6.1 Threshold photoelectron photoion coincidence results

6.1.2 Threshold photoelectron spectrum and total ion yield

Figure 6.1 shows the TPES of *c*-C_5F_8 recorded from 12 – 22 eV with an optical resolution of 0.2 nm on beamline 3.2 at the Daresbury SRS. The onset of ionisation was determined to be 12.25 ± 0.05 eV. Due to second-order effects and low flux on this beamline for $\lambda > 105$ nm, scans were not performed below 11.8 eV. However, in a survey scan from 11.8 –12.2 eV no signal is observed above background. To our knowledge there has only been one previous experimental measurement of the IE of *c*-C_5F_8 and one *ab initio* calculation. From an electron ionisation study Jiao *et al*.[9] determined the IE to be 11.6 ± 0.7 eV, while Hiraoka *et al.*[10] calculated the IE to be 11.2 eV using B3LYP methods. To help resolve these issues, at our instigation a new electron ionisation study was performed at the Institut für Ionenphysik in Innsbruck,[25] and a He(I) photoelectron spectrum was recorded at the University of Southampton with Professor John Dyke. The He(I) spectrum is also shown in Figure 6.1. The electron ionisation and photoelectron spectrometers have been described in detail elsewhere.[26,27] Briefly the electron ionisation apparatus consists of a trochoidal electron monochromator, an effusive molecular beam and a quadrupole mass spectrometer to detect product ions. Optimally the electron resolution can be as high as 30 meV with an electron current of ~ 0.5 nA. The He(I) spectrometer has a hemispherical detector, the hemispheres have a 10 cm mean radius and the optimal resolution is 30 meV. The electron transmission function of the detector is linear for all electron kinetic energies above 0.3 eV. From these studies, the IE of *c*-C_5F_8 from electron ionisation was found to be 11.24 ± 0.10 eV, and from He(I) photoionisation to be 11.30 ± 0.03 eV (for the v=0 peak). The weak peaks below 11 eV in the He (I) spectrum are most likely due to hot bands. The vibrational spacing of the first band in the He (I) spectrum has an average spacing of 0.20 eV (1613 cm^{-1}) which is

probably the C=C stretch in the ground electronic state of $C_5F_8^+$. We note that the C=C stretching frequency of neutral ethene is 1623 cm^{-1}.[14]

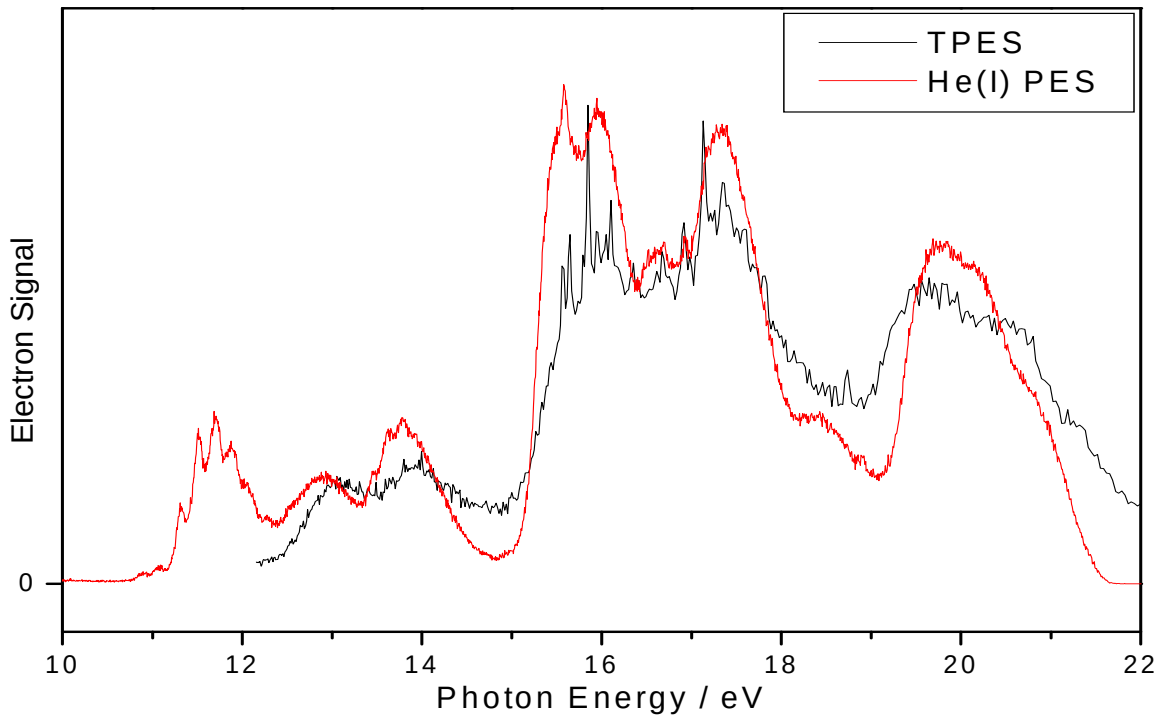

Figure 6.1: He(I) (University of Southampton) and threshold photoelectron (Daresbury Laboratory) spectra of *c*-C_5F_8. The resolution of the two spectra are 0.025 eV and 0.2 nm, respectively. Note the flat baseline in the threshold spectrum for $E < ca.$ 12.2 eV, whereas the He (I) spectrum has Franck-Condon intensity over the range 11.2–12.2 eV.

Both these new experimental data give an IE *ca.* 1 eV lower than the threshold electron measurement.[28] From 11 –12 eV the He (I) spectrum shows a band with clearly-resolved vibrational structure which is completely absent from the threshold spectrum. Unfortunately, due to the experimental limitations described above, scans were not performed below 11.8 eV under threshold conditions. Added confirmation that the IE is indeed lower than the value obtained from TPEPICO measurements comes from the observation of non-dissociative charge transfer for reactions of ions whose RE spans the range 11.2–12.2 eV with *c*-C_5F_8 (Section 6.2). Attempts have therefore been made to measure the TPES below 11.8 eV to check whether this band is truly absent. Firstly an ion-pair study was performed on *c*-C_5F_8, see Figure 6.2. [29]

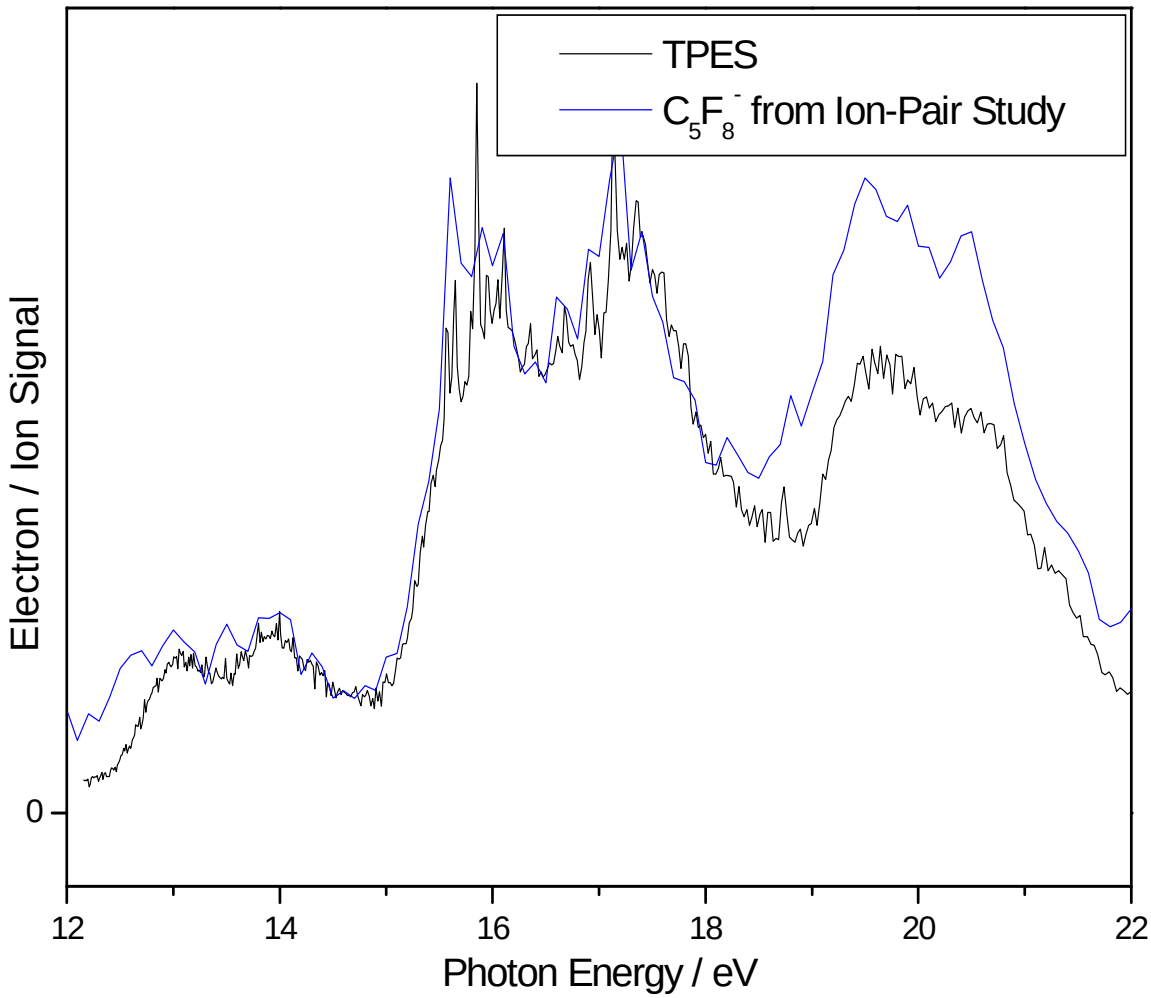

Figure 6.2: TPES for c-C5F8 on beamline 3.2 of the SRS at a resolution of 0.2 nm with the signal of $C_5F_8^-$ from photoion-pair production,[29] both are over the photon range 12 – 22 eV.

The parent anion $C_5F_8^-$ was detected, and this ion cannot be produced *via* a photoion-pair process. Therefore, it must arise from electron attachment to neutral *c*-C_5F_8. The low energy electrons needed for the attachment process are produced from threshold photoionisation during the photoion-pair experiment. This means that the signal of $C_5F_8^-$ should mirror the TPES signal. This technique to acquire the TPES *via* electron attachment is similar to a method pioneered by Ajello and Chutjian using SF_6 as a scavenger gas for low-energy electrons.[30,31] Figure 6.2 compares our TPES with the $C_5F_8^-$ signal from the ion-pair study. As can be seen the spectra are almost identical except for some minor intensity differences at around 20 eV. This is undoubtedly due to the different conditions used and the possibility of higher-energy electron attachment

resonances contributing to the signal; a similar effect has been observed with SF_6.[32,33] There appears to be some signal down to ~12 eV, however scans to lower energy with and without a lithium fluoride window, which cuts out photons with $\lambda < 105$ nm, suggests that this signal is produced by second-order radiation and that the onset of ionisation is 12.25 eV. This appears to confirm that this band is completely absent under threshold conditions.

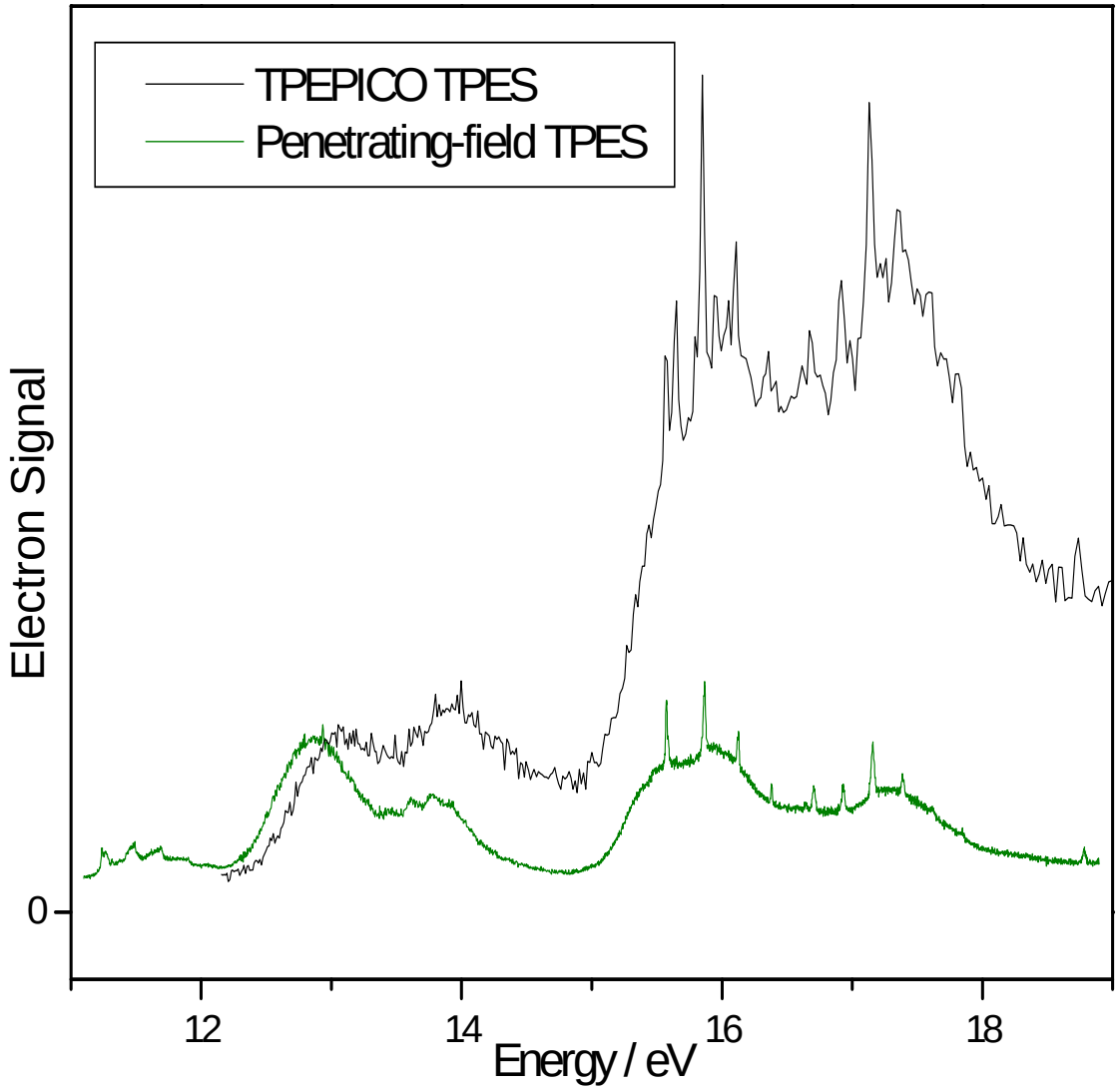

Figure 6.3: Threshold photoelectron spectrum from the TPEPICO experiment and from a penetrating-field spectrometer. The resolution of the former is 0.2 nm, the later 0.005 nm.

To confirm whether this band is truly completely absent under threshold conditions a TPES was recorded independently at the Daresbury SRS. We used the penetrating-field analyser of King

which combines high resolution (~ 0.002 eV) with excellent sensitivity.[34] The spectrum recorded with a resolution of 0.005 nm is shown in Figure 6.3, together with the threshold spectrum extracted from the coincidence experiment at a resolution of 0.2 nm. We have scaled the relative intensities of the two spectra such that the peak at ~13 eV has comparable intensity. Two points are apparent. First, the ground-state photoelectron band *is* observed under the enhanced sensitivity conditions of the penetrating-field spectrometer, but its intensity is indeed very weak. We determine the adiabatic IE of *c*-C_5F_8 to be 11.237 ± 0.002 eV. We conclude that the sensitivity of the threshold analyser in the coincidence apparatus is not sufficient to observe this very weak band, but we note that this apparatus is a compromise for efficient detection of both threshold electrons and mass-selected ions, see chapter 1 section 4.1.3.[35] Second, as both spectra are recorded nominally under threshold conditions, the relative intensities of all peaks should be similar. In practice, the relative intensity of the bands from 15 – 18 eV are significantly higher in the TPEPICO experiment. There are also many more autoionising peaks in this region recorded by the coincidence spectrometer (see later). We conclude that the threshold analyser of the coincidence spectrometer has a greater high-energy electron tail than the penetrating-field analyser. The small partial ionisation cross-section into the ground state of *c*-$C_5F_8^+$ under threshold conditions may be explained by fluorescence from, or predissociation of the initially-excited Rydberg state(s) into neutral fragments.

From the Gaussian 03 calculations in C_s symmetry the valence orbitals of *c*-C_5F_8 can be labelled as

... $(22a')^2$ $(14a")^2$ $(15a")^2$ $(23a')^2$ $(24a")^2$ $(16a")^2$ $(17a")^2$ $(25a')^2$ $(18a")^2$ $(26a')^2$ $(27a')^2$ $(19a")^2$ $(28a')^2$ $(20a")^2$ $(29a')^2$ $(21a")^2$ $(30a')^2$

where the numbering includes the core orbitals. The highest occupied molecular orbital has a' symmetry and is made up of the C=C bond π orbitals, an assignment which is confirmed by the vibrational spacing of the first band in the He(I) spectrum. The lower-energy orbitals are then combinations of C-F and C-C bonds with no clear localization of electron density into a single bond. This is the expected result for such a large molecule. Figure 6.4(a) shows the TPES of *c*-C_5F_8 recorded on beamline 3.2 at resolution of 0.2 nm. The positions of the OVGF IE values are indicated by red drop lines. The agreement with experiment is poor, with only the VIE of the measured threshold ground state showing any correlation. At higher energies the OVGF results are significantly higher in energy than peaks in the measured TPES. This is surprising because the agreement between equivalent data in *c*-C_4F_8 is excellent, see chapter 5. It is interesting that the OVGF calculations do not show the presence of the missing electronic state shown in the

He(I) PES. We note a shift of around 2 eV to lower energy in all the OVGF calculations would produce a much better agreement with the photoionisation results; this could be coincidental or significant.

In Figure 6.4(a) there are several sharp peaks in the TPES between 16-18 eV. These peaks are not due to vibrational structure because they also appear in the total relative photoion yield. Therefore they can only arise from autoionisation, indicated by resonances superimposed on non-resonant step functions. Further evidence for autoionisation is that these resolved peaks are not present under He(I) conditions (Figure 6.1), whilst they are present in reduced numbers under much higher-resolution threshold electron conditions (Figure 6.3). Figure 6.5 shows the total relative photoion yield recorded from onset to 22 eV, with the insert highlighting the autoionising features from 15.5–17.0 eV.

6.1.2 Scanning TPEPICO spectrum

The scanning energy TPEPICO spectrum was recorded from 12 – 22 eV with an optical resolution of 0.3 nm and a TOF resolution of 128 ns. Three product ions were observed (Figure 6.4(b)), $C_5F_8^+$, $C_5F_7^+$ and $C_4F_6^+$, and their appearance energies are listed in Table 6.1. The first product observed is the parent ion, $C_5F_8^+$, at 12.25 ± 0.05 eV. This is the major ion up to around 13.5 eV, before the signal drops to essentially zero at 15 eV. Above 18 eV the parent ion signal rises above zero for an energy range of *ca* 4 eV before returning to zero at 22 eV. The first fragment ion formed is $C_4F_6^+$ with an AE_{298} of 12.73 ± 0.05 eV which dominates till ~15 eV. The second and final fragment ion formed is $C_5F_7^+$ with an AE_{298} value of 15.14 ± 0.15 eV. It should be noted that some structure occurs in the $C_5F_7^+$ signal below this energy. However, as this onset is sharp, it is felt that the lower-energy features between 13 and 15 eV are artefacts of the analysis from the background subtraction technique which has been used. Above 18 eV all three ions form with roughly equal percentage.

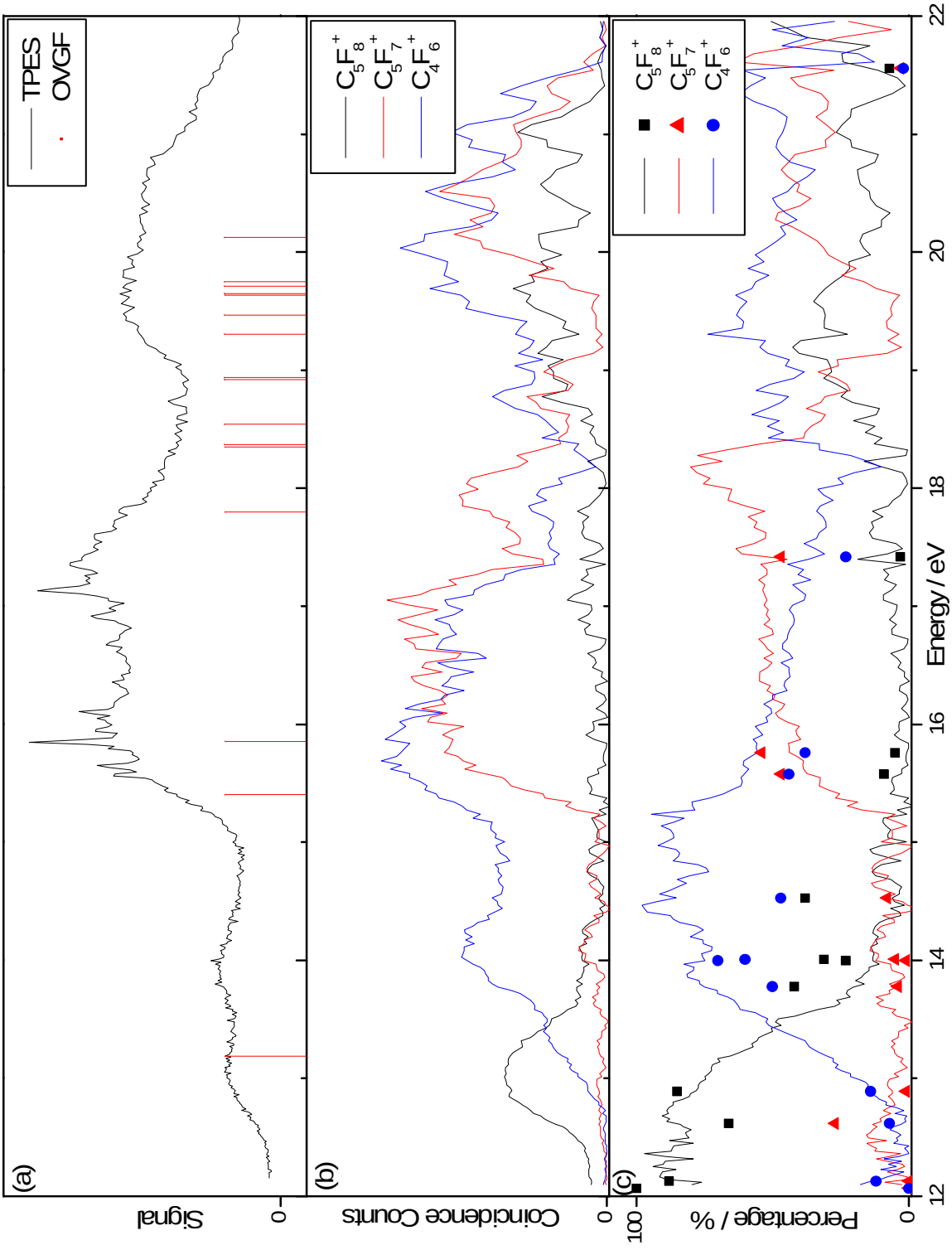

Figure 6.4: Threshold photoelectron photoion coincidence data for *c*-C_5F_8 (a) Threshold photoelectron spectrum and calculated OVGF ionisation energies, (b) ion yield curves, (c) SIFT-TPEPICO breakdown diagram.

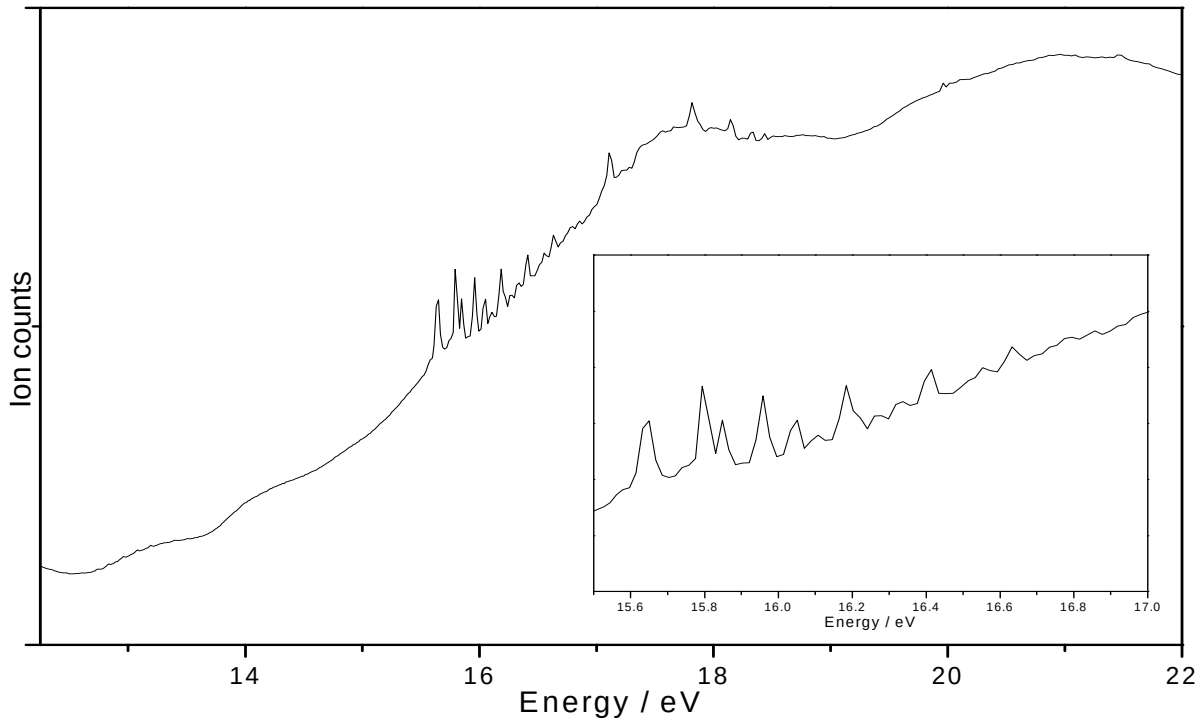

Figure 6.5: Total relative photoion yield for *c*-C_5F_8 from 12 – 22 eV recorded on beamline 3.2 with a resolution of 0.2 nm. The insert from 15.5–17.0 eV shows the features due to autoionisation of Rydberg states.

It is interesting to note that formation of $C_4F_6^+$, involving the breaking of two C-C bonds, has a lower appearance energy than formation of $C_5F_7^+$,where only a single C-F bond is broken, and this fact has been noted for other fluorocarbons by Bauschlicher and Ricca.[18] Jiao *et al* also saw the same ordering of appearance energies for $C_5F_8^+$, $C_5F_7^+$ and $C_4F_6^+$ following electron ionisation of *c*-C_5F_8.[9] They also observed $C_4F_5^+$, $C_3F_3^+$, $C_3F_4^+$, CF^+ and CF_2^+ as products. Their appearance energies, however, for $C_4F_6^+$ and $C_5F_7^+$, 14.2 and 17.5 eV, are significantly higher than our values. An obvious explanation for such differences is that their work was carried out in a FTMS where ions are trapped for an appreciable length of time. Such long storage times could lead to further fragmentation of product ions if they are metastable, giving rise to the extra fragments which we do not observe. We should note that the recent electron ionisation study performed by Feil *et al*,[25] whilst observing the same range of ions as detected in the FTMS experiment, gives similar appearance energies for $C_4F_6^+$ and $C_5F_7^+$ to our coincidence study.

Table 6.1: Thermochemistry of the observed dissociative ionisation pathways of *c*-C_5F_8 at 298 K.

	AE_{298} / eV	$\Delta_r H^o_{298,exp}$ / eV	$\Delta_r H^o_{298,calc}$ / eV
Major Products of *c*-C_5F_8 (–1495)			
c-$C_5F_8^+$(–411) + e^-	12.25	-	-
$C_5F_7^+$(–223) + F(+79)	15.14	15.44	14.00
Minor Products of *c*-C_5F_8			
$C_4F_6^+$(–21) + CF_2 (–182) + e^-	12.73	13.11	13.39
c-$C_4F_6^+$(+76) + CF_2 (–182) + e^-	12.73	13.11	14.39

In Table 6.1 the measured appearance energies have been converted into $\Delta_r H^0_{298}$ values using the method of Traeger and McLoughlin.[13] This method was applied to formation of $C_4F_6^+$, although it is an approximation for the reasons outlined in section 3, and $C_5F_7^+$. These experimental values were compared to the thermochemical values. For $C_4F_6^+$ the experimental value is actually below the thermochemical value. The difference is around 27 kJ mol^{-1}, and undoubtedly arises due to uncertainty in the calculated enthalpy of formation of *c*-C_5F_8 and our application of the Traeger and McLoughlin method. However, within reasonable error limits, it seems that the $C_4F_6^+$ onset cannot be associated with formation of *cyclic*-$C_4F_6^+$ but must involve formation of *linear*-$C_4F_6^+$. This is in agreement with the retro Diels-Alder mechanism suggested by Jiao *et al.* for formation of *linear*-$C_4F_6^+$.[9] The calculated enthalpy of reaction for $C_5F_7^+$ + F lies 0.92 eV below the experimental value. For such a simple C-F bond cleavage, an exit-channel barrier or kinetic shift of this magnitude is very unlikely. However, it is possible that the loss of an F-atom may involve a more complicated rearrangement than we assume. The lack of agreement may reflect on the *ab initio* values used for the enthalpy of formation of both *c*-C_5F_8 and $C_5F_7^+$.

6.2 Selected ion flow tube results

6.2.1 Rate coefficients

The reactions of *c*-C_5F_8 with twenty two atomic and molecular reactant ions have been studied using the SIFT apparatus with recombination energies (RE) in the range 6.27 – 21.56 eV. Five ions did not react; H_3O^+, SF_3^+ NO^+, SF_5^+ and SF_2^+. The fact that H_3O^+ did not react by proton transfer shows that the proton affinity of *c*-C_5F_8 is less than that of H_2O, *i.e.* < 691 kJ mol^{-1}. Comparisons can be made between the calculated MADO rate coefficient and the experimentally measured rate coefficient to determine the efficiency of the reaction (see Table 6.2). To calculate the MADO value the dipole moment of *c*-C_5F_8 is needed, and we used a value of 1.87 D from our Gaussian 03 *ab initio* calculations. There is excellent agreement between experimental and theoretical rate coefficients, suggesting that our values for μ and α' are essentially correct.

Most of the reactions go at or near (within 30%) of the collisional rate, and so are very efficient. However, there are two slow reactions. The slowest is the reaction of SF^+ with *c*-C_5F_8 which is only 10% efficient. There is unlikely to be significant steric hindrance for such a reaction and the disagreement is most likely because the reaction is slightly endothermic. The absence of reaction of SF_3^+, SF_5^+ and SF_2^+ with *c*-C_5F_8 can then allow the fluoride ion affinity, FIA, of $C_5F_7^+$ to be bracketed between that of SF_5^+ and SF^+, *i.e.* $1001 \leq$ FIA $[C_5F_7^+] \leq 1045$ kJ mol^{-1}. As there is a slow reaction with SF^+ but not with SF_5^+, the data suggests that the FIA[*c*-$C_5F_7^+$] probably lies closer to the FIA[SF] value, see chapter 1 for more details. The second slow reaction is H_2O^+ + *c*-C_5F_8 which reacts with only 55% efficiency. The main product is *c*-$C_5F_8^+$. We note that N_2O^+, with a similar RE to H_2O^+, reacts with *c*-C_5F_8 at the collisional rate. We suggest that H_2O^+ does not react with *c*-C_5F_8 *via* long range charge transfer, but *via* a shorter range mechanism where steric effects may be important.

6.2.2 Ion-molecule branching Ratios

Table 6.2 shows the experimental and MADO rate coefficients (Column 2) and the ionic products and branching ratios (Column 3) for the reactions of *c*-C_5F_8 with the cations used in this study. Proposed neutral products based on mass conservation and thermodynamics are given in column 4, and column 5 lists corresponding enthalpies of reactions. The pathways shown are those which are both the most exothermic and chemically feasible. In cases where there is more

than one possible pathway an indicative selection is presented. Emphasis has been placed on products due to charge transfer reactions.

Table 6.2: Rate coefficients at 298 K, product cations and branching ratios, and suggested neutral products for reactions of gas-phase cations with *c*-C_5F_8. The dashed line indicates the position of the IE of *c*-C_5F_8 at 11.24 eV.

Reagent ion (RE / eV)	Rate coefficient / 10^{-9} cm^3 molecule^{-1} s^{-1}	Product ions (%)	Proposed neutral products	$\Delta_r H^o_{298}$ / kJ mol^{-1}
H_3O^+ (6.27)	- [2.8]	No Reaction	-	-
SF_3^+ (8.32)	- [1.5]	No Reaction	-	-
CF_3^+ (9.04)	1.2 [1.6]	$C_5F_7^+$ (100)	CF_4	-66
CF^+ (9.11)	2.0 [2.3]	$C_5F_7^+$ (100)	CF_2	-43
NO^+ (9.26)	- [2.3]	No Reaction	-	-
SF_5^+ (9.78)	- [1.3]	No Reaction	-	-
SF_2^+ (10.24)	- [1.6]	No Reaction	-	-
SF^+ (10.31)	0.2 [1.8]	$C_5F_7^+$ (100)	SF_2	-21
CF_2^+ (11.44)	2.0 [1.9]	$C_5F_7^+$ (100)	CF_3	-115
O_2^+ (12.07)	2.4 [2.2]	$C_5F_8^+$ (100)	O_2	-80
Xe^+ (12.13/13.44)	1.3 [1.3]	$C_5F_8^+$ (88) $C_4F_6^+$ (12)	Xe Xe + CF_2	-86 +122
H_2O^+ (12.62)	1.6 [2.9]	$C_5F_8^+$ (66) $C_5F_7^+$ (27) $C_4F_6^+$ (7)	H_2O H_2O + F CF_2 + H_2O	-132 +136 +75
N_2O^+	2.1	$C_5F_8^+$ (85)	N_2O	-159

(12.89)	[1.9]	$C_5F_7^+$ (1)	$N_2O + F$	+109
		$C_4F_6^+$ (14)	$N_2O + CF_2$	+48
			$OCF_2 + N_2$	-491
O^+	2.6	Not Recorded	-	-
(13.62)	[3.0]			
CO_2^+	2.0	$C_5F_8^+$ (42)	CO_2	-244
(13.76)	[2.0]	$C_5F_7^+$ (4)	$CO_2 + F$	+24
		$C_4F_6^+$ (50)	$CO_2 + CF_2$	-37
			$CO + OCF_2$	-210
		$C_4F_5^+$ [f](4)	$CO_2 + CF_3$	-114
Kr^+	1.6	$C_5F_8^+$ (23)	Kr	-266
(14.00)	[1.5]	$C_5F_7^+$ (1)	Kr + F	+2
		$C_4F_6^+$ (70)	$Kr + CF_2$	-59
		$C_4F_5^+$ (6)	$Kr + CF_3$	-136
CO^+	2.4	$C_5F_8^+$ (31)	CO	-267
(14.01)	[2.4]	$C_5F_7^+$ (5)	CO + F	+1
			COF	-143
		$C_4F_6^+$ (60)	$CO + CF_2$	-60
		$C_4F_5^+$ (4)	$CO + CF_3$	-137
N^+	2.5	$C_5F_8^+$ (38)	N	-318
(14.53)	[3.3]	$C_5F_7^+$ (8)	N + F	-50
			NF	-354
		$C_4F_6^+$ (47)	$N + CF_2$	-110
			FCN + F	-286
		$C_4F_5^+$ (5)	$N + CF_3$	-188
		$C_3F_3^+$ (2)	$N + C_2F_5$	-800 - $\Delta_f H^o_{298}[C_3F_3^+]$
			$CF_3CN + F_2$	-875 - $\Delta_f H^o_{298}[C_3F_3^+]$
N_2^+	1.9	$C_5F_8^+$ (9)	N_2	-419
(15.58)	[2.4]	$C_5F_7^+$ (47)	$N_2 + F$	-151
		$C_4F_6^+$ (44)	$CF_2 + N_2$	-211
Ar^+	1.9	$C_5F_8^+$ (5)	Ar	-437
(15.76)	[1.6]	$C_5F_7^+$ (54)	Ar + F	-169
		$C_4F_6^+$ (38)	$Ar + CF_2$	-229
		$C_4F_5^+$ (3)	$Ar + CF_3$	-307
F^+	2.9	$C_5F_8^+$ (3)	F	-596
(17.42)	[2.8]	$C_5F_7^+$ (47)	F + F	-279
			F_2	-487
		$C_4F_6^+$ (23)	$F + CF_2$	-389
			CF_3	-752
		$C_4F_5^+$ (6)	$F + CF_4$	-466
			CF_4	-1013
		$C_3F_3^+$ (21)	$F + C_2F_5$	-1079 - $\Delta_f H^o_{298}[C_3F_3^+]$
			C_2F_6	-1609 - $\Delta_f H^o_{298}[C_3F_3^+]$
Ne^+	2.2	$C_5F_8^+$ (7)	Ne	-996

(21.56)	[2.7]	$C_5F_7^+$ (3)	Ne + F	-728
		$C_5F_6^+$ (2)	Ne + F_2	-585 - $\Delta_f H^o_{298}[C_5F_6^+]$
		$C_4F_6^+$ (2)	Ne + CF_2	-788
		$C_4F_5^+$ (15)	Ne + CF_3	-866
		$C_3F_5^+$ (3)	Ne + C_2F_3	-733
		$C_4F_4^+$ (2)	Ne + CF_4	-958
		$C_3F_4^+$ (12)	Ne + C_2F_4	-788
		$C_2F_4^+$ (2)	Ne + C_3F_4	-863
		$C_3F_3^+$ (43)	CF_4 + CF_3 + Ne	-1984 - $\Delta_f H^o_{298}[C_3F_3^+]$
		CF_3^+ (7)	$2C_2F_4$ + F + Ne	-1417

Eight ions whose RE falls below 11.24 eV were studied. Five did not react. The remaining three, CF_3^+, CF^+ and SF^+ react by fluoride abstraction to form $C_5F_7^+$ as the ionic product. The TPEPICO experiment shows that when fragmentation is initiated by a photon it is more facile to break C-C σ-bonds than C-F σ-bonds. However, the reactions with these three ions break the C-F bond. This shows the differences that can occur when reactions are initiated chemically, rather than by photons. CF_2^+ has an RE of 11.44 eV and so non-dissociative electron transfer is possible, instead only a F^- abstraction channel occurs to form $C_5F_7^+$. The dominant ion as a result of ion-molecule reactions from 11.24 eV to 13.5 eV is $C_5F_8^+$. For higher RE, $C_4F_6^+$ becomes as strong as the parent ion until ~15 eV when $C_5F_7^+$ is the major ion. From ~ 17 eV upwards the branching ratio to $C_3F_3^+$ becomes significant, and for Ne^+(RE = 21.56 eV) it is the major product ion.

There are only two other studies of the ion-molecule reactions of *c*-C_5F_8 available to compare these results with; the work of Jiao *et al* using a FTMS and of Hiraoka *et al* using an electron mass spectrometer.[9,10] The work of Hiraoka *et al* largely concentrates on negative ions and cluster formation. There is only one comparable reaction:

$$c\text{-}C_5F_8 + N_2^+ \rightarrow C_5F_8^+ + N_2 \qquad \textbf{(re 6.3)}$$

Parent ion is the only product, while in the SIFT experiment three product ions are detected of which the parent is only a minor channel. However, the experiment of Hiraoka *et al.* is performed at higher pressures (several Torr). Furthermore the reactant ions are formed by a 2 kV electron pulse and could be either N_2^+ or $N_2 \cdot N_2^+$. If N_2^+ is the reactant ion then the lack of products other than $C_5F_8^+$ could be due to collisional stabilisation at the high pressures used. The work of Jiao *et al* contains three reactions with which we can make comparisons:[9]

$$c\text{-}C_5F_8 + CF_3^+ \rightarrow C_5F_7^+ + CF_4 \qquad \textbf{(re 6.4)}$$

$$c\text{-}C_5F_8 + CF^+ \rightarrow C_5F_7^+ + CF_2 \qquad \textbf{(re 6.5)}$$

$$c\text{-}C_5F_8 + Ar^+ \rightarrow \text{Various} \qquad \textbf{(re 6.6)}$$

For reactions 6.4 and 6.5 the same ionic product is seen in the SIFT study, for reaction 6.6 there are some differences in branching ratios, but only of the minor channels; for example, $C_5F_8^+$ is detected at the 5 % level in the SIFT and $C_3F_3^+$ is not detected, whereas this situation is reversed in the FTMS study. Such differences are most likely due to the extremely low pressure in a FTMS and hence absence of collisional stabilisation of metastable ions. This can lead to more fragmentation in comparison to a higher-pressure experiment such as the SIFT. We note that Jiao *et al.* are only able to quote rate coefficients for the three reactions relative to that measured for the Ar^+ reaction. Our absolute values do not agree with these relative values. The difference could be due to uncertainties in the translational energy of ions in a FTMS, and the difficulties of measuring accurately absolute pressures in a FTMS system.[36]

We comment that many of the channels forming $C_5F_7^+$ and $C_4F_6^+$ with significant branching ratios are calculated to be endothermic. We are using the more negative value for $\Delta_f H^0_{298}[C_5F_7^+]$, -223 kJ mol^{-1}, of the possible values described in section 3. The experimental value from the TPEPICO experiment, -84 kJ mol^{-1}, leads to an even higher endothermicity for all reactions forming $C_5F_7^+$. Interpretations of reactions forming $C_4F_6^+$ are hindered by the lack of knowledge of the isomer formed, either linear or cyclic, although we note that the values of Table 6.2 assume the linear form is produced. We believe that the apparent endothermicities of such reactions arise from the accumulation of errors for $\Delta_f H^0_{298}$ values of *c*-C_5F_8, $C_5F_7^+$ and linear-$C_4F_6^+$.

7. Comparison of SIFT and TPEPICO branching ratios

In Figure 6.4 (c) shows the branching ratios from the TPEPICO, continuous lines, and SIFT, discrete points at RE of reactant ion, as a function of energy. Only fragment ions from the SIFT study which are also observed in the TPEPICO experiment are indicated. A comparison of the branching ratios may indicate which mechanism is occurring in the ion-molecule reactions. If the branching ratios are similar to those from photon ionisation, long-range charge transfer may be dominant; if they are different, short-range charge transfer or a chemical reaction is probably occurring. Agreement between the two experiments is good in the range 12 - 13 eV which covers the Franck-Condon envelope of the $\tilde{A}$ state of $C_5F_8^+$. The only anomalous ion in this range is

H_2O^+ which, as stated earlier, reacts with low efficiency. This is further evidence that H_2O^+ may not react by long-range charge transfer, but form a tight collision complex where steric effects and orientation will be important and inhibit the reaction channel. Other ions in this energy range probably react *via* long-range charge transfer. For energies in the range 13 -17 eV the agreement is slightly less satisfactory between TPEPICO and SIFT results. Both experiments, however, show the same trends for the fragment ions. Therefore, it seems likely that a long-range mechanism, not a short-range mechanism, operates for ions in this range. The only ion which shows a significant variation from the TPEPICO branching ratios is N^+ (RE = 14.53 eV), as observed in previous work.[37,38] It appears that reaction with N^+ causes much 'softer' ionisation (*i.e.* less fragmentation) than expected for a cation with this RE value. One explanation may be that some fraction of the N product is formed as N* (^{2}D) with an internal energy of 2.38 eV. Less energy would then be available for ionisation and subsequent fragmentation of *c*-C_5F_8. For F^+ (RE = 17.42 eV), the agreement between the branching ratios is much better, within the 15% error we define as indicative of agreement.[39] For Ne^+ (RE = 21.56 eV), however, there is poor agreement, and many more fragments are formed than from photoionisation at this energy. For Ne^+, therefore, it is likely that a compact collision complex is forming and reaction proceeds by a short-range process.

8. Conclusions

The threshold photoelectron, the threshold photoelectron photoion coincidence spectrum, and the total ion yield have been recorded for *c*-C_5F_8 from 12–22 eV. We have made the first measurement of the ionisation energy of *c*-C_5F_8 using threshold photoionisation to be 12.25 eV, which corresponds to the first excited electronic state of the parent ion, *i.e.* the ground state is undetectable in our TPEPICO measurements. The energy selected ion yields of the three product ions, $C_5F_8^+$, $C_5F_7^+$ and $C_4F_6^+$, from 12-22 eV have been measured. A He(I) photoelectron spectrum has been recorded and gives an ionisation energy for *c*-C_5F_8 of 11.30 eV for the v=0 peak. A high resolution electron ionisation study has also been performed, yielding an ionisation energy of 11.24 eV. A much higher-resolution TPES has also been performed which shows that the ground ionic state is present but only with very low intensity; the adiabatic IE is 11.237 eV.

Branching ratios and rate coefficients at 298 K for the reaction of twenty two cations with *c*-C_5F_8 have been recorded in a selected ion flow tube. Most of the ions studied react with a high

efficiency. The absence of reaction between H_3O^+ and *c*-C_5F_8 has allowed an upper limit to be placed on the proton affinity *c*-C_5F_8. Similarly, the fluoride abstraction reactions with SF_x^+ (x = 1–5) and CF_n^+ (n=1–3) have allowed upper and lower limits to be placed on the fluoride ion affinity of *c*-C_5F_8. Comparison with TPEPICO data suggests that the majority of ions react *via* a long-range charge transfer mechanism. N^+ behaves in this, as in several previous studies as a 'soft' chemical ioniser. One explanation may be that some of the product N atoms are formed electronically excited, leading to less internal energy being available to fragment $C_5F_8^+$. Using Gaussian 03 the enthalpy of formation of *c*-C_5F_8 has been calculated to be –1495 kJ mol^{-1}.

The most interesting result in this comprehensive study of the formation of positive ions from *c*-C_5F_8 is found in the photoionisation data. The first photoelectron band, which is clearly visible in the He(I) spectrum with vibrationally-resolved structure, is almost absent from the threshold photoelectron spectrum. This result may be due to either autoionisation of the Rydberg state under threshold conditions to give a distinctly non-Franck-Condon intensity distribution, or predissociation of the Rydberg state into neutrals rather than ionisation. It is well known that different vibrational distributions of a molecular photoelectron band can be observed under resonant and non-resonant conditions. However, to our knowledge, this is a very rare example of a molecular photoelectron spectrum showing a band under one set of ionisation (*i.e.* non-resonant) conditions, whilst being almost completely absent under different (*i.e.* resonant or threshold) conditions.

9. References

1 L.G. Christophorou, J.K. Olthoff: *Fundamental Electron Interactions with Plasma Processing Gases*, Kluwer Academic / Plenum Publishers, New York, (2004).
2 M. Ooka, S. Yokoyama, *Jpn. J. Appl. Phys.*, **44**, (2005) 6476.
3 A. Chutjian, S.H. Alajajian, *J. Phys. B*, **18**, (1985) 4159.
4 B.G. Zollars, K.A. Smith, F.B. Dunning, *J. Chem. Phys.*, **81**, (1984) 3158.
5 R.Y. Pai, L.G. Christophorou, A.A. Christodoulides, *J. Chem. Phys.*, **70**, (1979) 1169.
6 C.-H. Chang, S.H. Bauer, *J. Phys. Chem.*, **75**, (1971) 1685.
7 P.K. Chowdhury, *J. Phys. Chem*, **99**, (1995) 12084.
8 P.K. Chowdhury, K.V.S.R. Rao, J.P. Mittal, *J. Phys. Chem.*, **90**, (1986) 2877.
9 C.Q. Jiao, C.A. De Joseph, Jr., A. Garscadden, *J. Phys. D*, **38**, (2005) 1076.
10 K. Hiraoka, K. Fujita, M. Ishida, T. Ichikawa, H. Okada, K. Hiizumi, A. Wada, K. Takao, S. Yamabe, N. Tsuchida, *J. Phys. Chem. A*, **109**, (2005) 1049.
11 C.R. Howle, S. Ali, R.P. Tuckett, D.A. Shaw, J.B. West, *Nucl. Instru. Meth. B*, **237**, (2005) 656.
12 D.M.P. Holland, J.B. West, A.A. Macdowell, I.H. Munro, A.G. Beckett, *Nucl. Instrum. Meth. B*, **44**, (1989) 233.
13 J.C. Traeger, R.G. McLoughlin, *J. Am. Chem. Soc.*, **103**, (1981) 3647.
14 T. Shimanouchi: *Tables of Molecular Vibrational Frequencies Consolidated Volume I*, National Bureau of Standards, (1972).
15 M.W. Chase, *J. Phys. Chem. Ref. Data*, (1998) Monograph no. 9.
16 S.G. Lias, J.E. Bartmess, J.F. Liebman, J.L. Holmes, R.D. Levin, W.G. Mallard, *J. Phys. Chem. Ref. Data*, **17**, (1988) supplement no 1.
17 G.A. Garcia, P.-M. Guyon, I. Powis, *J. Phys. Chem. A*, **105**, (2001) 8296.
18 C.W. Bauschlicher, A. Ricca, *J. Phys. Chem. A*, **104**, (2000) 9026.
19 C.W. Bauschlicher, A. Ricca, *J. Phys. Chem. A*, **104**, (2000) 4581.
20 C.W. Bauschlicher, A. Ricca, *J. Phys. Chem.*, **102**, (1998) 4722.
21 T. Su, *J. Chem. Phys.*, **88**, (1988) 4102.
22 T. Su, *J. Chem. Phys.*, **89**, (1988) 5355.
23 T. Su, W.J. Chesnavich, *J. Chem. Phys.*, **76**, (1982) 5183.
24 K.J. Miller, *J. A. Chem. Soc.*, **112**, (1990) 8533.
25 S. Feil, P. Scheier, T.D. Märk, C.A. Mayhew, *Unpublished Data*, (2006)
26 V. Grill, H. Drexel, W. Sailer, M. Lezius, T.D. Märk, *Int. J. Mass spec.*, **205**, (2001) 209.
27 J.M. Dyke, A. Morris, N. Jonathon, *Int. Rev. Phys. Chem.*, **2**, (1982) 3.
28 M.A. Parkes, S. Ali, R.P. Tuckett, V.A. Mikhailov, C.A. Mayhew, *PCCP*, **9,** (2007) 5222.
29 M.J. Simpson, R.P. Tuckett, C.J. Latimer, K.F. Dunn, *Unpublished Data*, (2007)
30 A. Chutjian, J.M. Ajello, *J. Chem. Phys.*, **66**, (1977) 4544.
31 J.M. Ajello, A. Chutjian, *J. Chem. Phys.*, **65**, (1976) 5524.
32 M.J. Simpson, R.P. Tuckett, C.J. Latimer, K.F. Dunn, A. Hunniford, *J. Phys. B*, (2007) Submitted.
33 A.J. Yencha, D.B. Thompson, A.J. Cormack, D.R. Cooper, M. Zubek, P. Bolognesi, G.C. King, *Chem. Phys.*, **216**, (1997) 227.
34 R.I. Hall, A. McConkey, K. Ellis, G. Dawber, L. Avaldi, M.A. MacDonald, G.C. King, *Meas. Sci. Tech.*, **3**, (1992) 316.
35 P.A. Hatherly, D.M. Smith, R.P. Tuckett, *Zeit. Phys. Chem.*, **195**, (1996) 97.

36 D. Schröder, H. Schwarz, D.E. Clemmer, Y. Chen, P.B. Armentrout, V.I. Baranov, D.K. Böhme, *Int. J. Mass Spec. Ion. Proc.*, **161**, (1997) 175.
37 V.A. Mikhailov, M.A. Parkes, R.P. Tuckett, C.A. Mayhew, *J. Phys. Chem. A*, **110**, (2006) 5760.
38 M.A. Parkes, S. Ali, R.P. Tuckett, V.A. Mikhailov, C.A. Mayhew, *Phys. Chem. Chem. Phys.*, **8**, (2006) 3643.
39 M.A. Parkes, R.Y.L. Chim, C.A. Mayhew, V.A. Mikhailov, R.P. Tuckett, *Mol. Phys.*, **104**, (2006) 263.

Chapter 7: Isomeric Effects in the Formation of Chloroethene Cations

1. Introduction

It is of key importance to both chemistry and physics that isomeric effects are studied in gas-phase reactions. Different structures can lead to both different reactivity and different dynamics. To this end studies have been performed on six different chloroethenes. The chloroethenes are monochloroethene, dichloroethene, trichloroethene and tetrachloroethene. Dichloroethene, $C_2H_2Cl_2$, can exist in three isomeric forms. They are the 1,1-dichloroethene isomer, where both chlorines are bonded to the same carbon, and the 1,2-dichloroethenes, where the chlorines are bonded to different carbons. The 1,2 isomer can itself take two forms. These forms are the *Z* (cis) isomer where the chlorines are on the same side of the double bond, and the *E* (trans) isomer where the chlorines are on opposite sides of the C=C bond. Figure 7.1 shows the structures of monochloroethene, all three isomers of dichloroethene, trichloroethene and tetrachloroethene.

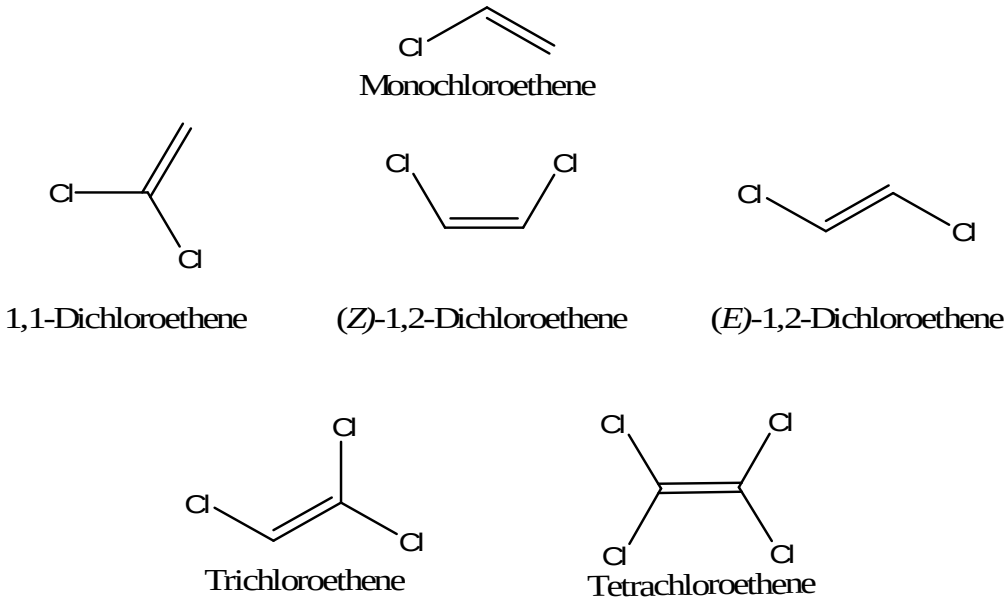

Figure 7.1: Structures of the Chloroethene isomers.

A study of these six molecules will yield much information; firstly, on the effect of additional chlorine substitution on reactivity and electronic processes, and secondly, on isomeric effects. For the three dichloroethenes it will, in essence, be a comparison between two different types of isomer. The 1,1 and 1,2 isomers are *connectivity* isomers, *i.e.* they have the same constituent atoms but the bonding arrangement is different. The relationship of the *E* to the *Z* isomers is of *stereoisomers, i.e.* the bonding is the same but, due to constrained motion around bonds, different structures result. This makes this set of isomers ideal to see how isomerisation can affect the reactivity and dynamics of molecules. The only major form of isomerisation not present is that of enantiomers.

To study how structure affects the reactions of the chloroethenes, the formation of positive ions by photoionisation and the reactions of a selection of cations with the six chloroethenes have been studied. No photoionisation study was performed on monochloroethene. This is a large study and as such will be broken into sections. Chapter 7 will deal exclusively with the formation and subsequent fragmentation of the chloroethenes following photon ionisation. Chapter 8 will compare the photon results with results from the cation-molecule study for ions whose recombination energy (RE) is greater than the ionisation energy (IE) of the isomers. Finally, chapter 9 will present the remaining cation-molecule reactions, when the RE is less than the IE of the isomers.

The ionisation of $C_2H_2Cl_2$ has been extensively studied. There have been many He(I) photoelectron studies,[1-4] but only one photoionisation study.[5] Recently, high-resolution laser-induced pulsed field ionisation-photoelectron and mass-analysed threshold ionisation spectra have been reported for the *E* isomer.[6,7] Walsh *et al* have also presented the ultra-violet absorption spectra for all three isomers.[8-10] As well as these photon-based studies electron ionisation has been performed, both the common variant,[11] and also as an (e,2e) coincidence experiment.[12-14] A theoretical analysis of vibrations in the dichloroethene photoelectron spectra has also been performed by Takeshita.[15] A study of Penning ionisation following collision of He^* (2^3S) with the dichloroethenes has also published by Ohno *et al*.[16] This formed part of a study which also examined Penning ionisation of monochloroethene.[17] For trichloroethene and tetrachloroethene both He(I) and He(II) studies have been published.[1,3] Their photoelectron spectra at a range of photon energies has also been studied by Potts *et al*., allowing insight of how the ionisation cross-section varies with energy.[18] Photoionisation studies have been performed on both tri- and tetrachloroethene.[5] Woo *et al* have studied trichloroethene in detail using high resolution photoionisation studies,[19,20] while REMPI spectra have been reported by Williams and Cool.[21]

Tetrachloroethene has been studied by two groups using multiphoton ionisation.[21,22] Electron ionisation cross sections have been reported for both tri- and tetrachloroethene from threshold to 200 eV.[23] To the best of our knowledge, surprisingly no threshold photoelectron spectra have been recorded for any of these molecules, or any measurements of energy-selected ion yields. An aim of this study is to fill this gap. So far one paper has been published from this work on the photoionisation of the dichloroethenes.[24]

2. Experimental

The experiment was performed as described in chapter 2. The three isomers of dichloroethene were purchased from Sigma-Aldrich with stated purities of 99.5, 97 and 98 % for the 1,1, *Z* and *E* isomers respectively. The trichloroethene and tetrachloroethene samples were also purchased from Sigma-Aldrich with purities of + 99 %. All samples were further purified by successive freeze-pump thawing cycles before use.

3. Energetics and theory

As previously explained in chapter 3 section 2.1, experimental appearance energies at 298 K, AE_{298}, can be converted into upper limits for $\Delta_r H^0_{298}$ for the major product ions. Major product ions are defined as those which are formed by fragmentation of only a single bond in the parent ion. In this study the only major fragments are $C_2H_2Cl^+$, $C_2HCl_2^+$ and $C_2Cl_3^+$, from C-Cl bond cleavage of di-, tri- and tetrachloroethene. The vibrational frequencies of these fragments have been calculated using Gaussian 03 at the B3LYP 6-311 G + (d,p) level. Any other vibrations needed were taken from standard sources.[25] All enthalpies of formation are from standard sources.[26,27] The exceptions are values of all neutral chloroethenes which are from Manion,[28] and values for C_2HCl^+ and $C_2Cl_2^+$ which were calculated from the enthalpy of formation of the neutral plus its respective IE (1237 kJ mol^{-1} and 1219 kJ mol^{-1}, respectively). No enthalpy of formation was available for the final fragment, C_2Cl^+, formed from tetrachloroethene.

The structures and molecular orbitals of the six neutral molecules were calculated in Gaussian 03 starting from experimental structures. The final structures were calculated at the MP2 level with a 6-311 G + (d,p) basis set. The structures are very similar to those given by gas-

phase electron diffraction and microwave measurements.[29-34] Ionisation energies of the orbitals were calculated using the outer valence Green's functions (OVGF) method.

4. Results

4.1 Threshold photoelectron spectra and total ion yields

Figure 7.2(a) – (f) presents the threshold photoelectron spectrum (TPES) and energies of the molecular orbitals calculated by the OVGF method from 9–23 eV for monochloroethene, 1,1-dichloroethene, (*Z*)-1,2-dichloroethene, (*E*)-1,2-dichloroethene, trichloroethene and tetrachloroethene, respectively. Except for monochloroethene, they were all recorded on beamline 3.2 at the Daresbury SRS with an optical resolution of 0.3 nm. The TPES of monochloroethene was taken from the work of Locht *et al*.[35] Figure 7.3(a) – (e) show the total ion yields for 1,1-dichloroethene, (*Z*)-1,2-dichloroethene,(*E*)-1,2-dichloroethene, trichloroethene and tetrachloroethene recorded at Daresbury with an optical resolution of 0.3 nm.

The adiabatic ionisation energies (IE) measured at Daresbury are 9.79, 9.66, 9.65, 9.46 and 9.30 eV for 1,1-dichloroethene, (*Z*)-1,2-dichloroethene, (*E*)-1,2-dichloroethene, trichloroethene and tetrachloroethene, respectively. The estimated error for all values is ± 0.05 eV. These are all in good agreement with the accepted literature values.[27] Recently, working under supersonic beam conditions Woo *et al.* and Bae *et al.* reported adiabatic ionisation energies for the (*E*)-1,2-dichloroethene of 9.6310 ± 0.0002 and 9.6306 ± 0.0002 eV.[6,7] Woo *et al* have also studied trichloroethene by the same technique, giving an adiabatic IE of 9.478 eV.[20] These values are slightly higher than the 298 K values which are reported here. This is to be expected because these values are quoted as 0 K values (see chapter 3 section 2.1) appropriate to a molecular beam.

The calculations performed for this thesis give the orbital energies and symmetries of the molecular orbitals (MO), and ionisation energies were obtained by the OVGF technique. Table 7.1 lists the electronic state and its symmetry, experimental and calculated vertical IE for the three dichloroethene isomers, whilst Table 7.2 lists the same results for trichloroethene and tetrachloroethene. The values in brackets in the OVGF column are the calculated pole strengths for ionisation from these states. The two states $\tilde{F}/\tilde{G}$ for 1,1 and (*E*)-1,2-dichloroethene and the states $\tilde{C}$-$\tilde{F}$ for tetrachloroethene are not resolved in our experiment.

Table 7.1: Experimental (VIE) and calculated (OVGF) vertical ionisation energies for the three isomers of dichloroethene, $C_2H_2Cl_2$.

1,1-dichloroethene			(*Z*)-1,2-dichloroethene			(*E*)-1,2-dichloroethene		
State	VIE / eV	OVGF / eV	State	VIE / eV	OVGF / eV	State	VIE / eV	OVGF / eV
$\tilde{X}\,(B_1)$	9.89	9.69 (0.91)	$\tilde{X}\,(B_1)$	10.03	9.45 (0.91)	$\tilde{X}\,(A_u)$	10.21	9.44 (0.91)
$\tilde{A}\,(B_2)$	11.68	11.41 (0.91)	$\tilde{A}\,(B_2)$	11.88	11.50 (0.91)	$\tilde{A}\,(A_g)$	11.88	11.65 (0.91)
$\tilde{B}\,(A_2)$	12.22	11.94 (0.91)	$\tilde{B}\,(A_1)$	12.08	11.78 (0.91)	$\tilde{B}\,(B_u)$	12.08	11.81 (0.91)
$\tilde{C}\,(A_1)$	12.55	12.32 (0.91)	$\tilde{C}\,(A_2)$	12.55	12.31 (0.91)	$\tilde{C}\,(B_g)$	12.77	12.48 (0.91)
$\tilde{D}\,(B_2)$	13.91	13.89 (0.91)	$\tilde{D}\,(B_1)$	13.91	13.71 (0.89)	$\tilde{D}\,(A_u)$	13.91	13.77 (0.90)
$\tilde{E}\,(B_1)$	14.19	14.20 (0.90)	$\tilde{E}\,(B_2)$	14.19	14.02 (0.91)	$\tilde{E}\,(A_g)$	14.01	13.94 (0.91)
$\tilde{F}\,/\,\tilde{G}$ $(A_1)\,/\,(B_2)$	16.15	15.95 (0.90) 16.58 (0.87)	$\tilde{F}\,(A_1)$	15.73	15.55 (0.89)	$\tilde{F}\,/\,\tilde{G}$ $(B_u)/\,(A_g)$	16.28	16.38 (0.88) 16.21 (0.89)
$\tilde{H}\,(A_1)$	18.49	18.93 (0.86)	$\tilde{G}\,(A_1)$	16.93	17.12 (0.88)	$\tilde{H}\,(B_u)$	18.99	N/A
			$\tilde{H}\,(B_2)$	18.90	N/A			

The experimental and calculated values are clearly in good agreement, although the agreement is worse at lower photon energies. The experimental values are also in good agreement with literature values of the vertical IEs, for example from von Niessen *et al.* and Lake and Thompson.[1,3]

For all chloroethenes the MOs were calculated at the MP2 level of theory, and the numbering includes all core orbitals.

In C_s symmetry, the outer valence MOs of monochloroethene are:

……$(8a')^2$ $(9a')^2$ $(10a')^2$ $(11a')^2$ $(12a')^2$ $(2a")^2$ $(13a')^2$ $(3a")^2$

In C_{2v} symmetry, the outer-valence MOs of the 1,1 isomer of $C_2H_2Cl_2$ are:

..... $(8a_1)^2$ $(9a_1)^2$ $(6b_2)^2$ $(10a_1)^2$ $(2b_1)^2$ $(7b_2)^2$ $(11a_1)^2$ $(2a_2)^2$ $(8b_2)^2$ $(3b_1)^2$.

The corresponding orbitals of (*Z*)-1,2-$C_2H_2Cl_2$, also in C_{2v} symmetry, are labelled:

…… $(7a_1)^2$ $(7b_2)^2$ $(8a_1)^2$ $(9a_1)^2$ $(8b_2)^2$ $(2b_1)^2$ $(2a_2)^2$ $(10a_1)^2$ $(9b_2)^2$ $(3b_1)^2$

(*E*)-1,2-$C_2H_2Cl_2$ has C_{2h} symmetry, and the orbitals are labelled:

..... $(7a_g)^2$ $(7b_u)^2$ $(8a_g)^2$ $(8b_u)^2$ $(9a_g)^2$ $(2a_u)^2$ $(2b_g)^2$ $(9b_u)^2$ $(10a_g)^2$ $(3a_u)^2$.

In C_s symmetry the outer valence MOs for trichloroethene can be labelled, from MP2 calculations as:

…. $(18a')^2$, $(19a')^2$, $(20a')^2$ $(21a')^2$ $(4a'')^2$ $(22a')^2$, $(5a'')^2$, $(23a')^2$, $(6a'')^2$,$(24a')^2$, $(25a')^2$, $(7a'')^2$.

Similarly in D_{2h} symmetry the outer valence MOs for tetrachloroethene are:

….$(7a_g)^2$ $(7b_{1u})^2$, $(8a_g)^2$, $(5b_{2u})^2$, $(2b_{3u})^2$, $(6b_{3g})^2$, $(2b_{2g})^2$, $(9a_g)^2$, $(8b_{1u})^2$, $(2b_{1g})^2$, $(6b_{2u})^2$, $(2a_u)^2$, $(7b_{3g})^2$ $(3b_{3u})^2$.

The relative ordering of the MOs is in excellent agreement with those previously obtained by von Niessen *et al* from OVGF calculations.[1] However, compared to the ordering proposed by Mei *et al.*[12-14] from Hartree-Fock (HF) calculations for the dichloroethenes, only the 1,1 isomer is in agreement. An obvious reason for this difference is the level of calculation. For this study a higher, though not necessarily more accurate, level of theory was used. It is well known that the ordering of closely spaced levels is affected by the level of theory used for a calculation. To check if the difference is due to the level of theory a HF calculation was performed from the MP2 optimised structure. The results of this gave the same ordering as the MP2 calculation. Therefore, it is most likely that the level of theory used for the optimisation, rather than for the self-consistent field calculations, is the cause of the difference.

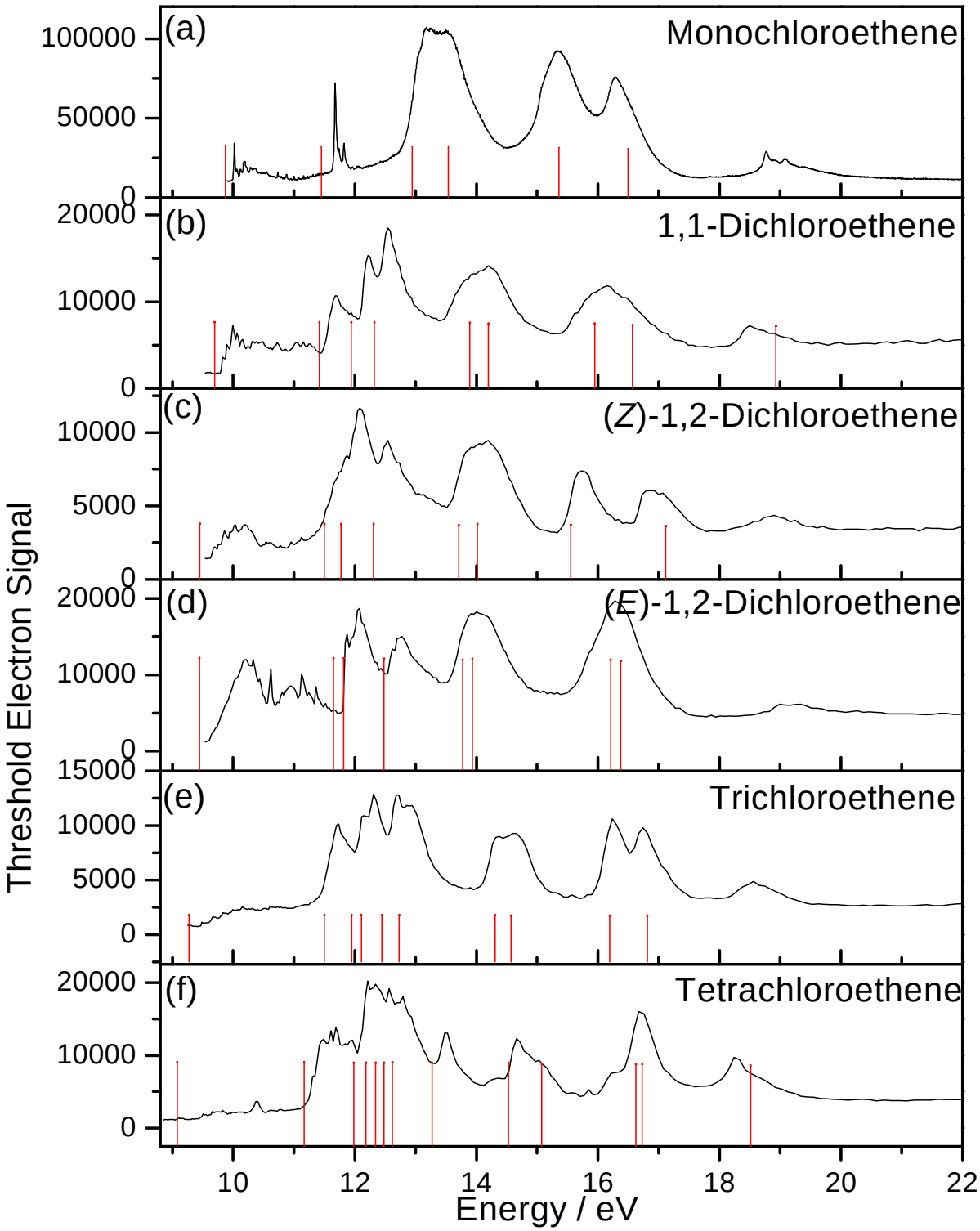

Figure 7.2: TPES for the six chloroethenes recorded with an optical resolution of 0.3 nm. The data for monochloroethene, spectrum (a), is taken from ref. 35. The red drop lines represent the calculated OVGF ionisation energies.

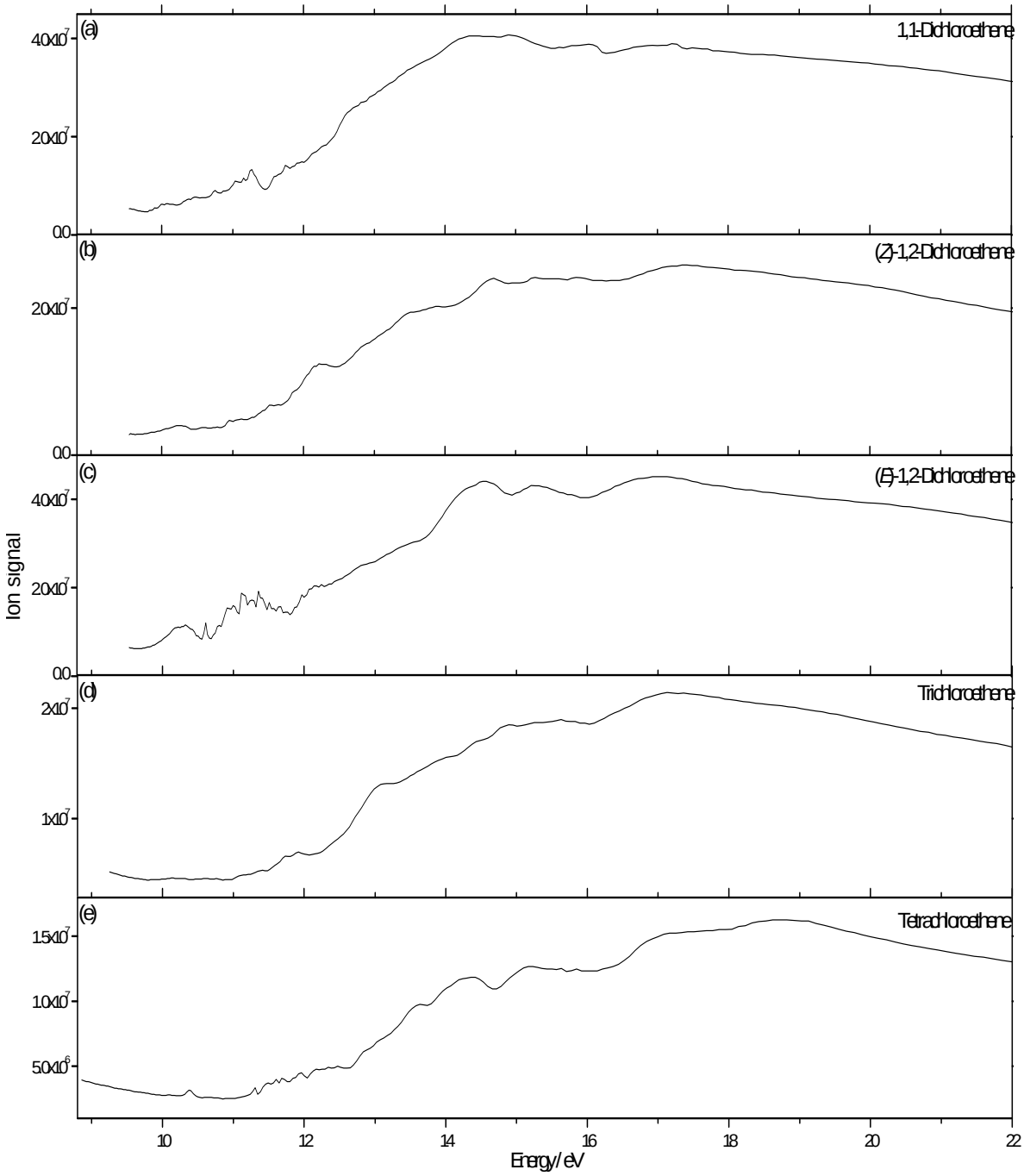

Figure 7.3: Total photoionisation yields for 1,1-dichloroethene, (*Z*)-1,2-dichloroethene, (*E*)-1,2-dichloroethene, trichloroethene and tetrachloroethene recorded with an optical resolution of 0.3 nm.

Table 7.2: Experimental and theoretical VIE for trichloroethene and tetrachloroethene

Trichloroethene			Tetrachloroethene		
State	VIE / eV	OVGF / eV	State	VIE / eV	OVGF / eV
$\tilde{X}$ (A")	10.15	9.28 (0.91)	$\tilde{X}$ (B_{3u})	9.65	9.08 (0.98)
$\tilde{A}$ (A')	11.73	11.50 (0.91)	$\tilde{A}$ (B_{3g})	11.5	11.17 (0.91)
$\tilde{B}$ (A')	12.15	11.95 (0.91)	$\tilde{B}$ (A_u)	11.96	11.98 (0.91)
$\tilde{C}$ (A")	12.31	12.11 (0.91)	$\tilde{C}$ (B_{2u})	-	12.18 (0.90)
$\tilde{D}$ (A')	12.68	12.45 (0.91)	$\tilde{D}$ (B_{1g})	-	12.34 (0.90)
$\tilde{E}$ (A")	12.94	12.73 (0.9)	$\tilde{E}$ (B_{1u})	-	12.48 (0.90)
$\tilde{F}$ (A')	14.38	14.31 (0.9)	$\tilde{F}$ (A_g)	-	12.62 (0.91)
$\tilde{G}$ (A")	14.66	14.57 (0.89)	$\tilde{G}$ (B_{2g})	13.53	13.27 (0.90)
$\tilde{H}$ (A')	16.24	16.20 (0.89)	$\tilde{H}$ (B_{3g})	14.66	14.53 (0.90)
$\tilde{I}$ (A')	16.74	16.81 (0.88)	$\tilde{I}$ (B_{3u})	15.03	15.08 (0.88)
$\tilde{J}$ (A')	18.56	-	$\tilde{J}$ / $\tilde{K}$	16.68	16.62 (0.88)
			(B_{2u}) / (B_{1u})		16.73 (0.89)
			$\tilde{L}$ (A_g)	18.23	18.51 (0.86)

It is illuminating to compare the TPES for all six molecules studied here. The first point to note is that as the number of chlorine atoms increases, the IE decreases. This is due to conjugation between the C=C π-orbitals and the out-of-plane chlorine lone pairs, and it has the effect of increasing the energy of the C=C orbital (hence lowering its IE) but decreasing the energy of the MO which largely consists of the out-of-plane Cl lone pair. This effect has been seen often before and is commented on by Lake and Thompson.[3]

All six molecules show a similar progression of states. The ground state is largely C=C π-bonding with some conjugation from out-of-plane Cl lone pairs. The next set of related states spans 11.0 – 13.5 eV. For monochloroethene there is only one state, for the three dichloroethenes there are three states, for trichloroethene five states, and for tetrachloroethene seven states. This increase in number of states by two for the addition of an extra chlorine atom strongly suggests

that they arise from lone pairs on the chlorines. Gaussian 03 calculations show this to be correct, and all these orbitals are essentially Cl lone pairs. It should be noted that the count of ionic electronic states in this region due to Cl lone pairs is one less than it should be. This is due to the conjugation of the out-of-plane Cl lone pairs with the C=C bond, which moves one of the Cl lone pair states to a higher IE. After this cluster of Cl lone pair states there is a peak which consists of two states. Gaussian 03 calculations show that one of these is due to the conjugated Cl lone pair, the other to C-Cl and C-H bonding. The ordering of these two states depends on the molecule. For monochloroethene, (*Z*)-1,2-dichloroethene and (*E*)-1,2-dichloroethene the state with lowest IE is derived from the conjugated Cl lone pair. For 1,1-dichloroethene, trichloroethene and tetrachloroethene the state of lowest IE is made up of C-Cl and C-H σ-bonds. It is not clear why the ordering reverses between these two sets of molecules.

The next peak at ~16 – 17 eV consists of two states and is resolved for monochloroethene, (*Z*)-1,2-dichloroethene and trichloroethene, but not for 1,1-dichloroethene, (*E*)-1,2-dichloroethene and tetrachloroethene. Both states are combinations of C-Cl, C=C and in some cases C-H bonding. In general the bonding in the state of lowest IE is σ-bonding along the C-Cl and C-H bond axis, in the higher IE state the C-Cl and C-H bonds are π-bonds in the plane of the molecule. It should be noted that, with states so close in energy, the ordering could easily change in *ab initio* calculations depending on the method and basis set used. Whether the peaks are resolved depends on the symmetry of the two states. For molecules where the two states are resolved, they both have the same symmetry which causes an enhanced separation of the states.

The total ionisation yields for photoionisation of the five chloroethenes studied (Figure 7.3) show some interesting features. The yields show clear contribution at several energies of autoionising states. This is especially noticeable in the vicinity of the first excited ionic state of all five molecules. The total ion yield for (*E*)-1,2-dichloroethene, Figure 7.3(c), shows a long progression of such states between the ground and first excited states of (*E*)-1,2-dichloroethene. These states have an approximate average spacing of between 0.10 and 0.11 eV (806 – 887 cm^{-1}). In gas-phase pulsed-field ionisation Woo *et al* measured frequencies of 873 cm^{-1} and 836 cm^{-1} for the ν_8 and the ν_6 modes of the (*E*)-1,2-dichloroethene cation.[6] In an argon matrix Zhou *et al.* [36] measured a value of 840 cm^{-1} for the ν_6 mode. There was no sign of chlorine isotopes effects in the ν_6 mode so Zhou *et al* assigned it to a C-H bend. For this thesis calculations were performed to obtain the vibrational frequencies of (*E*)-$C_2H_2Cl_2^+$ using DFT B3LYP and a 6-311G + (d,p) basis set. This calculation gave two vibrations in the correct energy range. However, one had A_u

symmetry while the second had B_g, as the vibration has to transform in A_g symmetry neither could be responsible for the detected vibration. There is a vibration at 940 cm^{-1} with A_g symmetry due to a symmetric C-Cl stretch. These calculations contradict the experimental results of Zhou, but due to the difference in energies it is likely that this vibrational Rydberg progression must be due to a C-H bend of some form.

It is interesting that the three dichloroethenes show such similar TPES. The sequence of states and their relative intensities are very similar. The largest differences are the energy separation of the two states at around 16 eV, $\tilde{F}$ and $\tilde{G}$. Another difference is that the intensity of the first band of (*E*)-1,2-dichloroethene is almost the same as other bands in the spectrum. For both 1,1-dichloroethene and (*Z*)-1,2-dichloroethene it is much weaker.

4.2 Scanning Energy TPEPICO spectra

4.2.1 Energy-selected ion yields and breakdown diagrams

Figure 7.4 (a) – (f) shows the energy-selected ion yields for the three dichloroethenes, trichloroethene and tetrachloroethene. Figure 7.5(a) – (d) shows the breakdown diagram for the three dichloroethenes and trichloroethene; due to poor signal-to-noise the breakdown diagram for tetrachloroethene is not presented. The spectra were recorded from onset of ionisation to 22 eV with an optical resolution of 0.3 nm and a TOF resolution of 64 ns. This TOF resolution is much lower than the highest achievable with the current time-to-digital converter (TDC) card of 8 ns, but it was then possible to record all ionic fragments on one 3D coincidence map. Use of such a degraded resolution means that any loss of hydrogen atoms cannot be resolved on the 3D map as it would shift the fragment TOF by only one acquisition channel of the TDC. However, measurement at a selection of fixed energies of the TOF distribution at higher TOF resolution for all products did not indicate the presence of any H-loss channels. Therefore it is assumed that the H-atom loss from any of the product channels is insignificant; for the dichloroethenes this is in broad agreement with the results of Momigny.[11] To be accurate, however, the branching ratios of all ionic products (*e.g.* $C_2H_2Cl^+$) should be considered as incorporating fragments formed due to H-atom loss (*i.e.* $C_2H_2Cl^+$, C_2HCl^+ and C_2Cl^+).

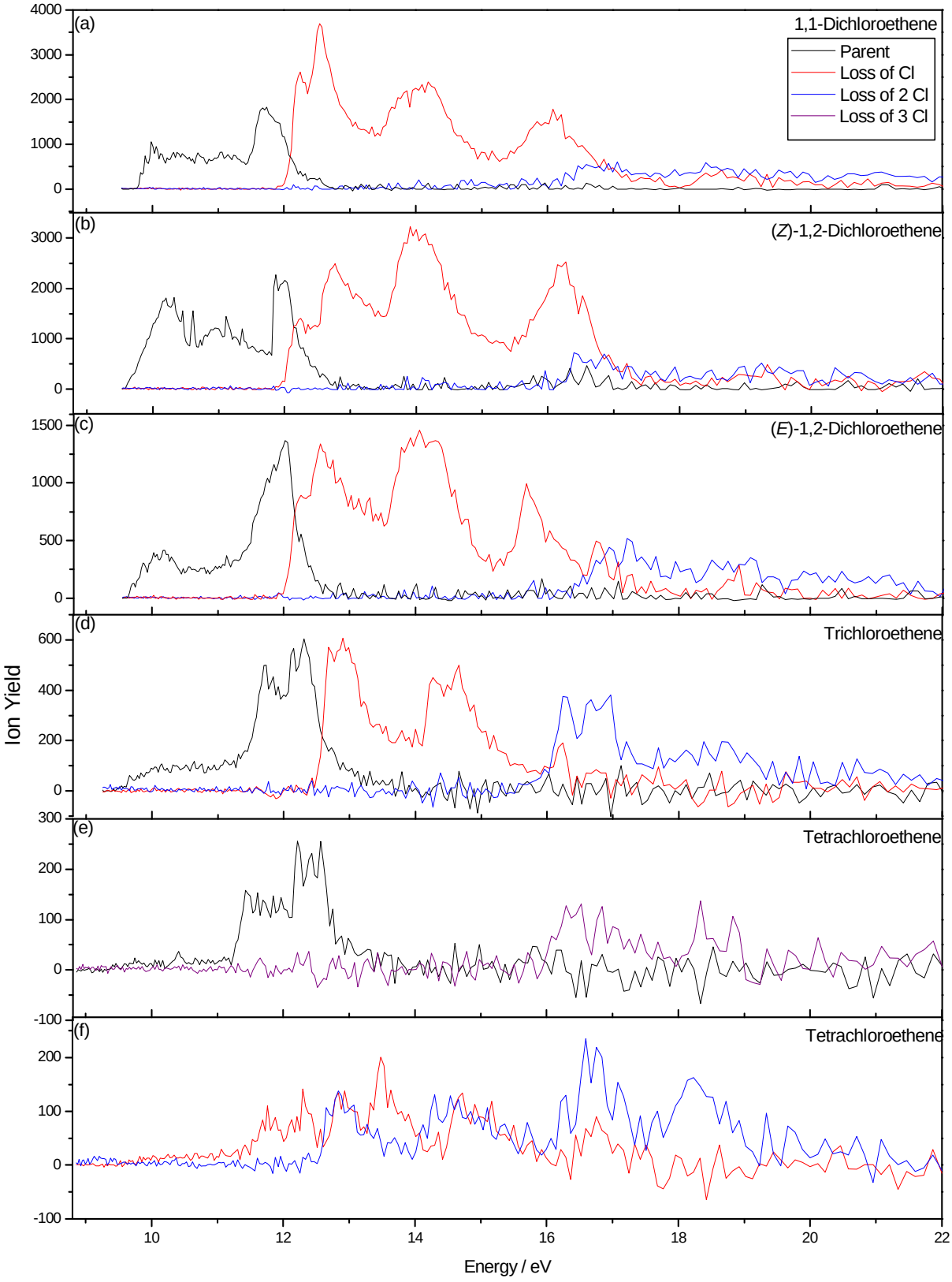

Figure 7.4: Energy-selected ion yields for five chloroethenes, recorded at an optical resolution of 0.3 nm.

For all of the five molecules studied there are very similar photoionisation products. Parent ion is detected at threshold. At higher energies first one Cl atom is lost and as the photon energy is raised a second Cl atom is lost. For tetrachloroethene three Cl atoms are lost at high photon energies. The product ions and their respective AE_{298} values are listed in Table 7.3 for the dichloroethenes and Table 7.4 for trichloroethene and tetrachloroethene. Also listed are the experimental $\Delta_r H^0_{298}$ values from applying the method of Traeger and McLoughlin to the values of AE_{298}, as well as the calculated values of $\Delta_r H^0_{298}$ and $\Delta_f H^0_{298}$ of the chemical species involved in the unimolecular dissociations. All values are given in eV except $\Delta_f H^0_{298}$ values which are in kJ mol^{-1}. It should be noted that there is no value for $\Delta_f H^0_{298}[C_2Cl^+]$ available, so no calculation has been made for this channel produced from C_2Cl_4.

Three products are detected for the dichloroethenes (Figure 7.4 (a) – (c) and Figure 7.5(a) – (c)), they are $C_2H_2Cl_2^+$, $C_2H_2Cl^+$ and $C_2H_2^+$. The parent ion is formed from the first two states and is the only product in this energy range. For the next five states, the energy range 12 – 17 eV, Cl-atom loss dominates. The AE_{298} for $C_2H_2Cl^+$ are 11.88 ± 0.05, 11.88 ± 0.05 and 11.84 ± 0.05 eV for the 1,1 and the Z and E isomers respectively. Formation of $C_2H_2^+$ begins at around 16 eV (16.28 ± 0.15, 16.47 ± 0.15 and 16.28 ± 0.15 eV for the 1,1, *Z* and *E* isomers of $C_2H_2Cl_2$, respectively) and is the main ion after ~ 17 eV. Kim *et al.* studied the lifetime of excited electronic states of dichloroethene cations using a charge-exchange technique in a reversed-geometry double-focussing mass spectrometer.[37] They found that, following electron ionisation at 17 eV, the $\tilde{B}$ states had long lifetimes, on the order of tens of microseconds, while states at higher energy rapidly dissociate. This confirms the results given here that the parent ion is not formed at energies above the energy of the $\tilde{B}$ state, but fragments instead.

It is interesting to note that, apart from a slight difference in the branching ratios for $C_2H_2Cl^+$ and $C_2H_2^+$ above 20 eV, there are no clear isomeric effects in the dichloroethene selected ion yields. This is less surprising for the (*Z*)-1,2- and (*E*)-1,2-dichloroethene isomers where the difference is due to the constrained rotation about the C=C double bond. This constraint may be lost upon ionisation, making all the ions formed from the *Z* and *E* isomers equivalent.[11] It is more surprising that the 1,1 isomer shows very similar ion yields to either 1,2 isomer. Now, the two chlorines are bonded on the same carbon and larger differences would be expected in comparison with the other isomers. This is probably because the dissociation is statistical and so the actual bonding arrangement of the molecules does not matter only the bond strengths, which are essentially the same for all three dichloroethenes.

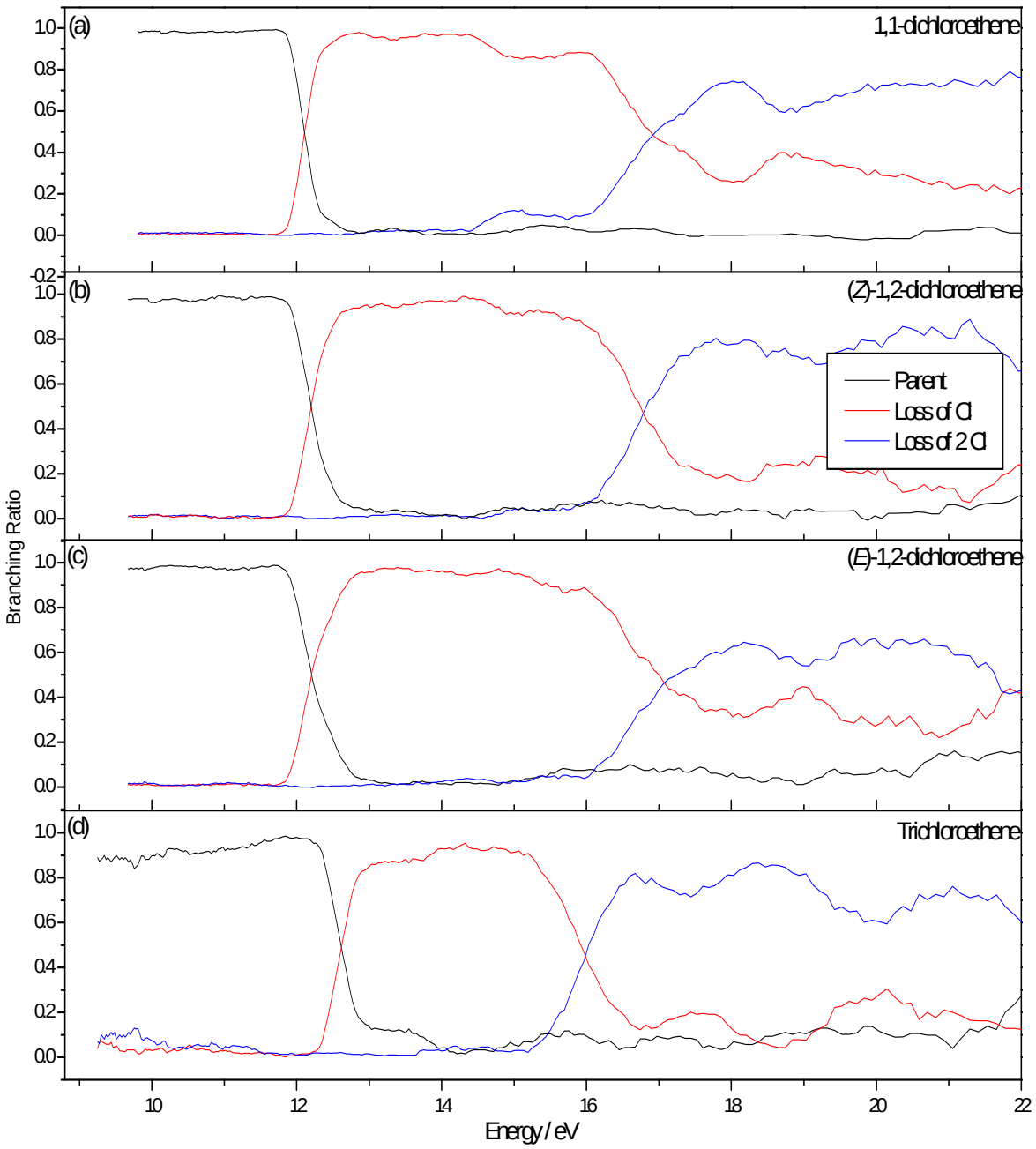

Figure 7.5 : Breakdown diagram for the dichloroethenes and trichloroethene recorded with an optical resolution of 0.3 nm.

For trichloroethene (Figure 7.4 (d) and Figure 7.5(d)) three products are also detected. They are the parent ion, $C_2HCl_2^+$ and C_2HCl^+. The parent ion is the only product formed from onset for the first four ionic states. The first fragment ion detected is $C_2HCl_2^+$ at 12.35 ± 0.05 eV. After this energy the signal for parent ion drops essentially to zero. From 13 – 16 eV $C_2HCl_2^+$ is the only fragment ion detected. At 15.5 ± 0.05 eV the third fragment C_2HCl^+ is formed and again the signal of the previous fragment decreases essentially to zero leaving C_2HCl^+ as the dominant ion.

The energy selected ion yields for tetrachloroethene from 9 – 25 eV with an optical resolution of 0.3 nm and 64 ns TOF resolution are shown in Figure 7.4(e) and (f). Though the experimental conditions were the same for both tri- and tetrachloroethene it is clear that the signal-to-noise ratio is much poorer for the tetrachloroethene study. Due to this poor signal-to-noise ratio the breakdown diagram was found to be of unusable quality, and for this reason it is not produced here.

Four products are observed for ionisation of tetrachloroethene. They are the parent ion ($C_2Cl_4^+$) and fragments due to loss of one chlorine atom ($C_2Cl_3^+$), two chlorine atoms ($C_2Cl_2^+$) and three chlorine atoms (C_2Cl^+). The AE_{298} for all four ions are listed Table 7.4. The values are 9.30 eV, 9.48, 12.52 eV and 15.92 eV, respectively. Due to the poor signal-to-noise ratio, errors are put conservatively at ± 0.1 eV, except for the formation of the first fragment $C_2Cl_3^+$ where the error is a lot greater. This fragment has a surprisingly low AE_{298} value, considering that a C-Cl bond is broken; the data on the other chloroethenes suggest an energy of about 2 eV excess above the IE is required. It is likely that the presence of the long low intensity peak from 9.48 – ~11.4 eV in the $C_2Cl_3^+$ cross-section is an artefact due to the low signal-to-noise ratio of these measurements. If it is assumed that this is correct then the $AE_{298} \approx 11.40$ eV, a value which seems more reasonable than 9.48 eV. In Table 7.4 both possible values for $AE_{298}[C_2Cl_3^+]$ have been included and the Traeger and McLoughlin correction has been applied in both cases, numbers in square brackets in the table represent the results when $AE_{298} = 11.4$ eV. Assuming that the AE_{298} of $C_2Cl_3^+$ is 11.4 eV then from onset to 12.50 eV the parent ion dominates. Its intensity drops down after this energy and has zero intensity from about 14 eV. From 12.5 eV $C_2Cl_3^+$ is the major ion for an interval of ~1 eV before $C_2Cl_2^+$ is formed. The production of $C_2Cl_2^+$ begins at 12.52 eV and from 13.5 eV it has roughly equal intensity with $C_2Cl_3^+$. From 16 eV $C_2Cl_2^+$ is the main ion fragment. At around 16 eV there is also a decline in the signal of $C_2Cl_3^+$ and the onset of formation of C_2Cl^+ is reached. C_2Cl^+ has only very weak intensity at all photon energies studied here.

Table 7.3: Energetics of the dissociative ionisation pathways of isomers of $C_2H_2Cl_2$ at 298 K. Values in the first column are given in kJ mol^{-1}.

	AE_{298} / eV	$\Delta_r H^0_{298,\,exp}$ / eV	$\Delta_r H^0_{298,\,calc}$ / eV
Major products of 1,1-$C_2H_2Cl_2$ (2)			
$C_2H_2Cl_2^+$ (946) + e^-	9.78	-	9.78
$C_2H_2Cl^+$ (1040) + Cl (121) + e^-	11.88	12.01	12.01
Minor products of 1,1-$C_2H_2Cl_2$ (2)			
$C_2H_2^+$ (1327) + Cl (121) + Cl (121) + e^-	16.28	-	16.24
$C_2H_2^+$ (1327) + Cl_2 (0) + e^-		-	13.73
Major products of (*Z*)-1,2-$C_2H_2Cl_2$ (-3)			
$C_2H_2Cl_2^+$ (925) + e^-	9.62	-	9.62
$C_2H_2Cl^+$ (1035) + Cl (121) + e^-	11.88	12.01	12.01
Minor products of (*Z*)-1,2-$C_2H_2Cl_2$ (-3)			
$C_2H_2^+$ (1327) + Cl (121) + Cl (121) + e^-	16.47	-	16.29
$C_2H_2^+$ (1327) + Cl_2 (0) + e^-		-	13.78
Major products of (*E*)-1,2-$C_2H_2Cl_2$ (-1)			
$C_2H_2Cl_2^+$ (923) + e^-	9.58	-	9.58
$C_2H_2Cl^+$ (1033) + Cl (121) + e^-	11.84	11.97	11.97
Minor products of (*E*)-1,2-$C_2H_2Cl_2$ (-1)			
$C_2H_2^+$ (1327) + Cl (121) + Cl (121) + e^-	16.28	-	16.27
$C_2H_2^+$ (1327) + Cl_2 (0) + e^-		-	13.76

Table 7.4: Energetics of the ionisation pathways of trichloroethene and tetrachloroethene at 298 K. Values in brackets are if the AE_{298} of $C_2Cl_3^+$ is assumed to be 11.4 eV. The values in the first column are given in kJ mol^{-1}.

	AE_{298} / eV	$\Delta_r H^0_{298,\,exp}$ / eV	$\Delta_r H^0_{298,\,calc}$ / eV
Major products of C_2HCl_3 (-19)			
$C_2HCl_3^+$ (894) + e^-	9.46	-	-
$C_2HCl_2^+$ (1066) + Cl (121) + e^-	12.35	12.5	-
Minor products of C_2HCl_3			
C_2HCl^+ (1237) + Cl (121) + Cl (121) + e^-	15.50	-	15.53
C_2HCl^+ (1237) + Cl_2 (0)+ e^-		-	13.01
Major products of C_2Cl_4 (-12)			
$C_2Cl_4^+$ (887) + e^-	9.30	-	-
$C_2Cl_3^+$ (798) + Cl (121) + e^-	9.48	9.66	-
	[11.40]	[11.58]	
Minor products of C_2Cl_4			
$C_2Cl_2^+$ (1165) + Cl (121) + Cl (121) + e^-	12.52	-	14.72
$C_2Cl_2^+$ (1165) + Cl_2 (0)+ e^-		-	12.20
C_2Cl^+ + Cl (121) + Cl (121) + Cl (121) + e^-	15.92	-	-
C_2Cl^+ + Cl_2 (0)+Cl (121) + e^-		-	

It is interesting to examine some of the trends between the chloroethenes. Upon going from dichloroethene to trichloroethene the difference between onset of ionisation and formation of the first fragment increases from ~2 eV to ~3 eV. While, allowing for the uncertainty in $AE_{298}[C_2Cl_3^+]$, going from trichloroethene to tetrachloroethene the difference is now ~ 2 eV again. For formation of the next fragment, for the dichloroethenes the energy difference is ~ 4 eV, for trichloroethene it is ~ 3 eV and for tetrachloroethene it is ~ 1 eV. It is likely these differences arise from the relative stability of the cations formed. The stability will depend on the interplay between conjugation and induction effects due to the chlorine atoms on the C=C double bond.

Another interesting trend is the formation of the fragment ion due to loss of two Cl atoms. It is clear that there are three possible channels for formation of this ion:

$$C_2H_xCl_{4-x} \xrightarrow{\Delta_r H^0_{298}} C_2H_xCl_{2-x}^{+} + Cl + Cl + e^- \qquad \textbf{(re 7.1)}$$

or

$$C_2H_xCl_{4-x} \xrightarrow{\Delta_r H^0_{298}} [C_2H_xCl_{3-x}^{+}]^* + Cl + e^- \xrightarrow{\Delta_r H^0_{298}} C_2H_xCl_{2-x}^{+} + Cl \qquad \textbf{(re 7.2)}$$

or

$$C_2H_xCl_{4-x} \xrightarrow{\Delta_r H^0_{298}} C_2H_xCl_{2-x}^{+} + Cl_2 + e^- \qquad \textbf{(re 7.3)}$$

where *x* is an integer value from 0 – 3. Reactions 7.1 and 7.2 are essentially the same process, and the distinction between them depends only on the time scale of the dissociation. For the dichloroethenes and trichloroethene the AE_{298} for this ionic fragment is very close in energy to the enthalpy of reaction of reaction 7.1. However the onset lies ~ 2 eV above the enthalpy of reaction for reaction 7.3, formation of a Cl_2 molecule. This second channel undoubtedly involves an exit-channel barrier, which could be around 2 eV, so energetics do not rule out this possibility. For 1,1-dichloroethene, (*Z*)-1,2-dichloroethene and trichloroethene, where two Cl atoms are adjacent, it is easy to see that following dissociation it would be simple to eject Cl_2. For (*E*)-1,2-dichloroethene where the Cl atoms are on opposite sides of the molecule it harder to see this happening, unless upon ionisation the C=C bond becomes weak enough for rotation to occur, as the transition state will be highly constrained. For the three dichloroethenes the consistency of the onset for this channel suggests that the same process must be occurring. However, for tetrachloroethene this product is formed at 12.52 eV, around 2 eV lower than formation of two chlorine atoms, but just above the limit for formation of Cl_2. This strongly indicates that reaction 7.3 is occurring for tetrachloroethene. It is possible that for dichloroethene and trichloroethene dissociation through reaction 7.3 is behind a large barrier, while reaction is 7.2 open at threshold. That tetrachloroethene reacts by forming Cl_2 could be because the cation is more unstable due to the electron withdrawing effect of the four Cl atoms than in the dichloroethenes and trichloroethene. So it appears that when two chlorine atoms are lost after ionisation the two mechanisms could both be active. For tetrachloroethene only reaction 7.3 takes place while for the other four chloroethenes studied here it is impossible to say whether either reaction 7.1 or 7.3 occurs or whether they both take place in competition.

4.2.2 Calculated thermochemistry

Several new thermochemical values have been calculated from the TPEPCIO data presented here. The enthalpies of formation of the parent ions were calculated from the enthalpy of formation of the neutral plus the measured ionisation energy from this study. For the $C_2H_2Cl^+$ product from the dichloroethenes and the $C_2HCl_2^+$ product from trichloroethene there was no enthalpy of formation available for the neutral forms $C_2H_2Cl^{\bullet}$ and $C_2HCl_2^{\bullet}$. Therefore the calculation for the enthalpy of formation of the ion was not as trivial as for the parent ions. To calculate the enthalpy of formation the following Hess' cycles were used:

$$C_2H_2Cl_2 \xrightarrow{\Delta_r H^0_{298}} C_2H_2Cl^+ + Cl + e^- \qquad \textbf{(re 7.4)}$$

and

$$C_2HCl_3 \xrightarrow{\Delta_r H^0_{298}} C_2HCl_2^+ + Cl + e^- \qquad \textbf{(re 7.5)}$$

where $\Delta_r H^0_{298}$ was calculated *via* conversion from the AE_{298} value for the respective chloroethene. This method of calculation for $\Delta_f H^0_{298}[C_2H_2Cl^+]$ and $\Delta_f H^0_{298}[C_2HCl_2^+]$ assumes that the appearance energy is the same as the thermochemical threshold, *i.e.* there is no barrier in the exit channel or any kinetic shift. As the reaction is a simple cleavage of a C-Cl bond the lack of a barrier seems a reasonable assumption to make. From this analysis new values for the upper limit for $\Delta_f H^0_{298}[C_2H_2Cl^+]$ have been established, they are +1040, +1035 and +1033 kJ mol^{-1} for Cl-atom loss from 1,1-, *Z* and (*E*)-$C_2H_2Cl_2^+$, respectively. The C_2H_2Cl ion formed after ionisation of the (*Z*)- and (*E*)-1,2-dichlroethenes will essentially be the same in both cases, leading to an average enthalpy of formation of +1034 kJ mol^{-1}. The enthalpy of formation of $C_2HCl_2^+$ from this work is $\leq$ 1066 kJ mol^{-1}.

For C_2Cl_4, there was also no value for the enthalpy of formation of $C_2Cl_3^+$ available in the literature. This has been calculated using the following Hess' cycle and the same assumptions as above:

$$C_2Cl_4 \xrightarrow{\Delta_r H^0_{298}} C_2Cl_3^+ + Cl + e^- \qquad \textbf{(re 7.6)}$$

As there is uncertainty in the value of AE_{298} ($C_2Cl_3^+$), two values of its enthalpy of formation have been calculated. If the AE_{298} is 9.48 eV then the enthalpy of formation is +798 kJ mol^{-1}, if the AE_{298} is 11.40 eV instead then the enthalpy of formation is now +984 kJ mol^{-1}.

4.3 Fixed Energy TPEPICO-TOF spectra

TPEPICO-TOF scans were performed with a TOF resolution of 8 ns at the energies of the peaks in the TPES. The parent ion TOF spectra show the expected convolution of the Gaussian distributions for the presence of chlorine isotopes. The TOF spectra for the ions due to the loss of a single chlorine atom, $C_2H_2Cl^+$, $C_2HCl_2^+$ and $C_2Cl_3^+$, have been analysed to produce the kinetic energy distribution (KERD) and hence average total kinetic energy release, $<KE>_t$. The analysis procedure was described in chapter 3. Briefly, the TOF spectra are fitted with a series of peaks which represent a discrete energy release using a least-squares method. Allowance is made in the fitting for the presence of the chlorine isotopomers in the daughter ion. Figure 7.6(a) shows the TOF for $C_2H_2Cl^+$ formed from dissociative photoionisation of (*E*)-1,2-$C_2H_2Cl_2$ at 12.77 eV, the peak of the $\tilde{C}\ ^2B_g$ state of the parent ion, and Figure 7.6 (b) shows the KERD from which a $<KE>_t$ value of 0.36 ± 0.03 eV is determined. The $<KE>_t$ values can be compared to the available energy to produce the fractional release into translational energy, $<f>_t$. $<f>_t$ can be predicted from both statistical and pure-impulsive models, so comparison with the experimental results can indicate whether a fragmentation is essentially impulsive or statistical in nature. Table 7.6 displays the results for the TOF peaks studied for the fragmentation into $C_2H_xCl_{4-x}^+ + Cl$ for all five chloroethenes. Values for $<KE>_t$ and $<f>_t$ from experiment and both impulsive and statistical theories are listed. For the statistical theories, values have been calculated using the formula of Klots (chapter 3 section 2.2)[38] and the estimate of the lower limit from Franklin (chapter 3 section 2.2).[39] For the formation of $C_2Cl_3^+$ from C_2Cl_4, two possible values of AE_{298} are possible, as described above (section 4.2.2). Hence the results have been calculated twice, the values for AE_{298} = 11.4 eV being given in square brackets.

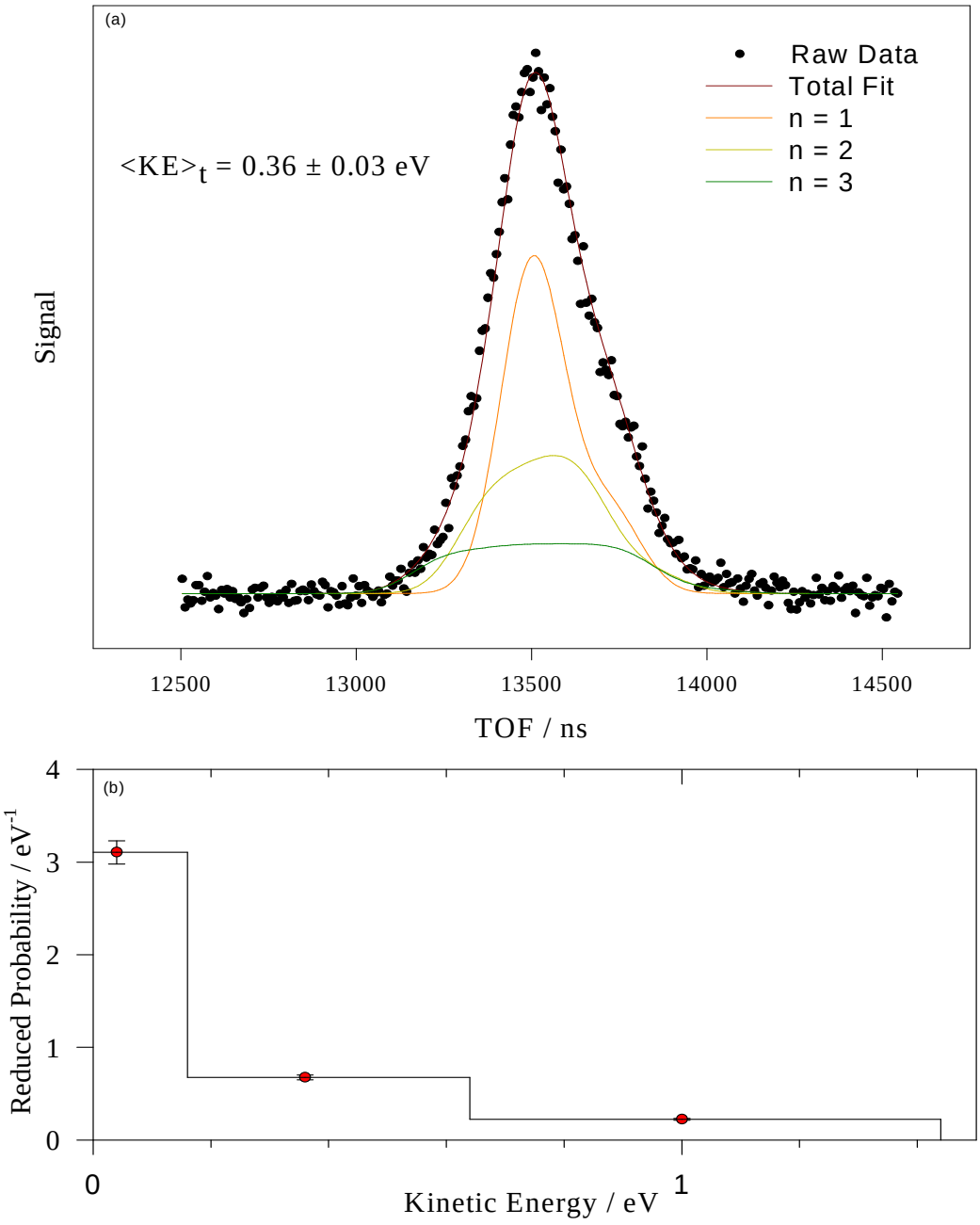

Figure 7.6: (a) TOF distribution of $C_2H_2Cl^+$ from (*E*)-dichloroethene at 12.77 eV, (b) Reduced probability for each discrete energy component fitted in (a).

Table 7.5: Total mean kinetic energy releases, $\langle KE \rangle_t$, for the two-body fragmentation of valence states of isomers of $C_2H_2Cl_2^+$ and $C_2HCl_3^+$ and $C_2Cl_4^+$. $\langle f \rangle_t$ is the fraction of energy released as translation calculated by various methods. Values in brackets apply if the AE_{298} of $C_2Cl_3^+$ is assumed to be 11.40 eV, and not 9.48 eV.

Parent Ion	State	Daughter Ion	hν / eV	E_{avail} / eV	$\langle KE \rangle_t$ / eV	$\langle f \rangle_t$ exp	$\langle f \rangle_t$ Klot	$\langle f \rangle_t$ stat	$\langle f \rangle_t$ imp
1,1-$C_2H_2Cl_2^+$	$\tilde{B}$	$C_2H_2Cl^+$	12.25	0.45	0.16	0.36	0.18	0.08	0.40
	$\tilde{C}$		12.59	0.79	0.24	0.30	0.15	0.08	0.40
	$\tilde{D}$ / $\tilde{E}$		14.19	2.39	0.60	0.25	0.12	0.08	0.40
	$\tilde{F}$ / $\tilde{G}$		16.21	4.41	0.77	0.17	0.11	0.08	0.40
	$\tilde{H}$		18.51	6.71	0.53	0.08	0.10	0.08	0.40
***(Z)*-1,2-$C_2H_2Cl_2^+$**	$\tilde{B}$	$C_2H_2Cl^+$	12.55	0.75	0.24	0.32	0.15	0.08	0.40
	$\tilde{D}$ / $\tilde{E}$		14.19	2.39	0.54	0.23	0.12	0.08	0.40
	$\tilde{F}$		15.73	3.93	0.58	0.15	0.11	0.08	0.40
	$\tilde{G}$		16.73	4.93	0.93	0.19	0.10	0.08	0.40
	$\tilde{H}$		18.90	7.10	0.49	0.07	0.10	0.08	0.40
***(E)*-1,2-$C_2H_2Cl_2^+$**	$\tilde{C}$	$C_2H_2Cl^+$	12.77	1.01	0.36	0.36	0.14	0.08	0.40
	$\tilde{D}$ / $\tilde{E}$		14.00	2.24	0.40	0.18	0.12	0.08	0.40
	$\tilde{F}$ / $\tilde{G}$		16.28	4.52	0.65	0.14	0.11	0.08	0.40
	$\tilde{H}$		19.34	7.58	0.53	0.07	0.10	0.08	0.40
$C_2HCl_3^+$	$\tilde{D}$	$C_2HCl_2^+$	12.68	0.44	0.141	0.32	0.16	0.08	0.35
	$\tilde{E}$		12.90	0.66	0.19	0.29	0.14	0.08	0.35
	$\tilde{F}$		14.28	2.04	0.40	0.19	0.11	0.08	0.35
	$\tilde{G}$		14.66	2.42	0.425	0.18	0.11	0.08	0.35
$C_2Cl_4^+$	$\tilde{D}$	$C_2Cl_3^+$	12.34	3.01 [1.09]	0.254	0.08 [0.23]	0.10 [0.11]	0.08	0.32
	$\tilde{F}$		12.84	3.51 [1.59]	0.343	0.1 [0.22]	0.10 [0.11]	0.08	0.32
	$\tilde{G}$		13.53	4.20 [2.28]	0.383	0.09 [0.17]	0.10 [0.10]	0.08	0.32
	$\tilde{H}$		14.72	5.39 [3.47]	0.47	0.09 [0.14]	0.10 [0.10]	0.08	0.32

For all five molecules, the value of $\langle f \rangle_t$ decreases as the photon energy increases above threshold. This result is predicted by statistical theories, such as RRKM and is shown here numerically by the statistical values calculated using the formula of Klots.[38] For the first state above the threshold for fragmentation (~12.5 eV) the value of $\langle f \rangle_t$, 0.32-0.36, is very close to the pure impulsive limit of 0.40 for the dichloroethenes and 0.35 for trichloroethene. It is interesting that Zhou *et al* found the $\tilde{B}$ state of the three dichloroethenes to be long-lived, yet this study suggests the opposite, that the state rapidly dissociates. It is difficult to reconcile these results. The KERDs for tetrachloroethene seem to confirm that AE_{298} = 9.48 eV is too low. For this energy the $\tilde{D}$ state has a $\langle f \rangle_t$ of only 0.08 and this then increases with increasing photon energy. If, however, the 11.4 eV value is used then the results for $\langle f \rangle_t$ are more reasonable. Now the fragmentation begins as slightly impulsive before becoming statistical. For all chloroethenes at higher energies, $\langle f \rangle_t$ approaches 0.08, the value calculated as the lower statistical limit for fractional kinetic energy release. Such behaviour was also seen in previous studies with this apparatus on similarly sized molecules.[40] It should be noted that at these higher energies the formula of Klots gives larger $\langle f \rangle_t$ values than are measured. This is probably due to errors in the calculation of the ionic fragments vibrational frequencies. That $\langle f \rangle_t$ decreases with increasing energy is easily reconciled with the theories of intramolecular energy redistribution. As the photon energy increases, successively more electronic and vibrational energy levels of the parent ion can be accessed. The available energy is shared between states and hence less likely to be localised in a vibrational mode that would lead to dissociation of the $C_2H_xCl_{3-x}^+$ ion. This seems to confirm that the fragmentation of the chloroethenes is statistical in nature at higher energies, but more non-statistical in character at energies close to threshold.

5. Conclusions

The photoionisation dynamics of 1,1-dichloroethene, (*Z*)-1,2-dichloroethene, (*E*)-1,2-dichloroethene, trichloroethene and tetrachloroethene have been studied using synchrotron radiation from onset of ionisation to 23 eV by threshold photoelectron photoion coincidence spectroscopy. Threshold photoelectron spectra and total ion yields have been recorded. The measured energies of the ion states are found to be in good agreement with those calculated using the outer valence Greens' functions method. For (*E*)-1,2-dichloroethene a vibrational Rydberg

series is recorded leading to the first excited electronic state. From Gaussian 03 calculations the vibration is found to be due to a C-H bend.

From energy-selected ion yields appearance energies and branching ratios have been determined for the fragments formed from the five chloroethenes. The fragments in all cases are found, in order of increasing AE_{298}, to be parent ion, a fragment formed from loss of a chlorine atom and a fragment formed from loss of two chlorine atoms. For tetrachloroethene a fourth product is seen in which three chlorine atoms are lost. Examination of thermochemistry and branching ratios suggest that when the two chlorine atoms are lost, they are lost separately and not as a Cl_2 molecule. Tetrachloroethene appears to be anomalous, and a chlorine molecule is formed instead.

Upper limits on the enthalpies of formation of the parent ions, $C_2H_2Cl_2^+$, $C_2HCl_3^+$ and $C_2Cl_4^+$ have been determined. Assuming there is no kinetic shift or exit-channel barrier upper limits on the enthalpies of formation for $C_2H_2Cl^+$ and $C_2HCl_2^+$ have also been determined. Three values have been determined for $C_2H_2Cl^+$, because if there is no rearrangement or free rotation around the C=C double bond upon ionisation then three distinct ions will be formed. Two values for the enthalpies of formation of $C_2Cl_3^+$ have been determined, depending on which value for the appearance energy of this fragment is taken. The translational energy released when the parent ion fragments by loss of Cl has been shown to be impulsive at low photon energies, but becomes more statistical in nature as the energy increases.

For the three dichloroethenes no clear sign of the isomeric effect has been discovered. Two small differences are noted. In the threshold photoelectron spectra the $\tilde{F}$ and $\tilde{G}$ states are resolvable in the *Z* isomer but not in either the 1,1 or *E* isomer, due to the symmetries of the two states. There are also slight differences in the branching ratios of the $C_2H_2Cl^+$ and $C_2H_2^+$ products above a photon energy of 20 eV.

Trends due to the increasing number of chlorine atoms are also noted. Firstly, we note the increase in ionic states present in the threshold photoelectron spectra due to the increasing number of chlorine lone pairs. This leads to a reduction in ionisation energy because of the increased conjugation of the C=C π-orbitals and the chlorine lone pairs. Secondly, we note the variation in energy difference between the onset of ionisation and the appearance of the first fragment ion.

6. References

1 W. Von Niessen, L. Åsbrink, G. Bieri, *J. Elec. Spec. Rel. Phen.*, **26**, (1982) 173.
2 K. Wittel, H. Bock, *Chem. Ber.*, **107**, (1974) 317.
3 R. F. Lake, H. Thompson, *Proc. Roy. Soc. Lond. A.*, **315**, (1970) 323.
4 N. Jonathon, K. Ross, V. Tomlinson, *Int. J. Mass. Spectrom. Ion Phys.*, **4**, (1970) 51.
5 K. Watanabe, T. Nakayama, J. Mottl, *J. Quant. Spectry. Radiat. Transfer*, **2**, (1962) 369.
6 H.K. Woo, P. Wang, K.C. Lau, X. Xing, C.Y. Ng, *J. Phys. Chem. A*, **108**, (2004) 9637.
7 Y.J. Bae, M. Lee, M.S. Kim, *J. Phys. Chem. A*, **110**, (2006) 8535.
8 A.D. Walsh, A. Warsop, J.A.B. Whiteside, *J. Chem. Soc. Fara. Trans.*, **64**, (1968) 1432.
9 A.D. Walsh, P.A. Warsop, *J. Chem. Soc. Fara. Trans.*, **63**, (1967) 524.
10 A.D. Walsh, P.A. Warsop, *J. Chem. Soc. Fara. Trans.*, **64**, (1967) 1418.
11 J. Momigny, *Bull. Soc. Chim. Belges*, **70**, (1961) 241.
12 M.H. Chuaqui, L. Mei, C.P. Mathers, M.L. Allison, J.F. Ying, K.T. Leung, *J. Chem. Phys.*, **102**, (1995) 90.
13 L. Mei, M. Chuaqui, C.P. Mathers, J.F. Ying, K.T. Leung, *Chem. Phys.*, **188**, (1994) 347.
14 L. Mei, M. Chuaqui, C.P. Mathers, J.F. Ying, K.T. Leung, *J. Chem. Phys.*, **101**, (1994) 3558.
15 K. Takeshita, *J. Chem. Phys.*, **110**, (1999) 6792.
16 K. Ohno, N. Kishimoto, H. Yamakado, *J. Phys. Chem.*, **99**, (1995) 9687.
17 N. Kishimoto, K. Ohshimo, K. Ohno, *J. Elec. Spec. Rel. Phenom.*, **104**, (1999) 145.
18 A.W. Potts, J.M. Benson, I. Novak, W.A. Svensson, *Chem. Phys.*, **115**, (1987) 253.
19 H.K. Woo, P. Wang, K.-C. Lau, X. Xing, C.Y. Ng, *J. Chem. Phys.*, **120**, (2004) 1756.
20 H.K. Woo, P. Wang, K.-C. Lau, X. Xing, C. Chang, C.Y. Ng, *J. Chem. Phys.*, **119**, (2003) 9333.
21 J. Duttont, A. Goodings, A.K. Lucas, A.W. Williams, *J. Phys. E*, **21**, (1988) 264.
22 B.A. Heath, M.B. Robin, *J. Am. Chem. Soc.*, **102**, (1980) 1796.
23 J.E. Hudson, C. Vallance, M. Bart, P.W. Harland, *J. Phys. B*, **34**, (2001) 3025.
24 C.A. Mayhew, A.D.J. Critchley, D.C. Howse, V. Mikhailov, M.A. Parkes, *Eur. Phys. D*, **35**, (2005) 307.
25 T. Shimanouchi: *Tables of Molecular Vibrational Frequencies Consolidated Volume I*, National Bureau of Standards, (1972).
26 M.W. Chase, *J. Phys. Chem. Ref. Data*, (1998) Monograph no. 9.
27 S.G. Lias, J.E. Bartmess, J.F. Liebman, J.L. Holmes, R.D. Levin, W.G. Mallard, *J. Phys. Chem. Ref. Data*, **17**, (1988) supplement no 1.
28 J.A. Manion, *J. Phys. Chem. Ref. Data*, **31**, (2002) 123.
29 R.C. Ivey, M.I. Davis, *J. Chem. Phys.*, **57**, (1972) 1909.
30 L. Schäfer, J.D. Ewbank, K. Siam, D.W. Paul, D.L. Monts, *J. Mol. Struc.*, **145**, (1986) 135.
31 M.I. Davies, H.P. Hanson, *J. Phys. Chem.*, **69**, (1965) 4091.
32 S. Sekino, T. Nishikawa, *J. Phys. Soc. Jpn.*, **12**, (1957) 43.
33 T.G. Strand, *Acta Chem. Scand.*, **21**, (1967) 2111.
34 Z. Kisiel, L. Pszczolkowski, *J. Mol. Spectrosc.*, **178**, (1996) 125.
35 R. Locht, B. Leyh, Hottmann, H. Baumgärtel, *Chem. Phys.*, **220**, (1997) 217.
36 H. Zhou, Y. Gong, M. Zhou, *J. Phys. Chem. A*, **111**, (2007) 603.
37 M. Kim, J.C. Choe, M.S. Kim, *J. Am. Soc. Mass Spectrom.*, **15**, (2004) 1266.
38 C.E. Klots, *Chem. Phys. Letts.*, **38**, (1976) 61.
39 J.L. Franklin, *Science*, **193**, (1976) 725.

40 C.R. Howle, D.J. Collins, R.P. Tuckett, A.E.R. Malins, *Phys. Chem. Chem. Phys.*, **7**, (2005) 2287.

Chapter 8: Isomeric effects in the reactions of chloroethenes with selected cations: 1. RE ≥ IE[$C_2H_xCl_{4-x}$]

1. Introduction

In the previous chapter the photoionisation dynamics of five chloroethenes, 1,1-dichloroethene, (*Z*)-1,2-dichloroethene, (*E*)-1,2-dichloroethene, trichloroethene and tetrachloroethene, were reported. In this chapter the study will be extended by examining the reactions of all six chloroethenes (including monochloroethene) with a range of cations in the selected ion flow tube (SIFT). Only those reactant ions whose recombination energy (RE) is greater than the ionisation energy (IE) of the reactant neutral will be considered in this chapter, ions where RE < IE will be discussed in the next chapter.

Monochloroethene is a major industrial gas especially for the production of polyvinyl chloride. It is also a class 1 carcinogen. Though the reactions of the monochloroethene parent cation with neutral monochloroethene has been extensively studied,[1,2] along with its reaction with a range of other neutrals such as methanol, ammonia and methane,[3-5] there are very few studies of the reactions of neutral monochloroethene with cations. Two of interest are the SIFT study of C_{60}^{n+} with monochloroethene by Ling *et al*.,[6] and the reactions of rare gas ions with monochloroethene in an ion-beam mass spectrometer.[7]

The dichloroethenes have recently attracted attention as environmental pollutants and possible carcinogens. Though the reactions of the three isomers with neutrals in the gas phase have been reasonably well studied, for example their oxidation by atmospheric radicals,[8-14] their reactions with gas-phase cations are much less studied. Using ion cyclotron resonance Bowers and Laudenslager studied the reactions of all three isomers with rare gas ions,[15,16] while Rebrion *et al.*[17] have investigated their reactions with N^+ and H_3^+.

A study of the reactions of all three dichloroethene isomers and trichloroethene with a selection of anions (O_2^-, O^-, OH^-, CF_3^- and F^-) was performed by Kennedy *et al*.[18] For these reactions there was a striking example of an isomeric effect; the vinyl anion, $C_2HCl_2^-$, was only

observed as a product for the *E* isomer, whereas Cl^- was the major product observed for the 1,1 and *Z* isomers. For the reaction of the dichloroethenes with Cl^- Bagno *et al* predicted that the adduct $C_2H_2Cl_3^-$ would be the only product formed, whereas this product was only seen for the *Z* isomer.[19]

Even less work seems to have been performed on trichloroethene and tetrachloroethene. Studies on the breakdown of trichloroethene in a corona discharge have been performed,[20] and a study of the reactions of both trichloroethene and tetrachloroethene with H_3O^+, NO^+ and O_2^+ has been carried out on a SIFT adapted for breath analysis.[21]

In this chapter the reactions of all six chloroethenes, monochloroethene, 1,1-dichloroethene, (*Z*)-1,2-dichloroethene, (*E*)-1,2-dichloroethene, trichloroethene and tetrachloroethene with a series of cations with RE in the range 9.78 – 21.56 eV will be reported. The reactions of ions with RE below this energy range will be described in the following chapter. The ion-molecule reactions of the dichloroethenes have been already published.[22]

2. Experimental

The experiments were performed as described in chapter 2. The six isomers were purchased from Sigma-Aldrich with stated purities of 99.5, 97 and 98 % for the 1,1, *Z* and *E* isomers respectively. The monochloroethene, trichloroethene and tetrachloroethene samples were also purchased from Sigma-Aldrich with purities of 99 + %. All samples were further purified by successive freeze-pump thawing cycles before use except for monochloroethene.

3. Theoretical considerations

For comparison to the experimental rate coefficients, k_{exp}, theoretical rate coefficients, k_c, were calculated. These were calculated using the corrected version of the modified average dipole orientation (MADO) model of Su and Chesnavich,[23,24] as explained in chapter 3 section 1.1.2. This requires values for both a polarisability volume, α', and a dipole moment, μ_D, for the neutral reactant. The values for α' for the 1,1-, (*Z*)-1,2- and (*E*)-1,2-dichloroethene isomers are 7.83, 8.15, and 8.03×10^{-30} m^3, respectively.[25] For monochloroethene, trichloroethene and tetrachloroethene the values for α' are 6.41, 10.03 and 12.02 x 10^{-30} m^3, the values for monochloroethene and trichloroethene have been taken from the CRC handbook;[25] for

tetrachloroethene the value was estimated using the method of Miller outlined in chapter 3 section 1.2.1. (*E*)-1,2-dichloroethene and tetrachloroethene have zero dipole moments but for monochloroethene, 1,1 and *Z* dichloroethene and trichloroethene μ_D has a non-zero value; the values are 1.45, 1.29, 1.90 and 0.90 D, respectively.[19,25,26]

For calculation of enthalpies of reaction, $\Delta_r H^o_{298}$, enthalpies of formation of ions and neutrals were required. The majority were taken from standard sources,[27,28] exceptions being the enthalpies of formation for CF_3^+ (+ 406 kJ mol^{-1}),[29] CClF (+ 31 kJ mol^{-1}),[30] SF_5^+ (+ 29 kJ mol^{-1}),[31] SF_5 (-915 kJ mol^{-1}),[32] SF_4^+ (-768 kJ mol^{-1}),[33] SF_2^+ (+ 693 kJ mol^{-1}),[33] SF_2 (-295 kJ mol^{-1}),[33] SF^+ (+ 998 kJ mol^{-1})[33] and NCl (+ 314 kJ mol^{-1}).[34] The values for the parent neutrals are taken from the compilation of Manion.[35] The enthalpies of formation for the parent ions formed from the dichloroethenes, trichloroethene and tetrachloroethene were taken from the TPEPICO study, as reported in the previous chapter. Values were also taken from the TPEPICO study for $C_2H_2Cl^+$, $C_2HCl_2^+$ and $C_2Cl_3^+$. It should be noted that for $C_2Cl_3^+$ the enthalpy of formation was derived using the measured AE_{298} of 9.48 eV, not the estimated AE_{298} of 11.4 eV. It is felt that it is better to use the actual measured value rather than the approximate value. The IE of the chloroethenes used in this chapter are 9.99 eV for monochloroethene, 9.79 eV for 1,1-dichloroethene, 9.66 eV for (*Z*)-1,2-dichloroethene, 9.65 eV for (*E*)-1,2-dichloroethene, 9.46 eV for trichloroethene and 9.30 eV for tetrachloroethene. These values were reported in chapter 7 for all the chloroethenes apart from monochloroethene which is taken from the compilation of Lias *et al.*[28]

4. Results

Table 8.1– Table 8.6 show the results for the SIFT experiments on monochloroethene, 1,1-dichloroethene, (*Z*)-1,2-dichloroethene (*E*)-1,2-dichloroethene, trichloroethene and tetrachloroethene, respectively. The first column shows the reagent ion and the RE of the ion, the second both the experimental and theoretical rate coefficients, the latter are shown in square brackets. Measured product ions are listed in column 3 along with branching ratios. Proposed neutral products and enthalpies of reactions are shown in columns 4 and 5, respectively. For several of the reactions branching ratios have not been measured because it was impossible to obtain a clean signal of a single reactant ion, leading to complications in calculating branching ratios. Only the reactions with ions whose RE > IE[$C_2H_xCl_{4-x}$] are shown. However, SF_5^+ is

shown even though it has a RE value (9.78 eV) below the IE of monochloroethene and 1,1-dichloroethene. This is because the value is within experimental error of the IE of the 1,1 isomer, 9.79 eV, so it is borderline whether charge transfer can occur. The reaction of SF_5^+ is also included for monochloroethene for ease of comparison with the other chloroethenes. Rate coefficients, but not branching ratios, have been measured for SF_4^+ as only a weak signal was obtainable. This is because SF_4^+ could only be formed by collision induced dissociation of SF_5^+ at the flow tube entrance. For trichloroethene and tetrachloroethene branching ratios have not been given as only one product was observed for reaction from both SF_5^+ and SF_4^+, simplifying analysis. However, for monochloroethene not even a rate coefficient could be measured as products formed from the reaction of monochloroethene and SF_5^+ occurred at masses 107 and 109 obscuring any reactive loss of SF_4^+ ions at mass 108. The O^+ results have not been recorded for the dichloroethenes. For the reactions of H_2O^+ and OH^+ with monochloroethene, trichloroethene and tetrachloroethene it was impossible to separate the two ions using the current injection quadrupole. Therefore only observed products are listed in the tables. One exception is the reaction with monochloroethene where some allowance could be made for the presence of OH^+, and approximate branching ratios are therefore given for this reaction.

Table 8.1: Rate coefficients, product ions and proposed neutral products for the reactions of monochloroethene with cations with RE in the range 9.7 – 21.6 eV. Dashed line indicates IE of monochloroethene of 9.99 eV.

Reagent ion (RE [b] / eV)	Rate coefficient / 10^{-9} cm^3 molecule^{-1} s^{-1}	Product ions (%)	Proposed neutral products	$\Delta_r H^o_{298}$ / kJ mol^{-1}
SF_5^+	0.4	SF_3^+ (50)	C_2H_2FCl + HF	38 - $\Delta_f H^o_{298}[C_2H_2FCl]$
(9.78)	[1.4]	$C_2H_3ClF^+$ (50)	SF_4	-819 +$\Delta_f H^o_{298}[C_2H_3ClF^+]$
SF_2^+	1.6	$C_2H_3SF_2^+$ (6)	Cl	-594 + $\Delta_f H^o_{298}[C_2H_3SF_2^+]$
(10.24)	[1.6]	$C_2H_3Cl^+$ (94)	SF_2	-25
SF^+	1.8	C_2HSF^+ (13)	H_2 + Cl	-899 + $\Delta_f H^o_{298}[C_2HSF^+]$
(10.31)	[1.8]	C_2SF^+ (22)	H_2 + HCl	-1113 + $\Delta_f H^o_{298}[C_2SF^+]$
		$C_2H_3Cl^+$ (40)	SF	-31
		$C_2H_3^+$ (25)	SFCl	80 + $\Delta_f H^o_{298}$[SFCl]
CF_2^+	1.8	$C_3H_3F_2^+$ (5)	Cl	-823 + $\Delta_f H^o_{298}[C_3H_3F_2^+]$
(11.44)	[1.8]	$CHFCl^+$ (25)	CF + CH_2	-3
			C_2FH	-75
		$C_2H_3Cl^+$ (70)	CF_2	-140
O_2^+	2.0	$C_2H_3Cl^+$ (100)	O_2	-161

(12.07)	[2.0]			
Xe^+	1.4	$C_2H_3Cl^+$ (78)	Xe	-206
(12.13)	[1.4]	$C_2H_3^+$ (21)	Xe + Cl	+29
		$C_2H_2^+$ (1)	Xe + HCl	+42
H_2O^+	2.4	$C_2H_3ClH^+$ (9)	OH	-958 + $\Delta_f H^o_{298}[C_2H_3ClH^+]$
(12.62)	[2.5]	$C_2H_3Cl^+$ (73)	H_2O	-253
		$C_2H_3^+$ (17)	H_2O + Cl	-18
N_2O^+	1.7	$C_2H_3Cl^+$ (56)	N_2O	-280
(12.89)	[1.8]	$C_2H_3^+$ (44)	N_2O + Cl	-159
OH^+	2.5	$C_2H_3Cl^+$ (-)	OH	-383
(13.25)	[2.6]	$C_2H_3^+$ (-)	OH + Cl	-55
		$C_2H_2^+$ (-)	OH + HCl	-42
O^+	2.1	Not Measured	-	-
(13.62)	[2.6]			
CO_2^+	2.0	$C_2H_3Cl^+$ (7)	CO_2	-365
(13.76)	[1.8]	$C_2H_3^+$ (90)	CO_2 + Cl	-129
		$C_2H_2^+$ (3)	CO_2 + HCl	-116
Kr^+	1.5	$C_2H_3Cl^+$ (1)	Kr	-387
(14.00 (&	[1.6]	$C_2H_2Cl^+$ (1)	Kr + H	-114
14.67))		$C_2H_3^+$ (91)	Kr + Cl	-152
		$C_2H_2^+$ (7)	Kr + HCl	-138
CO^+	2.1	$C_2H_3Cl^+$ (2)	CO	-388
(14.01)	[2.1]	$C_2H_3^+$ (92)	CO + Cl	-152
		$C_2H_2^+$ (6)	CO + HCl	-139
N^+	2.5	$C_2H_3Cl^+$ (57)	N	-438
(14.53)	[2.7]	$C_2H_3^+$ (41)	N + Cl	-203
		$C_2H_2^+$ (2)	N + HCl	-190
N_2^+	2.0	$C_2H_3Cl^+$ (2)	N_2	-539
(15.58)	[2.1]	$C_2H_2Cl^+$ (8)	N_2 + H	-266
		$C_2H_3^+$ (76)	N_2 + Cl	-304
		$C_2H_2^+$ (14)	N_2 + HCl	-291
Ar^+	1.7	$C_2H_3Cl^+$ (1)	Ar	-557
(15.76)	[1.9]	$C_2H_2Cl^+$ (10)	Ar + H	-284
		C_2HCl^+ (3)	Ar + H_2	-306
		HCl^+ (4)	Ar + C_2H_2	-179
		$C_2H_3^+$ (68)	Ar + Cl	-322
		$C_2H_2^+$ (13)	Ar + HCl	-309
F^+	2.1	$C_2H_3Cl^+$ (5)	F	-717
(17.42)	[2.5]	$C_2H_2Cl^+$ (13)	F + H	-444
		$C_2H_3^+$ (72)	F + Cl	-481
		$C_2H_2^+$ (10)	F + H + Cl	-37

			F + HCl	-468
Ne^+	2.1	$C_2H_3Cl^+$ (5)	Ne	-1116
(21.56)	[2.4]	$C_2H_2Cl^+$ (1)	Ne + H	-843
		C_2HCl^+ (4)	Ne + H + H	-429
			Ne + H_2	-865
		Cl^+ (8)	Ne + C_2H_3	-432
		$C_2H_3^+$ (4)	Ne + Cl	-881
		$C_2H_2^+$ (74)	Ne + H + Cl	-478
			Ne + HCl	-868
		C_2H^+ (4)	Ne + H + HCl	-379
			Ne + H_2 + Cl	-384

4.1 Rate coefficients

The general ordering of the measured rate coefficients is (*Z*)-1,2-dichloroethene > monochloroethene > 1,1-dichloroethene > trichloroethene > tetrachloroethene > (*E*)-1,2-dichloroethene. This order is related primarily to the magnitude of the dipole moment of the molecule as well as its mass and polarisability volume. The larger μ_D then the larger the rate coefficient, an effect modelled in the MADO theory. α' has the same effect, while an increase in molecular mass will give a smaller rate coefficient.

Comparison of the k_c to k_{exp} values shows that the majority of the reactions go at, or very near to, the collisional rate. For most ions the efficiency is in the range 68 – 100 %. For some of the reactions k_{exp} has been measured as ~ 20 – 30 % larger than k_c. Although the experimental error for the SIFT measurement can explain most of these errors, it could also be a sign of the presence of excited ionic reagents.

The reactions with SF_5^+ (RE = 9.78 eV) are in general slow and inefficient (~25%) for all six chloroethenes, although the reaction with tetrachloroethene is 50% efficient. The slowness of the SF_5^+ reaction has previously been seen with $CHCl_2F$, $CHClF_2$ and CH_2ClF.[36] There are two possible explanations for this reactions inefficiency. Firstly, there could be steric effects due to the size of the SF_5^+ cation; if orientation of the molecules is important then it is likely that there will not be unit probability of reaction upon collision. Secondly, for the dichloroethenes, the RE[SF_5^+] is very close to the neutral IE, and it is possible that the cross section for charge transfer is very low at threshold, again leading to a smaller rate coefficient. For monochloroethene, only a chemical reaction can take place, so steric effects will be important.

For tetrachloroethene there is a second slow reaction, the reaction with SF_2^+ (RE = 10.24 eV); this reaction is 58 % efficient. It is possible that this reaction is slow due to the presence of four chlorine atoms. These large atoms could possibly create steric hindrance, blocking the accesses of SF_2^+ to electrons located in the molecular orbitals of tetrachloroethene.

The rate coefficients for the reactions of the dichloroethenes with rare gas ions were measured by Su and Bowers using an ICR.[16] After allowance was made for long-range collisions in their data their rate coefficients agree fairly well with ours, especially considering the difficulties of measuring absolute rate coefficients in an ICR apparatus.[37]

Table 8.2: Rate coefficients, product ions and proposed neutral products for the reactions of 1,1-dichloroethene with cations with RE in the range 9.7 – 21.6 eV. The dashed line indicates the ionisation energy of 1,1-dichloroethene of 9.79 eV.

Reagent ion (RE [b] / eV)	Rate coefficient / 10^{-9} cm^3 molecule^{-1} s^{-1}	Product ions (%)	Proposed neutral products	$\Delta_r H^o_{298}$ / kJ mol^{-1}
SF_5^+ (9.78)	0.3 [1.2]	$C_2H_2Cl_2F^+$ (71) $C_2H_2Cl_2^+$ (16) $C_2H_2Cl^+$ (13)	SF_4 SF_5 SF_5Cl	800 + $\Delta_f H^o_{298}[C_2H_2Cl_2F^+]$ -0.4 -30
SF_2^+ (10.24)	1.4 [1.5]	$C_2H_2Cl_2^+$ (100)	SF_2	-45
SF^+ (10.31)	1.6 [1.6]	$C_2H_2Cl_2^+$ (59) $C_2H_2ClSF^+$ (8) C_2HClSF^+ (8) $C_2H_2Cl^+$ (21) $CHCl_2^+$ (4)	SF Cl HCl SFCl CS + HF	-52 -879 + $\Delta_f H^o_{298}[C_2H_2ClSF^+]$ –1093 + $\Delta_f H^o_{298}[C_2H_2ClSF^+]$ 39 + $\Delta_f H^o_{298}$[SFCl] -106 [f]
CF_2^+ (11.44)	1.9 [1.6]	$C_2H_2Cl_2^+$ (100)	CF_2	-160
SF_4^+ (11.99)	1.4 [1.3]	Not Measured	-	-
O_2^+ (12.07)	2.5 [1.9]	$C_2H_2Cl_2^+$ (77) $C_2H_2Cl^+$ (23)	O_2 O_2 + Cl OClO or ClOO	-221 -6 -30 -29
Xe^+ (12.13)	1.3 [1.3]	$C_2H_2Cl_2^+$ (81) $C_2H_2Cl^+$ (19)	Xe Xe + Cl	-227 -12
N_2O^+ (12.89)	1.7 [1.7]	$C_2H_2Cl_2^+$ (15) $C_2H_2Cl^+$ (85)	N_2O N_2O + Cl N_2OCl	-300 -85 -275

CO_2^+ (13.76)	1.5 [1.7]	$C_2H_2Cl_2^+$ (13) $C_2H_2Cl^+$ (87)	CO_2 CO_2 + Cl	-385 -170
Kr^+ (14.00 (& 14.67))	1.3 [1.4]	$C_2H_2Cl^+$ (93) C_2HCl^+ (7)	Kr + Cl Kr + HCl	-407 -192
CO^+ (14.01)	2.0 [2.0]	$C_2H_2Cl^+$ (100)	CO + Cl COCl	-193 -266
N^+ (14.53)	2.7 [2.7]	$C_2H_2Cl_2^+$ (40) $C_2H_2Cl^+$ (54) C_2HCl^+ (6)	N N + Cl NCl N + HCl	-459 -243 -524 -261
N_2^+ (15.58)	2.0 [2.0]	$C_2H_2Cl^+$ (83) C_2HCl^+ (17)	N_2 + Cl N_2 + HCl	-344 -361
Ar^+ (15.76)	1.5 [1.8]	$C_2H_2Cl^+$ (84) C_2HCl^+ (16)	Ar + Cl Ar + HCl	-362 -379
F^+ (17.42)	2.0 [2.3]	$C_2H_2Cl_2^+$ (14) $C_2H_2Cl^+$ (41) $C_2H_2^+$ (45)	F F + Cl FCl F+Cl_2	-737 -522 -773 -356
Ne^+ (21.56)	2.0 [2.3]	$C_2H_2Cl_2^+$ (5) $C_2H_2^+$ (50) C_2HCl^+ (35) CCl^+ (4) Cl^+ (6)	Ne Ne + Cl + Cl Ne + Cl_2 Ne + H + Cl Ne + HCl Ne + CH_2 +Cl Ne+ CH+HCl Ne + C_2H_2Cl Ne + Cl+C_2H_2	-1136 -513 -756 -507 -938 -332 -338 -711 + $\Delta_f H^o_{298}[C_2H_2Cl]$ -364

4.2 Ion-molecule branching ratios

For monochloroethene, trichloroethene and tetrachloroethene reactions with nineteen ions have been recorded. For the dichloroethenes only 16 ions have been studied, the H_2O^+, O^+ and OH^+ reactions being omitted. The cations have RE values ranging from 9.78 to 21.56 eV. The ion with lowest RE, SF_5^+, is a special case in that for monochloroethene charge transfer should not be able to occur, charge transfer is a borderline process for the dichloroethenes, but is allowed for trichloroethene and tetrachloroethene. The measured products reflect these differences in the IE of the chloroethenes.

The reaction of monochloroethene and SF_5^+ cannot occur by charge transfer, so it must go *via* a chemical reaction in which bonds break and form. Two ionic products, SF_3^+ and $C_2H_3ClF^+$, are observed. As expected, neither of the products is due to charge transfer. The production of SF_3^+ is interesting as neutral fluorine atoms have been transferred rather than the normal transfer of an F^- anion, leaving a fragment of the reagent ion as the product. Normally, the reagent ion is either incorporated into the product ion or it is left without any charge. F^+-transfer leads to the formation of the other ionic product $C_2H_3ClF^+$.

For all three dichloroethenes F^+-transfer to form $C_2H_2Cl_2F^+$ is the major channel with minor channels forming the parent ion and $C_2H_2Cl^+$. For these reactions the loss of a chloride ion can only be due to a chemical reaction to form SF_5Cl as a neutral partner, since there is not enough energy for charge transfer to be followed by unimolecular dissociation of the parent ion. This suggests that, because the RE of SF_5^+ is only just above the IE of the dichloroethenes, the cross-section for long-range charge transfer is low. Thus, the neutrals and SF_5^+ will approach to a small internuclear distance and form a reactive ion-molecule complex. It is in this complex that the chemical reaction takes place which will form $C_2H_2Cl_2F^+$ and $C_2H_2Cl^+$. The formation of the parent ion ($C_2H_2Cl_2^+$) can take place in two ways; either *via* a short-range mechanism inside the complex where it is competing with the chemical reaction, or at a large separation of ion and neutral. In this second case the charge transfer is classed as long-range. That long-range charge transfer is inefficient and a complex is formed is highlighted by the small reaction rate coefficient. It should be noted that, due to uncertainties in thermochemistry it is possible that only vibrationally-excited SF_5^+ can react *via* charge transfer. It cannot be discounted that any parent ion forms from excited SF_5^+, and that there is only a chemical reaction taking place for ground-state SF_5^+.

For trichloroethene the major channel for reaction with SF_5^+ is now formation of parent ion ($C_2HCl_3^+$) with the only other product been due to F^+ transfer ($C_2HCl_3F^+$). The reaction is also slightly more efficient than for the dichloroethenes. When tetrachloroethene is the reactant neutral only non-dissociative charge transfer takes place and the reaction is 60 % efficient. This large change in product yields is due to the decrease in IE with increasing chlorine substitution. This leads to an increase in the long-range charge transfer cross-section for this reaction. Chemical reaction can still compete for trichloroethene, but for tetrachloroethene long-range charge transfer is so efficient that it can dominate.

Table 8.3: Rate coefficients, product ions and proposed neutral products for the reactions of *Z*-1,2-dichloroethene with cations with RE in the range 9.7 – 21.6 eV. The IE of (*Z*)-1,2-dichloroethene is 9.66 eV.

Reagent ion (RE [b] / eV)	Rate coefficient / 10^{-9} cm^3 molecule^{-1} s^{-1}	Product ions (%)	Proposed neutral products	$\Delta_r H^o_{298}$ / kJ mol^{-1}
SF_5^+	0.2	$C_2H_2Cl_2F^+$ (69)	SF_4	-794 + $\Delta_f H^o_{298}[C_2H_2Cl_2F^+]$
(9.78)	[1.6]	$C_2H_2Cl_2^+$ (14)	SF_5	-16
		$C_2H_2Cl^+$ (17)	SF_5Cl	-30
SF_2^+	1.7	$C_2H_2Cl_2^+$ (100)	SF_2	-60
(10.24)	[1.8]			
SF^+	1.5	$C_2H_2Cl_2^+$ (88)	SF	-67
(10.31)	[2.0]	$C_2H_2ClSF^+$ (6)	Cl	-874 + $\Delta_f H^o_{298}[C_2H_2ClSF^+]$
		C_2HClSF^+ (6)	HCl	-1088 + $\Delta_f H^o_{298}[C_2HClSF^+]$
CF_2^+	1.6	$C_2H_2Cl_2^+$ (100)	CF_2	-176
(11.44)	[2.0]			
SF_4^+	1.4	Not Measured	-	-
(11.99)	[1.6]			
O_2^+	2.3	$C_2H_2Cl_2^+$ (78)	O_2	-237
(12.07)	[2.4]	$C_2H_2Cl^+$ (22)	O_2 + Cl	-5
			OClO	-29
			ClOO	-30
Xe^+	1.4	$C_2H_2Cl_2^+$ (82)	Xe	-242
(12.13)	[1.5]	$C_2H_2Cl^+$ (18)	Xe + Cl	-11
N_2O^+	1.9	$C_2H_2Cl_2^+$ (15)	N_2O	-316
(12.89)	[2.1]	$C_2H_2Cl^+$ (85)	N_2O + Cl	-85
			N_2 + OCl	-186
			N_2OCl	-275
CO_2^+	1.9	$C_2H_2Cl_2^+$ (18)	CO_2	-400
(13.76)	[2.1]	$C_2H_2Cl^+$ (75)	CO_2 + Cl	-169
		C_2HCl^+ (7)	CO_2 + HCl	-181
Kr^+	1.6	$C_2H_2Cl^+$ (83)	Kr + Cl	-192
(14.00)	[1.7]	C_2HCl^+ (17)	Kr + HCl	-204
CO^+	1.7	$C_2H_2Cl_2^+$ (10)	CO	-423
(14.01)	[2.5]	$C_2H_2Cl^+$ (78)	CO + Cl	-192
			COCl	-266
		C_2HCl^+ (12)	CO + HCl	-204
N^+	2.8	$C_2H_2Cl_2^+$ (56)	N	-474
(14.53)	[3.3]	$C_2H_2Cl^+$ (37)	N + Cl	-243
			NCl	-523

		C_2HCl^+ (7)	N + HCl	-262
N_2^+	2.3	$C_2H_2Cl_2^+$ (10)	N_2	-574
(15.58)	[2.5]	$C_2HCl_2^+$ (6)	N_2 + H	-216
		$C_2H_2Cl^+$ (68)	N_2 + Cl	-344
		C_2HCl^+ (16)	N_2 + HCl	-363
Ar^+	1.5	$C_2H_2Cl_2^+$ (4)	Ar	-592
(15.76)	[2.2]	$C_2HCl_2^+$ (4)	Ar + H	-234
		$C_2H_2Cl^+$ (75)	Ar + Cl	-361
		C_2HCl^+ (17)	Ar + HCl	-381
F^+	2.4	$C_2H_2Cl_2^+$ (25)	F	-752
(17.42)	[2.9]	$C_2H_2Cl^+$ (29)	F + Cl	-521
			FCl	-772
		$C_2H_2^+$ (46)	F + Cl_2	-358
Ne^+	2.3	$C_2H_2Cl_2^+$ (11)	Ne	-1152
(21.56)	[2.8]	$C_2H_2^+$ (60)	Ne + Cl + Cl	-508
			Ne + Cl_2	-750
		C_2HCl^+ (21)	Ne + HCl	-933
		Cl^+ (8)	Ne + C_2H_2Cl	-706 + $\Delta_f H^o_{298}[C_2H_2Cl]$

The reactions of SF_2^+ (RE = 10.24 eV) and SF^+ (RE = 10.31 eV) show interesting results across the six chloroethenes. For all six neutrals charge transfer is energetically allowed, so parent ions can be formed. When monochloroethene is the neutral, the parent ion is the major product for both reactions, however, several other products form. For reaction with SF_2^+ the other product is $C_2H_3SF_2^+$ which can only be formed by a chemical reaction. For the reaction with SF^+ the other products are C_2HSF^+, C_2SF^+ and $C_2H_3^+$. All three products form from a chemical reaction, and there is not enough energy to form a parent ion which would fragment to $C_2H_3^+$ + Cl. For the other five neutrals, reaction with SF_2^+ only forms parent ions, whilst with the reactions of the dichloroethenes with SF^+ several non-charge transfer products are produced. For the 1,2 isomers of dichloroethene two other ions are formed in small, ~ 6 %, yields along with the parent ion. They are $C_2H_2ClSF^+$ and C_2HClSF^+. For the 1,1 isomer these two ions are formed with the parent in a small percentage but also formed are $C_2H_2Cl^+$ and $CHCl_2^+$. Apart from the parent ion all the other products must have been formed in a chemical reaction. For trichloroethene and tetrachloroethene only parent ion is formed with SF^+. This pattern with increasing chlorine substitution, *i.e.* charge transfer and competing chemical reactions for monochloroethene changing to charge transfer only as the number of Cl atoms increases, is the same as for the SF_5^+ reactions. The pattern can be explained in a similar way. For the

monochloroethene and the dichloroethene reactions the RE of the two ions is not much greater than the IE of the neutrals. So, although charge transfer is favourable it may be slightly inefficient, so not all reactant pairs of ion and neutral react *via* charge transfer. It is likely that only charge transfer occurs for the dichloroethenes for the reaction with SF_2^+ because no chemical reactions are energetically open. For trichloroethene and tetrachloroethene, the IE is far enough below the RE of the ions that long-range charge transfer is very efficient and no ion-molecule complexes are formed. This trend is confirmed for the reaction of monochloroethene with CF_2^+ (RE = 11.44 eV). For all the other chloroethenes this ion reacts *via* charge transfer, but for monochloroethene, although the parent ion is dominant, two other products are also formed, $C_3H_3F_2^+$ and $CHFCl^+$.

Another ion in this energy range which does not just react by charge transfer alone with monochloroethene is H_2O (RE = 12.62 eV). For this reaction a small percentage of protonated monochloroethene is formed ($C_2H_3ClH^+$). This shows that the proton affinity of monochloroethene is greater than that of OH.

Table 8.4: Rate coefficients, product ions and proposed neutral products for the reactions of *E*-1,2-dichloroethene with cations with RE in the range 9.7 – 21.6 eV. The IE of (*E*)-1,2-dichloroethene is 9.65 eV.

Reagent ion (RE [b] / eV)	Rate coefficient / 10^{-9} cm^3 molecule^{-1} s^{-1}	Product ions (%)	Proposed neutral products	$\Delta_r H^o_{298}$ / kJ mol^{-1}
SF_5^+ (9.78)	0.2 [0.9]	$C_2H_2Cl_2F^+$ (77) $C_2H_2Cl_2^+$ (16) $C_2H_2Cl^+$ (7)	SF_4 SF_5 SF_5Cl	-797 + $\Delta_f H^o_{298}[C_2H_2Cl_2F^+]$ -20 -35
SF_2^+ (10.24)	1.4 [1.0]	$C_2H_2Cl_2^+$ (100)	SF_2	-64
SF^+ (10.31)	1.3 [1.2]	$C_2H_2Cl_2^+$ (89) $C_2H_2ClSF^+$ (6) C_2HClSF^+ (5)	SF Cl HCl	-71 -877 + $\Delta_f H^o_{298}[C_2H_2ClSF^+]$ -1090 + $\Delta_f H^o_{298}[C_2HClSF^+]$
CF_2^+ (11.44)	1.3 [1.2]	$C_2H_2Cl_2^+$ (100)	CF_2	-180
SF_4^+ (11.99)	1.1 [1.0]	Not Measured	-	-
O_2^+ (12.07)	1.2 [1.4]	$C_2H_2Cl_2^+$ (68) $C_2H_2Cl^+$ (32)	O_2 O_2 + Cl OClO	-240 -11 -35

			or ClOO	-34
Xe^+	0.9	$C_2H_2Cl_2^+$ (85)	Xe	-246
(12.13)	[0.9]	$C_2H_2Cl^+$ (15)	Xe + Cl	-17
N_2O^+	0.9	$C_2H_2Cl_2^+$ (24)	N_2O	-320
(12.89)	[1.2]	$C_2H_2Cl^+$ (76)	N_2O + Cl	-90
			or N_2 + OCl	-192
			or N_2OCl	-281
CO_2^+	1.1	$C_2H_2Cl_2^+$ (15)	CO_2	-404
(13.76)	[1.2]	$C_2H_2Cl^+$ (74)	CO_2 + Cl	-174
		C_2HCl^+ (11)	CO_2 + HCl	-184
Kr^+	1.2	$C_2H_2Cl^+$ (80)	Kr + Cl	-197
(14.00 (& 14.67))	[1.0]	C_2HCl^+ (20)	Kr + HCl	-207
CO^+	1.6	$C_2H_2Cl_2^+$ (11)	CO	-427
(14.01)	[1.4]	$C_2H_2Cl^+$ (74)	CO + Cl	-198
			COCl	-271
		C_2HCl^+ (15)	CO + HCl	-207
N^+	2.0	$C_2H_2Cl_2^+$ (47)	N	-478
(14.53)	[1.9]	$C_2H_2Cl^+$ (42)	N + Cl	-249
			NCl	-529
		C_2HCl^+ (11)	N +HCl	-260
N_2^+	1.6	$C_2H_2Cl_2^+$ (9)	N_2	-579
(15.58)	[1.4]	$C_2HCl_2^+$ (4)	N_2 + H	-219
		$C_2H_2Cl^+$ (66)	N_2 + Cl	-349
		C_2HCl^+ (21)	N_2 + HCl	-358
Ar^+	1.1	$C_2H_2Cl_2^+$ (5)	Ar	-597
(15.76)	[1.3]	$C_2HCl_2^+$ (7)	Ar + H	-237
		$C_2H_2Cl^+$ (66)	Ar + Cl	-367
		C_2HCl^+ (22)	Ar + HCl	-376
F^+	1.4	$C_2H_2Cl_2^+$ (23)	F	-756
(17.42)	[1.7]	$C_2H_2Cl^+$ (32)	F + Cl	-527
			FCl	-778
		$C_2H_2^+$ (45)	F + Cl + Cl	-113
			F + Cl_2	-356
Ne^+	1.8	$C_2H_2Cl_2^+$ (5)	Ne	-1156
(21.56)	[1.6]	$C_2H_2^+$ (56)	Ne + Cl + Cl	-510
			Ne +Cl_2	-752
		C_2HCl^+ (34)	Ne + HCl	-935
		Cl^+ (5)	Ne + C_2H_2Cl	-708 + $\Delta_f H^o_{298}[C_2H_2Cl]$

When the RE of the reagent ion is greater than the IE of the neutral molecule, several clear patterns appear in the branching ratios. Firstly, after the RE of the ion exceeds the IE of the neutral, only parent ion is formed from charge transfer. After an energy gap of approximately 2 – 3 eV the first product ion due to fragmentation of the parent ion is formed. This product is due to loss of a chlorine atom, or in the case of monochloroethene a hydrogen atom. This ion is then formed in large percentages until, after another gap of several eV, a product ion is formed from which two chlorine atoms have been lost. These are the main channels. Other smaller channels occur which involve loss of hydrogen atoms, either with or without loss of chlorines at the same time.

Table 8.5: Rate coefficients, product ions and proposed neutral products for the reactions of trichloroethene with cations with RE in the range 9.7 – 21.6 eV. The IE of trichloroethene is 9.46 eV.

Reagent ion (RE / eV)	Rate coefficient / 10^{-9} cm^3 molecule^{-1} s^{-1}	Product ions (%)	Proposed neutral products	$\Delta_r H^o_{298}$ / kJ mol^{-1}
SF_5^+ (9.78)	0.4 [1.1]	$C_2HCl_3F^+$ (16)	SF_4	-780 – $\Delta_f H^o_{298}[C_2HCl_3F^+]$
		$C_2HCl_3^+$ (84)	SF_5	-33
SF_2^+ (10.24)	1.4 [1.5]	$C_2HCl_3^+$ (100)	SF_2	-77
SF^+ (10.31)	1.2 [1.3]	$C_2HCl_3^+$ (100)	SF	-995
CF_2^+ (11.44)	1.9 [1.5]	$C_2HCl_3^+$ (100)	CF_2	-193
SF_4^+ (11.99)	1.5 [1.1]	$C_2HCl_3^+$ (100)	SF_4	-247
O_2^+ (12.07)	1.8 [1.7]	$C_2HCl_3^+$(100)	O_2	-253
Xe^+ (12.13)	1.1 [1.1]	$C_2HCl_3^+$ (82) $C_2HCl_2^+$ (18)	Xe Xe + Cl	-259 34
H_2O^+ (12.62)	2.2 [2.2]	$C_2HCl_3^+$ (-) $C_2HCl_2^+$ (-)	H_2O H_2O + Cl	-306 -12
N_2O^+ (12.89)	2.0 [1.5]	$C_2HCl_3^+$ (49) $C_2HCl_2^+$ (51)	N_2O N_2O + Cl N_2 + OCl	-333 -39 -142
OH^+	2.3	$C_2HCl_3^+$ (-)	OH	-343

(13.25)	[2.2]	$C_2HCl_2^+$ (-)	OH + Cl	-50
			O + HCl	-53
			HOCl	-285
O^+	2.3	$C_2HCl_3^+$ (-)	O	-403
(13.62)	[2.3]	$C_2HCl_2^+$ (-)	O + Cl	-109
			OCl	-379
CO_2^+	1.7	$C_2HCl_3^+$ (21)	CO_2	-417
(13.76)	[1.5]	$C_2HCl_2^+$ (79)	CO_2 + Cl	-124
Kr^+	1.3	$C_2HCl_3^+$ (5)	Kr	-440
(14.00 (& 14.67))	[1.2]	$C_2HCl_2^+$ (95)	Kr + Cl	-146
CO^+	1.5	$C_2HCl_3^+$ (11)	CO	-440
(14.01)	[1.8]	$C_2HCl_2^+$ (89)	CO + Cl	-147
			COCl	-221
N^+	3.3	$C_2HCl_3^+$ (44)	N	-491
(14.53)	[2.5]	$C_2HCl_2^+$ (43)	N + Cl	-198
			NCl	-478
		C_2HCl^+ (13)	N + Cl_2	-148
			NCl + Cl	-186
N_2^+	1.3	$C_2HCl_3^+$ (3)	N_2	-592
(15.58)	[1.8]	$C_2HCl_2^+$ (88)	N_2 + Cl	-299
		$CHCl_2^+$ (9)	N_2 + CCl	-96
			NCN + Cl	-4
Ar^+	1.5	$C_2HCl_3^+$ (6)	Ar	-610
(15.76)	[1.6]	$C_2HCl_2^+$ (90)	Ar + Cl	-317
		$CHCl_2^+$ (4)	Ar + CCl	-114
F^+	2.3	$C_2HCl_3^+$ (17)	F	-770
(17.42)	[2.2]	$C_2HCl_2^+$ (18)	F + Cl	-476
			FCl	-727
		C_2HCl^+ (65)	F + Cl_2	-427
			FCl + Cl	-435
Ne^+	2.3	$C_2Cl_2^+$ (13)	Ne + HCl	-1936
(21.56)	[2.1]	C_2HCl^+ (78)	Ne + Cl_2	-826
		CCl^+ (9)	Ne + $CHCl_2$	-1452

Two reactions which are interesting to compare are those of Kr^+ (RE = 14.00) and CO^+ (RE = 14.01). The RE of these two ions only differs by 0.01 eV. Thus any difference between the branching ratios of these two ions must be due to differences in reaction mechanism rather than energetics. For monochloroethene the main difference is that for Kr^+ an extra channel due to loss of a hydrogen atom from the parent ion is seen. For reaction with 1,1-dichloroethene a similar

extra channel is seen for Kr^+ compared with CO^+. For the1,2-dichloroethenes the difference is that a percentage of parent ion is seen for reaction with CO^+. With both trichloroethene and tetrachloroethene no difference is observed between Kr^+ or CO^+. The differences suggest that the two ions may be reacting *via* different mechanisms. However, they could be due to the presence of some excited Kr^+ in the flow tube which leads to the extra fragmentation measured for monochloroethene and the dichloroethenes.

Another interesting ion is N^+ (RE = 14.53 eV). Examination of the branching ratios for reaction of the six chloroethenes with N^+ show that more parent ion is produced than would be expected from the branching ratios of ions with a similar RE value. This has been observed for most of the reactions of N^+ studied in this thesis, and a detailed discussion is given in Chapter 1.

The reactions of Xe^+ and Ar^+ with monochloroethene have been previously studied in a two-stage ion-beam mass spectrometer by Izod and Tedder.[7] For the Xe^+ reaction our branching ratios agree within experimental error, except no $C_2H_2^+$ is formed in the ion-beam equipment. For the Ar^+ reaction the branching ratios are in good agreement for formation of both $C_2H_3^+$ and $C_2H_2^+$, however the only other ion formed in the ion-beam study is $C_2H_3Cl^+$. None of the other three ions seen in the SIFT results are detected. The differences are undoubtedly due to the different reaction conditions between the two experiments.

The reactions of trichloroethene and tetrachloroethene with O_2^+ have been studied by Španěl *et al*.[21] This work was performed in a version of the SIFT and only relative rate coefficients were recorded. O_2^+ reacted to form the parent ion in both cases. These results agree with those recorded here. The measured rate coefficients are in reasonable agreement between the two experiments.

Examination of the results for the six dichloroethenes shows trends which depend on the amount of chlorine substitution, for example the products and efficiency of the reaction with SF_5^+. Signs of trends which depend on the position of the chlorine substituents, *i.e.* the differences between the dichloroethene isomers are less clear. No differences outside experimental error have been found between the *E* and (*Z*)-1,2-dichloroethene isomers. This is probably because upon ionisation the rotation around the C=C bond becomes free so that *E* and *Z* form the same parent ion. More conclusive differences have been observed between the 1,1 and the 1,2-dichloroethene isomers. For example, from the reaction of SF^+ with 1,1-dichloroethene both $CHCl_2^+$ and $C_2H_2Cl^+$ are detected, yet neither of these products are observed for the reaction with the 1,2-dichloroethenes. Similarly, the reaction of 1,1-dichloroethene with Ne^+ produces CCl^+ which is not formed from *E* or (*Z*)-1,2-dichloroethene. Another example is the reactions of

CO^+ with the dichloroethenes. Here, when either *E* or (*Z*)-1,2-dichloroethene is the neutral reactant parent ion is detected; when 1,1-dichloroethene is the neutral reactant no parent ion is detected. Finally, when *E* or (*Z*)-1,2-dichloroethene react with N_2^+ or Ar^+ both $C_2H_2Cl_2^+$ and $C_2HCl_2^+$ are products, but they are not formed in reaction with 1,1-dichloroethene.

Table 8.6: Rate coefficients, product ions and proposed neutral products for the reactions of tetrachloroethene with cations with RE in the range 9.7 – 21.6 eV. The IE of tetrachloroethene is 9.30 eV.

Reagent ion (RE / eV)	Rate coefficient / 10^{-9} cm^3 molecule^{-1} s^{-1}	Product ions (%)	Proposed neutral products	$\Delta_r H^o_{298}$ / kJ mol^{-1}
SF_5^+ (9.78)	0.6 [1.0]	$C_2Cl_4^+$ (100)	SF_5	-44
SF_2^+ (10.24)	0.7 [1.3]	$C_2Cl_4^+$ (100)	SF_2	-89
SF^+ (10.31)	1.2 [1.2]	$C_2Cl_4^+$ (100)	SF	-96
CF_2^+ (11.44)	1.5 [1.3]	$C_2Cl_4^+$ (100)	CF_2	-204
SF_4^+ (11.99)	1.0 [1.0]	$C_2Cl_4^+$ (100)	SF_4	-258
O_2^+ (12.07)	1.3 [1.6]	$C_2Cl_4^+$ (100)	O_2	-265
Xe^+ (12.13)	0.9 [0.9]	$C_2Cl_4^+$ (55) $C_2Cl_3^+$ (45)	Xe Xe + Cl	-271 -227
H_2O^+ (12.62)	1.6 [2.0]	$C_2Cl_4^+$ (-) $C_2Cl_3^+$ (-)	H_2O H_2O + Cl	-317 -273
N_2O^+ (12.89)	1.7 [1.4]	$C_2Cl_4^+$ (22) $C_2Cl_3^+$ (78)	N_2O N_2O + Cl	-344 -300
OH^+ (13.25)	1.7 [2.1]	$C_2Cl_4^+$ (-) $C_2Cl_3^+$ (-)	OH OH + Cl	-342 -317
O^+ (13.62)	2.0 [2.1]	$C_2Cl_4^+$ (-) $C_2Cl_3^+$ (-)	O O + Cl	-414 -370
CO_2^+ (13.76)	1.4 [1.4]	$C_2Cl_4^+$ (18) $C_2Cl_3^+$ (82)	CO_2 CO_2 + Cl	-422 -391
Kr^+ (14.00 (& 14.67))	1.1 [1.1]	$C_2Cl_4^+$ (4) $C_2Cl_3^+$ (96)	Kr Kr + Cl	-451 -407

CO^+	1.8	$C_2Cl_4^+$ (7)	CO	-452
(14.01)	[1.7]	$C_2Cl_3^+$ (93)	CO + Cl	-408
N^+	2.3	$C_2Cl_4^+$ (43)	N	-503
(14.53)	[2.3]	$C_2Cl_3^+$ (57)	N + Cl	-459
N_2^+	1.7	$C_2Cl_4^+$ (7)	N_2	-603
(15.58)	[1.7]	$C_2Cl_3^+$ (67)	N_2 + Cl	-559
		CCl_3^+ (3)	N_2 + CCl	-115
			NCN + Cl	-23
		$C_2Cl_2^+$ (17)	N_2 + Cl_2	-314
			N_2 + Cl + Cl	-71
		CCl_2^+ (5)	N_2 + CCl_2	-77
Ar^+	1.4	$C_2Cl_4^+$ (3)	Ar	-621
(15.76)	[1.4]	$C_2Cl_3^+$ (42)	Ar + Cl	-577
		CCl_3^+ (3)	Ar + CCl	-133
		$C_2Cl_2^+$ (44)	Ar + Cl_2	-332
			Ar + Cl + Cl	-89
		CCl_2^+ (8)	Ar + CCl_2	-95
F^+	1.4	$C_2Cl_2^+$ (100)	F + Cl_2	-492
(17.42)	[2.0]		F + Cl + Cl	-249
			FCl + Cl	-500
Ne^+	2.0	$C_2Cl_3^+$ (1)	Ne + Cl	-1136
(21.56)	[1.9]	$C_2Cl_2^+$ (54)	Ne + Cl_2	-891
			Ne + Cl + Cl	-648
		CCl_2^+ (10)	Ne + CCl_2	-654
		C_2Cl^+ (10)	Ne + Cl_2 + Cl	-1935 – $\Delta_f H^o_{298}[C_2Cl^+]$
		CCl^+ (25)	Ne + CCl_3	-733
			Ne + CCl_2 + Cl	-453

5. Comparison of product branching ratios from SIFT and TPEPICO experiments

Figure 8.1(a) – (f) show the branching ratios from ion-molecule reactions recorded on the SIFT with all six chloroethenes over the RE range 9.7 – 21.6 eV. In Figure 8.1 (b) – (e) the TPEPICO results from chapter 7 from onset of ionisation to 22 eV are also plotted. The TPEPICO breakdown data for tetrachloroethene are not produced here as the quality is poor.

Examination of Figure 8.1 shows that the agreement between the SIFT and TPEPICO branching ratios in general is good. The overall trends are mirrored. That is, after onset the parent ion is formed, followed by fragmentation by chlorine-atom loss at higher energies. In the range 9.7 – 12 eV there is no disagreement for trichloroethene. For the dichloroethene isomers the

major disagreement is for reaction with SF_5^+; this is expected as these reactions predominately occur by a chemical mechanism, as discussed earlier. For 1,1-dichloroethene there is another disagreement in this energy range for SF^+, due to a large percentage of chemical products occurring in this reaction. There is also some disagreement for the reactions of the 1,2-dichloroethenes with SF^+, but not a large amount. This suggests that the reactions with SF^+ are not purely long-range charge transfer, but some other mechanisms are operative as well.

From 12 – 15 eV the agreement between branching ratios is not as good, but except for N^+ (RE = 14.53 eV) the overall trends are the same for the two experiments. For N^+ the yield of parent ions is around 50 % in all cases. We note that the SIFT branching ratios for the reaction with the dichloroethenes agree with those of Rebrion *et* al.[17] As mentioned in previous chapters N^+ is often an anomalous ion, seeming to act as a softly-ionising species compared to photons of this energy.

For the reactions with F^+ (RE = 17.42 eV) none of the dichloroethene isomers show any agreement between the SIFT and TPEPICO results. For example, parent ion is formed in the ion-molecule reactions but not from photon ionisation. F^+, therefore cannot be reacting *via* a pure long-range mechanism. Trichloroethene shows fair agreement between the two sets of experimental data, suggesting that long-range charge transfer is taking place.

For Ne^+ (21.56 eV) (*E*)-1,2-dichloroethene and trichloroethene show fair agreement, especially for the *E* isomer. The agreement is poor for 1,1-dichloroethene and (*Z*)-1,2-dichloroethene. It should be noted that for Ne^+ other ions are formed which are not seen in the TPEPICO data. The broad agreement between the experiments for Ne^+ suggests that the charge transfer mechanism is largely of a long-range nature with some interaction leading to production of Cl^+ as well. In general, all the ion-molecule reactions where the RE > 13 eV produce a greater percentage of parent ion than at the comparable photon energy.

Though data for TPEPICO branching ratios of monochloroethene and tetrachloroethene is not available, comparison with the other four chloroethenes is interesting. The overall trends clearly agree for all the isomers. The appearance of $C_2Cl_3^+$ in the SIFT experiments occurs around 12 eV, this seems to agree with the belief that the measured $AE_{298}[C_2Cl_3^+]$ of 9.48 eV is too low and that the real value is closer to 11.4 eV.

For the dichloroethenes no new isomeric effects have been observed when the ion-molecule results are compared to the photoionisation data. This is expected because no clear isomeric effects were seen in the TPEPICO data, see chapter 7, and long-range charge transfer seems to be the dominant mechanism.

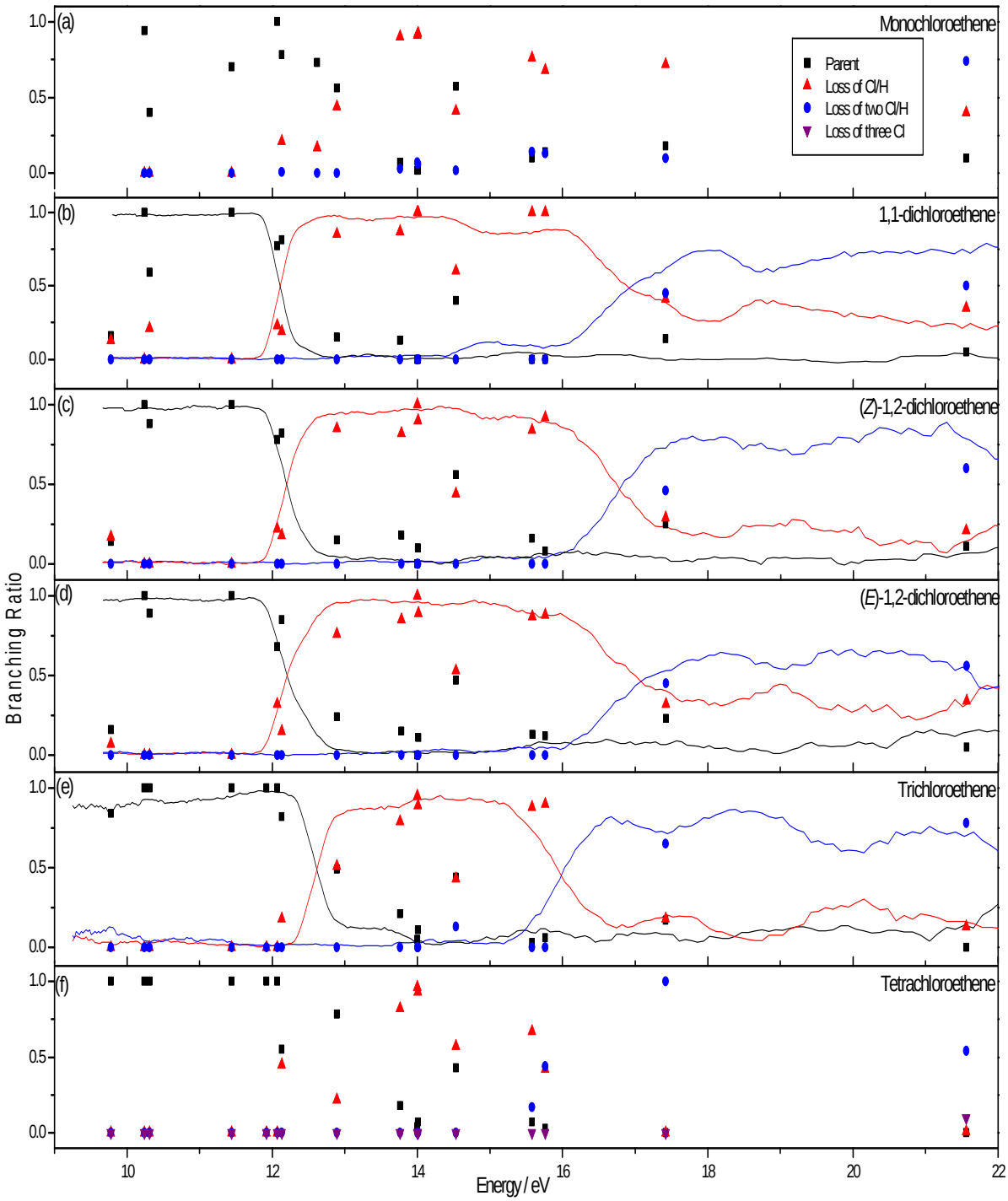

Figure 8.1: (a) – (f) SIFT branching ratios and for (b) – (e) TPEPICO branching ratios with an optical resolution of 0.3 nm for the chloroethenes.

6. Conclusions

Results have been presented for the ion-molecule reactions of the six different chloroethenes: monochloroethene, 1,1-dichloroethene, (*Z*)-1,2-dichloroethene, (*E*)-1,2-dichloroethene, trichloroethene and tetrachloroethene with a selection of cations with RE in the range 9.78 – 21.56 eV. Comparison has been made with photon ionisation results over the same energy range for the dichloroethenes and trichloroethene. Overall, agreement is good between the two methods, suggesting that the charge transfer mechanism for the ion-molecule reactions is mainly long-range in nature. For the few exceptions, chemical reaction or short-range charge transfer is postulated as the main mechanism likely to occur.

Some weak isomeric effects have been seen for the reactions of a few ions. All the isomeric effects seen are differences between the 1,1 and 1,2 isomers, so due to connectivity isomerisation. Effects due to conformational isomerisation, *i.e.* differences between the *Z* and (*E*)-1,2 isomers, have not been seen in this study.

7. References

1 V.G. Anicich, M.T. Bowers, *Int. J. Mass. Spectrom. Ion Phys.*, **11**, (1973) 329.
2 J.L. Beauchamp, L.R. Anders, J.D. Baldeschwieler, *J. Am. Chem. Soc*, **89**, (1967) 4569.
3 A. Nixdorf, H.-F. Grützmacher, *Chem. Eur. J.*, **7**, (2001) 1248.
4 L.i. Bian, E.G. Alley, B.C. Lynn, *Environ. Sci. Technol.*, **33**, (1999) 1528.
5 A. Nixdorf, H.-F. Gru1tzmacher, *J. Am. Chem. Soc.*, **119**, (1997) 6544.
6 Y. Ling, G.K. Koyanagi, D. Caraiman, A.C. Hopkinson, D.K. Bohme, *Int. J. Mass. Spec.*, **192**, (1999) 215.
7 T.P.J. Izod, J.M. Tedder, *Int. J. Mass. Spectrom. Ion Phys.*, **22**, (1976) 85.
8 M.T. Baumgartner, R.A. Taccone, M.A. Teruel, S.I. Lane, *Phys Chem Chem Phys*, **4**, (2002) 1028.
9 E.V. Avzianova, P.A. Ariya, *Int. J. Chem. Kinetics*, **34**, (2002) 678.
10 T. Yamada, A. El-Sinaw, M. Siraj, P.H. Taylor, J. Peng, X. Hu, P. Marshall, *J. Phys. Chem. A*, **105**, (2001) 7588.
11 M.A. Teruel, R.A. Taccone, S.I. Lane, *Int. J. Chem. Kinetics*, **33**, (2001) 415.
12 C.E. Canosa-Mas, T.J. Dillon, H. Sidebottom, K.C. Thompson, R.P. Wayne, *Phys Chem Chem Phys*, **3**, (2001) 542.
13 Z. Zhang, R. Liu, R.E. Huie, M.J. Kurylo, *J .Phys. Chem*, **95**, (1991) 194.
14 M.B. Blanco, P.M. Cometto, R.l.A. Taccone, S.I. Lane, M.A. Teruel, *J. Phys. Org. Chem.*, **19**, (2006) 752.
15 M.T. Bowers, J.B. Laudenslager, *J. Chem. Phys.*, **56**, (1972) 4711.
16 T. Su, M.T. Bowers, *J. Chem. Phys.*, **58**, (1973) 3027.
17 C. Rebrion, J.B. Marquette, B.R. Rowe, C. Chakravarty, D.C. Clary, N.G. Adams, D. Smith, *J. Phys. Chem*, **92**, (1988) 6572.
18 R.A. Kennedy, C.A. Mayhew, R. Peverall, P. Watts, *Phys. Chem. Chem. Phys.*, **2**, (2000) 3145.
19 A. Bagno, A. Donò, S. Martinucci, C. Paradisi, G. Scorrano, *Int. J. Mass. Spectrom.* , **179/180**, (1998) 349.
20 A. Dono, C. Paradisi, G. Scorrano, *Rap. Comm. Mass Spec.*, **11**, (1997) 1687.
21 P. Španěl, D. Smith, *Int. J. Mass Spec.*, **184**, (1999) 175.
22 V. A. Mikhailov, M. A. Parkes, R. P. Tuckett, C. A. Mayhew, *J. Phys. Chem.*, **110**, (2006) 5760.
23 T. Su, *J. Chem. Phys.*, **88**, (1988) 4102.
24 T. Su, W.J. Chesnavich, *J. Chem. Phys.*, **76**, (1982) 5183.
25 D.R. Lide: *Handbook of Chemistry and Physics 87th Edition*, Taylor and Francis, London, (2006).
26 J.L.M. Abboud, R. Notari, *Pure App. Chem.*, **71**, (1999) 645.
27 M.W. Chase, *J. Phys. Chem. Ref. Data*, (1998) Monograph no. 9.
28 S.G. Lias, J.E. Bartmess, J.F. Liebman, J.L. Holmes, R.D. Levin, W.G. Mallard, *J. Phys. Chem. Ref. Data*, **17**, (1988) supplement no 1.
29 G.A. Garcia, P.-M. Guyon, I. Powis, *J. Phys. Chem. A*, **105**, (2001) 8296.
30 J.C. Poutsma, J.A. Paulino, R.R. Squires, *J. Phys. Chem. A*, **101**, (1997) 5327.
31 R.Y.L. Chim, R.A. Kennedy, R.P. Tuckett, W. Zhou, G.K. Jarvis, D.J. Collins, P.A. Hatherly, *J. Phys. Chem. A*, **105**, (2001) 8403.
32 E.R. Fisher, B.L. Kickel, P.B. Armentrout, *J. Chem. Phys.*, **97**, (1992) 4859.
33 C.W. Bauschlicher, A. Ricca, *J. Phys. Chem.*, **102**, (1998) 4722.

34 K.R. Shamasundar, E. Arunan, *J. Phys. Chem. A*, **105**, (2001) 8533.
35 J.A. Manion, *J. Phys. Chem. Ref. Data*, **31**, (2002) 123.
36 C.R. Howle, C.A. Mayhew, R.P. Tuckett, *J. Phys. Chem. A*, **109**, (2005) 3626.
37 D. Schröder, H. Schwarz, D.E. Clemmer, Y. Chen, P.B. Armentrout, V.I. Baranov, D.K. Böhme, *Int. J. Mass. Spectrom. Ion Proc.*, **161**, (1997) 175.

Chapter 9: Isomeric effects in the reactions of the chloroethenes with selected cations: 2. RE ≤ IE[$C_2H_xCl_{4-x}$]

1. Introduction

The previous two chapters have dealt with the photoionisation of five of the chloroethenes (1,1-dichloroethene, (*Z*)-1,2-dichloroethene, (*E*)-1,2-dichloroethene, trichloroethene and tetrachloroethene) and their reactions with a series of cations with recombination energies (RE) ranging from 9.78 – 21.56 eV. Comparisons between the two data sets have been discussed. Ion-molecule reactions in the energy range have also been reported for the sixth chloroethene, monochloroethene. This chapter will deal with a sequence of cations that have RE values below the ionisation energies (IE) of the six chloroethenes. In this energy range charge transfer is not allowed energetically, so that all reactions must occur by an intimate chemical reaction in which bonds form and break in a complex. In such a situation steric effects will be significant and isomeric differences should become more important than in the previously-reported results.

In this chapter the reactions of ions with RE values which span the range 4.73 eV to 9.11 eV with all six chloroethenes are reported. The reaction with NH_4^+ was only performed with the three dichloroethene isomers. The reactions were studied on the SIFT apparatus. As before, the main aim was to look for examples of the effects of structural isomerisation upon reaction rates and products, and the effects of increasing the number of chlorine atoms. Data on the ion-molecule reactions of the dichloroethenes have previously been published.[1]

2. Experimental

The experiments were performed as described in chapter 2. The six isomers were purchased from Sigma-Aldrich with stated purities of 99.5, 97 and 98 % for the 1,1, *Z* and *E* isomers respectively. The monochloroethene, trichloroethene and tetrachloroethene samples were also purchased from Sigma-Aldrich with purities of + 99 % All samples were further purified by successive freeze-pump thawing cycles before use except for monochloroethene.

3. Theoretical Considerations

The values used for calculating thermochemistry and reaction coefficients are the same as those listed in the previous chapter (chapter 8 section 3).

4. Results

4.1 Rate coefficients

Tables 9.1 – 9.6 show the results for SIFT experiments on monochloroethene, 1,1-dichloroethene, (*Z*)-1,2-dichloroethene, (*E*)-1,2-dichloroethene, trichloroethene and tetrachloroethene, respectively. The first column shows the reagent ion and its RE, the second both the experimental and theoretical rate coefficients, the latter values are in square brackets. Measured product ions are listed in column 3 along with branching ratios. Proposed neutral products and enthalpies of reaction are shown in columns 4 and 5, respectively. Only the five ions with an RE less than the IE of the chloroethenes are listed.

Of the five ions studied in this range two did not react with any of the neutrals. These ions are SF_3^+ and NO^+. For NO^+ there was sign of some reaction, however it was very slow and there was a large amount of curvature in the plot of ln(Ion signal) *vs* neutral concentration (chapter 2). This suggests that all the reaction was due to excited NO^{+*} ions. The reaction of NO^+ with trichloroethene and tetrachloroethene has been studied by Španěl *et al.*[2] They found that it reacted to form an adduct only. No adduct was observed in our studies, but high enough flows of neutral gas may not have been used for the product to become detectable. NH_4^+ did not react with any of the dichloroethenes. The other three ions, H_3O^+, CF_3^+ and CF^+, reacted with all six chloroethenes.

Table 9.1: Rate coefficients, product ions and proposed neutral products for the reactions of monochloroethene with cations with RE in the range 6.27 - 9.26 eV. The IE of monochloroethene is 9.99 eV.

Reagent ion (RE / eV)	Rate coefficient / 10^{-9} cm^3 molecule^{-1} s^{-1}	Product ions (%)	Proposed neutral products	$\Delta_r H^o_{298}$ / kJ mol^{-1}
H_3O^+ (6.27)	2.2 [2.5]	$C_2H_3ClH^+$ (100)	H_2O	-815 + $\Delta_f H^o_{298}[C_2H_3ClH^+]$
SF_3^+ (8.32)	No Reaction [1.5]	-	-	-
CF_3^+ (9.04)	1.1 [1.6]	$CHFCl^+$ (35) $C_2H_3^+$ (65)	$C_2F_2H_2$ CF_3Cl	-25 -36
CF^+ (9.11)	2.0 [2.1]	$CHFCl^+$ (27) $C_2H_3^+$ (73)	C_2H_2 CFCl	-186 -25
NO^+ (9.26)	No Reaction [2.0]	-	-	-

Unlike the reactions with RE ≥ IE[neutral] there is a large variation in the efficiency of the reactions for ions with RE < IE[neutral]. This is because when RE ≥ IE[neutral] charge transfer is energetically allowed and in general tends to be an efficient process, so reactions are likely to occur with every collision. When RE < IE[neutral], then charge transfer is not allowed, and only a chemical reaction can take place. Chemical reactions only occur when the ion and neutral are in close contact. Here the orientation of the ion and neutral relative to each other and steric effects can make significant changes to reaction efficiencies. Also, there could be exit channel barriers and energetic constraints for some of the product channels. The most prominent example is for the reactions of H_3O^+ (RE = 6.27 eV). With monochloroethene, 1,1-dichloroethene and trichloroethene the rate coefficient is essentially the same as the collisional value, however, for both 1,2 isomers the reaction is only around 15 % efficient whilst for tetrachloroethene it is 50 % efficient. Such a difference must clearly be due to the structures of the molecules, the relative positions of the chlorine atoms, and the energetics of the reaction products.

Table 9.2: Rate coefficients, product ions and proposed neutral products for the reactions of 1,1-dichloroethene with cations with RE in the range 4.73 - 9.26 eV. The IE of 1,1-dichloroethene is 9.79 eV.

Reagent ion (RE / eV)	Rate coefficient / 10^{-9} cm^3 molecule^{-1} s^{-1}	Product ions (%)	Proposed neutral products	$\Delta_r H^o_{298}$ / kJ mol^{-1}
NH_4^+ (4.73)	No Reaction [1.68]	-	-	-
H_3O^+ (6.27)	2.0 [2.0]	$C_2H_2Cl_2H^+$ (100)	H_2O	$-808 + \Delta_f H^o_{298}[C_2H_2Cl_2H^+]$
SF_3^+ (8.32)	No Reaction [1.4]	-	-	-
CF_3^+ (9.04)	1.2 [1.5]	$C_2H_2Cl^+$ (100)	CF_3Cl	-76
CF^+ (9.11)	2.1 [2.0]	$CHCl_2^+$ (6) $CHClF^+$ (25) $C_2H_2Cl^+$ (69)	C_2HF C_2HCl CFCl	-142 -180 -65
NO^+ (9.26)	No Reaction [1.9]	-	-	-

The reactions of all six chloroethenes with CF^+ are fairly efficient, the lowest efficiency being 80 % for (*E*)-1,2-dichloroethene. For the reactions with CF_3^+ the efficiency shows more variation across the chloroethenes. For monochloroethene and (*E*)-1,2-dichloroethene the reaction is 70 % efficient, for 1,1-dichloroethene it is 80 % efficient, and for trichloroethene and tetrachloroethene it is 100 % efficient. (*Z*)-1,2-dichloroethene has the lowest efficiency, only 50 %.

Table 9.3: Rate coefficients, product ions and proposed neutral products for the reactions of (*Z*)-1,2-dichloroethene with cations with RE in the range 4.73 - 9.26 eV. The IE of (*Z*)-1,2-dichloroethene is 9.66 eV.

Reagent ion (RE / eV)	Rate coefficient / 10^{-9} cm^3 molecule^{-1} s^{-1}	Product ions (%)	Proposed neutral products	$\Delta_r H^o_{298}$ / kJ mol^{-1}
NH_4^+ (4.73)	No Reaction [3.0]	-	-	-
H_3O^+ (6.27)	0.4 [2.9]	$C_2H_2ClOH_2^+$ (65) $C_2H_2Cl_2H^+$ (35)	HCl H_2O	-688 + $\Delta_f H^o_{298}[C_2H_2ClOH_2^+]$ -837 + $\Delta_f H^o_{298}[C_2H_2Cl_2H^+]$
SF_3^+ (8.32)	No Reaction [1.7]	-	-	-
CF_3^+ (9.04)	1.0 [1.8]	$CHCl_2^+$ (100)	C_2HF_3	10
CF^+ (9.11)	2.0 [2.4]	$CHCl_2^+$ (41) $CHClF^+$ (59)	C_2HF C_2HCl	-137 -181
NO^+ (9.26)	No Reaction [2.4]	-	-	-

4.2 Ion-molecule branching ratios

Branching ratios were measured for the reactions of all six chloroethenes with the three cations which reacted; H_3O^+, CF_3^+ and CF^+. For the three dichloroethenes, striking isomeric effects are seen in the branching ratios for reactions with ions of RE < IE[neutral], much more significant than for ions with a higher RE. For clarity each of the ions which reacted will be dealt with in turn.

Table 9.4: Rate coefficients, product ions and proposed neutral products for the reactions of (*E*)-1,2-dichloroethene with cations with RE in the range 4.73 - 9.26 eV. The IE of (*E*)-1,2-dichloroethene is 9.65 eV.

Reagent ion (RE / eV)	Rate coefficient / 10^{-9} cm^3 molecule^{-1} s^{-1}	Product ions (%)	Proposed neutral products	$\Delta_r H^o_{298}$ / kJ mol^{-1}
NH_4^+ (4.73)	No Reaction [1.7]	-	-	-
H_3O^+ (6.27)	0.3 [1.7]	$C_2H_2ClOH_2^+$ (43) $C_2H_2Cl_2H^+$ (57)	HCl H_2O	$-685 + \Delta_f H^o_{298}[C_2H_2ClOH_2^+]$ $-834 + \Delta_f H^o_{298}[C_2H_2Cl_2H^+]$
SF_3^+ (8.32)	No Reaction [1.0]	-	-	-
CF_3^+ (9.04)	0.7 [1.0]	$CHCl_2^+$ (100)	C_2HF_3	8
CF^+ (9.11)	1.4 [1.4]	$CHCl_2^+$ (51) $CHClF^+$ (49)	C_2HF C_2HCl	-140 -177
NO^+ (9.26)	No Reaction [1.4]	-	-	-

4.2.1 Reactions of H_3O^+

The reactions of H_3O^+ with the chloroethenes produce three different products indicated here for a dichloroethene isomer:

$$H_3O^+ + C_2H_2Cl_2 \rightarrow C_2H_2Cl_2H^+ \quad \text{(proton transfer)} \quad \textbf{(re 9.1)}$$

$$\rightarrow C_2HClOH_2^+ + HCl \quad \text{(chemical reaction)} \quad \textbf{(re 9.2)}$$

$$\rightarrow C_2H_2Cl_2 \cdot H_3O^+ \quad \text{(adduct formation)} \quad \textbf{(re 9.3)}$$

All three of these different products are seen for the reaction of H_3O^+ with (*Z*)-1,2-dichloroethene and (*E*)-1,2-dichloroethene, whereas only the proton-transfer channel is seen for monochloroethene, 1,1-dichloroethene, trichloroethene and tetrachloroethene. The reactions of trichloroethene and tetrachloroethene were studied by Španěl *et al*, [2] and protonated parent was the only detected product for trichloroethene, in agreement with our data. For tetrachloroethene a small percentage of $C_2Cl_3^+$ was also detected by Španěl *et a*l. No sign of this product was observed during our studies.

Table 9.5: Rate coefficients, product ions and proposed neutral products for the reactions of trichloroethene with cations with RE in the range 6.27 - 9.26 eV. The IE of trichloroethene is 9.46 eV.

Reagent ion (RE / eV)	Rate coefficient / 10^{-9} cm^3 molecule^{-1} s^{-1}	Product ions (%)	Proposed neutral products	$\Delta_r H^o_{298}$ / kJ mol^{-1}
H_3O^+ (6.27)	2.1 [2.2]	$C_2HCl_3H^+$ (100)	H_2O	-815 + $\Delta_f H^o_{298}[C_2HCl_3H^+]$
SF_3^+ (8.32)	No Reaction [1.2]	-	-	-
CF_3^+ (9.04)	1.3 [1.3]	$CFCl_2^+$ (24) $C_2HCl_2^+$ (54) CF_2Cl^+ (22)	C_2HClF_2 CF_3Cl C_2HCl_2F	315 + $\Delta_f H^o_{298}[C_2HClF_2]$ -33 168 + $\Delta_f H^o_{298}[C_2HCl_2F]$
CF^+ (9.11)	1.8 [1.8]	$CFCl_2^+$ (39) $CHCl_2^+$ (23) $CHClF^+$ (37)	C_2HCl CF + CCl C_2FCl C_2Cl_2	-200 -251 -230 + $\Delta_f H^o_{298}[C_2FCl]$ -164
NO^+ (9.26)	No Reaction [1.79]	-	-	-

As all the chloroethenes react with H_3O^+ by proton transfer their proton affinity (PA) must be larger than that for H_2O (691 kJ mol^{-1}).[3] Using this fact, upper limits for $\Delta_f H^o_{298}$ of protonated monochloroethene, 1,1-dichloroethene, (*Z*)-1,2-dichloroethene, (*E*)-1,2-$C_2H_2Cl_2$, trichloroethene and tetrachloroethene have been determined as 124, 117, 146, 143, 124 and 118 kJ mol^{-1}, respectively. As there is no reaction with NH_4^+ but there is a protonation reaction with H_3O^+, the PAs of the dichloroethenes can be bracketed using the following inequality:

$$\text{PA}[H_2O] \text{ or } 691 \leq \text{PA}[C_2H_2Cl_2] \leq \text{PA}[NH_3] \text{ or } 854 \text{ kJ mol}^{-1}$$

If the formation of $C_2H_2ClOH_2^+$ from (*Z*)-1,2-dichloroethene and (*E*)-1,2-dichloroethene is assumed to occur with HCl as the neutral partner and the enthalpy of reaction is zero, then upper limits for $\Delta_f H^o_{298}$ for this ion are 688 and 685 kJ mol^{-1} for the *Z* and *E* isomers of dichloroethene. It is usually assumed that all reactions with H_3O^+ occur by a proton transfer reaction and cause very little fragmentation. It is therefore surprising to see $C_2H_2ClOH_2^+$ as an ionic product. However, such processes have been seen before in other chlorocarbons. Španěl *et al.*[2] saw an analogous product from reaction of H_3O^+ with some chloroethanes.

Table 9.6: Rate coefficients, product ions and proposed neutral products for the reactions of tetrachloroethene with cations with RE in the range 6.27 - 9.26 eV. The IE of tetrachloroethene is 9.30 eV.

Reagent ion (RE / eV)	Rate coefficient / 10^{-9} cm^3 molecule^{-1} s^{-1}	Product ions (%)	Proposed neutral products	$\Delta_r H^o_{298}$ / kJ mol^{-1}
H_3O^+ (6.27)	1.1 [2.0]	$C_2Cl_4H^+$ (100)	H_2O	-809 + $\Delta_f H^o_{298}[C_2Cl_4H^+]$
SF_3^+ (8.32)	No Reaction [1.1]	-	-	-
CF_3^+ (9.04)	1.9 [1.2]	$C_2Cl_3^+$ (9) $CFCl_2^+$ (16) CF_2Cl^+ (75)	CF_3Cl $C_2F_2Cl_2$ C_2FCl_3	-294 +321 + $\Delta_f H^o_{298}[C_2F_2Cl_2]$ +174 + $\Delta_f H^o_{298}[C_2FCl_3]$
CF^+ (9.11)	1.8 [1.6]	$CFCl_2^+$ (100)	C_2Cl_2	-197
NO^+ (9.26)	No Reaction [1.6]	-	-	-

Combining the branching ratios with the rate coefficients gives useful insight into the reaction mechanisms for the protonation of the six chloroethenes. Monochloroethene, 1,1-dichloroethene and trichloroethene react with high efficiency to form only one product, the protonated neutral molecule. Tetrachloroethene reacts with ~50 % efficiency to form only $C_2Cl_4H^+$. The 1,2-dichloroethenes react very slowly and two other products are formed as well as the protonated neutral. For the 1,2 isomers the slow rate suggest that there is a small barrier to protonation. The presence of the barrier not only slows down the reaction but also allows other product channels to be accessed, in this case the ion formed by loss of a hydrogen halide, $C_2H_2ClOH_2^+$. Also a small percentage of the H_3O^+ adduct was detected, indicating that the ion-neutral complex is relatively long-lived and it survives long enough for collisional cooling with the He buffer gas to occur. This cooling means that any barriers to reaction can no longer be surmounted, leading to detection of the adduct. It should be noted that no attempt was made to investigate the dependence of the association reaction on pressure of the buffer gas, hence the rate coefficient is an effective two-body rate.

For formation of the $C_2H_2ClOH_2^+$ product, attempts were made to ascertain which hydrogen atom was being ejected by use of D_3O^+. This attempt was unsuccessful due to rapid deuterium and hydrogen exchange in the reagent ion. Monochloroethene, 1,1-dichloroethene and

trichloroethene do not appear to have a barrier to protonation as they react rapidly to form only one product. For tetrachloroethene the reaction is fairly slow; there could be a barrier, or bulky chlorine atoms in the molecule block access of H_3O^+. The difference between the isomers of dichloroethene must be explained by the two chlorine atoms being on the same carbon in 1,1-dichloroethene. Under these conditions, the H_3O^+ can easily attach onto the end of the ethene with two hydrogens on it. One problem with this explanation, however, is that trichloroethene should have more hindrance to the attachment of a H_3O^+ due to chlorine substituents then either *E* or (*Z*)-1,2-dichloroethene, but this is not borne out by the experiments performed here.

4.2.2 Reactions of CF_3^+

The reactions of CF_3^+ produce a range of different products. They can be broken down into four groups exemplified by the following reactions:

$$CF_3^+ + C_2H_3Cl \rightarrow C_2H_3^+ + CF_3Cl \quad \textbf{(re 9.4)}$$

$$CF_3^+ + C_2H_2Cl_2 \rightarrow CHCl_2^+ + C_2HF_3 \quad \textbf{(re 9.5)}$$

$$CF_3^+ + C_2HCl_3 \rightarrow CF_2Cl^+ + C_2HCl_2F \quad \textbf{(re 9.6)}$$

$$CF_3^+ + C_2Cl_4 \rightarrow CFCl_2^+ + C_2F_2Cl_2 \quad \textbf{(re 9.7)}$$

Reaction 9.4 takes place for monochloroethene, 1,1-dichloroethene, trichloroethene and tetrachloroethene. It is a simple Cl^- extraction, which is driven by the formation of trifluorochloromethane as the neutral product. Reaction 9.5 is only seen for the 1,2-dichloroethenes, and there is no evidence for this channel in the reactions of any of the other chloroethenes. The formation of the ionic product, $CHCl_2^+$, in reaction 9.5 is very complicated, since it involves breaking the C=C π-bond of dichloroethene and transfer of a chlorine atom from one carbon to the other. Considering how complicated this mechanism is, reaction 9.5 occurs with a relatively high efficiency of 50 – 70 %. Reactions 9.6 and 9.7 are seen to take place for trichloroethene and tetrachloroethene. Reaction 9.7 also occurs for monochloroethene. Again, to form the ionic products CF_2Cl^+ and $CFCl_2^+$, cleavage of the C=C π-bond must take place; the efficiencies are 69 and 100 % for monochloroethene and trichloroethene. Tetrachloroethene reacts with a rate coefficient which is larger than the collisional value. The difference falls within the normal experimental errors, but might indicate that the reagent ion is energetically excited.

This set of reactions with CF_3^+ provides the most dramatic example of an isomeric effect found in this study of the photoionisation and ion-molecule reactions of the chloroethenes. 1,1-

dichloroethene reacts to give a single product, $C_2H_2Cl^+$, by Cl^- transfer. The (*E*)-1,2-dichloroethene and (*Z*)-1,2-dichloroethene also react to give a single product, but now the product is $CHCl_2^+$. This is a clear and distinct difference between the isomeric forms of dichloroethene.

From thermochemistry it was found that for reaction 9.5 the neutral partner could only feasibly be C_2HF_3, a fluorinated ethene. Formation of a new C=C π-bond in C_2HF_3 helps compensate for the energy required to break the original C=C π-bond. Even then, $\Delta_r H^o_{298}$ is predicted to be slightly endothermic, by around 10 kJ mol^{-1}. However, the error in $\Delta_f H^o_{298}$ [C_2HF_3] is ±8 kJ mol^{-1}, so the reaction could easily be slightly exothermic.[4] Even if the value for the enthalpy of formation of C_2HF_3 is taken without any error, this neglects the role of entropy. Although it is generally assumed that it is enthalpy which dictates whether a gas-phase reaction will occur, in reality it is the Gibbs free energy which indicates if a reaction is spontaneous or not,[5] and only a small change in entropy would be required to make this a favourable reaction. For reactions 9.6 and 9.7 it has been assumed that the neutral partner is the appropriate fluorochloroethene. So for the reaction of monochloroethene with CF_3^+ to form $CHFCl^+$, analogous to reaction 9.7, the product is $C_2F_2H_2$ and the enthalpy of reaction is -32 kJ mol^{-1}. For trichloroethene and tetrachloroethene, the enthalpies of formation of the fluorochloroethenes formed from reactions 9.6 and 9.7 are not known. Assuming that the products must contain a C=C bond and that the enthalpy of reaction is zero, upper limits can be set on the enthalpy of formation for these fluorochloroethenes of 315 kJ mol^{-1} for C_2HClF_2, 168 kJ mol^{-1} for C_2HCl_2F, 321 kJ mol^{-1} for $C_2F_2Cl_2$ and 174 kJ mol^{-1} for C_2FCl_3.

To explain these results attempts have been made to suggest reaction mechanisms. The starting point for all the mechanisms is to assume that initially CF_3^+ attacks electrophilically at the π orbitals of the double bond. Figure 9.1 is the proposed first step in the electrophilic attack of CF_3^+ to a chloroethene, in this case monochloroethene. This initial insertion step forms the trigonal-bridged intermediate cation shown in step 2. The CF_3^+ can then move from one side or another to form the two resonance structures shown. It is assumed that this is how the insertion step occurs for all the reactions proposed, therefore we will start the mechanisms from the most appropriate resonance form for the reaction of interest.

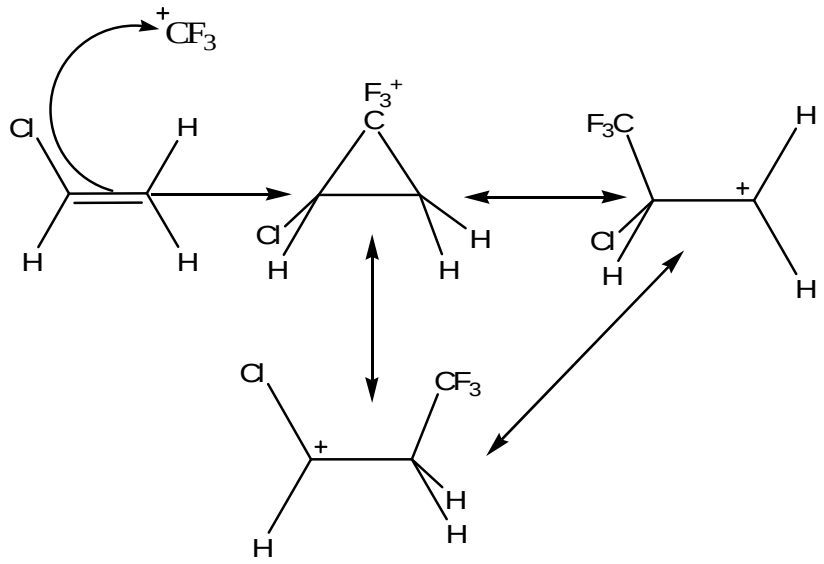

Figure 9.1: Inital insertion step of CF_3^+ into a chloroethene double bond

Figure 9.2 shows the proposed mechanism for formation of $C_2H_3^+$ from monochloroethene, reaction 9.4. Any of the other reactions in which Cl^- transfer to CF_3^+ takes place should follow the same, or a similar, mechanism. Firstly, CF_3^+ adds to the C=C bond.

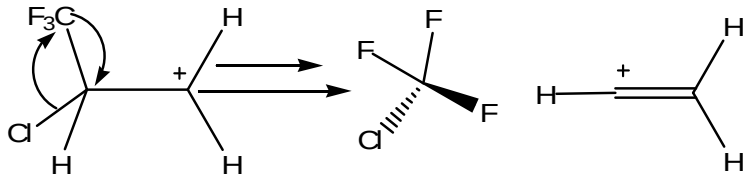

Figure 9.2: Proposed scheme for the reaction of monochloroethene with CF_3^+. Reaction 9.4

This is followed by the migration of the Cl to the CF_3 group. The next step will be the breaking of the C-CF_3 bond. These two steps may be either sequential or concerted. We assume that the chlorine transfer, and subsequent loss, takes place when the CF_3 is attached to the same carbon as the chlorine. The $C_2H_3^+$ product is formed by rearrangement of the initially-formed cation carbene after the loss of $CClF_3$.

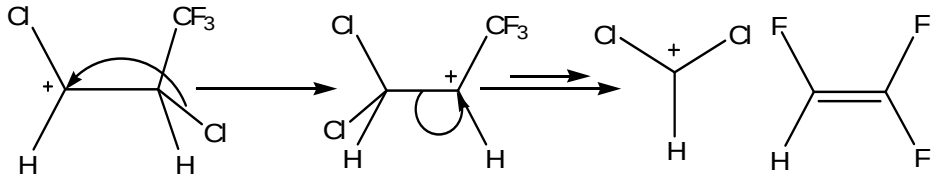

Figure 9.3: Proposed scheme for reaction of CF_3^+ with *Z* & (*E*)-1,2-dichloroethene. Reaction 9.5

Figure 9.3 shows the proposed mechanism for the reaction to form $CHCl_2^+$ from *Z* and (*E*)-1,2-dichloroethene, reaction 9.5. In this mechanism the first step is addition of CF_3^+ to the C=C bond; for these two chloroethenes the different resonance forms are identical. In the next step a chlorine atom moves across the C-C bond to the adjacent carbon. The C-C σ-bond then fragments to give $CHCl_2^+$ and F_3C-CH. This neutral product then rearranges by a fluorine shift to give C_2HF_3.

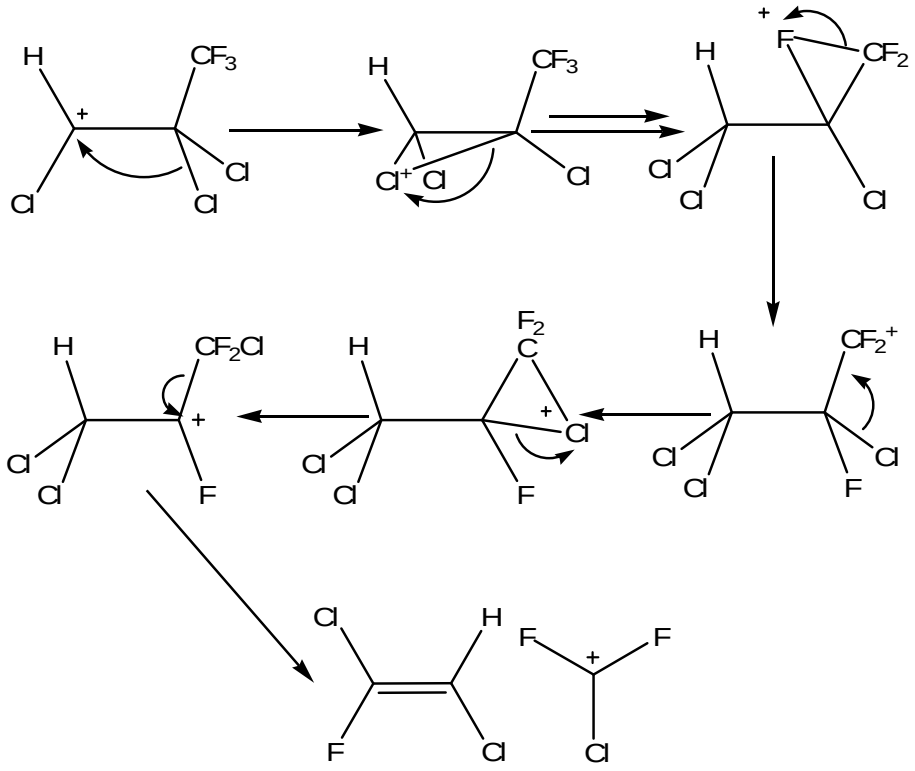

Figure 9.4: Proposed scheme for reaction of CF_3^+ with trichloroethene. Reaction 9.6

Figure 9.4 is a proposed mechanism to explain the formation of CF_2Cl^+ following reaction of CF_3^+ with trichloroethene, reaction 9.6. A similar mechanism should take place for formation of CF_2Cl^+ from tetrachloroethene. Again the first step is addition of CF_3^+. After this the chlorine

and fluorine atoms move between carbons *via* trigonal intermediates, until finally the CF_2Cl group breaks off as CF_2Cl^+ leaving behind a new halogenated ethene.

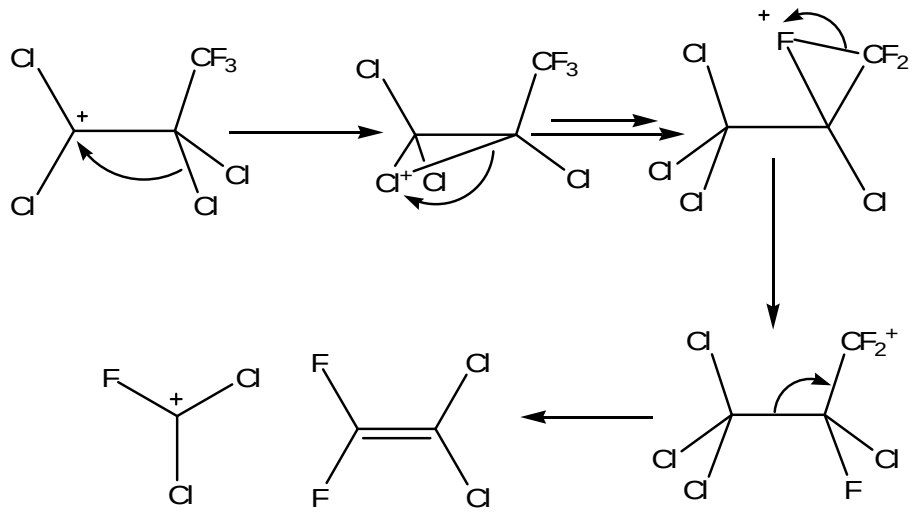

Figure 9.5: Proposed scheme for reaction of CF_3^+ with tetrachloroethene. Reaction 9.7

Figure 9.5 shows the mechanism for the formation of $CFCl_2^+$ from tetrachloroethene in reaction 9.7. This mechanism should also be suitable for the same reaction with monochloroethene and trichloroethene. The first step is as before addition of CF_3^+. As in Figure 9.4 the succeeding step is F transfer from the CF_3 group *via* a sequence of chlorine and fluorine atom transfer through trigonal intermediates. This gives the same intermediates as seen for reaction 9.6. To produce $CFCl_2^+$ the intermediate in step 3 fragments in a different way, one of the C-C σ-bond breaks, the electrons transferring to the C-C σ-bond between the second carbon atom and the CF_2^+ group. This leads to formation of a new C=C π-bond between the two carbons.

It is interesting to note which channels are open for each chloroethene and which are not. Monochloroethene reacts mainly (65 %) *via* reaction 9.4, it also reacts by reaction 9.7 (35 %). 1,1-dichloroethene reacts only *via* reaction 9.4, Cl^- transfer, while the 1,2-dichloroethenes react only by reaction 9.5. Trichloroethene reacts by reaction 9.4 (54 %), reaction 9.6 (22 %) and reaction 9.7 (24 %). Tetrachloroethene reacts by reaction 9.4 (9 %), reaction 9.6 (75 %) and by reaction 9.7 (16 %). In the absence of energy barriers, which channels are open and which are closed undoubtedly depends on the structures of the chloroethenes and the energetics of the reactions. It is interesting that as the number of chlorine atoms increases reaction 9.6, loss of CF_2Cl^+, dominates. A possible explanation is that, as there are now more chlorine atoms, there is

a greater chance that a chlorine can be transferred back to the CF_2^+ group of the intermediate. It could also be that transfer of chlorine atoms in the trigonal bridging intermediate is more favourable. For example, in tetrachloroethene it is unfavourable to have the positive charge next to two chlorines, so by transferring a chlorine across the double bond the positive charge is moved so that it is only next to one chlorine and a CF_3 group, relieving the unfavourable interaction. It is clear that which reactions are favoured depends on a complex interplay between inductive effects and conjugation due to the chlorine atoms on the stability of the cation intermediates.

What are most interesting are the results for the dichloroethenes. Neither reactions 9.6 or 9.7 occur for these three chloroethenes. This cannot be due to a requirement of at least three chlorines because reaction 9.7 is open for monochloroethene. For some reason the presence of only two chlorines in these molecules inhibits these two channels. The other interesting result is that 1,1-dichloroethene only reacts by reaction 9.4 and this is probably because transfer of a hydrogen across the double bond in reaction 9.5 is unfavourable, as hydrogen cannot form the trigonal intermediate necessary for transfer across the bond. It could be unfavourable because of steric crowding around the carbon due to chlorines being present. With CF^+, however, reaction 9.5 does occur to produce a chloroethyne. This suggests that there is a barrier to H transfer which is overcome with the increase of available energy, 0.07 eV, in changing from CF_3^+ to CF^+ as the reagent ion. It is unclear why the simple reaction of chloride abstraction is not seen for either of the 1,2-dichloroethene isomers. *Ab initio* calculations of the potential energy surface and reaction dynamics upon it are required to clarify the chloroethene reactions.

4.2.3 Reactions of CF^+

All six chloroethenes react with CF^+. Similar ionic reaction products are seen as for the reactions of CF_3^+. This time, however, the reactions are nearly all 100 % efficient. Monochloroethene reacts to form the same two ionic products $CHFCl^+$ and $C_2H_3^+$ in essentially the same percentages as for the reaction with CF_3^+. It is assumed that the mechanisms for the reactions are the same as for the CF_3^+ but with slightly different neutral partners, *i.e.* ethynes rather than ethenes are formed. The dichloroethenes all react to produce $CHCl_2^+$ and $CHClF^+$. For the 1,2-dichloroethene isomers these two channels have about equal percentage. For 1,1-dichloroethene these channels are weak (6 % and 25 % respectively) and the main channel is still chloride transfer to produce $C_2H_2Cl^+$. Trichloroethene reacts to form three ionic ions. One is

$CFCl_2^+$, as was seen for reaction with CF_3^+, the other two are new products, $CHCl_2^+$ and $CHClF^+$. Neither $C_2HCl_2^+$ nor CF_2Cl^+ are detected for the reactions of CF^+ with trichloroethene. Tetrachloroethene only reacts to form $CFCl_2^+$. Due to similarities in the products formed for the reactions of CF^+ and CF_3^+, it is assumed that the reaction mechanisms will be similar to those shown in Figure 9.2 – 9.5, with the major difference being that CF^+ is the reactant ion. It should be noted that this is only an assumption, and there is no reason that the mechanisms should be the same for production of the same product ions.

Since $CHCl_2^+$ is formed from the reaction of CF^+ with 1,1-dichloroethene and trichloroethene but not for their reactions with CF_3^+, this suggests that there is a barrier to formation of this product in the latter reactions. This barrier is overcome when CF^+ is used instead of CF_3^+. This suggests that it is not a high barrier as only 0.07 eV extra energy is available. The reactions with CF^+ also allows a new channel, formation of $CHClF^+$, to open for the reactions with the dichloroethenes and trichloroethene, a channel which has previously been seen only for the reaction of CF_3^+ with monochloroethene. This suggests that it is formed as a product from reaction 9.7 (Figure 9.5), however, it is also possible that another mechanism is taking place which can only occur for CF^+. One possible way to test whether there is a barrier to reaction or whether it is a chemical-specific reaction is to perform another experiment in which the collision energy of the ion-neutral system is varied. For example, this could be done by changing the temperature of the system. The best method would probably be to use a guided ion beam of CF_3^+. If there is a barrier to formation of products, then as the ion beam energy is increased the product channels should ‘switch on’ at the threshold for formation. If there was no barrier but an effect due to the chemical differences between CF_3^+ and CF^+, then no such onset should occur. It is noted that the simple Cl^- transfer channel is not observed at all for trichloroethene and tetrachloroethene, even though it is energetically allowed if CFCl is the neutral partner. The reasons are unclear.

5. Isomeric effects in the ionisation processes of the dichloroethenes

This chapter completes the study of the reactions of the dichloroethenes with both photons and a range of cations. Previously the reactions of the dichloroethenes with a selection of anions has also been performed on the SIFT.[6] Therefore this is an ideal place to summarise the isomeric effects which have been observed in that and these studies.

For the studies of photoionisation, chapter 7,[7] no clear sign of isomeric effects were seen. There seemed to be no real difference in the breakdown diagrams or ion yields for any of the three isomers. The only difference was in the position of the $\tilde{F}$ and $\tilde{G}$ states in the threshold photoelectron spectra (TPES). For both 1,1-dichloroethene and (*E*)-1,2-dichloroethene these two peaks were experimentally unresolved, but for (*Z*)-1,2-dichloroethene the peaks were clearly resolved. The ability to resolve the two states for the *Z* isomer has been explained as due to a symmetry interaction pushing them apart, because they have the same symmetry, A_1. However, this difference does not seem to translate into a difference in the fragmentation yields, probably due to the statistical nature of the dissociation at these high energies.

For the reactions of cations with recombination energies which are greater than the ionisation energy of the dichloroethenes, only very weak isomeric effects have been detected, chapter 8.[1] The largest such effect was found for the reactions with SF^+, but smaller effects were also seen for reactions with Ne^+, CO^+, N_2^+ and Ar^+. The effects were only ever observed between the 1,1 and 1,2 isomers, and no differences between the *E* and *Z* isomers were observed.

For the reactions of cations with recombination energies below the ionisation energy of the dichloroethenes, this chapter,[1] clear isomeric effects have been seen for the reactions of H_3O^+, CF_3^+ and CF^+. Again the differences were only between the 1,1 and 1,2 isomers.

The anion study was performed with O_2^-, O^-, OH^-, CF_3^- and F^-.[6] For these reactions very striking isomeric effects were observed, and is the only example of a difference between the *E* and *Z* isomers. The difference was that $C_2H_2Cl^-$ was only observed for the *E* isomer, whereas Cl^- was the major product for the other two isomers.

These results suggest that isomeric effects will only show up to a significant extent when chemical reactions occur. This must be because chemical reactions occur when the ion and the neutral molecule are positioned very close together. Here the geometric differences in structure and steric effects will influence reactions outcomes. For processes such as charge transfer reaction occurs when the ion and neutral are well separated, and structural differences will then not have a significant effect. For photoionisation the dissociation process appears to take place statistically and so the bond orientation will have no effect on the formation of products.

6. Conclusions

The reactions of the six chloroethene molecules have been studied with a range of cations with recombination energies of 4.73 – 9.26 eV. There were five cations, H_3O^+, SF_3^+, CF_3^+, CF^+ and NO^+ studied for monochloroethene, trichloroethene and tetrachloroethene. For the dichloroethenes a sixth cation, NH_4^+, was also studied. Only three of the ions reacted, H_3O^+, CF_3^+ and CF^+.

The reactions with H_3O^+, and for the dichloroethenes with NH_4^+, have allowed limits to be placed on the proton affinities of the chloroethenes. For monochloroethene, trichloroethene and tetrachloroethene the proton affinity is greater than or equal to the proton affinity of water. For the dichloroethenes due to the lack of reaction with NH_4^+ the following inequality has been derived: PA[H_2O] or 691 $\leq$ PA [$C_2H_2Cl_2$] $\leq$ PA[NH_3] or 854 kJ mol^{-1}.

Examination of the reactions with CF_3^+ has shown several different reaction pathways. Many of these pathways involve breaking of the chloroethene C=C double bond and formation of a new double bond. Similar channels have also been seen for reactions with CF^+. It seems that a complex interplay between the position of the chlorine atoms and the C=C double bond dictates which channels are formed and in what percentages. It must certainly dictate the stability of the intermediate cations in the reaction pathways.

For the dichloroethene isomers very clear isomeric effects have been observed for the reactions of all three ions in this study. The results for the CF_3^+ reactions, where only Cl^- loss is seen for the reaction of 1,1-dichloroethene but two completely different products occur for the 1,2-dichloroethenes, are particularly striking. The data on the reactions of dichloroethenes studied for this thesis, and previously by our group,[6] has found that major isomeric effects are only seen for chemical reactions, and not for charge transfer reactions.

7. References

1 V. A. Mikhailov, M. A. Parkes, R. P. Tuckett, C. A. Mayhew, *J. Phys. Chem. A.*, **110**, (2006) 5760.

2 P. Španěl, D. Smith, *Int. J. Mas Spec.*, **184**, (1999) 175.

3 E.P. Hunter, S.G. Lias, *J. Phys. Chem. Ref. Data*, **27**, (1998) 413.

4 P.J. Linstrom, W.G. Mallard, *NIST Chemistry WebBook, NIST Standard Reference Database Number 69*, National Institute of Standards and Technology,, Gaithersburg MD, 20899, (2005).

5 K.K. Irikura, *J. Am. Chem. Soc*, **121**, (1999) 7689.

6 R.A. Kennedy, C.A. Mayhew, R. Peverall, P. Watts, *Phys. Chem. Chem. Phys.*, **2**, (2000) 3145.

7 M.A. Parkes, S. Ali, C.R. Howle, R.P. Tuckett, A.E.R. Malins, *Mol. Phys.*, **105**, (2007) 907.

Chapter 10: Electron Attachment Studies

1. Introduction

Electron attachment (EA) is one of the most fundamental of all chemical processes. In one sense it is the prototype for all chemical reactions. During EA an electron and a neutral molecule, AB, interact to form a transient negative ion:

$$e^- + AB \leftrightharpoons AB^- \qquad \textbf{(re 10.1)}$$

Once this anion is formed there are several subsequent reactions which can occur. The electron can detach to regenerate the starting molecule, AB^- can be stabilised either by collision or a Feshbach resonance can occur. However, the most common reaction is for AB^- to fragment into $A + B^-$ or $A^- + B$. EA is the major process that occurs in all plasmas and when electrical breakdown occurs, as well as in the upper regions of the Earth's atmosphere (*e.g.* the mesosphere). EA will occur in any environment where a large concentration of free electrons is present, and it is also important in chemistry occurring in interstellar space. It is crucial to have EA data to model gaseous discharges and industrial plasmas.[1,2]

For many gas-phase molecules, EA cross-sections show a maximum at an electron energy around 0 eV and, as EA tends to occur dissociatively, much interesting chemistry can therefore be initiated by very low-energy electrons. EA can be of importance biologically, it has been shown to cause strand breaking of DNA molecules.[3] There also links between the ability of carbon halide molecules to produce radical species by EA and whether the molecules carcogenic.[4,5] Many very accurate high-resolution measurements of *relative* electron attachment cross-sections have been made as a function of electron energy. To put these relative values on an absolute scale requires knowledge of the thermal electron attachment rate coefficient, k_a.[6-9] Measurements of k_a can only be done in a swarm environment, where the electrons are present in a broad distribution of energies. Many such rates have been measured in flowing afterglow Langmuir probe instruments or electron swarm spectrometers. This chapter reports further development of the Birmingham swarm apparatus, the Electron Attachment Mass Spectrometer (EAMS). This is an adapted ion-mobility spectrometer and details of its original mode of operation are available.[10] The operation of the experiment before this latest series of upgrades is detailed in chapter 2.[11]

2. Theoretical

Theoretical electron attachment rate coefficients, k_{th}, were calculated from *s*-wave capture theory based on the analytical formula of Klots.[12] More detail is given in chapter 3 on the applications and limits of these models. For these models polarisability volumes, α', are needed. We have studied EA to several molecules and the results are given later in the chapter. For octafluorocyclobutane the value was 1.25 x 10^{-29} m^3 from a semi-empirical calculation.[13] The value of α' for octafluorocyclopentene is 9.38 × 10^{-30} m^3, for octafluorobut-2-ene 8.36 x 10^{-30} m^3, for hexfluorobuta-1,3-diene 7.27 x 10^{-30} m^3 and for di-trifluoromethyl-hexafluorocyclobutane the value is 1.20 x 10^{-29} m^3. These values of α' were all estimated using the method of Miller outlined in chapter 3. For chloroform α' is 8.53 x 10^{-30} m^3.[14]

3. Experimental

The EAMS has been upgraded in several ways, which was a project undertaken as a part of this work. Each upgraded component will be considered in order. The first upgrade was to the electronic systems of the apparatus.

3.1 Electronics

The EAMS has several electronic systems that are required to run the experiment. One provides the pulse to the electron gate, another system converts and amplifies the small current pulse registered at the Faraday plate at the end of the drift tube. The final system digitises the data, and allows recording and analysis to take place. Circuit diagrams are given in appendix 3.

The original pulse unit used arrays of batteries to provide the voltage needed to open and shut the gate. This could lead to problems if one of the arrays discharged more than the other; different voltages applied to the separate wires of the gate would give misshapen pulse shapes, making data analysis difficult. The batteries have therefore been replaced with a transformer attached to the mains. Following the transformer is a rectifier to smooth the a.c. input to a d.c. output and a series of diodes which limit the maximum voltage to ± 30 V. As the voltage source is connected to the mains a series of capacitors have been added to decouple the output from

ground. A dual voltage regulator is then used to make sure that both positive and negative voltage outputs have the same magnitude. The pulse switch still consists of a pair of Schmitt triggers, but the inclusion of field-effect transistors improves further the sharpness of the pulse switching.

Once the pulses have been generated they must be detected at the Faraday plate. This is achieved using a high gain, 10^9 V A^{-1}, amplifier. Amplification is one of the most important stages of the experiment as very weak currents must be measured.[15] The amplifier contains three low-drift operational amplifiers and has several switchable gain ranges. Two potentiometers allow fine control of the performance of the amplifier. One alters the time constant for the amplification. Using a larger time constant can improve the signal-to-noise ratio, but at the cost of peak shape; the faster the amplifier response the squarer the pulse. Figure 10.1 shows examples of the pulse shapes with different response times. Figure 10.1 (a) shows the pulse with the fastest response time, Figure 10.1 (c) is the pulse with the slowest response time of our system and Figure 10.1 (b) is the pulse with an intermediate response time. It is clear that the pulse in (a) is much squarer than the pulse in (c). The ideal situation is to have a sharp, well-defined onset. (a) therefore represents an optimum situation in this regard. However, the recorded pulse has a lower signal-to-noise ratio and there are sharp peaks at the onset of the peak and at around 500 μs. This ringing is pick up from the electronic circuit, which can be reduced by slowing the response time. Therefore the actual time constant used is a compromise between obtaining a square pulse and removing the spurious peaks. The second potentiometer allows fine control of the gain range with a calibrated 10-turn dial.

The amplifier is contained in a sealed metal enclosure physically attached to the EAMS over the vacuum feed-through which connects to the Faraday plate. By making the connection inside the enclosure any electrical noise is reduced prior to the amplification step. A reed switch allows easy switching from measuring the current on the Faraday plate to applying a voltage to the Faraday plate. This makes it simple to switch between the two modes of operation of the EAMS; the pulsed measurement for electron attachment rate coefficients, and the non-pulsed measurement for detection of product anions.

The amplified pulse is then passed to the data acquisition system. The data acquisition card is manufactured by National Instruments (PCI 6014) and is located in a Pentium based PC. The card has several analogue inputs, two analogue outputs and many digital inputs/outputs. The connection is made through a National Instruments SCB-68 shielded connection box and the National Instruments SH68-68 cable assembly. The pulse is recorded through a differential

analogue channel. The differential channel digitises the difference between the signal and the shielding of the connector (which is nominally ground). This increases the common-mode rejection of noise in comparison to, a non-differential, single-ended measurement where the signal is compared to the ground of the acquisition card. To further lower electrical noise, the wire along which the signal is transmitted from amplifier to connection box runs through an earthed metal conduit.

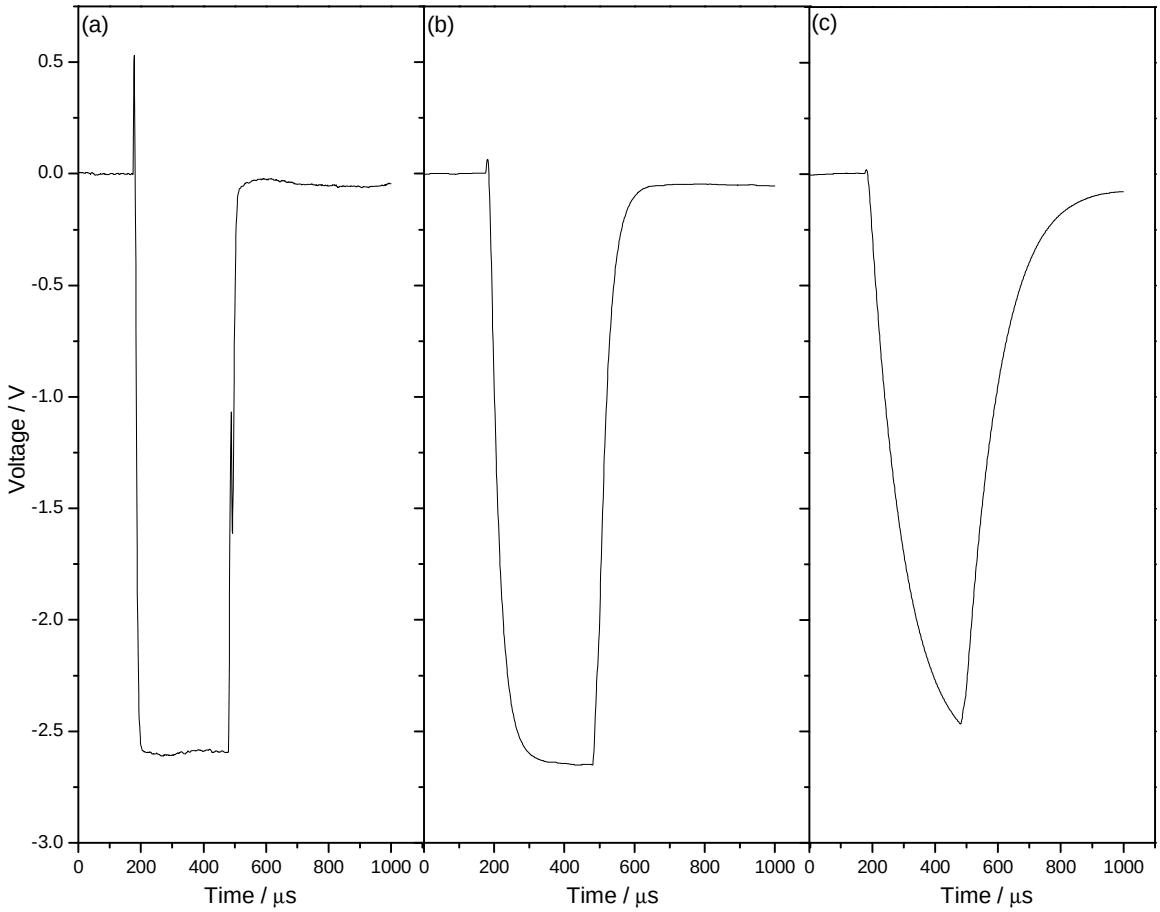

Figure 10.1: Examples of pulses as amplifier response time is varied.

The digitised pulse is recorded in a custom-designed labVIEW application. In this application measurement is obtained by averaging several hundred pulses, normally ~300, and then integrating across the width of the pulse. This method can drastically improve the signal-to-noise ratio compared to the previous method using a boxcar integrator. The application is also used to analyse the data using an exponential fit; it also allows automated control of some aspects of the experiment. The high-voltage applied to the drift tube can be varied from within the programme using analogue communication with the high-voltage supply (Stanford Research

Systems model PS350). It is also possible to control the mass spectrometer of the EAMS in a similar way.

Figure 10.2 shows an example of how the pulse height varies with increasing sample gas concentration. At zero flow rate there is one large peak followed by a flat background. As the sample flow rate is increased the peak height decreases. At later times a large broad peak appears due to product ions being formed in the system.

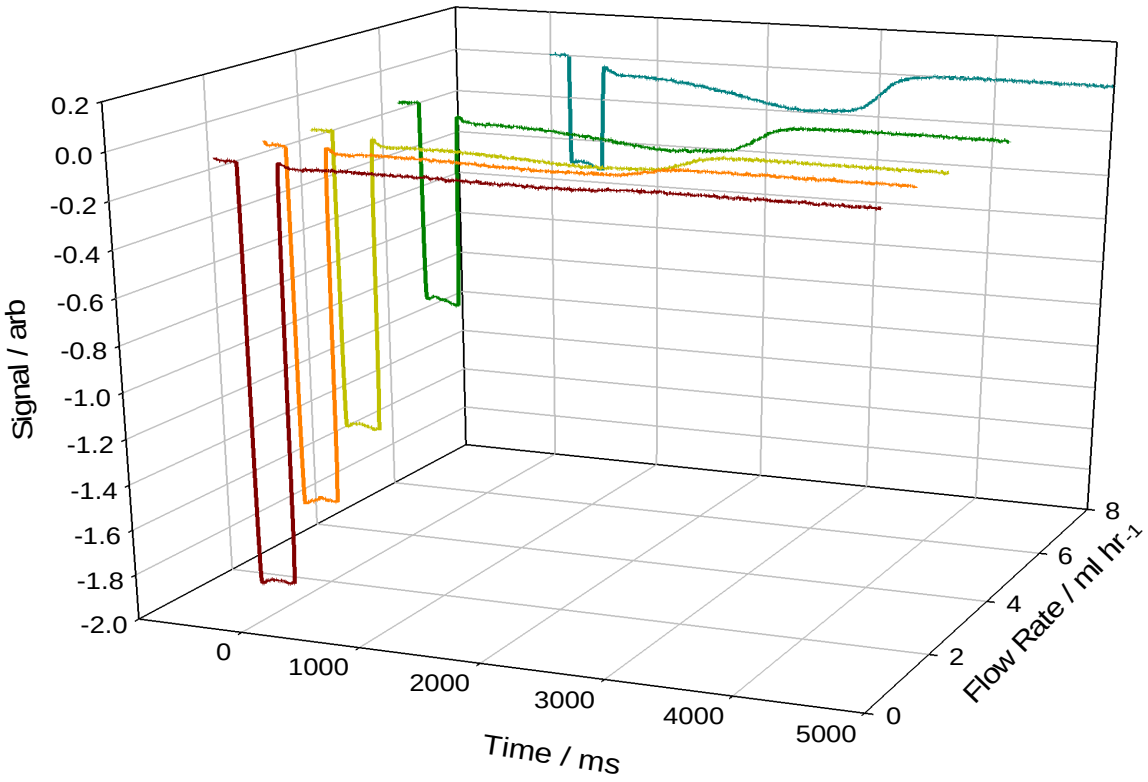

Figure 10.2: Variation of pulse height with sample concentration.

3.2 Drift tube

Several improvements have been made to the drift tube design. In the original ion mobility design the drift tube was inside a small glass envelope contained in a much larger vacuum chamber filled with buffer gas. Use of two gas flows meant that the sample gas would only have to mix within the glass envelope. Due to problems with concentration gradients the glass envelope was removed and only a single flow was used. This reduced the concentration

problem, but as the sample had to mix throughout the whole of a large vacuum chamber it could take a long time for measurements to take place. To speed up the mixing time a new vacuum chamber was constructed to house the drift tube. This chamber has much smaller dimensions, equivalent in size to the glass envelope, and mixing times are now much quicker. The small chamber has also made it more practical to bake-out the drift tube using heating wire.

Figure 10.3 shows an example of how the average pulse height varies with time in the new drift tube. The steps show where an increase in sample flow rate has been made. Apart from the first step, the mixing is rapid and quickly completed. The length of this first step is probably due to the need for equilibrium to be reached between the sample and the surfaces in the chamber. The small slope at the beginning is due to charging effects inside the drift tube.

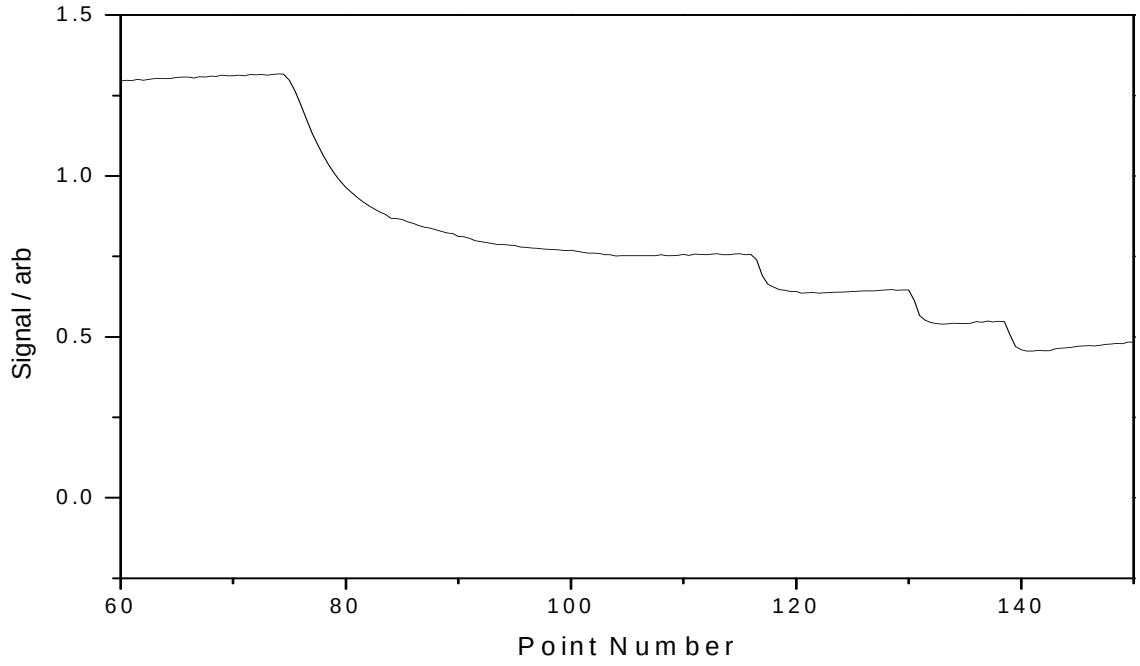

Figure 10.3: Average signal with time for the EAMS. Each point represents a measurement of the pulse height for 30 s, this is followed by a 30 s delay before the next point is taken.

3.3 Sample handling

As explained in chapter 2 sample preparation is very important for accurate measurements of k_a. The method outlined to prepare samples in chapter 2 has several failings. Firstly, gas must be pumped off at several stages in the procedure. This can lead to changes in expected

concentration as the pumping efficiency of either the buffer gas maybe higher than the sample gas or *vice versa*. This will reduce the amount of one gas relative to the other. A second problem is that the mixture can take days to prepare. It is almost certain that if the gas mixture is left for that long, changes in concentration will occur as equilibrium is reached due to wall losses. To overcome these problems a second preparation method was devised.

The new method removes the need for multiple evacuations and refills of the tanks. Instead a different procedure is followed:

1. The sample is first allowed into a small evacuated chamber (V_1 on Figure 10.4) at a low pressure (~ 1 mbar) which can be accurately read by a capacatron gauge (Leybold CTR 90) in the range 0 – 14 mbar.
2. The small chamber is then filled to ~ 2000 mbar with buffer gas.
3. A Speedivalve which connects V_1 and V_2 is then opened. The gas in V_1 thus expands into V_2. V_2 is approximately ten times the volume of V_1.
4. The two chambers are then filled with ~2000 mbar of buffer. This gives a ten fold dilution from the mixture in V_1 without recourse to pumping the tank.
5. If required the method from chapter 2 can also be used if even lower concentrations of sample are necessary.

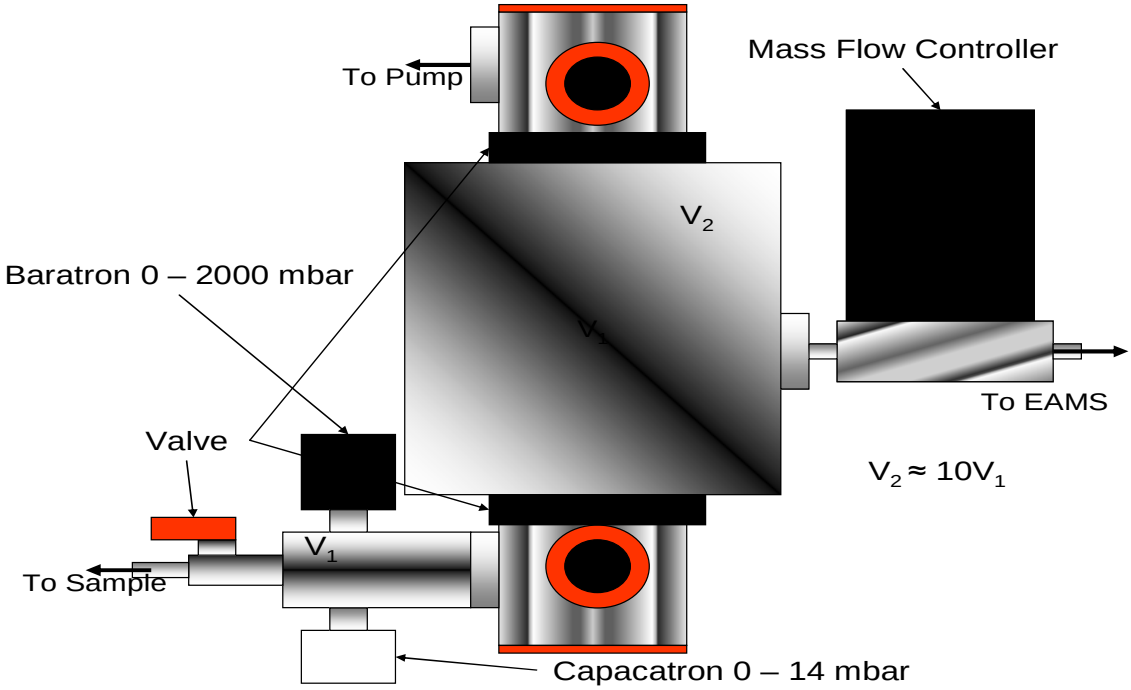

Figure 10.4: Mixing apparatus for preparation of samples for the EAMS.

This second method is more accurate than the first because there is no removal of mixture by pumping. The expansion from V_1 to V_2 keeps the proportions of buffer to sample gas the same. A second advantage is that the mixture can be made on the day of its use rather than days in advance. This reduces problems due to sample adsorption by, or reaction with, the walls of the tanks. From these considerations it is clear that method 2 should be used for mixing all samples. To improve mixing heated wire is wrapped around V_2. This creates a temperature gradient which will encourage diffusion of the gases.

Samples are removed from the tank for injection into the apparatus using either a syringe, or a mass flow controller. When the syringe is used sample is injected via a septum into the buffer gas flow. A mass flow controller (MKS 1179A, 20 sccm flow rate, or a Sierra Instruments Smart-Trak Series 100L, 5 sccm flow rate, depending on the required flow range) can also be used. In this case the sample does not need to be withdrawn from the tank as a direct connection is made to the EAMS. The preferred method is to use one of the mass flow controllers. However, sometimes the attachment rate of the neutral being studied is either too high or too low for the flow range of one of the mass flow controllers. In these situations the use of a syringe may be the better option.

3.4 Samples

The samples were bought from various suppliers. Sulphur hexafluoride was purchased from Apollo with a high purity of 99.9 %. Octafluorocyclobutane was purchased from Fluorochem UK with a purity of 99 %, octafluorocyclopentene from Apollo Scientific with a purity of 99 %. Perfluorobut-2-ene and hexafluorobuta-1,3-diene were provided by Apollo Scientific with purities of 97 %. Di-trifluoromethyl-hexafluorocyclobutane was synthesised for us by Dr N Simpson and was used as provided. Chloroform was purchased from BDH and is analytical grade; it was further purified by a freeze-pump thaw cycle before use.

4. Results

Results are presented for several molecules studied on the EAMS. The most important molecule studied is sulphur hexafluoride, SF_6, due to its high k_a value. This molecule has been extensively studied, and is the benchmark gas for electron attachment studies.[11,13,16] To this end SF_6 has been used to check the results of the improved EAMS. The measured rate is 2.38×10^{-7}

cm^3 $molecule^{-1}$ s^{-1}. This should be compared to the generally accepted value of 2.25 x 10^{-7} cm^3 $molecule^{-1}$ s^{-1}.[13] The agreement between the results provides confidence in the EAMS technique and upgrades.

A study has been begun on perfluorinated compounds due to their importance in industrial processes and generally high electron attachment rate coefficients. So far five perfluorocarbon molecules have been studied, octafluorocyclobutane (*c*-C_4F_8), octafluorobut-2-ene (2-C_4F_8), octafluorocyclopentene (*c*-C_5F_8), hexafluorobuta-1,3-diene (1,3-C_4F_6) and di-trifluoromethyl-hexafluorocyclobutane (*c*-$C_4F_6(CF_3)_2$). Thermal electron attachment coefficients were recorded for all five molecules in 1 atmosphere of CO_2 buffer gas. The data on *c*-C_4F_8 and 2-C_4F_8 have been published.[16] The measured rate coefficient for *c*-C_4F_8 is 1.81 ± 0.17 x 10^{-8} cm^3 $molecule^{-1}$ s^{-1}, the *s*-wave capture rate coefficient is 3.12 x 10^{-7} cm^3 $molecule^{-1}$ s^{-1}. Many measurements have been made on the electron attachment of *c*-C_4F_8, and Christophorou and Olthoff give the average thermal value as 1.5 x 10^{-8} cm^3 $molecule^{-1}$ s^{-1}.[13] Our value is in good agreement with this average, and even better agreement with the value of 1.81 x 10^{-8} cm^3 $molecule^{-1}$ s^{-1} obtained by Christodoulides *et al*. in their laboratory.[17] Low-energy electron attachment to *c*-C_4F_8 gives only a single product, the parent anion, *c*-$C_4F_8^-$. This in agreement with the electron beam mass spectrometry study of Sauers *et al*.[18]

2-C_4F_8 has been less extensively studied than *c*-C_4F_8 and the thermal rate coefficient is measured in this work to be 4.2 ± 0.2 x 10^{-8} cm^3 $molecule^{-1}$ s^{-1} for a mixture of the two *E*- and *Z*-isomers; the theoretical value is 3.14 x 10^{-7} cm^3 $molecule^{-1}$ s^{-1}. Our experimental value is in good agreement with a value obtained by Sauers *et al*.[18] Again only a single product is detected, $C_4F_8^-$. Sauers *et al* also studied the mass spectrum of 2-C_4F_8 following electron attachment in an adapted mass spectrometer.[18] The main product was parent anion, however, they also saw small amounts of $C_4F_7^-$ and $C_4F_6^-$. This difference is because they produced and detected the products under single collision conditions, there will be no collisional stabilisation of the initially formed anion. Thus extra fragmentation will occur, when compared to the products in the high-pressure swarm environment.[19]

The thermal rate coefficient for *c*-C_5F_8 was measured as 3.97 ± 1.34 x 10^{-7} cm^{-3} $molecule^{-1}$ s^{-1}, *s*-wave theory gives a value of 3.21 x 10^{-7} cm^3 $molecule^{-1}$ s^{-1}. This agrees well with the value measured by Pai *et al*. of 3.62 x 10^{-7} cm^3 $molecule^{-1}$ s^{-1},[20] however there are very large error bars in our value. These error bars probably arise from wall losses of *c*-C_5F_8 inside the mixing chamber before use, and it is also possible that *c*-C_5F_8 may decompose after injection.

This is a very fast rate coefficient for electron attachment, higher even than that for SF_6 which is considered one of the fastest attaching gases. The theoretical value is lower than the experimental value. However, the *s*-wave theory ignores the effect of the dipole moment of the molecule, 1.87 Debye, on the electron attachment rate. The mass spectrum of the products of EA to *c*-C_5F_8 was also recorded, and again only parent anion was detected. Only a thermal rate coefficient was measured for *c*-$C_4F_6(CF_3)_2$ and it was found to be $1.39 \pm 0.5 \times 10^{-7}$ cm^3 $molecule^{-1}$ s^{-1}, *s*-wave gives 3.36×10^{-7} cm^3 $molecule^{-1}$ s^{-1}. The sample used was a mixture of the different isomers. No products anions were measured.

For 1,3-C_4F_6 the thermal rate coefficient was $1.45 \pm 0.2 \times 10^{-8}$ cm^3 $molecule^{-1}$ s^{-1}, this does not agree at all with the previously measured value of 1.2×10^{-7} cm^3 $molecule^{-1}$ s^{-1} measured by Christodoulides *et al*.[21] Using the *s*-wave model of Klots gives 3.36×10^{-7} cm^3 $molecule^{-1}$ s^{-1}. To try and understand this disagreement rate coefficients were measured for 1,3-C_4F_6 in N_2 buffer gas as a function of mean electron energy, ε. Our swarm results are compared to those of Christodoulides *et al* in Figure 10.5.[21] It is clear that there is total disagreement between the two sets of data. A GC-MS was performed on the sample of 1,3-C_4F_6 to check that the supplied gas cylinder contained the correct sample. Examination of the mass spectrum suggests that the sample probably was indeed 1,3-C_4F_6 and not another C_4F_6 isomer. However, further work is needed to clarify the situation. It is difficult to explain why there is such a difference, although it could be that an inhibitor was mixed in with 1,3-C_4F_6 to lower the explosion risk. If there was a large concentration of this inhibitor then it would alter the concentration of the sample mixture injected into the EAMS and hence the measured rate coefficients.

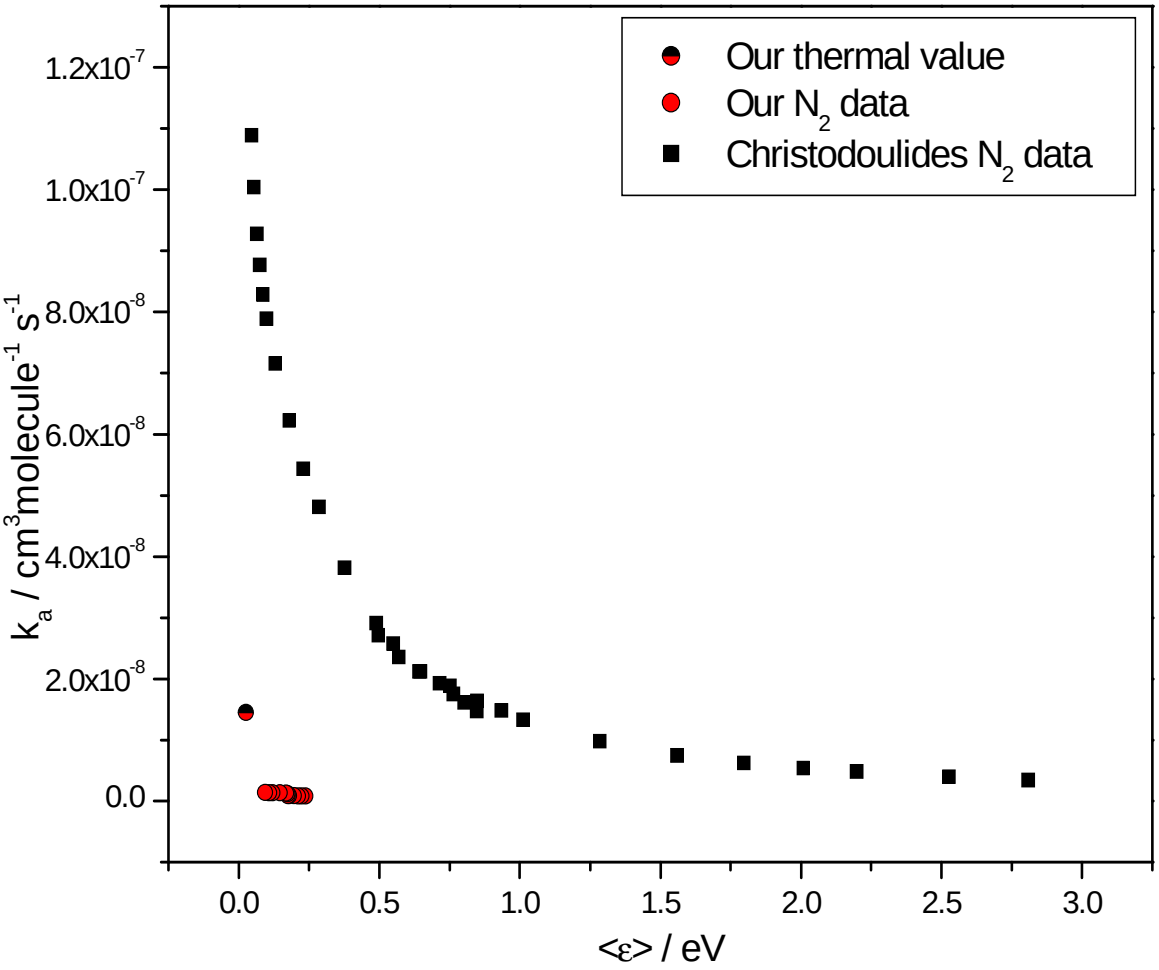

Figure 10.5: Comparison of N_2 swarm data for 1,3-C_4F_6.

It should be noted that the majority of the predicted *s*-wave capture rate coefficients are far larger than the actual measured values of k_a. There are several reasons for this. As noted in chapter 3 the *s*-wave capture theories are unphysical, since they do not model the underlying physics of the EA process because they ignore the resonance nature of EA and many quantum effects. This model therefore gives an upper limit but will not show any effects due to Feshbach resonaces or vibrational cusps.[22] Another reason for the disagreement is that the attachment coefficient measured during the EAMS experiments is an effective attachment rate coefficient. It is a balance between processes which remove electrons from the swarm, *e.g.* electron attachment and stabilisation of the anions, and processes which generate electrons, *e.g.* electron detachment from AB^-. This means it is likely that the effective rate coefficient will always be lower than the attachment rate coefficient.

It is useful at this point to try and link the trends in thermal electron attachment coefficient to the changes in structure; this is made more difficult by the unavailability of some perfluorocarbons of interest. For example it has not been possible to obtain a sample of hexafluorocyclobutene, which would give an interesting comparison between a cyclic alkane and a cyclic alkene. It appears that the presence of mulitple bonds increases the attachment rates, ignoring the anomalous results for 1,3-C_4F_6. To confirm this hypothesis, electron attachment needs to be performed with the linear alkane compound decafluorobutane, *n*-C_4F_{10}. Studying this molecule will also highlight the effect of cyclisation.

The difference in results between *c*-C_4F_8 and *c*-$C_4F_6(CF_3)_2$ is very interesting. The rate coefficient is almost an order of magnitude larger in the second molecule than the first. This must be due to the effect of the additional trifluoromethyl groups. It would be useful to acquire a sample of *c*-$C_4F_7CF_3$ to see if the attachment rate coefficient falls between the values for the other two molecules. This would indicate whether the addition of CF_3 groups in place of F atoms causes a systematic shift in rate coefficients.

Another molecule studied was chloroform, $CHCl_3$. One reason for studying this molecule is because it is cacinogenic.[4] It is carcinogenic because it attaches electrons dissociatively.[5] Therefore, it is interesting to study on the EAMS to see what ionic products are formed. $CHCl_3$ has been extensively studied by many groups and the accepted value seems to be 3.1×10^{-9} cm^3 $molecule^{-1}$ s^{-1} from ion cyclotron resonance and swarm measurements.[5] However, there is a large range of measured values, for example a FALP study measured a value of 3.6×10^{-9} cm^3 $molecule^{-1}$ s^{-1},[23] and a recent review found the average value of ten studies to be 2.7×10^{-9} cm^3 $molecule^{-1}$ s^{-1}.[24] Our value is $1.81 \pm 0.22 \times 10^{-9}$ cm^3 $molecule^{-1}$ s^{-1}, which falls on the low side of the range, the *s*-wave capture value is 3.16×10^{-7} cm^3 $molecule^{-1}$ s^{-1}. The differences probably arise due to different experimental conditions and sample qualities. The main product ion formed is Cl^-, which was the only product seen in the FALP study.[23] Cl_2^- was also detected in this work, but it is probably a secondary product from reaction of Cl^- with $CHCl_3$.

A final molecule studied was SF_5Cl. The thermal and non-thermal rate coefficients for this molecule have been studied previously.[16,25] When these results were compared to beam studies,[4] there were major differences in branching ratios; SF_4^- appears to be the major product under non-thermal conditions, which is difficult to reconcile with thermochemistry. Therefore the non-thermal study was repeated. The products were found to be the same. To further clarify the issue a GC-MS was performed on the SF_5Cl sample that was being used. This found that there

was a SF_4 impurity. This seems to suggest that the entire SF_4^- signal arises from this SF_4 impurity rather than from dissociative electron attachment.

5. Conclusions

Improvements to the electron attachment mass spectrometer have been reported. These have included upgrades to both the pulsing electronics and amplifying units. The old data acquisition system has been replaced with a new system based on labVIEW and National Instruments components. This has allowed the speeding up of experiments and better control of the apparatus.

The drift tube has been rehoused in a smaller vacuum chamber. This smaller design allows faster mixing of sample gases and the ability to easily bake the system. A new sample preparation rig and procedure have also been developed. This method removes the need for multiple evacuating of sample mixtures as well as the need to leave the mixtures for large amounts of time.

Results are reported for a series of molecules that have been studied on the apparatus. Trends can be seen within the perfluorocarbons. However, gaps in the series make it hard to quantify the effect of substitutions upon the attachment rate coefficients. Comparisons have been made with capture rate theories. The agreement is found to be poor; due to the non-resonant nature of the models and their limiting assumptions.

6. References

1 T.A. Field, A.E. Slattery, D.J. Adams, D.D. Morrison, *J. Phys. B*, **38**, (2005) 255.
2 K. Becker, H. Deutsch, M. Inokuti, *Adv. Atom. Mol. Phys.*, **43**, (2000) 406.
3 B. Boudaïffa, P. Cloutier, Darel Hunting, M.A. Huels, L. Sanche, *Science*, **287**, (2000) 1658.
4 J.J. Kaufman, W.S. Koski, S. Roszak, K. Balasubramanian, *Chem. Phys.*, **204**, (1996) 233.
5 L.G. Christophorou, D. Hadjiantoniou, *Chem. Phys. Letts*, **419**, (2006) 405.
6 M. Braun, M.-W. Ruf, H. Hotop, P. Cicman, P. Scheier, T.D. Märk, E. Illenberger, R.P. Tuckett, C.A. Mayhew, *Int. J. Mass Spec.*, **252**, (2006) 234.
7 J. Langer, I. Martin, G. Karwasz, E. Illenberger, *Int. J. Mass Spec.*, **249-250**, (2006) 477.
8 S. Marienfeld, I.I. Fabrikant, M. Braun, M.-W. Ruf, H. Hotop, *J. Phys. B*, **39**, (2006) 105.
9 J.-P. Ziesel, N.C. Jones, D. Field, L.B. Madsen, *J. Chem. Phys.*, **122**, (2005) 024309.
10 Y. Liu, C.A. Mayhew, R. Peverall, *Int. J. Mass Spec. Ion Phys.*, **152**, (1996) 225.
11 G.K. Jarvis, R.A. Kennedy, C.A. Mayhew, *Int. J. Mass Spec.*, **205**, (2001) 253.
12 C.E. Klots, *Chem. Phys. Letts.*, **38**, (1976) 61.
13 L.G. Christophorou, J.K. Olthoff: *Fundamental Electron Interactions with Plasma Processing Gases*, Kluwer Academic / Plenum Publishers, New York, (2004).
14 K.J. Miller, *J. Am. Chem. Soc.*, **112**, (1990) 8533.
15 J. Duttont, A. Goodings, A.K. Lucas, A.W. Williams, *J. Phys. E*, **21**, (1988) 264.
16 C.A. Mayhew, A.D.J. Critchley, D.C. Howse, V. Mikhailov, M.A. Parkes, *Eur. Phys. D*, **35**, (2005) 307.
17 A.A. Christodoulides, L.G. Christophorou, D.L. McCorkle, *Chem. Phys. Letts.*, **139**, (1987) 350.
18 I. Sauers, L.G. Christophorou, J.G. Carter, *J. Chem. Phys.*, **71**, (1979) 3016.
19 S.H. Alajajian, A. Chutjian, *J. Phys. B*, **20**, (1987) 2117.
20 R.Y. Pai, L.G. Christophoru, A.A. Christodoulides, *J. Chem. Phys.*, **70**, (1979) 1169.
21 A.A. Christodoulides, L.G. Christophorou, R.Y. Pai, C.M. Tung, *J. Chem. Phys.*, **70**, (1979) 1156.
22 H. Hotop, M.-W. Ruf, M. Allan, I.I. Fabrikant, *Adv. Atom. Mol. Phys.*, **49**, (2003) 85.
23 P. Spanel, S. Matejcik, D. Smith, *J. Phys. B*, **28**, (1995) 2941.
24 W. Barszczewska, J. Kopyra, J. Wnorowska, w. Szamrej, *J. Phys. Chem. A*, **107**, (2003) 11427.
25 C.A. Mayhew, G.K. Jarvis, A. Critchley, *Int. J. Mass Spec.*, **233**, (2004) 259.

Chapter 11: Conclusions

In this thesis nine molecules have been studied using both photoionisation and ion-molecule reactions. The photoionisation has been studied using a threshold photoelectron photoion coincidence spectrometer. Using this apparatus not only are the threshold photoelectron spectrum and the total photoion yields recorded but also the energy- and mass-selected ion yields. This allows the easy production of branching ratios for the ion products from threshold to around 22 eV. The ion-molecule reactions have been performed on a selected ion flow tube. Reactions have been performed with at least 22 different ions whose recombination energies range from 6 – 22 eV.

One of the main aims of these studies was to compare ionisation by photons and ions. Another aim was to gain insight into the charge transfer mechanism taking place for the ion-molecule reactions. For these molecules, when the recombination energies of the reactant ions were greater than the ionisation energies of the neutral reactants, long-range charge transfer seems to be the main reaction mechanism. These results seem to suggest that many of the criteria put forward for when long-range charge transfer should occur are not as critical as previously thought. It is probable that in polyatomic molecules the generally large rovibrational density of states makes the energy resonance criterion facile to meet, and that only a non-zero value for the Franck-Condon factors is necessary for favourable charge transfer. It also seems that the need for an unshielded orbital is also less important than was thought.

A comparison of the photon and ion initiated reactions of fluoroform with other molecules in the CXF_3 series was made. These comparisons showed many similarities and trends in the reactions. Most of the differences between the molecules can be explained based on the relative C-X bond strengths. However, some of the differences highlight the non-halogen nature of the hydrogen atom in CHF_3.

Both photoionisation and ion-molecule reactions have been studied with both octafluorocyclobutane and octafluorocyclopentene. For octafluorocyclobutane all the ion-molecule reactions were found to have experimental rate coefficients greater than those calculated using Langevin theory. Inclusion of a quadrupole moment in the calculation of the theoretical rate coefficient gave better agreement. The quadrupole moment should be considered as a correction factor to allow for errors in the Langevin assumptions, such as point particles. Photoionisation of octafluorocyclopentene showed the interesting result that the ground

electronic state of the parent cation has very weak intensity under threshold conditions. Photoionisation experiments were performed under a range of conditions; He(I) photoelectron conditions, a high-resolution threshold photoelectron spectrum and with electrons as the ionisation source. These experiments showed that the intensity of the ground electronic state is massively increased when either electrons or He(I) photons are used. In future it would be interesting to determine whether the weakness of the signal under threshold conditions is due to an intrinsically weak cross-section or due to other competing processes, for example fluorescence or predissociation. No value was available for the enthalpy of formation of either octafluorocyclopentene or $C_5F_7^+$. Use of *ab initio* methods allowed these values to be obtained.

An extensive study was performed on the six chloroethene molecules. The aim of this study was to examine how chlorination of molecules affects ionisation processes. The addition of chlorine atoms created clear trends in the studies, for example an increase in electronic states around 2 eV above onset of ionisation due to the chlorine lone pairs. Another aim was to see how isomeric effects alter the processes when the neutral molecules are the dichloroethenes which can exist in three isomeric forms. No clear sign of isomeric effects were seen in the photoionisation of the dichloroethenes or when long-range charge transfer was energetically allowed. When only chemical reactions could take place several interesting isomeric effects were detected. The clearest evidence was for the reactions of the dichloroethenes with CF_3^+. Here completely different products are seen depending on whether the neutral was 1,1-dichloroethene or 1,2-dichloroethene. It appears that isomeric effects are only detectable when the ionisation processes occur in a non-statistical fashion. If it is statistical then the small structural differences between the isomers will have little effect. It would also be of great value to study the chloroethenes by ion-pair production. This is an inherently non-statistical process and so isomeric effects may be more noticeable. Products formed from the chemical reactions indicate that very complicated mechanisms must be taking place. These products involve extensive rearrangement of atoms across the double bond. Future studies will be to examine the ion-molecule reactions of the fluoroethenes to see the effects of fluorine substitution on reactivity and compare them to the chloroethenes. Of real interest is whether some of the intricate mechanisms observed in the chloroethene reactions take place with the fluoroethenes.

Finally upgrades to the electron attachment mass spectrometer have been described. Characterisation of the new system shows improved performance over previous versions.

Appendix 1:

Rice Ramsperger Kassel Marcus (RRKM) Calculations

To aid in interpretation of the photoionisation results RRKM calculations were attempted. A programme as written in labVIEW based on BASIC code given in: *Unimolecular Reaction Dynamics : Theory and Experiment*, T. Baer and W. L. Hase, Oxford University Press, Oxford, (1996)

Table A1.1 shows the results for density of states and sum of states if the following vibrations are used in the calculations:

3030, 3020, 3010, 3005, 1503, 1401, 1383, 999, 951, 877, 652, 333, 278, 250, 89 cm^{-1} all are singly degenerate.

To calculate density of states set R, number of rotations to 0 and Q_r, rotational partition constant to 1. For the sum of states R to 1 and Q_r to 1.

Table A1.1: Test results for RRKM calculations.

Energy / cm^{-1}	Density of States / $(cm^{-1})^{-1}$	Sum of States
0	-	-
100	0.01	1.70
200	0.02	3.37
300	0.04	6.14
400	0.05	10.35
500	0.08	16.50
600	0.11	25.23
800	0.19	53.86
1000	0.34	105.4
2000	3.3	1466
3000	19.2	10704
4000	83.6	55098

5000	300	226143
6000	937	789568
8000	6736	6.83×10^6
10000	36600	4.28×10^7
12000	161100	2.13×10^8
14000	605900	8.91×10^8
16000	2.01×10^6	3.25×10^9

To test the RRKM calculation the dissociation of the parent cation formed from 1,1-dichloroethene by loss of a Cl atom was studied.

$$C_2H_2Cl_2^+ \rightarrow C_2H_2Cl^+ + Cl \qquad \textbf{(re A1.1)}$$

This required the vibrations of both the parent cation and the transition state (TS) of the fragmentation. The TS was found using the Berny-TS optimisation routine included in Gaussain 03, as explained in chapter 3. The TS structure is shown in Figure A1.1.

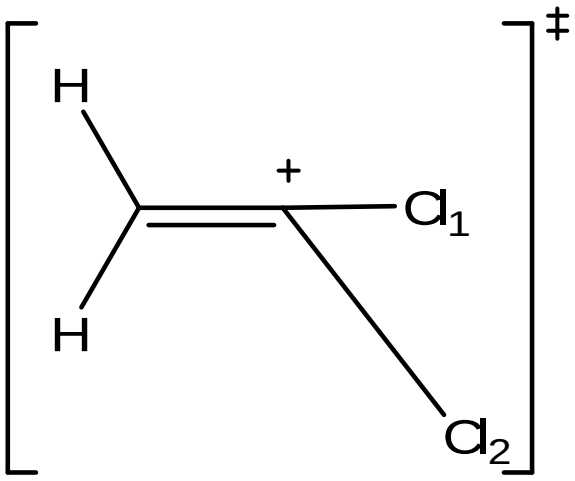

Figure A1.1: Transition structure for dissociation of 1,1-dichloroethene.

The structural parameters are: C-Cl_1 = 1.55 Å, C-Cl_2 = 3.6 Å, C-C = 1.28 Å, C-H = 1.09 Å, $\angle Cl_1CCl_2$ = 79.71°, $\angle Cl_1CC$ = 180.0°, $\angle Cl_2CC$ = 100.3°, $\angle HCH$ = 120.1°. The calculated vibrations are 400.1, 570.8, 584.6, 690.4, 843.8 893.8, 1200.8, 1354.4, 3090.3, 3287.1 and 4210.6 cm^{-1}.

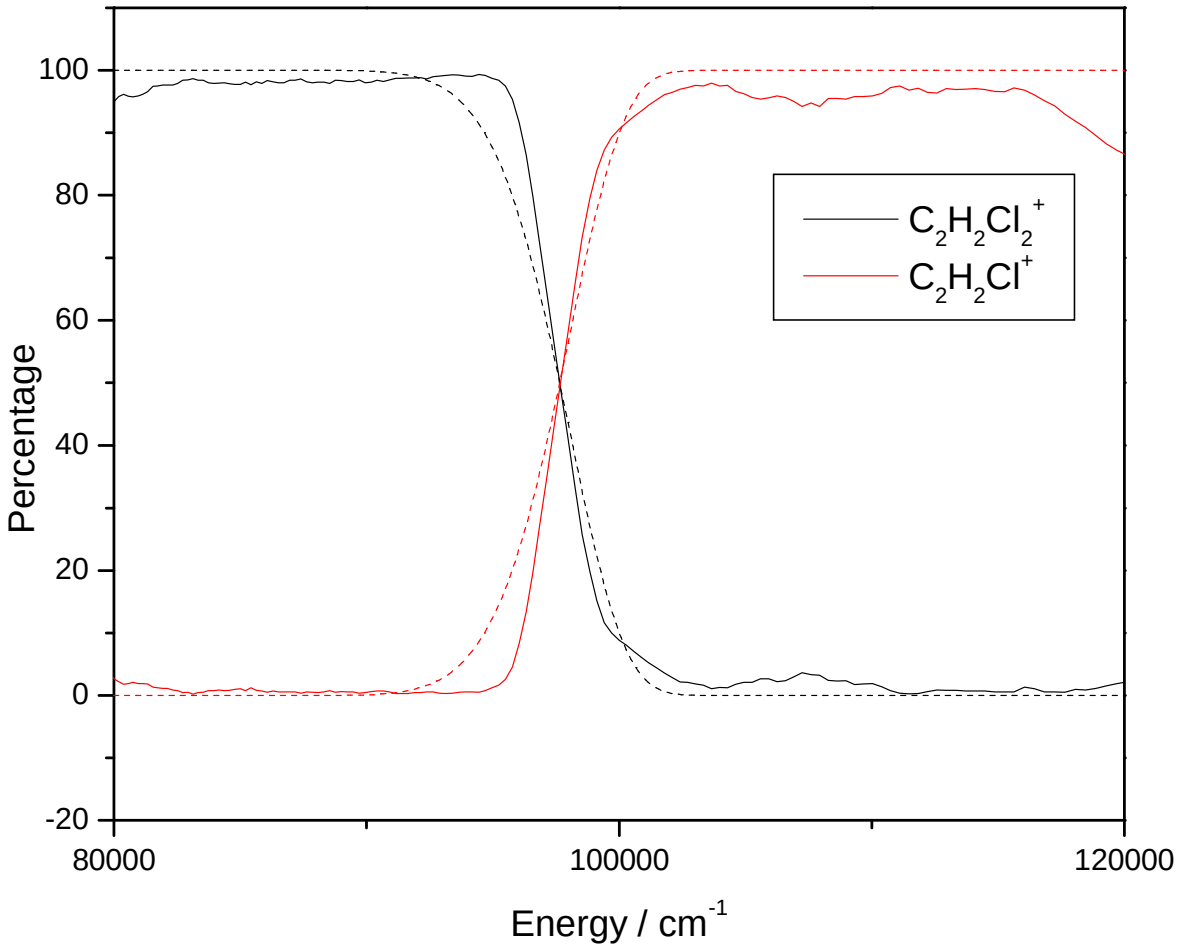

Figure A1.2: Breakdown diagram for dissociation of $C_2H_2Cl_2^+$ from TPEPICO data with RRKM fit.

Figure A1.2 shows the measured breakdown diagram for reaction A1.1 recorded using the TPEPICO experiment with a theoretical breakdown diagram calculated using RRKM theory. The fit gives an appearance energy at 298 K for the $C_2H_2Cl^+$ fragment as 10.85 eV. The experimental AE_{298} is 11.88 eV. This gives a difference in 1 eV between measured and calculated values. This difference is probably too large to be due to kinetic shift, normal values are < 0.5 eV. Another reason could be that there is a barrier in the exit channel. Though it is a simple single bond fragmentation, and therefore it is normal to assume that there is no barrier, it does involve the rearrangement of several bonds. The Cl atom which is to remain on the molecule needs to move in wards as the carbon will now be sp not sp^2 hybridised. As this occurs along with the removal of the other Cl atom some interaction may take place between them which causes a barrier to arise.

Other reasons for the large difference could be related to the calculation itself. It is possible that the TS which was used in the calculation is not the correct one. There could be another barrier at a smaller reaction coordinate, *i.e*. with C-Cl_2 bond length is shorter or $\angle Cl_1CC$ is smaller. Another reason could also be that the thermal distribution of energies of the parent ion has not been taken into account. To take this into account the calculated breakdown diagram must be convoluted with the internal energy distribution of the sample gas, in this case it is a thermal sample at 298 K, and an instrument resolution function. More work is needed to improve the RRKM calculations shown here.

Appendix 2:

Values used for the calculation of the enthalpy of formation of *c*-C_5F_8

Table A2.1: Calculated enthalpies used to calculate enthalpy of formation of *c*-C_5F_8.

Molecule	E + thermal (H_{298}) / Har	$\Delta_f H_{298}$ Calculated / kJ mol^{-1}
CF_3	-338	-465
CF_4	-438	-933
C_2F_4	-476	-677
C_2F_2	-276	0.13
CF_2	-238	-197
C_5F_8	-989	Unknown
C_4F_8	-951	-1572
C_3F_4	-514	-554
C_3F_6	-714	-1030
C_3F_8	-913	-1766
CF	-138	249

Table A2.1 lists the molecules used in the calculation of the enthalpy of formation of *c*-C_5F_8 as outlined in chapters 3 and 6. The first column lists the molecule; the second column gives the calculated enthalpy of formation from our DFT calculations. The final column lists calculated enthalpies of formation from high-level coupled cluster calculations. These calculations include corrections for basis set superposition errors as well as spin-orbit corrections. These values are taken from the following papers:

C.W. Bauschlicher, A. Ricca, *J. Phys. Chem. A*, **104**, (2000), 4581
C.W. Bauschlicher, A. Ricca, *J. Phys. Chem. A*, **104**, (2000), 9026.

Appendix 3: Electronic Circuits for the Electron Attachment Mass Spectrometer

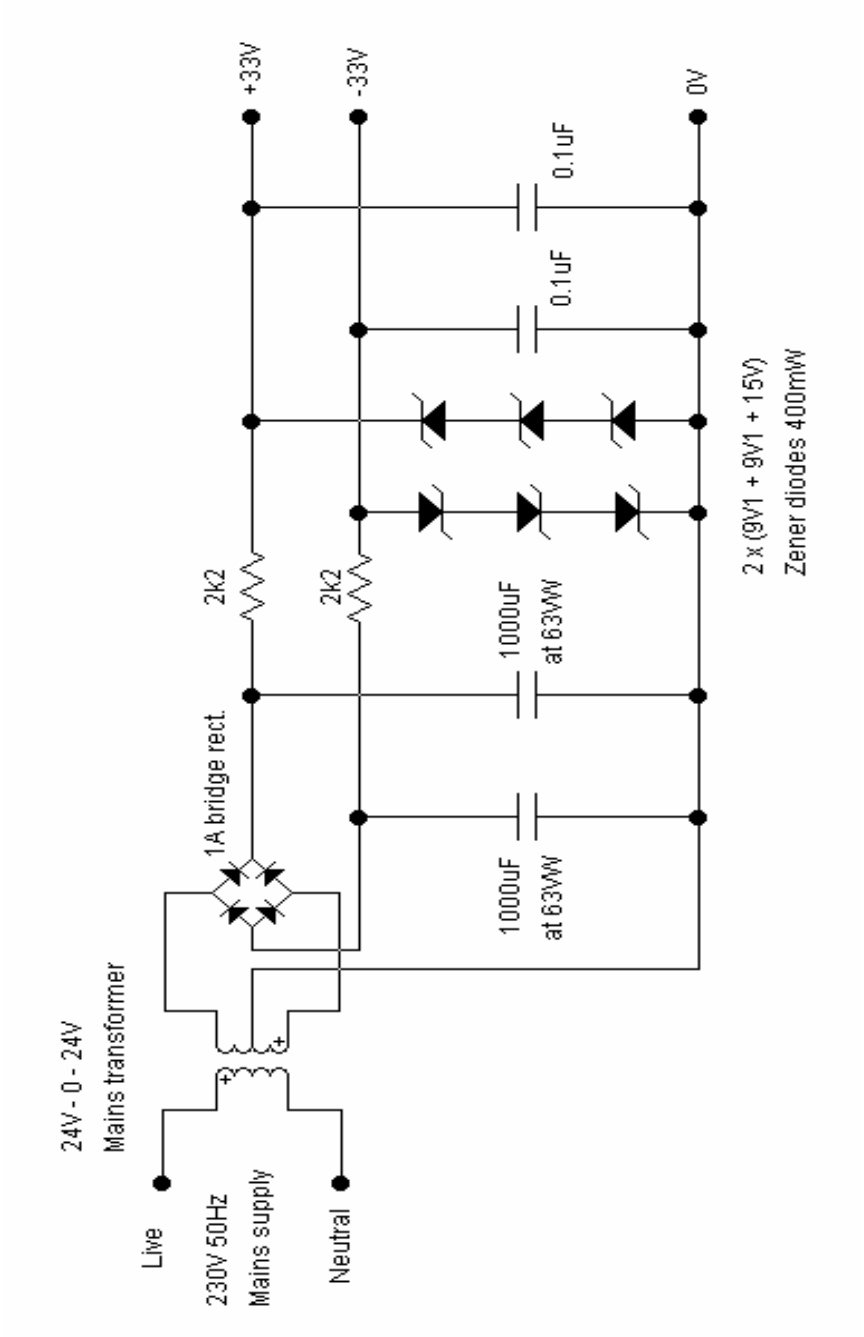

Figure A3.1: Circuit diagram for mains voltage supply to EAMS gate pulsing unit.

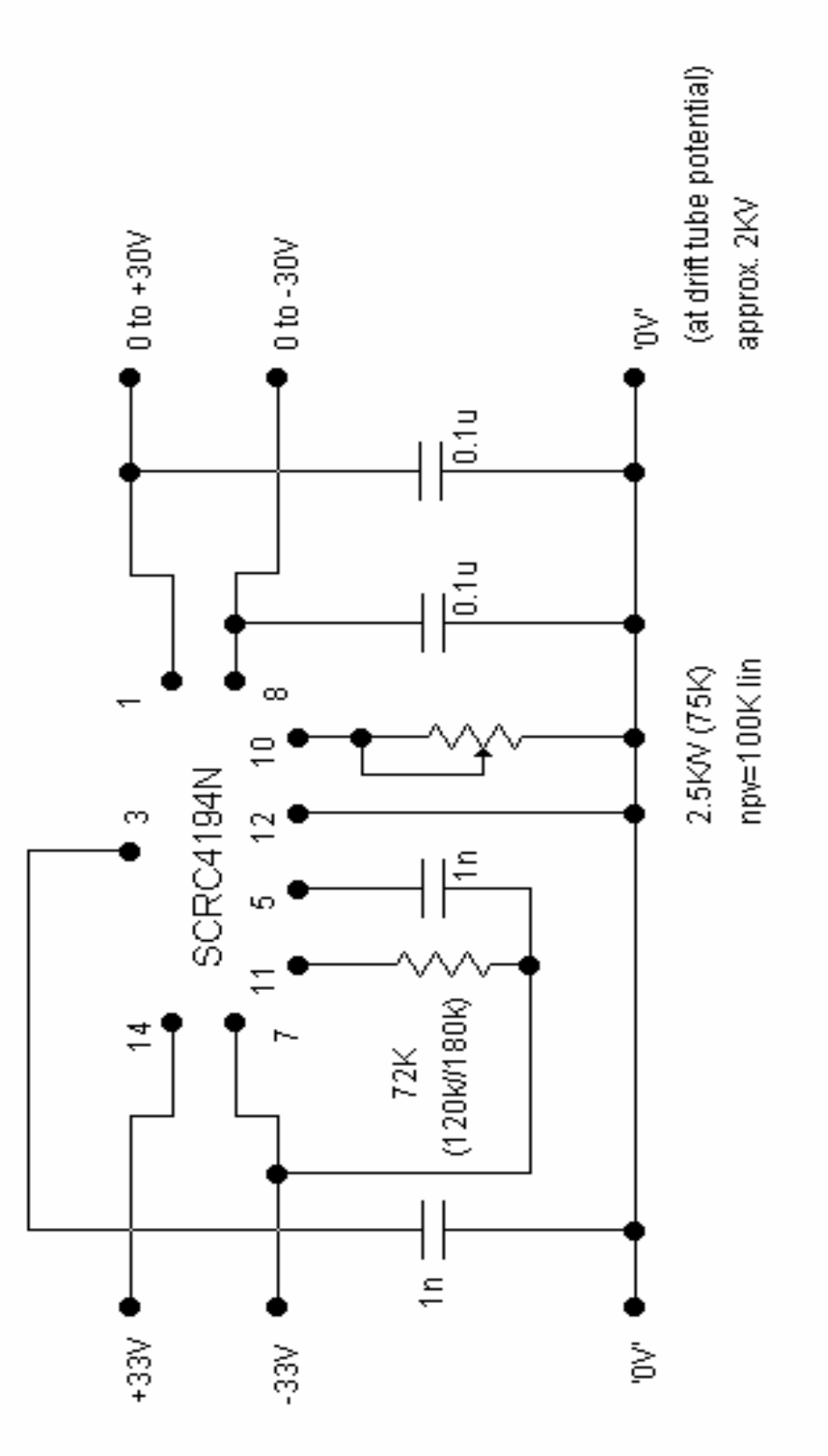

Figure A3.2: Dual tracking voltage regulator for EAMS gate pulsing unit.

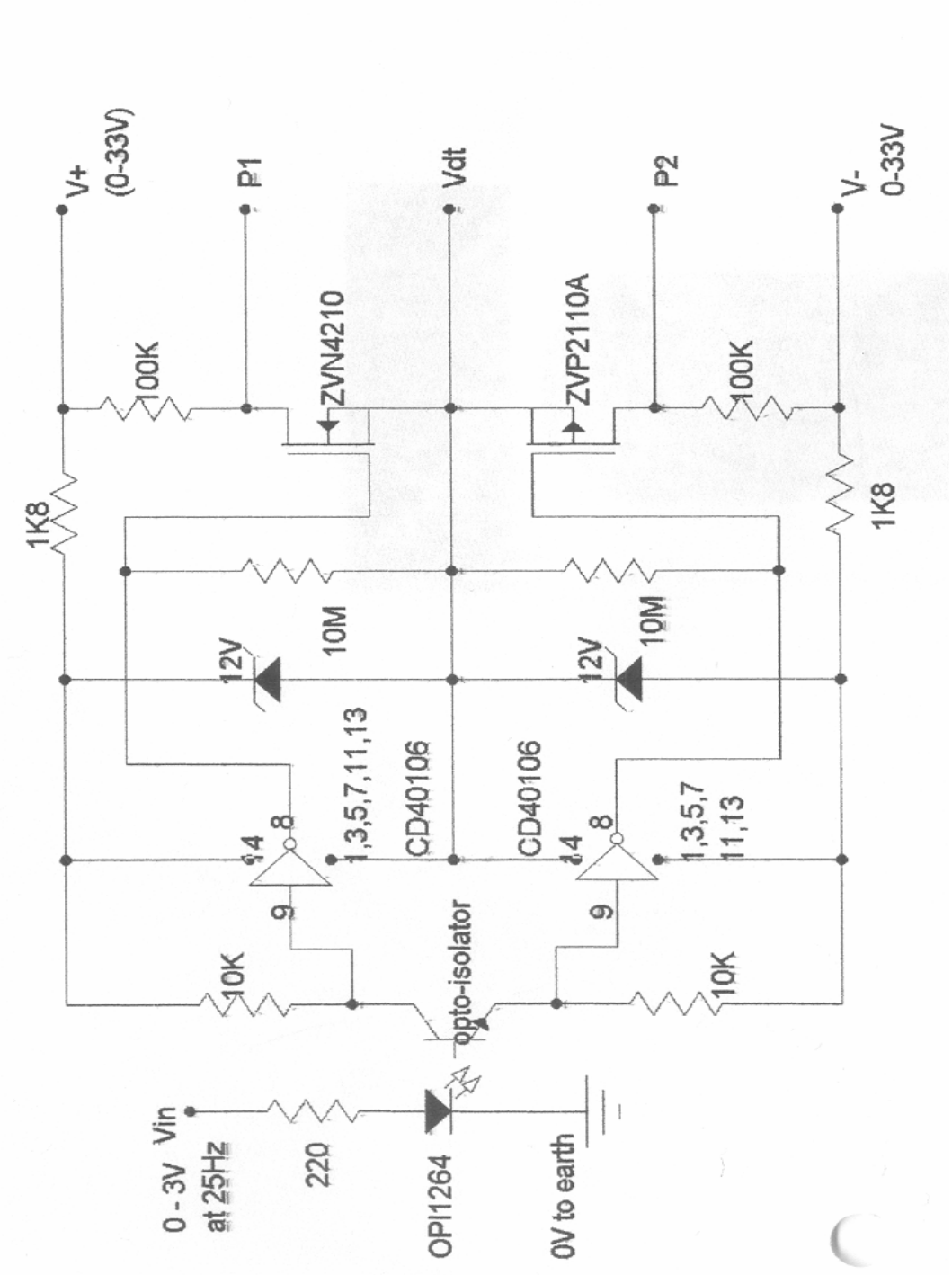

Figure A3.3: Pulse circuit for EAMS gate pulsing unit.

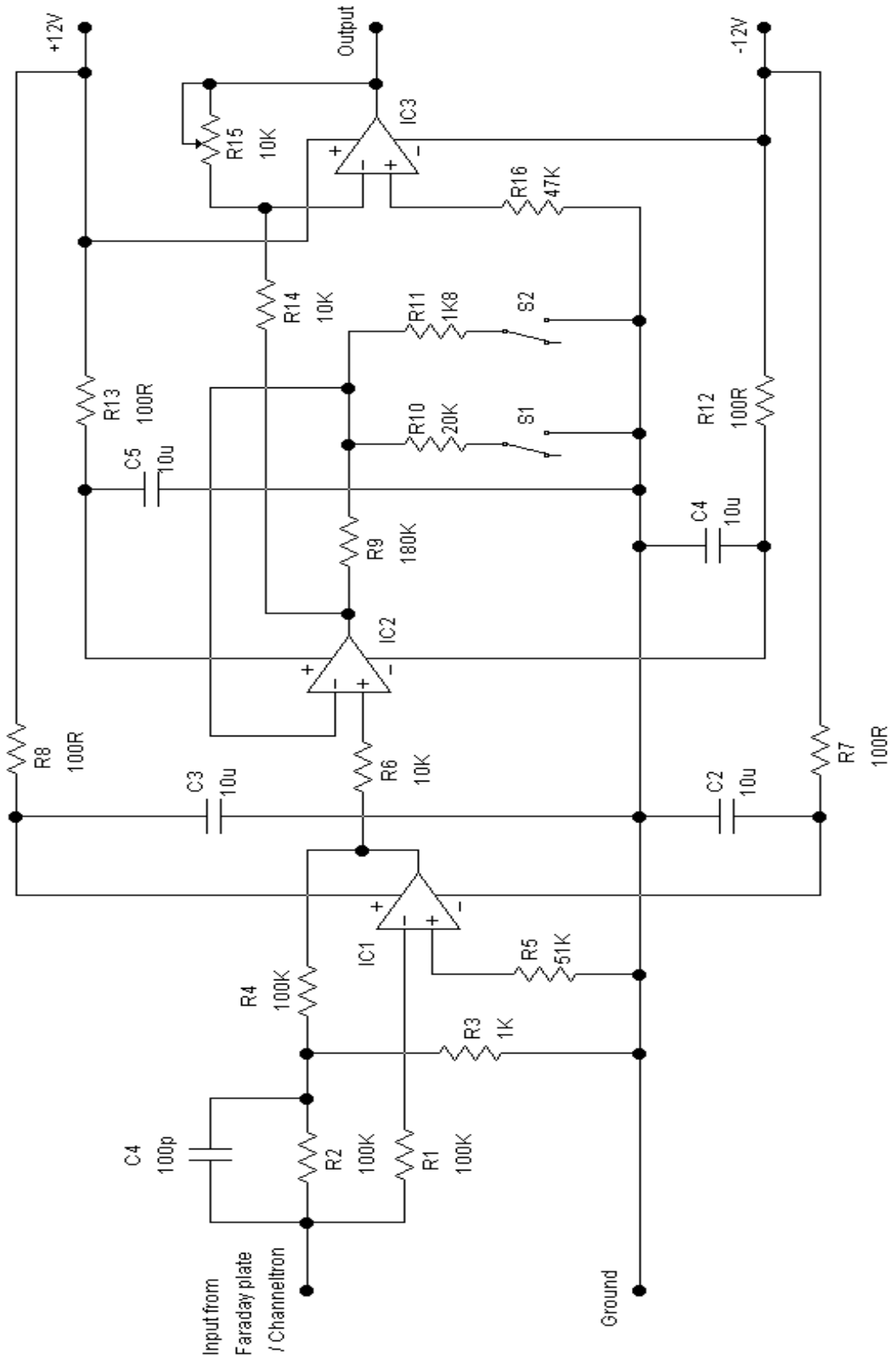

Figure A3.4: High-gain amplifier circuit for EAMS.